UNIVERZITA KARLOVA

Přírodovědecká fakulta

Doktorský studijní program: Biochemie



Mgr. Veronika Fojtíková

Kinetická analýza enzymové aktivity modelových hemových senzorových proteinů

Enzyme activity analysis of function domains belonging to model heme-containing sensor proteins

Disertační práce

Vedoucí disertační práce: doc. RNDr. Markéta Martínková, Ph.D.

Praha, 2018

Prohlášení: Prohlašuji, že jsem závěrečnou práci zpracovala samostatně a že jsem uvedla všechny použité informační zdroje a literaturu. Tato práce ani její podstatná část nebyla předložena k získání jiného nebo stejného akademického titulu.

V Praze, 20.6.2018

Poděkování

Na tomto místě bych ráda poděkovala své školitelce doc. RNDr. Markétě Martínkové, Ph.D. za profesionální vedení, poskytnutou pomoc, energii a čas, který se mnou strávila v průběhu mého studia.

Děkuji také doc. RNDr. Václavu Martínkovi, Ph.D. za pomoc při vývoji metod pro měření enzymové aktivity a RNDr. Petru Manovi, Ph.D. za hmotnostně-spektroskopická měření.

Dále bych chtěla poděkovat svým starším kolegům Mgr. Martinu Stráňavovi, Ph.D., RNDr. Janu Milichovskému, Ph.D. a Mgr. Janu Bláhovi, Ph.D., kteří mi vždy rádi a ochotně se vším pomohli a poradili.

V neposlední řadě bych ráda poděkovala svému příteli a své rodině za neustálou podporu v průběhu mého studia a všem svým spolupracovníkům z katedry biochemie za vytvoření příjemného pracovního prostředí.

Abstrakt CZ

Předkládaná disertační práce se zabývá studiem hemových senzorových proteinů, které detekují plynné molekuly. Tyto proteiny se nachází především v bakteriálních systémech, kde se podílí na regulaci procesů, jako např. sporulace, rezistence k antibiotikům a další. Hemové senzorové proteiny jsou tvořeny dvěma doménami – senzorovou, která obsahuje molekulu hemu, jenž interakcí s plynnými molekulami ovlivňuje aktivitu druhé, funkční domény. Součástí této práce je rešerše, která shrnuje poznatky ohledně problematiky hemových senzorů. V další části jsme se zaměřili na studium tří senzorových hemoproteinů, a to histidinkinasy *Af*GcHK, diguanylátcyklasy YddV a fosfodiesterasy *Ec*DOS.

Hlavním cílem předkládané práce bylo objasnit mechanismus intraproteinového/interdoménového přenosu signálu u hemových senzorových proteinů s globinovým uspořádáním senzorové domény (*Af*GcHK a YddV) s použitím kinetické analýzy enzymové aktivity a metod strukturní biologie. Dalším cílem bylo prozkoumat interproteinový přenos signálu mezi proteinem *Af*GcHK a jeho interakčním partnerem RR proteinem. V neposlední řadě byl zkoumán vlivu sulfidu sodného na katalytické vlastnosti proteinů *Ec*DOS, *Af*GcHK.

Výsledky kinetické analýzy odhalily, že redukce hemového železa a absence hemu v senzorové doméně výrazně snižuje enzymovou aktivitu hemových senzorů s globinovou strukturou. Strukturní analýzou bylo zjištěno, že redukce hemového železa u *Af*GcHK vyvolá strukturní změny v oblasti senzorové domény (helix H5), v dimerizační oblasti (helixy H6 a H7) a v oblasti funkční domény (helixy H9 a H11).

Studiem interakce *Af*GcHK s RR proteinem bylo odhaleno, že v roztoku dochází k tvorbě komplexu dimeru *Af*GcHK a monomeru RR proteinu. Přítomnost RR proteinu v reakční směsi snižuje autofosforylační aktivitu *Af*GcHK, což naznačuje, že RR protein je vázán do blízkosti vazebného místa pro ATP. Interakční rozhraní těchto proteinů je tvořeno oblastmi v regulační doméně č. 1 RR proteinu a dimerizační oblasti *Af*GcHK.

Přítomnost sulfidu sodného ovlivňuje spektrální vlastnosti všech zkoumaných hemových senzorových proteinů (*Ec*DOS, *Af*GcHK, YddV). U mutantních forem Arg97Ile proteinu *Ec*DOS a určitých mutantních forem Leu68 proteinu *Af*GcHK došlo k tvorbě tzv. verdohemu. U proteinu *Ec*DOS došlo po inkubaci se sulfidem sodným ke zvýšení enzymové aktivity proteinu, u *Af*GcHK přítomnost sulfidu sodného neovlivnila enzymovou aktivitu proteinu.

Abstract EN

This Ph.D. thesis focuses on the heme containing gas sensor proteins. These proteins are predominantly present in bacteria, in which play an important role in processes like, sporulation, antibiotic resistance and so on. Heme containing sensor proteins composed of two domains. First one is a globin domain, which contains the heme molecule. Interaction of heme with gas molecule acts as a signal for the activation/inactivation of the second functional domain. Part of this thesis is formed by a review, which summarized the current knowledge about heme containing sensor proteins. In the next part of this thesis we focused on three representatives from the group of oxygen sensor proteins – histidine kinase *Af*GcHK, diguanylate cyclase YddV and phosphodiesterase *Ec*DOS.

The main aim of this thesis was to solve the mechanism of interdomain/intraprotein signal transduction in two oxygen sensor proteins with globin fold of their sensor domain (*Af*GcHK, YddV). For this purpose, we used the kinetic analysis of their functional domain activity and the methods of structural biology. We also studied the mechanism of interprotein signal transduction in *Af*GcHK and its cognate partner RR protein. It was also tested, how the presence of sodium disulfide affects the functional properties of oxygen sensor proteins *Ec*DOS, *Af*GcHK.

Kinetic studies reveal that the Fe(II) form and heme free form of the sensor globin domain exhibited low activity comparing to Fe(III) form. Major conformational differences between the active and inactive forms were observed in the sensor domain (helix H5), at the dimerization interface (helices H6 and H7) and also in the functional domain (helices H9 and H11).

It was found, that in the relatively dilute solutions, *Af*GcHK and RR protein exist in the 2:1 complex (one dimeric *Af*GcHK and one monomeric RR protein). The presence of RR protein influences the autophosphorylation activity of *Af*GcHK, which suggest, that RR protein is bound close to the ATP binding site. The interaction interface of *Af*GcHK and RR protein is in the regulation domain 1 of the RR protein and in the *Af*GcHK's dimerization domain.

Presence of sodium disulfide influences the spectral properties of *Af*GcHK, *Ec*DOS and YddV. In the case of Arg97Ile mutant of *Ec*DOS and some of Leu68 mutants of *Af*GcHK the small proportion of verdoheme were formed after the treatment

with sodium disulfide. The catalytic enhancement due to the presence of sodium disulfide was observed in the case of *Ec*DOS, but not in the case of *Af*GcHK.

Obsah

Seznam zkratek 8

1. Cíle disertační práce 9

2. Výsledky, komentáře k souboru publikací a diskuse všech dosažených poznatků 10

3. Publikace BLOKU I 27

3.1 Gaseous O_2, NO, and CO in signal transduction: structure and function relationships of heme-based gas sensors and heme-redox sensors 28

3.2 Kinetic analysis of a globin-coupled histidine kinase, *Af*GcHK: effects of the heme iron complex, response regulator, and metal cations on autophosphorylation activity 72

4. Publikace BLOKU II 86

4.1 Catalytic enhancement of the heme-based oxygen sensing phosphodiesterase *Ec*DOS by hydrogen sulfide is caused by changes in heme coordination structure ... 87

4.2 Effects of hydrogen sulfide on the heme coordination structure and catalytic activity of the globin-coupled oxygen sensor *Af*GcHK 104

5. Publikace BLOKU III 120

5.1 Structural characterization of the heme-based oxygen sensor, *Af*GcHK, its interactions with the cognate response regulator, and their combined mechanism of action in a bacterial two-component signaling system 121

5.2 Coordination and redox state-dependent structural changes of the heme-based oxygen sensor *Af*GcHK associated with intraprotein signal transduction 137

6. Závěr 153

7. Curicullum vitae Veroniky Fojtíkové včetně seznamu publikací 155

Seznam zkratek

Aer-sal	protein regulující odpověď bakterie *Aeromonas salmonicida*
*Af*GcHK	histidinkinasa s globinovou strukturou senzorové domény izolovaná z bakterie *Anaeromyxobacter sp.*, kmen Fw 109-5
ATP	adenosintrifosfát
c-di GMP	cyklický bis-guanosinmonofosfát
*Ec*DOS	fosfodiesterasa s PAS strukturou senzorové domény bakterie *E. coli*
E. coli	*Escherichia coli*
*Gs*GCS	protein detekující kyslík s globinovou strukturou senzorové domény bakterie *Geobacter sulfurreducens*
GTP	guanosintrifosfát
HD výměna	vodík – deuteriová výměna
HK853	histidinkinasa bakterie *Thermotoga maritima*
HPLC	vysoce účinná kapalinová chromatografie
MBP	protein vázající maltosu
PAS	strukturní motiv prostorového uspořádaní proteinů; akronym odvozený z anglických názvů tři proteinů: „Drosophila period clock protein‘‘, „vertebrate aryl hydrocarbon receptor nuclear translocator‘‘ a „Drosophila single minded protein‘‘
RR protein	protein regulující odpověď (z angl. response regulator protein)
Tris	tris(hydroxymethyl)aminomethan
WT	přirozená forma proteinu (z angl. wild type)
YddV	diguanylátcyklasa s globinovou strukturou senzorové domény bakterie *Escherichia coli*
YddV-hem	globinová senzorová doména proteinu YddV

1. Cíle disertační práce

Cílem předkládané disertační práce bylo objasnit intraproteinový/interdoménový přenos signálu u modelových zástupců hemových senzorových proteinů s globinovým uspořádáním senzorové domény (*Af*GcHK, YddV). Dalším cílem bylo prostudovat interproteinový přenos signálu u proteinu *Af*GcHK a jeho partnera RR proteinu, tvořící tzv. dvousložkový signální systém. Rovněž byl kladen důraz na studium strukturních vlastností těchto proteinů. V neposlední řadě bylo cílem této disertační práce prostudovat vliv sulfidu sodného na strukturu senzorových domén a katalytickou aktivitu funkčních domén hemových senzorových proteinů (*Af*GcHK, YddV, *Ec*DOS).

V rámci studia intraproteinového/interdoménového přenosu signálu byly definovány tyto cíle:

- Určit kinetické parametry autofosforylační reakce *Af*GcHK a diguanylátcyklasové reakce YddV za různých oxidačních stavů iontu hemového železa a v přítomnosti různých ligandů hemu.
- Prozkoumat mechanismus přenosu signálu proteinu *Af*GcHK pomocí strukturně biologických metod (HD výměna spojená s hmotnostní spektrometrií, vyřešení krystalové struktury senzorové domény proteinu).

Pro objasnění interproteinového přenosu signálu byly stanoveny tyto cíle:

- Pomocí enzymové analýzy zjistit, jestli a jakým způsobem přítomnost RR proteinu ovlivní autofosforylační aktivitu *Af*GcHK
- Charakterizovat oligomerní stavy proteinů *Af*GcHK a RR, určit stechiometrii těchto proteinů v komplexu a charakterizovat jejich interakční rozhraní.

V rámci studia vlivu sulfidu sodného na strukturní a katalytické vlastnosti hemových senzorových proteinů byly definovány tyto cíle:

- Zjistit, jaký vliv má přítomnost sulfidu sodného na spektrální vlastnosti proteinů *Ec*DOS, *Af*GcHK a YddV a jak tento stav senzorové domény ovlivní katalytickou aktivitu proteinů *Ec*DOS a *Af*GcHK.

2. Výsledky, komentáře k souboru publikací a diskuse všech dosažených poznatků

Předkládaná disertační práce se zabývá studiem hemových senzorových proteinů, které detekují kyslík. Důraz byl kladen zejména na zkoumání fungování těchto proteinů na molekulární úrovni. K tomuto účelu byly vybrány tři proteiny z kategorie hemových senzorových proteinů, které se liší proteinovým uspořádáním jejich senzorových a funkčních domén, různou afinitou ke kyslíku, zapojením do buněčné signalizace. Nalezení vlastností, ve kterých se tyto proteiny shodovaly a/nebo naopak lišily, umožnilo přispět k odhalení mechanismu interdoménového a intraproteinového přenosu signálu.

Disertační práce je rozdělena do tří bloků. V BLOKU I (kapitoly 3.1, 3.2) jsou obsaženy výsledky publikace, která byla zaměřena na analýzu funkční domény modelového senzorového hemoproteinu – histidinkinasy s globinovou strukturou senzorové domény bakterie *Anaeromyxobacter sp* (*Af*GcHK). Výsledky popsané v kapitole 3.2 jsou porovnány s naměřenými daty kinetické analýzy hemového senzorového proteinu diguanalátcyklasy s globinovou strukturou senzorové domény bakterie *Escherichia coli* (YddV), se kterým *Af*GcHK sdílí globinovou senzorovou doménu, ale liší se ve funkci (data jsou součástí připravované publikace, proto nejsou uvedena v samostatné kapitole). BLOK I také obsahuje souhrnnou publikaci, která se věnuje rozsáhlému výčtu dosavadních poznatků o hemových senzorových proteinech (kapitola 3.1). Publikace BLOKU II (kapitoly 4.1, 4.2) jsou výsledkem studia vlivu sulfidu sodného na spektroskopické a funkční vlastnosti hemových senzorových proteinů. Pro tuto výzkumnou část byly vybrány dva proteiny s rozdílným prostorovým uspořádáním senzorových a funkčních domén – fosfodiesterasa s PAS strukturou senzorové domény bakterie *Escherichia coli* (*Ec*DOS) a *Af*GcHK. Obsahem BLOKU III (kapitoly 5.1, 5.2) je studium přenosu signálu mezi senzorovou a funkční doménou hemového senzorového proteinu *Af*GcHK a dále přenosu signálu mezi dvěma proteiny dvousložkového signálního systému, jehož je protein *Af*GcHK součástí.

Obsahem úvodní kapitoly 3.1 BLOKU I je souhrnný článek, který se detailně věnuje tématu hemových senzorových proteinů detekujících plynné molekuly. Tato tématika se dostává do oblasti zájmu mnoha vědeckých týmů po celém světě a za posledních deset let bylo objeveno mnoho doposud neznámých hemových senzorových proteinů a byl

také rozšířen výzkum těchto proteinů. Bylo proto na místě tyto vědecké výsledky sjednotit a uspořádat. Nejrozsáhleji je v této publikaci pojednáno o hemových senzorových proteinech detekujících kyslík, kterým se věnuje také tato předkládaná disertační práce. V další části je rozebrána problematika hemových senzorových proteinů detekujících oxid uhelnatý a oxid dusnatý. Je také zmíněn sulfan jako další signální molekula, která se v posledních letech dostává do popředí zájmu mnohých vědeckých týmů. Problematikou interakce hemových senzorových proteinů a sulfanu se věnuje i tato disertační práce, viz kapitoly 4.1 a 4.2.

Následující kapitola 3.2 BLOKU I a výsledky z připravované publikace uvedené na stranách 13 - 18 se věnují studiu enzymové aktivity dvou hemových senzorových proteinů. Oba tyto proteiny mají globinovou strukturu senzorové domény, ale liší se ve svých funkcích – histidinkinasové a diguanylátcyklasové. Shodná globinová struktura senzorových domén těchto proteinů nám umožnila podrobněji prozkoumat, jak velký vliv má stav senzorové domény na enzymovou aktivitu hemových senzorových proteinů detekujících kyslík. Výsledkem těchto studií bylo určení kinetických parametrů jednotlivých enzymových reakcí. Právě diference parametrů enzymových reakcí funkčních domén v důsledku změny redoxních a ligandových stavů iontu železa v senzorových doménách nám částečně pomohly objasnit, jakým způsobem probíhá přenos signálu ze senzorové na funkční doménu a odhadnout strukturní změny, které tento proces provází. Tyto výsledky jsme následně aplikovali a diskutovali i při dalších studiích, využívajících strukturně biologické postupy pro sledování strukturních změn proteinu *Af*GcHK (viz kapitoly 5.1, 5.2 BLOKU III).

Protein *Af*GcHK je jedinou doposud objevenou histidinkinasou s globinovou strukturou senzorové domény [Martinkova et al. *J Biol Chem* 288, 27702 (2013)]. Tento unikátní protein byl identifikován v anaerobní bakterii *Anaeromyxobacter speciens*, Fw 109-5, která byla izolována z půdy obsahující vysoký podíl dusičnanů a urania v Oak Ridge Reservation [Hwang et al. *Genome Announc* 3, e01449 (2015)]. Funkce této histidinkinasy je úzce spjata s proteinem regulujícím odpověď (RR protein) se kterým tvoří takzvaný dvousložkový signální systém [Kitanishi et al. *J Biol Chem* 286, 35522 (2011)]. Tyto systémy prostřednictvím mimobuněčných stimulů regulují procesy, které řídí správné fungování daného organismu [Grebe et al. *Adv. Microb. Physiol* 41, 139, (1999)] Po stimulaci *Af*GcHK signálem (vazbou molekuly kyslíku k hemu v senzorové doméně) dochází prostřednictvím γ-fosfátového zbytku hydrolyzovaného ATP k

autofosforylaci His183. Poté je fosfátový zbytek přesunut z *Af*GcHK na aspartátový zbytek (Asp52, Asp169) RR proteinu, čímž dochází k jeho aktivaci. Funkce RR proteinu v tomto dvousložkovém signálním systému nebyla zatím objasněna, předpokládá se však, že se podílí na regulaci procesů spojených s přechodem z aerobního do anaerobního prostředí, jako je například sporulace. Tento systém byl poprvé popsán v roce 2011 [Kitanishi et al. *J Biol Chem* 286, 35522 (2011)] nicméně se jednalo pouze o pilotní studii, kterou jsme se rozhodli v rámci předkládané disertační práce rozšířit.

Naším prvním úkolem specifikovaným v kapitole 3.2 BLOKU I bylo zjistit, jakým způsobem různé redoxní a koordinační stavy hemového železa ovlivní autofosforylační reakci. Stanovili jsme proto kinetické parametry autofosforylační reakce pro jednotlivé redoxní a ligandové stavy iontu železa hemu v senzorové doméně plno délkového proteinu *Af*GcHK a výsledky mezi sebou porovnali. Hodnoty k_{cat} *Af*GcHK, jehož hem v senzorové doméně byl ve stavu Fe(III)-OH^-, Fe(III)-CN^-, Fe(III)-imidazol a Fe(II)-O_2 byly velmi podobné (1,1 - 1,2 min^{-1}), naměřené hodnoty K_m^{ATP} těchto forem se pohybovaly v rozmezí 18,9 - 35,4 μM. Prostorové uspořádání těchto forem *Af*GcHK je tedy příznivé pro vazbu ATP a následnou autofosforylační reakci. Na druhé straně, pokud bylo hemové železo v redukované formě nebo pokud hem v senzorové doméně chyběl (byla vytvořena mutantní forma *Af*GcHK His99Ala) byla aktivita proteinu velmi nízká, což bylo prokázáno nízkou hodnotou k_{cat} 0,4 min^{-1}, respektive 0,3 min^{-1}. Zvláštním případem byla forma Fe(II)-CO, kdy k_{cat} byla 1,0 min^{-1}, ale hodnota K_m^{ATP} 357 μM byla mnohonásobně vyšší, než tomu bylo o ostatních forem. Vazba oxidu uhelnatého k hemu v redukované formě pravděpodobně vyvolá významné strukturní změny v okolí vazebného místa pro ATP, které jsou ale odlišné od změn vyvolaných vazbou jiných axiálních ligandů, jako kyslíku imidazolu nebo kyanidu. Z hlediska poměru k_{cat} a K_m^{ATP}, je katalytická účinnost enzymu ve formě Fe(II)-O_2 (700 $M^{-1}.s^{-1}$) mnohonásobně vyšší než enzymu ve formě Fe(II)-CO (50 $M^{-1}.s^{-1}$), což znamená, že vazba kyslíku k hemu má odlišný vliv na katalytickou regulaci než vazba oxidu uhelnatého k hemu. Rozdílné hodnoty K_m^{ATP} pro jednotlivé formy hemového železa v senzorové doméně indikují, že koordinační a redoxní stav hemu v senzorové doméně *Af*GcHK má výrazný vliv na histidinkinasovou aktivitu proteinu, a to prostřednictvím změny afinity k substrátu reakce, tedy ATP.

Kinetickou studii jsme použili také pro další úkoly kapitoly 3.2 BLOKU I tj. prozkoumání přenosu signálu mezi *Af*GcHK a jeho partnerem RR proteinem. V tomto

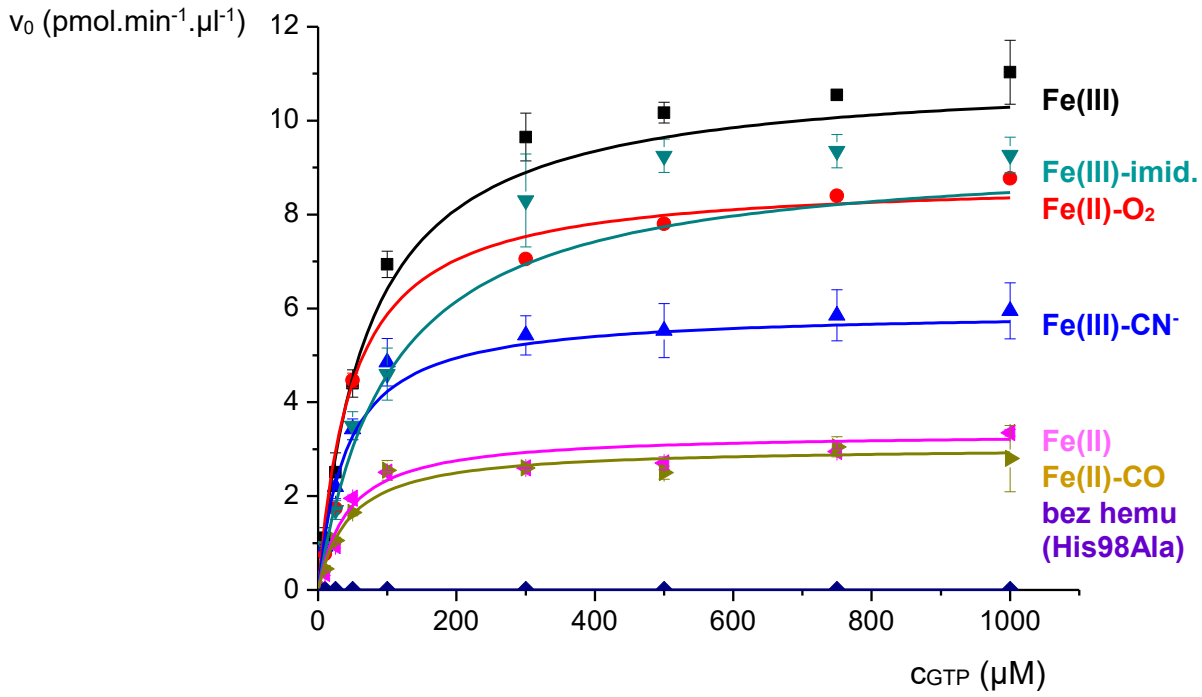
případě jsme studovali, jestli se změní kinetické parametry autofosforylační reakce *Af*GcHK, pokud bude v reakční směsi přítomen také RR protein. Byl vybrán *Af*GcHK ve stavu Fe(III)-OH^-, tedy ve stavu nejvíce enzymově aktivním, a RR protein s mutovanými fosforylačními místy, aby nedocházelo k přenosu fosfátového zbytku z *Af*GcHK na tento protein a bylo tak možné měřit množství produktu fosforylační reakce. Překvapivě došlo k nárůstu K_m^{ATP}, což svědčí o snížení afinity ATP k *Af*GcHK v případě, kdy je přítomen RR protein. RR protein tak zřejmě interaguje s *Af*GcHK v blízkosti vazebného místa pro ATP a dochází ke snížení efektivity fosforylační reakce. Tyto výsledky byly ověřeny také použitím jiných experimentálních metod v kapitolách 5.1, 5.2. Na základě výsledků vodík-deuteriové (HD) výměny bylo zjištěno, že vlivem přítomnosti RR proteinu docházelo ke změnám deuterace v oblasti helixu H11 proteinu *Af*GcHK, ve které se nachází také vazebné místo pro ATP. Lze tedy s jistotou říci, že RR protein během fosforylační reakce interaguje s oblastí vazebného místa pro ATP.

Enzymovou analýzu senzorového proteinu obsahujícího hem jsme se rozhodli použít také v případě funkční studie proteinu YddV. Výsledky této studie jsou součástí připravované publikace, v následujícím textu bude tedy kromě diskuze těchto výsledků stručně shrnuta i metodika a samotné výsledky.

Protein YddV bakterie *E. coli* se podílí na vzniku biofilmu a to prostřednictvím regulace syntézy adhezních látek a exopolysacharidů, které jsou jeho významnými složkami [Gong et. al. *Proc. Natl. Acad. Sci. U.S.A.* 95, 15177 (1998)]. Senzorová doména proteinu YddV má, stejně jako u proteinu *Af*GcHK, globinovou strukturu a jeho funkční doména vykazuje diguanylátcyklasovou aktivitu [Tuckerman et al. *Biochemistry* 48, 9764 (2009)]. Spolu s proteinem *Ec*DOS se podílí na udržení homeostázy cyklického guanosin-bismonofosfátu (c-di GMP), který je důležitým bakteriálním druhým poslem. Na základě signálu z okolí dojde k aktivaci YddV a následné syntéze c-di GMP ze dvou molekul GTP. *Ec*DOS je naproti tomu zodpovědný za degradaci c-di GMP tím, že katalyzuje jeho linearizaci [Delgado-Nixon et al. *Biochemistry* 39, 2685 (2000)]. Stejně jako v případě *Af*GcHK jsme se rozhodli prozkoumat, které oxidoredukční a koordinační stavy hemového železa způsobí enzymovou aktivaci a které protein naopak inaktivují. V předchozí studii zabývající se funkční charakterizací proteinu YddV byl použit semi-rekonstituovaný systém, kdy GTP byl přidán ke směsi obou proteinů YddV-*Ec*DOS [Tuckerman et al. *Biochemistry* 48, 9764 (2009); Kitanishi et al. *Biochemistry* 49, 10381 (2010)]. Pro naše účely, kdy

jsme porovnávali kinetické parametry dvou různých enzymů (*Af*GcHK a YddV), však bylo nutné pracovat pouze se samostatným proteinem. Exprese proteinu YddV v prokaryotních systémech je však obtížná a výtěžky získaného proteinu jsou velmi nízké. Proto jsme se rozhodli pomocí molekulárně biologických metod na N-konec proteinové sekvence YddV přidat protein vázající maltosu (MBP). Tímto došlo ke zvýšení solubility exprimovaného proteinu a po následné purifikaci byl získán protein o vysoké čistotě a výtěžku dostatečném pro kinetická měření.

Pro stanovení kinetických parametrů diguanylátcyklasové reakce byla vytvořena reakční směs obsahující 10 μM YddV, 10 – 1000 μM GTP, 50 mM Tris-HCl (pH 8,0), 50 mM KCl a 5 mM $MgCl_2$. Reakce byla zahájena přídavkem GTP o příslušné koncentraci a probíhala 2,5 minuty při laboratorní teplotě. Následně byla ukončena prostřednictvím inkubace reakční směsi při 100 °C. Směs byla centrifugována a supernatant byl aplikován na chromatografickou kolonu (LUNA 5 μC18 column, 15x4,6 cm, Phenomenex, USA). Pro analýzu byly použity dva pufry – A (100 mM KH_2PO_4, 4 mM tetrabutylamoniumhydrogen sulfát, pH 6,0) a B (75 % pufru A, 25 % methanolu). Analýza probíhala při průtoku 0,7 $ml.min^{-1}$ s gradientovou elucí – 0 min 40 % B/ 60 % A; 15 min 100 % B; 20 min 100 % B a 21 min 40 % B a 60 % A. Tato měření byla provedena s proteinem YddV s různými redoxními a koordinačními stavy hemového železa v jeho senzorové doméně – Fe(III), Fe(II), Fe(II)-CO, Fe(II)-O_2, Fe(III)-imidazol, Fe(III)-CN^- a také v případě, kdy hem v senzorové doméně zcela chyběl (byla použita mutantní forma proteinu His98Ala). Koordinační a redoxní stav hemového železa v senzorové doméně proteinu YddV byl vždy ověřen pomocí UV-VIS spektroskopie na základě charakteristické polohy Soretova pásu ve spektru jednotlivých forem (data nejsou ukázána). Každý experiment byl minimálně třikrát opakován. Byl sledován nárůst produktu enzymové reakce c-di GMP a pomocí standardů o daných koncentracích bylo vypočítáno množství c-di GMP vzniklé v průběhu enzymové reakce a počáteční rychlost enzymové reakce. Kinetické parametry reakce (K_m^{GTP}, V_{max}^{GTP}) byly získány nelineární regresí s využitím rovnice Michaelise a Mentenové v programu Origin. Výsledky jsou ukázány na obrázku 1 (strana 15) a v tabulce 1 (strana 16).



Obrázek 1: Vliv redoxního a koordinačního stavu hemového železa v senzorové doméně na kinetiku diguanylátcyklasové reakce proteinu YddV dle Michaelise a Mentenové

Reakční směs obsahovala 10 µM YddV, 10 – 1000 µM GTP, 50 mM Tris-HCl (pH 8,0), 50 mM KCl a 5 mM $MgCl_2$, reakce byla zahájena přídavkem GTP o příslušné koncentraci a probíhala 2,5 minuty při laboratorní teplotě. Byla ukončena inkubací reakční směsi při 100 °C. Směs byla centrifugována a supernatant byl aplikován na chromatografickou kolonu (LUNA 5 µC18 column, 15x4,6 cm, Phenomenex, USA). Pro analýzu byly použity dva pufry – A (100 mM KH_2PO_4, 4 mM tetrabutylamoniumhydrogen sulfát, pH 6,0) a B (75% pufru A, 25% methanol). Analýza probíhala při průtoku 0,7 $ml.min^{-1}$ s gradientovou elucí – 0 min 40 % B/ 60 % A; 15 min 100 % B; 20 min 100 % B a 21 min 40 % B a 60 % A. Měření byla provedena s proteinem YddV s různými redoxními a koordinačními stavy hemového železa v jeho senzorové doméně – Fe(III) (černé čtverce a křivka), Fe(III)-imidazol (zelené trojúhelníky a křivka), Fe(II)-O_2 (červené kruhy a křivka), Fe(III)-CN^- (modré trojúhelníky a křivka), Fe(II) (růžové trojúhelníky a křivka), Fe(II)-CO (žluté trojúhelníky a křivka), forma bez hemu – His98Ala (fialové kosočtverce a přímka)

Tabulka 1: Vliv redoxního a koordinačního stavu hemového železa v senzorové doméně na kinetické parametry diguanylátcyklasové reakce katalyzované proteinem YddV

Stav hemového železa v senzorové doméně YddV	K_m^{GTP} **(μM)**	V_{max}^{GTP} **(pmol.min^{-1}.μl^{-1})**	k_{cat} **(min^{-1})**	k_{cat}/K_m^{GTP} **(M^{-1}.s^{-1})**
Fe(III)	71,9 ± 15,7	11,1 ± 0,6	1,1	257
Fe(II)-O_2	49,2 ± 17,3	8,8 ± 0,5	0,9	299
Fe(II)-CO	44,8 ± 10,9	3,1 ± 0,2	0,3	126
Fe(II)	43,2 ± 14,2	3,4 ± 0,3	0,3	131
bez hemu (His98Ala)	reakce neprobíhá			
Fe(III)-CN^-	40,8 ± 7,1	6,2 ± 0,2	0,6	239
Fe(III)-imidazol	114,5 ± 22,4	10,8 ± 0,6	1,1	157

Ze získaných výsledků vyplývá, že stav hemového železa v senzorové doméně výrazným způsobem ovlivňuje katalytickou aktivitu proteinu YddV. To je v pozitivní korelaci s výsledky získanými při sledování vlivu stavu hemového železa na autofosforylační aktivitu *Af*GcHK (viz kapitola 3.2) se kterým protein YddV sdílí stejné prostorové uspořádání senzorové domény (globinová struktura). Stejně jako u *Af*GcHK, enzymově nejvíce aktivní byl enzym v případě, kdy hemové železo bylo ve formě Fe(III), Fe(II)-O_2 a Fe(III)-imidazol. Zajímavým zjištěním bylo rozdílné chování těchto dvou enzymů v případě, že šestým ligandem hemového železa byl kyanidový aniont. Zatímco u proteinu *Af*GcHK byla tímto ligandem autofosforylační aktivita ovlivněna minimálně, u enzymu YddV došlo k poklesu maximální rychlosti reakce a tím i snížení efektivity reakce (obrázek 1, strana 15, modrá křivka). Ani u proteinu *Af*GcHK, ani u YddV vlivem vazby kyanidového iontu k hemovému železu nedošlo ke změně hodnoty K_m a lze tak konstatovat, že tento ligand neovlivní afinitu enzymu k substrátu. Tato informace je také důležitá pro experimenty strukturní biologie, kdy je kyanidový iont často využíván pro stabilizaci krystalu hemových senzorových proteinů (viz kapitola 5.2).

K výraznému snížení enzymové aktivity YddV došlo po redukci hemového železa v senzorové doméně (FeII) (obrázek 1, strana 15, růžová křivka) a po vazbě oxidu uhelnatého k hemovému železu (FeII-CO) (obrázek 1, strana 15, žlutá křivka). Výrazné snížení enzymové aktivity vyvolané redukcí hemového železa v senzorové

doméně bylo pozorováno rovněž u proteinu *Af*GcHK. Vědeckému týmu Tarnawski a kol. [Tarnawski et al. *Acta Crystallogr. D Biol. Crystallogr.* 71, 2158 (2015)] se podařilo získat krystalovou strukturu senzorové domény proteinu YddV a to v jeho redukované a neredukované formě. Porovnáním těchto struktur dospěli k závěru, že redukce hemového železa nevyvolá výrazné strukturní změny v senzorové doméně. Nicméně pozorovali několik minoritních strukturních změn, kdy nejvýraznější změna byla pozorována v oblasti helixu F, který obsahuje His98, jenž koordinuje molekulu hemu. Další rozdíly byly nalezeny u helixů C a E a smyček, které propojují helixy C E a F G. Nám se podařilo získat krystalové struktury senzorové domény *Af*GcHK a to rovněž v neaktivním a aktivním stavu (kapitola 5.2). V našem případě však po ponoření krystalu *Af*GcHK v jeho aktivní formě do redukčního prostředí nedošlo k redukci všech iontů železa a vznikly tak dvě různé populace, které nám umožnily lépe vyhodnotit vzniklé diference. Tímto se nám podařilo zjistit, že po redukci hemového železa v senzorové doméně dochází k mnohem markantnějším strukturním změnám, než je uvedeno v publikaci [Tarnawski et al. *Acta Crystallogr. D Biol. Crystallogr.* 71, 2158 (2015)], viz kapitola 5.2. Kombinací strukturních a enzymových metod u dvou různých hemových senzorových proteinů s globinovou strukturou senzorové domény jsme dospěli k závěru, že redukce hemového železa vyvolá konformační změny senzorové domény, které vedou k výraznému snížení enzymové aktivity daných proteinů.

Zatímco vliv redukované formy hemového železa na enzymovou aktivitu YddV byl velmi podobný jako u proteinu *Af*GcHK, vazba oxidu uhelnatého k hemovému železu přinesla rozdílné výsledky. V obou případech (tedy *Af*GcHK a YddV) došlo k poklesu enzymové aktivity proteinu (u proteinu YddV byl tento pokles výraznější a byl srovnatelný s formou Fe(II)), nicméně výrazný rozdíl byl pozorován v naměřených hodnotách K_m. Hodnota K_m^{GTP} v případě YddV Fe(II-CO) je srovnatelná s hodnotami K_m^{GTP} naměřenými v případě, kdy je iont železa v těchto stavech Fe(II)-O_2, Fe(III)-CN^-, Fe(II). Hodnota K_m^{ATP} proteinu *Af*GcHK ve stavu Fe(II)-CO je však téměř dvacetkrát vyšší, než je tomu u ostatních redoxních a koordinačních stavů hemového železa. V případě proteinu *Af*GcHK je tedy afinita k substrátu reakce (ATP) výrazně snížena a strukturní změny vyvolané vazbou CO tak budou pro vazbu ATP nevýhodné. V případě YddV je afinita ke GTP podobná jako u jiných redoxních a koordinačních stavů, je ale výrazně snížena počáteční rychlost reakce. Pravděpodobně tak interakce oxidu uhelnatého s hemovým železem senzorové domény vyvolá různé strukturní změny u

těchto dvou proteinů a to i přesto, že mají podobné (homologní) globinové uspořádání této domény.

Bylo také testováno, jak se změní aktivita hemových senzorových proteinů v případě, kdy molekula hemu bude v senzorové doméně zcela chybět (byly připraveny mutantní formy proteinů, kdy nebyla umožněna koordinace hemu do struktury senzorové domény – His99Ala v případě *Af*GcHK a His98Ala v případě YddV). YddV s chybějícím hemem v senzorové doméně nevykazoval žádnou enzymovou aktivitu (obrázek 1, strana 15, fialová přímka). U proteinu *Af*GcHK byl pozorován vznik velmi malého množství produktu reakce, hodnota k_{cat} však byla téměř třikrát nižší než u *Af*GcHK v aktivní formě. Lze proto říci, že absence hemu v senzorové doméně vyvolá strukturní změny, které výrazně ovlivní enzymovou aktivitu hemových senzorových proteinů ve smyslu jejich inaktivace.

Na základě získaných výsledků studia enzymové aktivity dvou různých hemových senzorových proteinů, které sdílí podobnou strukturu senzorové domény lze konstatovat, že koordinační a ligační stav hemového železa v senzorové doméně hemových senzorových proteinů výrazně ovlivňuje jejich funkční doménu a tím i jejich aktivitu.

BLOK II této disertační práce je souhrnem poznatků věnujících se výzkumu sulfanu a jeho účinku na strukturní a funkční vlastnosti hemových senzorových proteinů. Sulfan byl do nedávna považován pouze za vysoce toxickou molekulu, byl však prokázán jeho pozitivní vliv na některé fyziologické procesy lidského organismu, jako například vazodilatace [Naik et al. *Am J Physiol Heart Circ Physiol* 311, H1437 (2016)]. Zajímavým zjištěním také bylo, že hem hemoglobinu a myoglobinu se sulfanem interaguje [Pietri et al. *Antioxid Redox Signal.* 15, 393 (2011)]. Jelikož pKa sulfanu je přibližně 6,9, ve vodných roztocích o neutrálním pH může docházet k vytvoření vazby mezi Fe(III) hemu a SH^- [Shimizu et al. *Curr Chem Biol* 7, 207 (2013)]. Pokud byl hemoglobin a myoglobin vystaven působení sulfanu a peroxidu vodíku, docházelo dokonce k inkorporaci atomu síry do porfyrinového kruhu a vzniku tzv. sulfhemu [Berzofsky et al. *J Biol Chem* 246, 3367 (1971)]. Tato schopnost interakce nás přivedla na myšlenku, zda u hemových senzorových proteinů bude také docházet k vazbě SH^- k hemu v jejich senzorové doméně a jestli bude tato vazba ovlivňovat jejich katalytickou funkci. K tomuto účelu jsme zvolili dva proteiny

s globinovou strukturou (jako je tomu u hemoglobinu a myoglobinu) – YddV a *Af*GcHK a jeden s PAS strukturou - *Ec*DOS.

V kapitole 4.1 BLOKU II jsou uvedeny výsledky vlivu sulfidu sodného na spektrální a katalytické vlastnosti proteinu *Ec*DOS s PAS strukturou jeho senzorové domény. Jak již bylo uvedeno dříve (strana 13), protein *Ec*DOS se nachází v bakterii *Escherichia coli*, kde na základě různých signálů z okolí katalyzuje přeměnu důležité signální molekuly c-di GMP na její lineární formu. Inkubací *Ec*DOS v jeho přirozené formě (WT) a stavu Fe(III) se sulfidem sodným došlo ke vzniku formy Fe(III)-SH^-, která byla po disociaci SH^- redukována na Fe(II). Jelikož experiment probíhal v aerobním prostředí došlo k vazbě kyslíku a následné autooxidaci na formu Fe(III)-OH^-. Tyto změny byly detekovány pomocí UV-VIS spektroskopie, konkrétně na základě změn Soretova pásu, který je charakteristický pro hemoproteiny. Fosfodiesterasová aktivita *Ec*DOS se po přídavku sulfidu sodného zvýšila, nicméně tento výsledek nebyl jednoznačný, právě kvůli možnosti, že ve směsi není pouze forma Fe(III)-SH^-, ale také Fe(II)-O_2, která může aktivitu ovlivňovat. Z tohoto důvodu byla hledána místa v senzorové doméně, jejichž mutace by problém s přítomností formy Fe(II)-O_2 vyřešila. Na základě publikací [Kurokawa et al. *J Biol Chem* 279, 20186 (2004); Park et al. *Biochemistry* 43, 2738 (2004)] jsme vybrali dvě takové aminokyseliny – Met95, který je axiálním ligandem hemu ve formě Fe(II) a Arg97, který stabilizuje vazbu molekuly kyslíku. Inkubací Met95Ala se sulfidem sodným došlo ke vzniku komplexu Fe(III)-SH^- bez přítomnosti více stavů iontů železa a byl také pozorován nárůst vzniku produktu enzymové reakce. Bylo tak prokázáno, že sulfid sodný stimuluje enzymovou aktivitu *Ec*DOS. V případě mutantní formy proteinu *Ec*DOS Arg97Ile došlo po přídavku sulfidu sodného ve spektru ke vzniku širokého píku v oblasti 650 nm. Píky v této oblasti spektra jsou charakteristické pro modifikované molekuly hemu jako například sulfhem nebo verdohem [Berzofsky et al. *J Biol Chem* 246, 3367 (1971); Andersson et al. *J Biol Chem* 259, 15340 (1984)]. Pomocí hmotnostní spektrometrie pak bylo prokázáno, že se jedná o derivát protoporfyrinu IX s inkorporovaným kyslíkem – verdohem, který vznikl pravděpodobně působením reaktivních forem kyslíku. Enzymová aktivita této formy proteinu však byla zvýšena jen málo, z čehož usuzujeme že verdohem, na rozdíl od formy Fe(III)-SH^-, nemá stimulační efekt na katalytickou funkci *Ec*DOS.

V kapitole 4.2 BLOKU II jsme zkoumali vliv sulfidu sodného na senzorové proteiny s globinovou strukturou, tedy analogickou k té jakou má myoglobin a

hemoglobin. Po inkubaci *Af*GcHK v jeho přirozené formě a stavu Fe(III)-OH^- se sulfidem sodným došlo k posunu Soretova pásu ze 412 nm na 424 nm. Na základě předchozích zkušeností byl pík o této vlnové délce přiřazen komplexu Fe(III)-SH^-. Tento komplex byl stabilní a nepřecházel na jiné formy, jako tomu bylo u *Ec*DOS, kdy docházelo ke vzniku komplexů Fe(II) a Fe(II)-O_2. Autofosforylační aktivita *Af*GcHK, jehož hemové železo v senzorové doméně bylo ve formě Fe(III)-SH^- se výrazně nelišila od formy Fe(III)-OH^-Z hlediska kinetických parametrů byla naměřena stejná hodnota V_{max} a vyšší hodnota K_m^{ATP}, došlo tedy ke snížení afinity enzymu k substrátu. V distální oblasti hemu proteinu *Af*GcHK se nachází dvě klíčové aminokyseliny. První z nich je Tyr45, který je vazebným místem pro kyslík. Druhou je Leu68, u kterého jsme předpokládali, že zabraňuje inkorporaci vody do aktivního centra senzorové domény, stejně jako je tomu u proteinu YddV v analogické pozici Leu65 [Stranava et al. *J Inorg Biochem* 140, 29 (2014)]. Mutace těchto aminokyselin nám umožnila prozkoumat, jakým způsobem změny ve specifických pozicích senzorové domény ovlivní koordinaci a strukturu hemu a enzymovou aktivitu *Af*GcHK. V případě mutantních forem Tyr45 nedošlo oproti přirozené formě k žádným změnám ve spektrech, a to ani po inkubaci se sulfidem sodným, rovněž nebyl pozorován vliv na enzymovou aktivitu. V případě mutantních forem Leu68Gly, Leu68Asn a Leu68Val došlo vlivem působení sulfidu sodného ke změně spektra v oblasti okolo 650 nm. V publikaci [Berzofsky et al. *J Biol Chem* 246, 3367 (1971)] je popsáno, že u myoglobinu dochází působením sulfanu k vytvoření sulfhemu. Díky určité strukturní podobnosti jsme se domnívali, že by tato situace mohla nastat i v případě *Af*GcHK. Hmotnostní spektrometrií však bylo prokázáno, že se jedná o verdohem. Pro tvorbu sulfhemových derivátů je zřejmě nutná přítomnost histidinu v distální části hemu, jehož orientace umožní vznik aktivního ternárního komplexu (Rios-Gonzales et al. *J Inorg Biochem* 133, 78 (2014)]. Enzymová aktivita nebyla ani u této mutantní formy proteinu vlivem přítomnosti sulfidu sodného ovlivněna.

Spektrální analýza vlivu sulfidu sodného na hemové senzorové proteiny byla provedena také s proteinem YddV, přesněji s jeho senzorovou doménou (YddV-hem). Ačkoliv sdílí *Af*GcHK a YddV stejnou strukturní homologii senzorové domény, jejich spektrální vlastnosti byly odlišné. V případě *Af*GcHK je iont železa v jeho oxidované formě hexakoordinovaný nízkospinový Fe(III)-OH^-, u YddV je Fe(III) pentakoordinový vysocespinový. Po přídavku sulfidu sodného k YddV-hem Fe(III) došlo k tvorbě Fe(II)-O_2. Po delším časovém úseku byla tato forma nahrazena Fe(II), kdy kyslíkový ligand

z původního Fe(II)-O_2 komplexu byl pravděpodobně převeden na superoxidový aniont nebo peroxid vodíku. Interakce YddV-hem a sulfidu sodného je tak odlišná od *Af*GcHK a *Ec*DOS. Byly také provedeny experimenty s mutantními formami Tyr43 a Leu65, u těchto však docházelo vlivem působení sulfidu sodného pouze k poklesu intenzity Soretova pásu, což ukazuje na probíhající degradaci molekuly hemu.

Z výsledků experimentů uvedených v BLOKU II (kapitoly 4.1, 4.2) této disertační práce vyplývá, že sulfid sodný ovlivňuje spektrální vlastnosti senzorových domén studovaných proteinů. Dva ze tří proteinů vykazují strukturní homologii senzorové domény, třetí protein má tuto strukturu odlišnou, i přes to byly nalezeny tři různé formy struktury a koordinace molekuly hemu těchto proteinů při inkubaci se sulfidem sodným. Byl také pozorován odlišný vliv na enzymovou aktivitu hemových senzorových proteinů. Zatímco u proteinu *Ec*DOS byla jeho fosfodiesterasová aktivita vlivem působení sulfidu sodného zvýšena, na autofosforylační aktivitu *Af*GcHK neměl sulfid sodný téměř žádný vliv. Tyto rozdíly mohou být zapříčiněny rozdílnými koordinačními stavy molekuly hemu – zatímco u proteinu *Af*GcHK vznikla pouze forma Fe(III)-SH^-, u *Ec*DOS byl pozorován výskyt Fe(III)-SH^- a Fe(II)-O_2. U mutantních forem *Ec*DOS, kde vznikal pouze Fe(III)-SH^- však také docházelo k nárůstu enzymové aktivity vlivem působení sulfanu, u homologních mutantních forem *Af*GcHK aktivita ovlivněna nebyla. Rozdíl v ovlivnění katalytických aktivit enzymů může být také zapříčiněn přítomností cysteinů na povrchu proteinu. Zatímco protein *Ec*DOS má na svém povrchu sedm thiolátových zbytků, po vystavení působení sulfidu sodného dokonce osm, *Af*GcHK nemá ve své struktuře jediný cystein. U proteinu *Ec*DOS bylo prokázáno, že nahrazením cysteinů za alaniny dojde k potlačení enzymové aktivity *Ec*DOS a pokud byly cysteiny mutovány jednotlivě, docházelo k poklesu enzymové aktivity [Takahashi et al. *J Inorg Biochem* 109, 66 (2012)]. Je tedy nutné přistupovat k tomu tématu komplexněji z hlediska celého proteinu, a ne pouze jeho senzorové domény, kde dochází k interakci hem-SH^-.

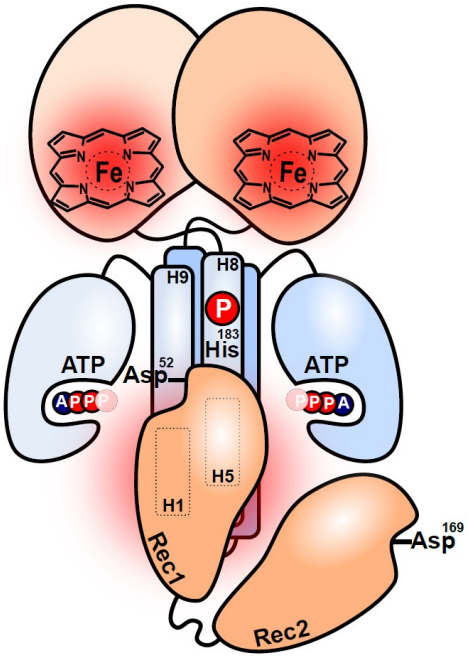
Publikace BLOKU III jsou věnované strukturně biologickým metodám studia *Af*GcHK. V publikacích BLOKU I (kapitola 3.2) a BLOKU II (kapitola 4.2), které se stejným proteinem také zabývají, jsou uvedeny výsledky enzymových studií a vlivu sulfidu sodného na spektrální a katalytické vlastnosti tohoto modelového proteinu. Výsledky uvedené v těchto kapitolách nám nastínily, jakým způsobem dochází k přenosu signálu ze senzorové na funkční doménu a jakým způsobem interaguje

protein *Af*GcHK se svým partnerem RR proteinem. Bylo však zapotřebí provést důkladnější strukturní analýzu těchto proteinů. Hemové senzorové proteiny pro své fungování potřebují, aby jejich struktura byla velmi flexibilní. Tato vlastnost je však obrovským problémem při studiu těchto proteinů pomocí konvenčních strukturních metod. V našem výzkumu jsme proto přistoupili k využití jiných metod, jako analytické ultracentrifugace, homologního modelování proteinové struktury a HD výměny spojené s hmotnostní spektrometrií.

V kapitole 5.1 byla nejprve provedena primární biofyzikální charakteristika *Af*GcHK a RR proteinu na základě sedimentačních koeficientů získaných pomocí analytické centrifugace. O většině doposud prozkoumaných histidinkinasach je známo, že za fyziologických podmínek vytváří homodimery. V případě *Af*GcHK tomuto tvrzení nasvědčovaly i výsledky získané pomocí gelové chromatografie. Nicméně bylo nutné toto potvrdit. Molekulová hmotnost *Af*GcHK vypočtená ze zastoupení aminokyselin je přibližně 43 kDa, avšak získaný sedimentační koeficient ($s_{20,w}$ = 4,74 S) odpovídá molekulové hmotnosti 82 kDa. Bylo tak prokázáno, že se *Af*GcHK v roztoku vyskytuje ve formě dimeru a to i případě nejnižší možné detekovatelné koncentrace proteinu (100 nM). Sedimentační koeficient RR proteinu ($s_{20,w}$ = 2,34 S) a z něj odvozená molekulová hmotnost 27 kDa odhalily, že RR protein se vyskytuje v roztoku ve formě monomeru. Nicméně na rozdíl od *Af*GcHK, který byl za všech měřených podmínek detekován jako dimer, 5 % RR proteinu nebylo v roztoku ve formě monomeru, ale jako dimer. Pokud byly oba proteiny v roztoku přítomny současně, došlo k vytvoření komplexu dimerní *Af*GcHK a monomerní RR protein. Komplex *Af*GcHK-RR byl transientní, s vysokou disociační konstantou. Pokud byla koncentrace RR proteinu zvyšována, vytvořil se komplex 2:2, jehož hodnota K_d byla o řád vyšší, než tomu bylo u komplexu 2:1. Podle známých struktur senzorových proteinů (*Gs*GCS bakterie *Geobacter sulfurreducens* pro senzorovou doménu [Pesce et al. *J Mol Biol* 386, 246 (2009)] a HK853 bakterie *Thermotoga maritima* pro funkční doménu [Casino et al. *Cell* 139, 325 (2009)]) byl vytvořen homologní model, který byl porovnán se strukturními daty získanými pomocí HD výměny. Experimenty HD výměny byly provedeny s plno délkovým *Af*GcHK v jeho enzymově nejaktivnější formě Fe(III)-OH^- (což bylo prokázáno pomocí získaných hodnot k_{cat} (1,1 min^{-1}) a k_{cat}/K_m^{ATP} (1000 $M^{-1}.s^{-1}$) v rámci enzymové studie viz kapitola 3.2). Globinová doména je tvořena sedmi helixy (H1-H7) a sedmi smyčkami (L1-L7) a s funkční doménou je spojena prostřednictvím smyčky L8, která je zároveň nejflexibilnější částí celého proteinu. Funkční doména obsahuje pět helixů (H8-

H12), pět β listů (B1-B5) a deset smyček (L9-L18). Experimenty HD výměny prokázaly, že oproti kinasové doméně je globinová doména *Af*GcHK mnohem rigidnější, zejména pak část helixu H4 a celé helixy H6 a H7, které pravděpodobně vytváří hydrofobní jádro globinové domény. Naproti tomu jediné flexibilní části senzorové domény tvoří krátký helix H3 a smyčky L3 a L4, které jsou součástí distální strany hemu.

Rovněž bylo provedeno homologní modelování (s využitím vyřešené struktury RR proteinu Aer-sal bakterie *Aeromonas salmonicida* [PDB code 3MF4]) a experimenty HD výměny pro RR protein. RR protein je tvořen dvěma doménami Rec1 (obsahující fosforylační místo Asp52) a Rec2 (obsahující fosforylační místo Asp169), jeho struktura je vysoce flexibilní a obsahuje devět α helixů, deset β listů a dvacet smyček. Nejzajímavějším cílem celé této publikace však bylo prostřednictvím metody HD výměny prozkoumat interakci *Af*GcHK a RR proteinu. Z hlediska *Af*GcHK docházelo k největší změně deuterace vlivem přítomnosti RR proteinu na helixech H8 a H9, které jsou zároveň i místem odpovědným za dimerizace proteinu. V menší míře dochází k interakci s RR proteinem také na helixu H11, tedy vazebné oblasti pro ATP. Tato data pozitivně korelují s výsledky získanými kinetickou studií, kdy docházelo k poklesu autofosforylační aktivity *Af*GcHK právě po interakci s RR proteinem a bylo tak předpokládáno, že se RR protein váže blízko této oblasti (kapitola 3.2). Z hlediska RR proteinu je interakce s *Af*GcHK zprostředkována prostřednictvím helixů H1 a H5, které se nacházejí v doméně Rec1. Zajímavým zjištěním bylo, že nebyly pozorovány výrazné změny v deuteraci domény Rec2, ačkoliv je doméně Rec1 strukturně velmi podobná. Zdá se, že interakce probíhá pouze mezi *Af*GcHK a Rec1 doménou RR proteinu. Toto zjištění je ve shodě s pozorováním, že nejprve dochází k fosforylaci Asp52 (doména Rec1) a teprve poté je fosforylován Asp169 (doména Rec2) [Kitanishi et al. *J Biol Chem* 286, 35522 (2011)]. Na základě všech získaných dat byl popsán interproteinový přenos signálu mezi *Af*GcHK a RR proteinem (přenos signálu mezi *Af*GcHK a RR proteinem je schematicky znázorněn na obrázku 2, strana 24). K přenosu fosfátu z His183 *Af*GcHK na Asp52 RR proteinu dochází v případě, kdy helix H9 kinasové domény *Af*GcHK interaguje s H1 helixem RR proteinu a helix H8 *Af*GcHK interaguje s helixem H5 RR proteinu. Nebyla pozorována žádná interakce mezi senzorovou doménou *Af*GcHK a RR proteinem.



Obrázek 2: Schematický model znázorňující interakci AfGcHK a RR proteinu
Dvě podjednotky dimeru AfGcHK (funkční domény jsou znázorněny odstíny modré barvy) a monomer RR proteinu (oranžová barva) spolu interagují prostřednictvím helixů H8 a H9 proteinu AfGcHK a helixů H1 a H5 RR proteinu. Nejprve dojde k fosforylaci Rec1 (konkrétně Asp52), poté je fosforylována Rec2 (konkrétně Asp169). Do interakce není zapojena senzorová doména AfGcHK (červená barva).

Kapitola 5.2 BLOKU III je věnována mechanismu intraproteinového přenosu signálu. V této části práce se nám podařilo získat krystal globinové domény *Af*GcHK, a to jak v jeho aktivní formě (Fe(III)-CN^-), tak také v neaktivní formě (Fe(II)). Porovnáním získaných struktur těchto krystalů bylo možné odvodit změny, ke kterým dochází při přeměně koordinačních stavů hemového železa. Pro určení diferencí mezi aktivním a neaktivním stavem senzorové domény a jeho vlivu na strukturu celého proteinu, byly provedeny experimenty HD výměny, a to rovněž v aktivním a neaktivním stavu.

Asymetrická jednotka krystalu globinové domény *Af*GcHK ve stavu Fe(III)-CN^- byla složena ze čtyř dimerů, které byly tvořeny osmi proteinovými řetězci (AB, CD, EF a GH). Každý monomer sestával ze sedmi helixů a sedmi smyček (byly tak potvrzeny údaje získané pomocí homologního modelování, viz kapitola 5.1). Tento krystal byl následně ponořen do roztoku se silnými redukčními vlastnostmi obsahující dithioničitan sodný. Tato redukce hemového železa vyvolala určité strukturní změny. Překvapivé bylo, že nedošlo k redukci veškerých iontů železa a vznikly tak dvě varianty (dvě populace) – varianta A, která byla konzistentní s formou, kdy bylo hemové železo ve

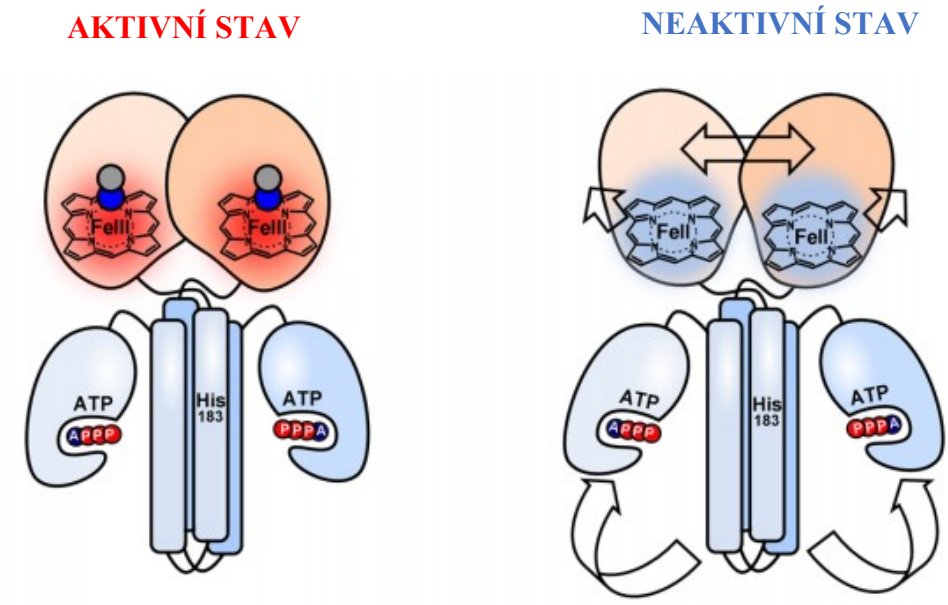
stavu Fe(III)-CN^- a varianta B, která odpovídá formě Fe(II). Toto pro nás bylo obrovskou výhodou, jelikož došlo k vytvoření formy, ve které bylo možné přímo pozorovat strukturní změny. Na rozdíl od výsledků publikovaných v [Tarnawski et al. *Acta Crystallogr D Biol Crystallogr* 71, 2158 (2015)], kde byly vytvořeny dva rozdílné krystaly v plně redukované a plně oxidované formě hemového železa globinové domény proteinu YddV a nebyly mezi nimi pozorovány žádné významné strukturní změny. V našem případě došlo k nejvýraznějším změnám v řetězci G (a to v oblasti helixů H2-H7) a v menší míře také řetězci H (oblast helixů H1 a H2).

Z důvodu obrovské flexibility plno délkové formy *Af*GcHK se nám bohužel nepodařilo připravit její krystal a studovat tak strukturní diference rovněž na funkční doméně. Namísto toho jsme, stejně jako v případě studia interproteinového přenosu signálu, použili metody HD výměny. Všechny aktivní formy proteinu *Af*GcHK, jmenovitě Fe(III)-OH^-, Fe(III)-CN^- a Fe(II)-O_2, viz kapitola 3.2, vykazovaly velmi podobné dynamické vlastnosti a přístupnost rozpouštědlu a to na rozdíl od neaktivní formy Fe(II). K nejvýraznějším změnám mezi aktivní a neaktivní formou došlo za a) v blízkosti molekuly hemu v senzorové doméně, za b) v oblasti dimerizace globinové domény (helixy H6 a H7) a za c) v helixech H11 a H9 kinasové domény, kde po redukci docházelo k rychlejší výměně vodíku za deuterium. Tento jev může být způsoben zvýšením pohyblivosti této oblasti, což je v přímé korelaci s hypotézou, že v neaktivním stavu dochází ke zvýšení vzdálenosti mezi těmito helixy.

V této kapitole jsme také prokázali, že pokud oddělíme funkční doménu od senzorové, nedochází k fosforylaci His183 a HD profil této izolované funkční domény je shodný s profilem funkční domény, kdy hem v senzorové doméně je v neaktivním Fe(II) stavu plno délkového *Af*GcHK. Srovnáním výsledků měření kinetické studie (kapitola 3.2) a studia HD výměny můžeme jednoznačně konstatovat, že všechny aktivní formy *Af*GcHK mají stejné strukturní uspořádání, které je však odlišné od toho, jaké mají stejné všechny enzymově neaktivní formy.

Pro vysvětlení, jak je autofosforylační aktivita funkční domény ovlivňována senzorovou doménou existují dvě odlišné teorie. První teorie, přímá, předpokládá, že autofosforylační místo je při určitých koordinačních stavech hemového železa senzorovou doménou stéricky blokováno [Cunnigham et al. *Mol Microbiol.* 71, 659 (2009)]. Druhá teorie, nepřímá, tuto přímou blokaci vylučuje. Data, která se nám podařilo získat v případě *Af*GcHK silně podporují druhý mechanismus a tedy nepředpokládáme přímou interakci senzorové a funkční domény. Intraproteinový přenos

signálu u kyslíkového senzoru *Af*GcHK tedy probíhá následujícím způsobem. Po vazbě kyslíku k iontu železa v koordinačním stavu Fe(II) v senzorové doméně dojde ke změnám v okolí molekuly hemu a signál je následně ze senzorové na funkční doménu přenesen skrz helixy H6 a H7 tvořící dimerizační rozhraní senzorové domény a helixy H8 a H9 tvořící dimerizační rozhraní funkční domény. Signál se pak šíří funkční doménou, kdy dojde k reorientaci helixů H11 a H9, což umožní vazbu ATP a následnou fosforylaci His183 (schematicky je intramolekulární přenos signálu zobrazen na obrázku 3, strana 26).



Obrázek 3: Schematické zobrazení intramolekulárního přenosu signálu proteinu AfGcHK

Redukce hemového železa (neaktivní stav, okolí molekuly hemu je znázorněno modře) vyvolá konformační změny v senzorové doméně (vyznačeny oranžovou barvou), zároveň dochází k rozšíření a rozdělení dimerizačního povrchu podjednotek senzorové domény. Signál se přes oblast spojující funkční a senzorovou doménu (linker) přenáší na funkční doménu (znázorněna modře), což vyústí v oddálení oblasti vázající ATP od His183, čímž je znesnadněna autofosforylace AfGcHK.

V kapitolách 5.1 a 5.2 BLOKU III předkládané disertační práce tak byl objasněn mechanismus interproteinového (*Af*GcHK a RR protein – viz obrázek 2, strana 24) a intraproteinového (senzorová a funkční doména *Af*GcHK – viz obrázek 3, strana 26) přenosu signálu.

3. Publikace BLOKU I

3.1 Gaseous O_2, NO, and CO in signal transduction: structure and function relationships of heme-based gas sensors and heme-redox sensors

Shimizu T., Huang D., Yan F., Stranava M., Bartosova M., **Fojtíková V**., Martínková M. *Chem. Rev.* (2015) 115, 6491 (**IF_{2016} 47,9**)

Podíl předkladatelky na této práci: 10 % (literární rešerše na téma kinetických studií hemových senzorových proteinů)

potvrzeno korespondujícím autorem, doc. RNDr. Markéta Martínková, Ph.D.

CHEMICAL REVIEWS

Review

pubs.acs.org/CR

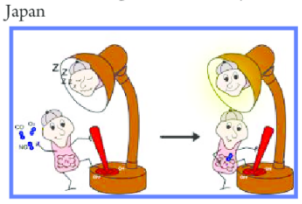
Gaseous O_2, NO, and CO in Signal Transduction: Structure and Function Relationships of Heme-Based Gas Sensors and Heme-Redox Sensors

Toru Shimizu,*[,†,‡,§] Dongyang Huang,[†] Fang Yan,[†] Martin Stranava,[‡] Martina Bartosova,[‡] Veronika Fojtíková,[‡] and Markéta Martínková*[,‡]

[†]Department of Cell Biology and Genetics and Key Laboratory of Molecular Biology in High Cancer Incidence Coastal Chaoshan Area of Guangdong Higher Education Institutes, Shantou University Medical College, Shantou, Guangdong 515041, China

[‡]Department of Biochemistry, Faculty of Science, Charles University in Prague, Prague 2 128 43, Czech Republic

[§]Research Center for Compact Chemical System, National Institute of Advanced Industrial Science and Technology (AIST), Sendai 983-8551, Japan



CONTENTS

1. Introduction 6492
2. Heme-Based O_2 Sensors 6492
2.1. Heme-Bound PAS Domain-Containing O_2 Sensors 6492
2.1.1. FixL 6493
2.1.2. *Ec*DOS (or *Ec*DosP) 6500
2.1.3. *Ax*PDEA1 6503
2.1.4. Aer2 6504
2.1.5. Gyc-88E 6504
2.1.6. ThkA 6504
2.2. Heme-Bound GAF Domain-Containing O_2 Sensors 6504
2.2.1. DosS (or DevS) 6505
2.2.2. DosT 6505
2.3. Heme-Bound Globin Domain-Containing O_2 Sensors: Globin-Coupled O_2 Sensor (GCS) 6506
2.3.1. HemAT 6506
2.3.2. YddV (or *Ec*DosC) 6506
2.3.3. *Af*GcHK 6507
2.3.4. HemDGC 6507
2.3.5. *Av*GReg 6507
2.3.6. *Bpe*GReg 6508
2.3.7. *Gs*GCS 6508
2.3.8. HemAC-*Lm* 6508
2.4. AppA: Heme Sensor Domain with a Central SCHIC Fold 6508
3. Heme-Based NO Sensors 6509
3.1. The Eukaryotic NO Sensor sGC 6509
3.1.1. Protein Structure 6509
3.1.2. Coordination Structures of the Heme Fe(II) Complex 6510
3.1.3. Catalytic Enhancement of sGC by Chemical Simulators and Activators 6510
3.2. Crystal Structures of the Heme-Bound, NO-Sensing H-NOX Domain of Bacterial NO Sensors: Stand-Alone Type 6511
3.2.1. *Tt*H-NOX 6511
3.2.2. *Ns*H-NOX 6511
3.2.3. *So*H-NOX 6512
3.3. Functions of Bacterial NO Sensors 6512
3.3.1. *So*H-NOX: Stand-Alone Type 6512
3.3.2. *Sw*H-NOX: Stand-Alone Type 6512
3.3.3. H-NOX from *Pseudoalteromonas atlantica*: Stand-Alone Type 6513
3.3.4. H-NOX from *Vibrio fischeri*: Stand-Alone Type 6513
3.3.5. H-NOX in *Vibrio harveyi*: Stand-Alone Type 6513
3.3.6. DNR: Fused Type 6513
3.3.7. YybT: Fused Type 6513
3.4. Insect E75: Fused Type 6513
3.5. Human Cystathionine β-Synthase: Fused Type 6514
4. Heme-Based CO Sensors 6514
4.1. CooA 6515
4.2. RcoM 6516
4.3. Cystathionine β-Synthase 6516
4.4. BK (Slo1) and Kv1.4 K^+ Channels, Nav1.5 Na^+ Channel, and Connexin Hemichannels 6516
4.5. NPAS2, CLOCK, Rev-erbα, Rev-erbβ, E75, Per1, and Per2 6516
5. Heme Redox Sensors with *c*-Type and Non-*c*-Type Heme Iron Complexes 6517
5.1. MA4561 6517
5.2. GSU582 and GSU935 6517
5.3. DcrA 6518
5.4. NtrY/NtrX 6518
5.5. OxdB 6518
5.6. Insect E75 6518
5.7. *Ec*DOS 6518
6. Heme-Based H_2S Sensors 6519
7. Common Characteristics of Heme-Based Gas Sensors 6519

Received: January 11, 2015
Published: May 29, 2015

ACS Publications © 2015 American Chemical Society

DOI: 10.1021/acs.chemrev.5b00018
Chem. Rev. 2015, 115, 6491−6533

8. Concerns That Need To Be Addressed 6519
9. Perspectives 6519
Author Information 6520
Corresponding Authors 6520
Notes 6520
Biographies 6520
Acknowledgments 6521
Abbreviations 6521
References 6522

1. INTRODUCTION

The heme iron complex is one of the most important cofactors in biological systems (Figure 1). The major functions of the heme iron complex are to serve as the O_2 binding site for hemoglobin (O_2 carrier protein), myoglobin (O_2 storage protein), and cytochrome P450 (O_2 activating enzyme); the peroxide activation site for peroxidase; and the electron transfer site for cytochromes.[1−8] The heme iron complex in well-known heme proteins acts as the functional active center by virtue of its binding to an O_2 molecule forming a heme iron−O_2 complex, which carries the O_2 molecule to peripheral tissues as hemoglobin, stores the O_2 molecule in muscle as myoglobin, and helps activate the O_2 molecule by cleaving the O−O bond in cytochrome P450 monooxygenase. Importantly, the O_2 molecule binds only to heme Fe(II) complexes and not to heme Fe(III) complexes. For cytochromes, electrons are transferred to/from the partner protein via the heme iron complex, whereas for peroxidases, the active heme iron species required for function, compound I and compound II, are formed by hydrogen peroxide, reinforcing the idea that the heme iron complex is the important active center for these heme proteins.[6]

The heme iron complex also functions as the binding site for toxic gaseous molecules, such as NO and CO. The binding of these non-O_2 gaseous molecules to the heme iron complex regulates various important physiological and pathological functions associated with O_2 binding, such as mitochondrial respiration, primarily inhibiting these functions.[9−22]

The heme iron complex of hemoglobin and myoglobin also functions to eliminate the toxicity of NO[23,24] and generate NO from nitrate and nitrite anions.[25−27] In contrast to O_2 and CO, which bind exclusively to the heme Fe(II) complex, the NO molecule binds to both the heme Fe(II) complex and the heme Fe(III) complex. Intriguingly, peroxynitrite, the reactive nitrogen species formed by NO and hydrogen peroxide under various pathological conditions, has various functional impacts on NO.[28,29] In addition to interacting with the heme iron complex, NO binds to cysteine thiolate and forms −SNO on the protein surface, thereby regulating numerous important functions;[30−32] it also binds to nonheme iron complexes.[33]

In contrast to NO and O_2 (as well as reactive oxygen species such as superoxide anion, hydrogen peroxide, and hydroxyl radical), CO is stable and inert, and thus binds exclusively to metal complexes, including heme iron and nonheme iron complexes, to inhibit their function, but it does not interact with nonmetal cofactors or amino acid residues on the protein surface.[13,16−19]

Noteworthy among the important novel and emergent physiological functions of the heme iron complex is its role as a gas-sensing site (Tables 1−3). Most heme-based gas sensors are composed of an N-terminal heme iron-bound gas-sensing domain and a C-terminal functional domain (Figure 2).[7,9,11,34−55] The ubiquitous and physiologically important gaseous molecule, O_2, plays an additional role as the signaling molecule for heme-based oxygen sensors. The notorious toxic gaseous molecules, NO and CO, have also come to be known as signaling molecules that regulate numerous important physiological functions. For heme-based gas sensors, a gaseous molecule, the first signal, associates with (or dissociates from) the heme iron complex in the N-terminal sensing domain, causing changes in the heme iron coordination structure that lead to concomitant changes in the surrounding protein. These changes in the protein structure within the sensing domain constitute the second signal, which is transduced to the functional domain, resulting in switching on/off various crucial physiological functions, such as catalytic activity (e.g., phosphodiesterase [PDE], diguanylate cyclase [DGC]), methyl-accepting chemotaxis, or transcription, which are mediated by the C-terminal functional domain (Figure 2). Many bacterial NO sensors are stand-alone heme-based NO sensors, in that the isolated NO sensing domain interacts with the isolated/separated functional domain and switches its functions on and off (Table 2).[56] In some gas sensors, the heme-bound gas-sensing domain is located in the central region between the N- and C-terminal domains.[57] Numerous heme-based gas sensors have been identified in archaea and bacteria, whereas among eukaryotes, the only heme-based NO sensor that has been reported is soluble guanylate cyclase (sGC).[36] The mechanisms by which the heme iron complex in heme-based gas sensors discriminates among these gaseous ligand molecules have been discussed.[47,48,55,58,59] Notably, the structure of the iron−sulfur cluster in gas-sensing nonheme iron proteins such FNR (fumarate and nitrate reduction regulator), which senses both O_2 and NO, is strikingly changed after these gaseous molecules bind to the cluster. Thus, the gas-sensing mechanisms of heme-based gas sensors, in which the heme iron complex structure is essentially retained after sensing the gaseous molecules, are substantially different from those of nonheme iron proteins.[33]

The emergent, novel role of gas sensing in various important physiological functions in bacteria and eukaryotes, as well as their involvement in disease processes, provides a compelling and timely rationale for presenting a summary of structure and function relationships of heme-based gas sensors. In this Review, we comprehensively summarize current knowledge of heme-based gas (O_2, NO, and CO) sensors and heme-redox sensors and delineate the structure/function relationships and common characteristics of the bacterial, archaeal, and mammalian sensors. We try to cite mainly new papers published after the year 2000 rather than citing numerous classical papers (even well-known ones). In this way, we are able to present many of the most recent papers.

2. HEME-BASED O_2 SENSORS

The O_2 molecule is the most important gaseous molecule for metabolism and the mitochondrial energy transfer system, playing a conserved role in nearly all organisms. Notably, additional important signaling roles of O_2 in bacterial and archaeal physiology are also emerging. Among all the gas sensors, the heme-based oxygen sensors of bacterial or archaeal origin are the best characterized (Table 1).[34,35,38−46,50,53−55]

2.1. Heme-Bound PAS Domain-Containing O_2 Sensors

The PAS (Per, ARNT, and Sim proteins) domain is characterized by its three-dimensional structure in which several parallel β-sheets are aligned and an α-helix crosses

DOI: 10.1021/acs.chemrev.5b00018
Chem. Rev. 2015, 115, 6491−6533

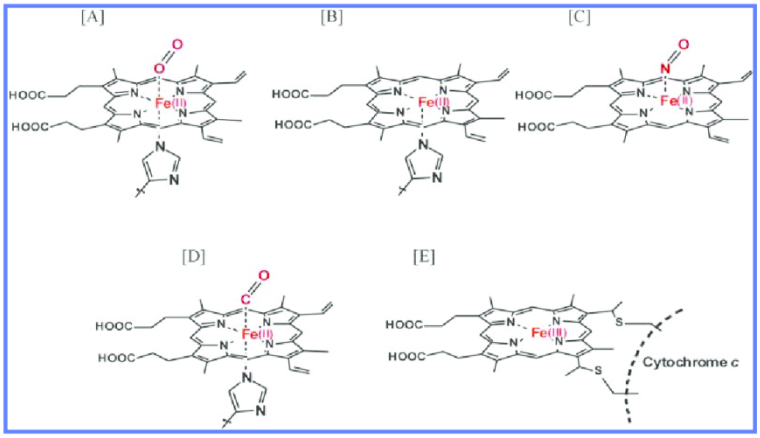


Figure 1. Heme iron/protoporphyrin IX iron complex. In hemoglobin, myoglobin, and many heme-based oxygen sensors, the heme Fe(II) complex is ionically bound to the imidazole of a histidine residue on the proximal side trans to the O_2-binding distal side [A].[1,6,8,50,51,81−83,85,190] The active form of FixL, a heme-based oxygen sensor containing a heme-bound PAS domain, is the O_2-free 5-coordinated Fe(II) complex [B],[41−43,66] whereas that of *Af*GcHK, a heme-based oxygen sensor containing a heme-bound globin domain, is the O_2-bound 6-coordinated Fe(II) complex [A].[73] For the heme-based NO sensor guanylate cyclase, the 5-coordinated Fe(II)-NO complex is the catalytically active form [C].[9,36] For the heme-based CO sensor CooA, the 6-coodinated Fe(II)-CO complex is the transcriptionally active form [D].[34,35,52,296] Cytochrome *c* contains a *c*-type heme in which the porphyrin ring is covalently bound to a cysteine residue of the protein [E].

from one end to the other, forming a shape similar to that of a fruit basket (Figure 3A).[49,51] The PAS domain often serves as the signaling site for protein−protein interactions as well as a signaling-accepting site for inter- and intramolecular signal transduction.[49,60−65] The PAS domain in heme-based O_2 sensors functions as the O_2 sensing/binding site, which is important for intramolecular signal transduction (Table 1).[35,41−43,50,53,55,60]

2.1.1. FixL. FixL is a heme protein kinase involved in nitrogen fixation. The discovery of FixL from *Rhizobium meliloti* (or *Sinorhizobium meliloti*), the first identified heme-based oxygen sensor, substantially changed our view of the role of the heme iron complex, showing that it can be an oxygen-sensing site for regulating histidine kinase function.[41−43,66] The structure−function relationships of FixLs from *R. meliloti* (*Rm*FixL), *S. meliloti* (*Sm*FixL), and *Bradyrhizobium japonicum* (*Bj*FixL) have been well characterized, partly because FixLs are suitable for overexpressing in *Escherichia coli* and can be readily purified as stable proteins.

2.1.1.1. Two-Component Signal Transduction Systems. FixL is an example of a two-component signal transduction system in which autophosphorylation at a histidine residue in the functional domain within the same FixL molecule is triggered by input from the external first signal and the phosphorylated group is then transferred to an aspartate residue in the response regulator (Figure 4).[67,68] Once this aspartate residue is phosphorylated, the output signal is manifested and transcription is switched on, resulting in enhanced nitrogen fixation in the plant root bacteria.[42,43,66] In its heme Fe(II)−O_2 complex form, FixL is inactive. Dissociation of the O_2 molecule from the heme Fe(II) complex switches on phosphorylation of the histidine residue. This oxygen-sensing system, in which O_2 dissociation acts as an "on" switch, is in contrast with other heme-based oxygen sensors such as *Ec*DOS and globin-coupled oxygen sensors, in which O_2 binding to the heme Fe(II) complex switches on their catalytic functions.[38,39,42,43,50] It has been proposed that the sensory/signaling module of the FixL network has been conserved such that its transcriptional output is adapted to the unique physiology of *Caulobacter crescentus* and nitrogen-fixing rhizobia.[69]

Note that there are additional types of two-component bacterial signal transduction systems (described in detail below), including (a) other heme-based oxygen sensors, such as DosS (DevS)/DosR and DosT/DosR from *Mycobacterium tuberculosis*,[70−72] and *Af*GcHK from *Anaeromyxobacter* sp. Fw109-5;[73] (b) stand-alone heme-based NO sensors, such as Hnox from *Shewanella oneidensis* (*So*H-NOX), *Vibrio cholera* (*Vc*H-NOX), *Vibrio harveyi* (*Vh*H-NOX), and *Vibrio fischeri* (*Vf*H-NOX);[56] and (c) the heme-redox sensor NtrY/NtrX from *Brucella abortus*.[74]

2.1.1.2. Catalytic Regulation. FixL with a heme Fe(II)−O_2 complex is inactive, whereas that with the O_2-free heme Fe(II) complex is active. FixL with a heme Fe(II)−CO or heme Fe(II)−NO complex is also inactive. In the absence of FixJ, a cognate response regulator, auto histidine kinase (autophosphorylation) activity of FixL is very low, but it becomes high in the presence of this partner protein.[42,43,75−78] However, this partner-protein-induced catalytic enhancement is not as obvious for the two-component signal transduction system *Af*GcHK, a globin-coupled, heme-based oxygen-sensing histidine kinase from soil bacteria.[73] Notably, turnover numbers for FixL, as well as those for other heme-based oxygen sensors and signaling enzymes, are relatively low as compared to those for metabolic enzymes. This is because, unlike the case for metabolic enzymes, the natural concentrations of their substrates (e.g., proteins to be phosphorylated) are usually comparable to the concentrations of the enzyme.[42,43] For signaling enzymes, the effective concentration of product

DOI: 10.1021/acs.chemrev.5b00018
Chem. Rev. 2015, 115, 6491−6533

depends on downstream signal transduction steps; thus, a vast excess of substrate is often unnecessary.[42,43]

A study of the role of FixL−FixJ complexation in catalytic regulation[78] showed that *Sm*FixL−*Sm*FixJ complexation precedes phosphorylation for a two-component regulatory system. An investigation of the effect of O_2 on formation of the *Rm*FixL−*Rm*FixJ complex by fluorescence polarization[77] further found that O_2 blocks the reaction of the FixL−FixJ complex with ATP, but does not influence binding of FixJ or ATP to FixL. These results suggest mechanistic roles for the signal and regulatory partner in this signal transduction system. The novel concept, termed "memory of oxygen binding", was introduced to explain the O_2 dose response of FixL.[79] A crucial role for the autophosphorylation domain of FixL in regulating coupling between O_2 binding and kinase activity has been suggested.[76] It has also been suggested that α4 and α5 helices not only serve as a dimerization interface, but are also involved in transferring the postphosphorylation/dimerization signal that unveils the DNA-binding activity of the C-terminal domain. It has been found that ADP reduces the O_2-binding affinity of FixL, suggesting the possibility of reciprocal enhancement of the kinase reaction.[80]

Table 1. Functions of Heme-Based O_2 Sensors[a]

	functions	refs
Heme-Bound PAS Domain		
FixL	HK, TCS with FixJ	66, 84, 107
*Ec*DOS (or *Ec*DosP)	PDE	117, 119, 121
*Ax*PDEA1	PDE	131
Aer2	MCP	165, 167
Gyc-88E	DGC	168
ThkA	HK, TCS with TrrA	169, 170
Heme-Bound GAF Domain		
DosS (or DevS)	HK, TCS with DosR	70−72, 172, 176
DosT	HK, TCS with DosR	71, 72, 174
Heme-Bound Globin Domain: GCS		
HemAT	MCP	188, 189, 192, 195
YddV (or *Ec*DosC)	DGC	115, 116
*Af*GcHK	HK, TCS with RR	73
HemDGC	DGC	200
*Av*GReg	putative DGC	201
*Bpe*GReg	DGC	202
*Gs*GCS	unknown	203
HemAC-*Lm*	adenylate cyclase	132, 133
Heme-Bound SCHIC Fold at the Central Region		
AppA	transcriptional regulation with PpsR	57

[a]HK, histidine kinase; TCS, two-component system; PDE, phosphodiesterase; MCP, methyl-accepting chemotaxis; DGC, diguanylate cyclase; SCHIC, sensor containing heme instead of cobalamin.

2.1.1.3. Ligand-Induced Global Protein Structural Changes Revealed by X-ray Crystal Structure and EXAFS (Extended X-ray Absorption Fine Structure) Studies. Similar to other heme-based oxygen sensors, the heme-binding domain is separated from the functional domain in FixL. The molecular mechanism underlying transduction of an intramolecular signal from the heme-binding domain to the functional domain is intriguing and thus worthy of exploration. Although only the crystal structure of the isolated heme-bound domain has been determined, efforts to resolve the crystal structure of the entire protein have not yet succeeded. Nevertheless, the crystal structure of the isolated heme-bound domain of FixL provides insight into the molecular mechanism of the oxygen-sensing system.[47,81−84]

Table 2. Functions of Heme-Based NO Sensors[a]

	functions	refs
Mammalian		
sGC	guanylate cyclase	9, 36, 232, 233
Insect		
E75	transcriptional regulator	227, 375, 377
Bacterial: Stand-Alone Type		
*Tt*H-NOX, TT-SONO	putative MCP: oxygen sensor?	245, 246
CB-SONO	putative MCP: oxygen sensor?	245
*Ns*H-NOX	putative guanylate cyclase	243, 244, 263, 265
*So*H-NOX	MCS: HnoX/HnoK/HnoD/PDE: biofilm	242, 266−268, 272
	MCS: HnoX/HnoK/HnoC: transcription	
*Vc*H-NOX	MCS: HnoX/HnoK/HnoD/PDE: biofilm	272, 273
	MCS: HnoX/HnoK/HnoC: transcription	
*Sw*H-NOX	HnoX/DGC/PDE: biofilm	274, 275
*Pa*H-NOX	TCS: H-NOX/HarK/HarR/PDE: biofilm	277
*Vf*H-NOX	TCS: HnoX/HnoK/Hpt?/Hur? heme uptake	278
*Vh*H-NOX	TCS: HnoX/HqaK/LuxU: quorum sensing	279, 280
Bacterial: Fused Type		
DNR	transcriptional regulator	282−284
*Bs*YybT	PDE	285
*Gf*YybT	PDE	285, 286

[a]*Bs*YybT, YybT PDE with a heme-bound PAS domain from *Bacillus subtilis*; CB-SONO, sensor of NO from *Clostridium botulinum*; DNR, dissimilative nitrate respiration regulator NO sensor from *Pseudomonas aeruginosa*; E75, nuclear receptor from *Oncopeltus fasciatus*; *Gf*YybT, YybT PDE with a heme-bound PAS domain from *Geobacillus thermodenitrificans*; MCS, multicomponent system; *Ns*H-NOX, H-NOX from *Nostoc punctiforme*; *Pa*H-NOX, H-NOX from *Pseudoalteromonas atlantica*; sGC, soluble guanylate cyclase; *So*H-NOX, H-NOX or NnoX from *Shewanella oneidensis*; *Sw*H-NOX, H-NOX from *Shewanella woodyi*; TCS, two-component system; *Tt*H-NOX, H-NOX from *Thermoanaerobacter tengcongensis*; TT-SONO, sensor of NO from *Thermoanaerobacter tengcongensis*; *Vc*H-NOX, H-NOX from *Vibrio cholera*; *Vf*H-NOX, H-NOX or HnoX from *Vibrio fischeri*; *Vh*H-NOX, H-NOX from *Vibrio harveyi*.

Global protein structural changes at the heme distal side are caused by association/dissociation of external axial ligands, including O_2, at the heme iron complex (Figure 5A).[81−83] Specifically, binding of O_2 to Arg220 in the heme Fe(II) complex in FixL results in flattening of the heme porphyrin and a shift of a critical loop, the FG loop, away from the heme pocket (Figure 6).[83] This type of profound protein structural change is unprecedented and had not been reported for prototypical heme proteins. The global changes in protein structure caused by O_2 are able to fully account for intramolecular signal transduction from the heme-bound domain to the functional domain. Similar global protein structural changes are induced by heme redox changes in *Ec*DOS, another heme-based oxygen sensor with the heme-bound PAS fold (Figure 5B).[51,85]

DOI: 10.1021/acs.chemrev.5b00018
Chem. Rev. 2015, 115, 6491−6533

Table 3. Functions of Heme-Based CO Sensors[a]

	functions	refs
Bacterial		
*Rr*CooA	transcription regulator	52, 296, 314, 317
*Ch*CooA	transcription regulator	325, 332, 334
$RcoM_{Bx}$-1 and $RcoM_{Bx}$-2	transcription regulator	294, 338, 339, 341
Mammalian		
CBS	cystathionine, H_2S, thiol ester synthesis	146, 147, 287, 289, 291
Slo1/BK	K^+ channel	351, 352, 354, 355, 361
Kv2.1	K^+ channel	357
Nav1.5	Na^+ channel	358
connexin hemichannel	ATP, glutathione, Ca^{2+} channel	359
NPAS2	transcription regulator: circadian rhythms	363, 364, 366−368
CLOCK	transcription regulator: circadian rhythms	369, 370
Per1	transcription regulator: circadian rhythms	378
Per2	transcription regulator: circadian rhythms	380, 382, 384
Rev-erbα	transcription regulator: circadian rhythms	371, 373
Rev-erbβ	transcription regulator: circadian rhythms	371, 374−376
Insect		
E75	transcription regulator	227, 375, 377

[a]CBS, mammalian cystathionine β-synthase; *Ch*CooA, CooA from *Carboxydothermus hydrogenoformans*; $RcoM_{Bx}$-1 and $RcoM_{Bx}$-2, RcoMs from *Burkholderia xenonorans*; *Rr*CooA, CooA from *Rhodospirillum rubrum*; Slo1/BK, large-conductance Ca^{2+}- and voltage-activated K^+ channel.

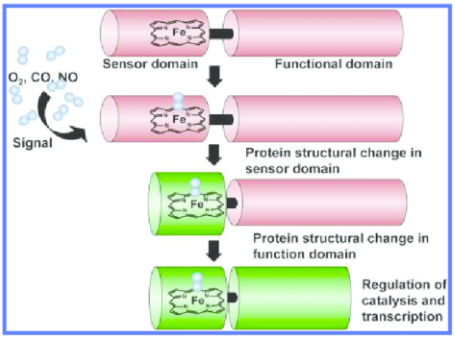


Figure 2. Heme-based gas sensor. The sensor is composed of an N-terminal heme-bound gas-sensing domain and a C-terminal functional domain.[41−43,50,66] For gas sensors, a gaseous molecule is the first signal. Binding of a gaseous molecule to the heme Fe(II) complex in the N-terminal sensing domain induces a structural change in the protein. This change in protein structure represents the second signal. This signal is transduced to the functional domain, switching on/off function in response to the association/dissociation of the gaseous molecule. For the heme-based oxygen sensors FixL and *Ax*PDEA1, dissociation of the O_2 molecule from the heme Fe(II) complex initiates the function, whereas for *Ec*DOS (or *Ec*DosP) and globin-coupled oxygen sensors, function is switched on by binding of the O_2 molecule to the heme Fe(II) complex.[50] For all heme-based NO and CO sensors reported to date, binding of gaseous molecules to the heme Fe(II) complex triggers the function.

The FG loop has been proposed to play an important role in domain−domain interactions.[84,86] Interactions between heme propionates and arginine side chains of the protein that occur upon O_2 binding[81,82,86] have been suggested as an explanation for intramolecular signal transduction from the heme-bound domain to the histidine kinase domain. Time-resolved crystallographic studies suggest that ligand (CO) binding causes structural changes in the FG loop and in the β-sheet distal to the heme, which are coupled to the movement of the main chain atoms of Leu236 in the I strand.[87] Conformational changes were also apparent at propionate 6 and in the FG loop residues Ile215 to Ile218. The sensing mechanism was proposed such that successive reactions would take place, including doming of the heme and subsequent propionate 6 movement and ligand shape sensed by steric clash of Leu236 with the bound ligand.[88]

Differences in the environment surrounding the heme structure between FixLs from *B. japonicum* (*Bj*FixL) and *R. meliloti* (*Rm*FixL) have been proposed on the basis of Fe K-edge EXAFS studies, crystal structures, and resonance Raman (RR) spectroscopic findings.[84,89] It was suggested that profound conformational changes in the FG loop are induced by steric repulsion between the bent, bound O_2 and Ile209 side chain, and that these changes are transmitted to the histidine kinase domain. The same research group also found a correlation between the heme-to-nitrogen (proximal His194) distance in the heme domain and the phosphorylation activity of the kinase domain.[89]

Heme redox-dependent substitution of the axial ligands of FixL was not observed, in contrast to *Ec*DOS, another PAS oxygen sensor, in which the axial ligands, hydroxide anion and histidine imidazole, of the heme Fe(III) complex are converted to methionine thiolate and histidine imidazole upon heme reduction to the heme Fe(II) complex.[51]

The Arg220 residue in the heme distal side is characteristic and important for O_2 binding (Figures 5A and 6[1]).[81−83] This is in contrast to hemoglobin and myoglobin, where a His residue in the distal side is important for O_2 binding and helps stabilize the heme Fe(II)−O_2 complex and thus should be beneficial for O_2 binding or storage.[1,6,8] This is also unlike P450, in which the threonine residue of the O_2-interacting site of the heme Fe(II)−O_2 complex serves to help activate the O_2 molecule or cleave the O−O bond of the heme Fe(II) complex-bound O_2 molecule with the aid of the cysteine residue of the proximal axial ligand by pushing electrons to the O_2 molecule.[2−6] Arg220 is reported to be involved in O_2-coupled structural changes[90] involved in caging O_2 near the heme[91−94] and in interactions with heme propionate 7.[95] Furthermore, the involvement of Arg226 in the formation of salt bridges[96] and contributions of Arg200, Arg208, Ile209, Ile210, and Arg214 to signal transduction between the heme and the kinase domain[86,97] have been proposed.

The importance of the heme proximal Arg206 in signal transduction has also been emphasized.[98] Crystal structure and oxygen kinetic data for an Arg206Ala mutant of *Bj*FixL suggest that the interaction between Arg206 and the heme propionate is important for the planarity of the porphyrin ring, tension of His214, and, ultimately, transmission during signal transduction.

DOI: 10.1021/acs.chemrev.5b00018
Chem. Rev. 2015, 115, 6491−6533

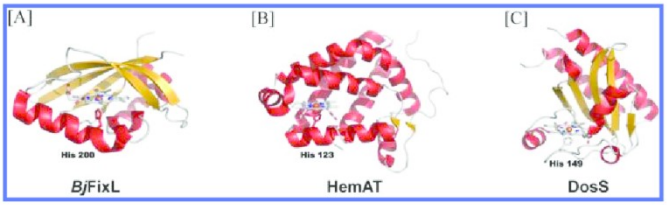


Figure 3. Typical protein structures of the heme-bound PAS [A],[81,82] globin [B],[190] and GAF [C][174] domains. The heme iron complex is bound to these domains, forming the gas-sensing site. FixL, *Ec*DOS, *Ax*PDEA1, and Aer2 are heme-based oxygen sensors containing a heme-bound PAS domain.

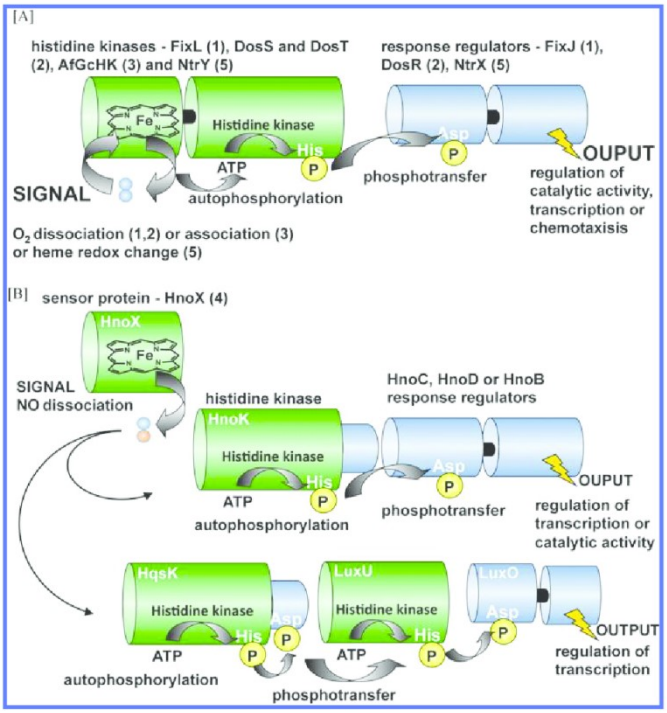


Figure 4. Bacterial two-component system of [A] fused type and [B] stand-alone type. Physical stimuli, such as light illumination or oxygen association/dissociation, interact with the sensing site of a signal-sensing protein, initiating an autophosphorylation reaction at a histidine residue in the functional domain. The self-added phosphate group is ultimately transferred to an aspartate residue of the response regulator, triggering a functional response, such as DNA binding and initiation of transcription of an important protein.[67,68] (1) FixL, a signal-sensing protein containing a heme-bound PAS domain, adopts a heme Fe(II)−O_2 complex form under resting conditions. Dissociation of O_2 from the heme Fe(II) complex triggers the autophosphorylation reaction and subsequent phosphotransfer reaction to FixJ, a response regulator.[41−43,66] (2) DosS and DosT are signaling proteins containing a heme-bound GAF domain.[70−72,171] Their response regulator is DosR. Similar to FixL, O_2 dissociation from the heme Fe(II) complex drives the autophosphorylation and phosphotransfer reaction to DosR. (3) *Af*GcHK is a signal-sensing protein containing a heme-bound globin domain.[73] Unlike the case for FixL and DosS/DosT, O_2 association with the heme Fe(II) complex significantly enhances autophosphorylation and phosphotransfer reactions to the response regulator. (4) HnoX is a stand-alone heme-based NO sensor.[56] NO association with or dissociation from the heme Fe(II) complex in HnoX triggers phosphorylation of HnoK or HqsK, which are not covalently bound to HnoX. The phosphotransfer reaction occurs from HnoK or HqsK to a response regulator or to another site within the same protein. Note that HnoK/HahK of *Pseudoalteromonas atlantica*,[277] HnoX/HnoK of *V. fischeri*,[278] and HnoX/HqsK of *V. harveyi*[279] also regulate NO-associated histidine kinase in a two-component signal transduction system. (5) NtrY is a heme redox sensor.[74] The heme Fe(II) complex form of NtrY autophosphorylates a histidine kinase domain at its C-terminus and stimulates phosphotransfer to NtrX, the response regulator, to control gene expression, whereas the heme Fe(III) complex form of NtrY does not.

DOI: 10.1021/acs.chemrev.5b00018
Chem. Rev. 2015, 115, 6491−6533

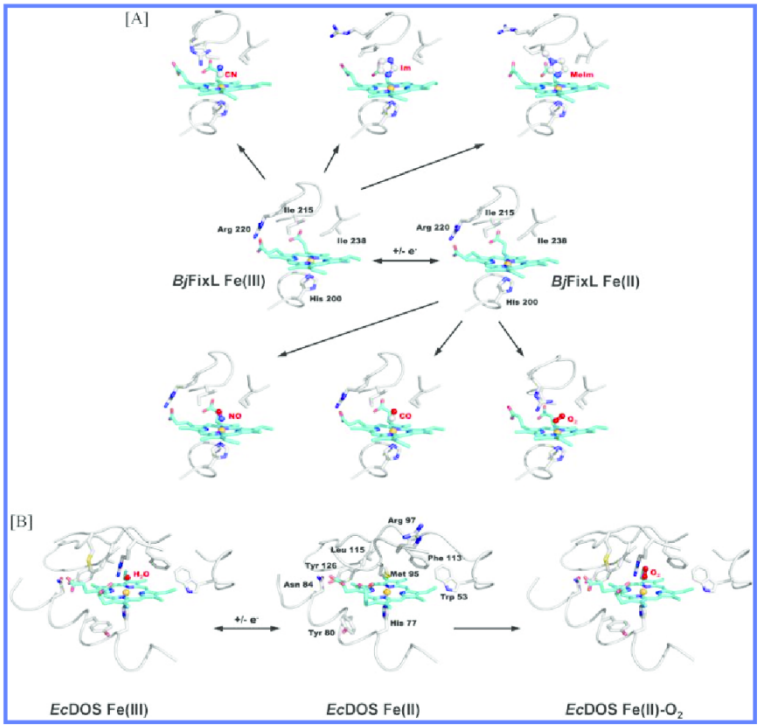


Figure 5. Ligand binding to the heme iron complex in *Bj*FixL induces global changes in protein structure [A][81−83] and in *Ec*DOS (or *Ec*DosP) [B].[51,85] The protein structure of the heme Fe(III) complex form of *Bj*FixL is virtually identical to that of the heme Fe(II) complex form. Binding of an external CN^- to the heme Fe(III) complex induces profound changes in protein structure involving both the FG loop and the heme axial ligands. The heme distal structure of inactive complexes, such as heme Fe(III)−CN, Fe(III)−imidazole, and Fe(II)−O_2, differs substantially from that of active complexes, such as heme Fe(III), Fe(II), and Fe(II)−CO. Unlike the case for *Bj*FixL, the protein structure of the heme Fe(III) complex in *Ec*DOS is substantially different from that of the heme Fe(II) complex. Here, O_2-binding to the heme Fe(II) complex induces changes in the protein structure of the distal side such that Arg97 interacts with O_2 bound to the heme Fe(II) complex. Amino acid residues that were discussed in the ultraviolet and time-resolved RR spectra of *Ec*DOS are shown in [B].[136,137,142,143]

Reduction of the heme Fe(III) complex by dithiothreitol was shown to be more effective in catalytic regulation by O_2 than reduction by treatment with sodium dithionite.[99] This suggests a significant role for a free cysteine thiol, or a relevant reduced state, in the catalysis of FixL.

Several recombinant, isolated, heme-bound domains of *Bj*FixL have been characterized by MALDI-TOF (matrix-assisted laser desorption/ionization-time-of-flight) mass spectrometry.[100] These studies included an assessment of the temporal mass stabilities of these domains, which revealed that as much as ~25% of the starting mass was not observed, a finding that could explain the "missing" terminal amino acids in published crystal structures. This phenomenon could be attributable to sample sterilization techniques and protease inhibitors usage, primary sequence variations, the presence/absence of a heme Fe(III) complex ligand, and the presence/absence of O_2.

2.1.1.4. O_2 Association/Dissociation Kinetics. Extensive studies have been conducted to examine the O_2 binding properties of FixL. Interestingly, these studies have shown that the equilibrium dissociation constant (K_d value) of O_2 from the heme Fe(II) complex in FixL, estimated at 29−140 μM, is unusually high as compared to that for other heme proteins.[66,81,98] By comparison, the well-known heme protein, myoglobin, has a K_d value of 0.88 μM.[50,101,102] The important role of the arginine residue in O_2 binding to FixL has been well characterized. The kinetic parameters for O_2 and CO binding to the heme Fe(II) complex of FixL are significantly changed by mutations at Arg220, the distal O_2 binding site, as well as by mutations at other hydrophobic amino acids and arginine residues that interact with the heme on the proximal side and with the heme propionate.[93,95,98,103] Different laboratories have reported different values for some kinetic parameters. Methods for determining these values appear critical for obtaining solid and reliable results.

A comparison of the mechanism of FixL autoxidation with that of *Aplysia* myoglobin[104] suggested a role for water interaction with the heme Fe(II) complex in determining the autoxidation rate of FixL, based on the dependence of this rate on O_2 concentration.

DOI: 10.1021/acs.chemrev.5b00018
Chem. Rev. 2015, 115, 6491−6533

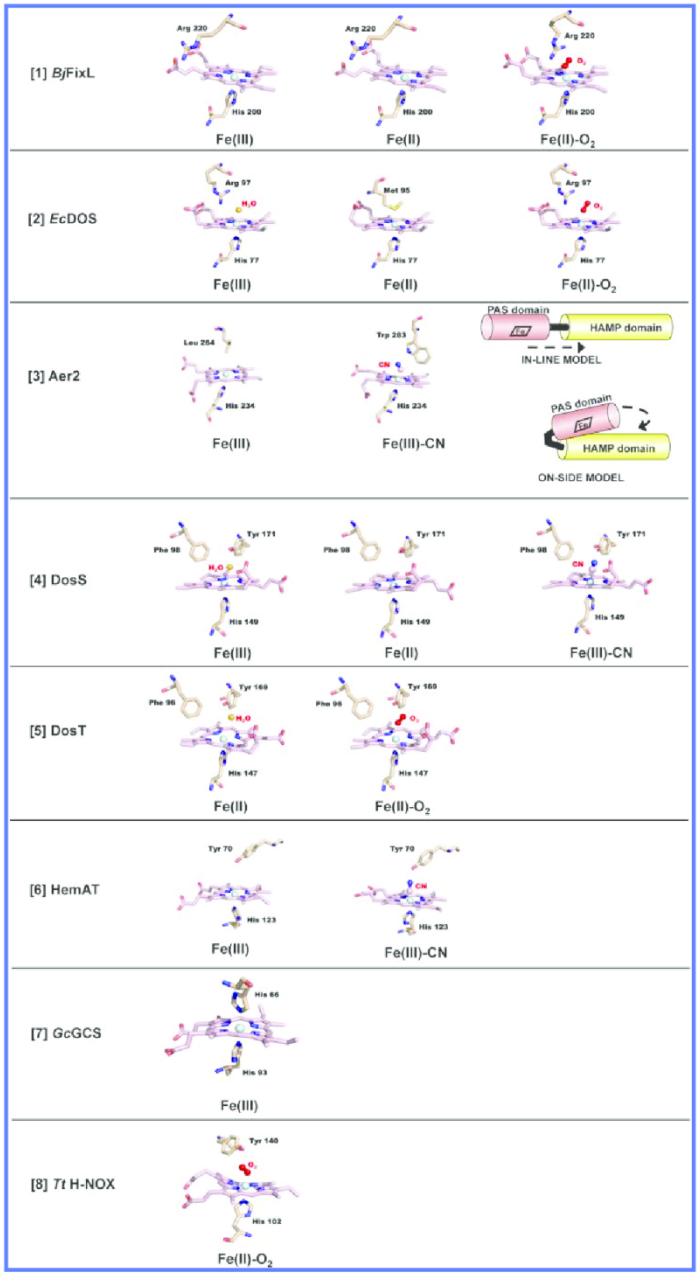


Figure 6. continued

DOI: 10.1021/acs.chemrev.5b00018
Chem. Rev. 2015, 115, 6491−6533

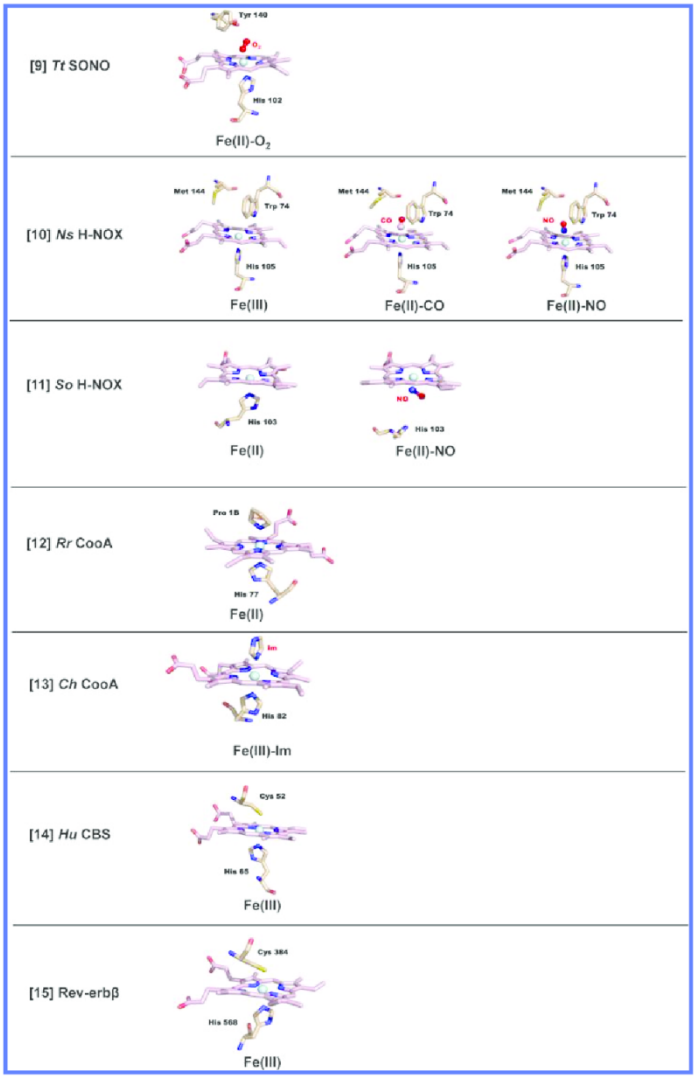


Figure 6. Heme-surrounding structures of heme Fe(III), Fe(II), and their ligand-bound complexes in heme-based gas sensors determined by X-ray crystallography. O_2 sensors: PAS fold, [1] FixL,[83] [2] *Ec*DOS (or *Ec*DosP),[51,85] and [3] Aer2;[165,167] GAF fold, [4] DosS (or DevS)[172] and [5] DosT;[174] globin fold, [6] HemAT[190] and [7] *Gs*GCS.[203] The in-line and on-side models of Aer2 are shown in [3]. NO sensors: [8] H-NOX from *T. tengcongensis*,[246] [9] SONO from *T. tengcongensis*,[245] [10] H-NOX from *Nostoc* sp.,[243,264] and [11] H-NOX from *S. oneidensis*.[242] CO sensors: [12] *Rr*CooA from *R. rubrum*,[312] [13] *Ch*CooA from *C. hydrogenoformans*,[333] and human [14] CBS[344,348,400] and [15] Rev-erbβ.[376]

Photodissociation of O_2 from the heme Fe(II) complex of *Sm*FixL has been studied by time-resolved RR spectroscopy.[90] On the basis of a comparison of the three steps in the dynamic structural changes that result from O_2 dissociation, the authors of this study proposed an FG loop switching mechanism to explain intramolecular signal transduction in this enzyme, in that the interactions of the heme propionates with the distal residues, including the FG loop region, change after O_2 dissociation.

2.1.1.5. CO Complex. Although CO is not a physiological axial ligand, extensive CO-binding kinetic studies have been conducted to explore the binding mechanism and access channel for this ligand.[96,105] CO-binding kinetic data suggest that interdomain signal transmission is coupled to heme ligand

DOI: 10.1021/acs.chemrev.5b00018
Chem. Rev. 2015, 115, 6491−6533

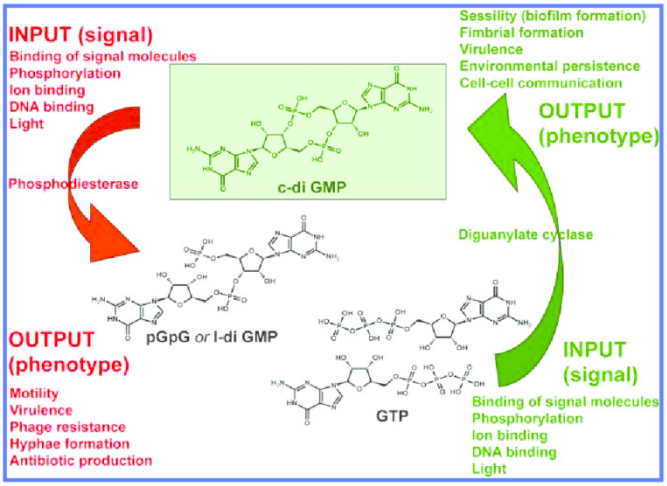


Figure 7. Cyclic-di-GMP is an important bacterial second messenger.[110−114] *Ec*DOS is a heme-based oxygen sensor PDE that linearizes c-di-GMP into l-di-GMP.[117,119] YddV is a heme-based oxygen sensor DGC that synthesizes c-di-GMP from GTP.[115,116] *Ec*DOS and YddV are *E. coli* enzymes that synergistically regulate the concentration of c-di-GMP to maintain intracellular c-di-GMP homeostasis.

release and that ligand-coupled protein oligomerization is physiologically relevant.[106] An ultrafast infrared spectroscopic analysis applied to the heme Fe(II)−CO complex of FixL[94] suggested that CO rotates toward the heme plane upon photodissociation in the heme pocket. Remarkably, CO bound to the heme iron is tilted by ∼30° with respect to the heme normal.

2.1.1.6. NO Complex. NO also is not a physiological axial ligand, but valuable information regarding ligand binding to the heme Fe(II) complex of FixL has been obtained on the basis of RR spectral data for the heme Fe(II)−NO complex of FixL. These studies suggested that the kinase domain influences the heme structure and that interdomain interactions between the heme and kinase domains are associated with ligand-binding-mediated kinase activity.[107]

2.1.1.7. pH Dependence and Tyrosine Residues. The pH-dependent behavior of the heme Fe(III) forms of both full-length Fix and the isolated heme-bound domain of FixLs was studied to ascertain how the spin state and ligation state of the heme iron complex respond to changes in pH by UV−visible, RR, and EPR spectroscopy.[108] The hemes of both FixL proteins were not fully ligated by hydroxide ion under strongly alkaline conditions, thus differing from the hemes of both myoglobin and hemoglobin. Both FixL proteins undergo additional alkaline transitions that involve the deprotonation of tyrosine residues, considering the pK_a values of tyrosine residues. Spectroscopic evidence indicates that the loss of activity at elevated pH was not due solely to the generation of a low-spin heme hydroxide. Rather, one or more tyrosines may be involved in signal transduction between the heme iron and kinase domain of FixL.

2.1.1.8. Chimeric Sensory Kinases. Chimeric sensory kinases composed of the heme-bound oxygen-sensor domain of FixL and the histidine kinase domain from the hyperthermophile, *Thermotoga maritima*, were constructed, and their molecular properties were characterized. An analysis of these chimeric kinases suggested that the interaction with the physiological sensor histidine kinase is strictly and finely controlled to mediate the signal ligand-dependent autophosphorylation activity in the histidine kinase domain.[109]

2.1.2. *Ec*DOS (or *Ec*DosP). Cyclic-di-GMP (c-di-GMP) is an important second messenger for bacteria, regulating numerous important physiological functions including cell motility, differentiation, development, virulence, biofilm formation, cell−cell communications, environmental persistence, photosynthesis, phage resistance, heavy metal resistance, and many others (Figure 7).[110−114] Homeostasis of c-di-GMP, regulated by diguanylate cyclase (DGC)-mediated synthesis and phosphodiesterase (PDE)-mediated degradation/linearization of c-di-GMP, is crucial for bacterial survival. These enzymes are controlled by phosphorylation, heavy metal binding, gas (O_2, NO) binding, DNA binding, and light illumination, among many other external stimuli. In *E. coli*, two heme-based oxygen sensors, *E. coli* direct oxygen sensor (*Ec*DOS, also known as *Ec*DosP) and YddV, with PDE and DGC activity, respectively, as well as numerous other enzymes with the same functions, work together in response to various external environmental stimuli such as changes in O_2 concentration.[115,116]

*Ec*DOS is a heme-based O_2-sensing PDE that catalyzes the conversion of c-di-GMP to linear di-GMP (pGpG) (Figure 7).[117] Similar to FixL, *Ec*DOS is composed of an N-terminal heme-bound O_2-sensing PAS domain, in which heme is bound to one of two tandem PAS domains, and a C-terminal PDE catalytic domain (Figure 2).[42,43,46,53] However, in contrast to FixL, where O_2 dissociation stimulates catalysis, the activity of *Ec*DOS is markedly enhanced by O_2 binding to the heme Fe(II) complex.[118−120] The molecular mechanism responsible for O_2-stimulated *Ec*DOS PDE activity has been characterized in numerous studies.

2.1.2.1. Catalytic Properties. The C-terminal catalytic domain of *Ec*DOS has the EAL subdomain typical for PDE,

DOI: 10.1021/acs.chemrev.5b00018
Chem. Rev. 2015, 115, 6491−6533

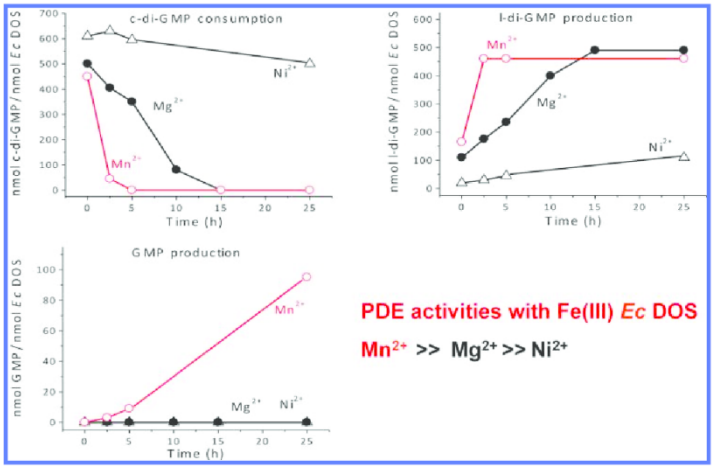


Figure 8. Role of Mn^{2+} in *Ec*DOS catalysis is different from that of Mg^{2+}. The heme Fe(III) complex form of *Ec*DOS in the presence of Mn^{2+} instead of Mg^{2+} exhibits robust PDE activity toward c-di-GMP in the absence of external ligands, such as O_2, CO, NO, cyanide, and imidazole.[129] This reaction also mediates the two-step hydrolysis of c-di-GMP all of the way to GMP via the linear di-GMP intermediate. Adapted from Honjo et al.[129] Adapted with permission from ref 129. Copyright 2012 Nova Science: Hauppaug.

which converts c-di-GMP into linear di-GMP (l-di-GMP); although it also possesses the GGDEF subdomain characteristic of DGC, which synthesizes c-di-GMP from GTP, DGC activity has not been reported for *Ec*DOS.[118−120] The C-terminal PDE activity is substantially enhanced by O_2 binding to the heme Fe(II) complex in the N-terminal sensing domain. Interesting features of ligand-induced catalytic stimulation include the fact that enhancement of catalysis by NO or CO binding to the heme Fe(II) complex is similar to that of O_2 and the observation that cyanide or imidazole binding to the Fe(III) complex stimulates catalysis to an extent similar to that of these gaseous molecules.[120] These axial ligand-induced increases in catalytic activity appear to be associated with the upward movement of the heme distal amino acids caused by ligand binding to the heme iron complex. As shown by the crystal structures of *Ec*DOS, catalytic enhancement of the heme Fe(II) complex by O_2, NO, and CO is achieved by dissociation of Met95;[51,85] in this scenario, the axial ligand Met95 on the heme distal side dissociates from the heme Fe(II) complex, and these gaseous molecules subsequently bind to the heme iron complex (Figures 5B and 6[2]). Therefore, it is reasonable to suppose that the activity of mutants containing a substitution at Met95, the axial ligand for the heme Fe(II) complex, is already high enough without those gaseous molecules, reinforcing the suggestion that the upward movement of the distal amino acids impelled by gaseous ligands is significantly involved in the resulting catalytic enhancement. The protein structure of the heme distal side is not clear from a study of the X-ray crystal structure of the heme Fe(III) complex of *Ec*DOS (Figure 6[2]).[51] However, it appears that similar movement of the protein in the heme distal side occurs upon binding of cyanide and imidazole, leading to catalytic enhancement via intramolecular signal transduction from the N-terminal heme-bound domain to the C-terminal catalytic domain.[120] The protein surface of the catalytic domain may interact, directly or indirectly, with the surface of the heme distal side in the heme-binding domain. Protein movement at the heme distal side may form an optimal structure at the protein surface of the heme-bound domain, thus stimulating catalysis in the functional domain.

YddV (or *Ec*DosC) is the heme-based oxygen-sensing DGC from *E. coli*,[115,116] as described in greater detail below (YddV section), whereas *Ec*DOS is the corresponding heme-based oxygen-sensing PDE toward c-di-GMP (Figure 7). Notably, the reactions catalyzed by YddV and *Ec*DOS leading to the synthesis and degradation of c-di-GMP in vitro are coupled, suggesting that both oxygen sensors function synergistically to regulate c-di-GMP concentration in response to external stimuli or O_2 concentration.[115,116]

*Ec*DOS also acts on the alternative substrate cyclic AMP (cAMP),[53,121−123] although its PDE activity toward this substrate is much lower than that of the native PDE enzyme in *E. coli*.[124] Intracellular cAMP concentrations in *Ec*DOS-knockout *E. coli* cells were ∼26-fold higher than those in wild-type cells,[125] and the morphologies of *Ec*DOS-knockout and wild-type *E. coli* cells were significantly different.[125] These results suggest that cAMP is also a native substrate of *Ec*DOS under physiological conditions. In its heme Fe(II) complex form, *Ec*DOS shows PDE activity toward cAMP, whereas the heme Fe(III) complex form of *Ec*DOS lacks PDE activity toward this substrate. It has been suggested that these heme redox-dependent catalytic differences in *Ec*DOS are partly caused by a heme redox-dependent domain−domain interaction at the C-terminal subdomain and protein flexibility (see next subsection for more detail).[51]

Mg^{2+} is essential for facilitation of the PDE activity of *Ec*DOS; it is also essential for kinase, phosphatase, PDE, guanylate cyclase, and numerous other nucleotide-associated reactions.[8,126−128] It is well-known that Mn^{2+} assists these nucleotide-associated reactions instead of Mg^{2+}.[8,126−128] A comparison of the effects of Mn^{2+} and Mg^{2+} on the PDE reaction of *Ec*DOS[129] showed that, in the presence of Mn^{2+} and

DOI: 10.1021/acs.chemrev.5b00018
Chem. Rev. 2015, 115, 6491−6533

in the absence of external ligands (cyanide, imidazole), the heme Fe(III) complex form of *Ec*DOS exhibited full PDE activity that was significantly faster than that in the presence of Mg^{2+} (Figure 8). This finding is in marked contrast to the case for the heme Fe(II) complex form of *Ec*DOS, in which binding of an external ligand (O_2, NO, or CO) is needed to stimulate PDE activity in the presence of Mg^{2+}.[118,119] Furthermore, in the presence of Mn^{2+}, the heme Fe(III) complex form of *Ec*DOS was found to mediate the two-step hydrolysis of c-di-GMP all of the way to GMP via the l-di-GMP intermediate. It was speculated that Mn^{2+} may be situated or coordinated at an active-site position that, even in *Ec*DOS heme Fe(III), is suitable for promoting optimal catalytic activity comparable to that observed for the heme Fe(II)−O_2 form with Mg^{2+}. Thus, one plausible explanation for the gas-sensing function of *Ec*DOS is that O_2 (or NO/CO) binding enhances Mg^{2+} affinity for the active site and/or creates a Mg^{2+} coordination structure that is optimal for efficient PDE catalysis.

2.1.2.2. Heme Redox-Induced and Ligand-Induced Changes in Global Protein Structure. Heme redox-dependent axial ligand substitution of *Ec*DOS should be a specific characteristic of *Ec*DOS distinct from that of FixL. This is because the axial ligand, hydroxide anion, on the distal side of the heme Fe(III) complex of *Ec*DOS is changed to Met95 upon the reduction of heme to the heme Fe(II) complex (Figures 5B and 6[2]).[51,85] Global protein rearrangements, including an ionic interaction between the heme propionate and protein arginine residue, are reported to occur upon heme reduction in *Ec*DOS. These heme redox-dependent axial ligand substitutions and global protein structural changes are not observed for FixL.

Heme redox-dependent changes in protein flexibility have also been reported. For the heme Fe(III) complex, the protein structure on the heme distal side cannot be definitely determined due to protein flexibility; in contrast, the corresponding structure of the heme Fe(II) complex is resolvable. Because it is assumed that the heme Fe(III) complex is inactive toward the alternative substrate, cAMP, as well as c-di-GMP, and that the heme Fe(II) complex is partially active toward both substrates, as described above,[53,118−123] the protein flexibility near the heme surrounding of *Ec*DOS should significantly contribute to the catalytic regulation of this enzyme. A high-pressure study revealed similar relationships between protein flexibility and the heme redox state of *Ec*DOS with respect to protein compressibility.[130]

Furthermore, upon O_2 binding to the heme Fe(II) complex, the heme distal side undergoes profound structurally changes, with Arg97 moving toward and eventually interacting with the O_2 molecule bound to the heme Fe(II) complex (Figures 5B and 6[2]).[85] This profound structural change induced by ligand binding and the interaction of Arg97 with the heme-bound O_2 molecule are similar to those observed for the heme-bound PAS domain of FixL.[81−83] For heme-based oxygen sensors, only limited O_2-free and O_2-bound structures have been determined for FixL and *Ec*DOS. However, on the basis of available information, it is reasonable to suggest that, in general, binding of the O_2 molecule to the heme Fe(II) complex in heme-based oxygen sensors profoundly changes the protein structure surrounding the heme, and these structural rearrangements, in turn, switch on intramolecular signal transduction to the C-terminal functional domain. It has also been suggested that the protein surface of the heme distal side and the functional domain face each other and directly or indirectly interact, as described above.

Notably, removal of the *Ec*DOS heme iron complex or truncation of the heme-bound PAS domain does not affect the catalytic activity toward c-di-GMP; in both cases, the catalytic activity of the heme-free form is as high as that of the O_2-stimulated form.[120] This finding suggests that the heme iron complex serves to suppress catalysis, and O_2 association with the heme Fe(II) complex releases this catalytic suppression. Similar findings have also been reported for the heme-based oxygen sensors, YddV and *Af*GcHK,[73,116] suggesting that the role of the heme iron complex in catalytic regulation is generally common among heme-based oxygen sensors. However, the heme-free forms of two other heme-based oxygen sensors, *Ax*PDEA1 and HemAC-*Lm*, have low activity.[131−133] Thus, one possibility for these oxygen sensors is that binding of the heme iron complex to the sensor domain is critical for maintaining an active site structure suitable for optimal catalysis. Further studies will be needed to elucidate the role of the heme iron complex in heme-based oxygen sensors.

2.1.2.3. O_2 Association/Dissociation Kinetics. The equilibrium dissociation constant (K_d) values of *Ec*DOS for O_2 are 13−21 μM for the isolated heme-bound domain, and 74−340 μM for the full-length protein.[50,117,134,135] As noted above, these values, like those for FixL (29−140 μM),[50] are substantially higher than that of myoglobin (0.88 μM). This suggests that both FixL and *Ec*DOS function under aerobic conditions, sensing slight differences in O_2 concentration and then increasing/decreasing their catalytic activity in response. Because the K_d value of the c-di-GMP synthetic enzyme YddV for O_2 (14 μM)[116] is lower than that of the c-di-GMP degradative enzyme *Ec*DOS, both YddV and *Ec*DOS would function synergistically to regulate c-di-GMP concentration in response to the stress imposed by changes in external O_2 concentration.

Not surprisingly, mutations at the heme distal side-localized Arg97, which interacts with the O_2 molecule bound to the heme Fe(II) complex, substantially change various O_2 binding kinetics, in particular, O_2 dissociation and auto-oxidation rate constants.[134] These observations suggest that Arg97 is important for the stability of the heme Fe(II)−O_2 complex in *Ec*DOS and for anchoring the O_2 molecule, thus preventing O_2 dissociation from the heme Fe(II) complex and/or rapid auto-oxidation. Furthermore, mutations at Met95, the axial ligand to the heme Fe(II) complex, cause more drastic changes in the O_2 association rate constant, suggesting that prior dissociation of Met95 from the heme iron plays a more crucial role than subsequent association of the O_2 molecule with the heme iron.[135]

2.1.2.4. CO and Cyanide Association Kinetics. CO association rate constants, unlike the case for O_2 association rate constants, are slightly increased in Arg97 mutants as compared to the wild-type protein.[134] This suggests that Arg97 does not have a significant direct effect on the CO access/escape channel in heme Fe(II) complex-bound *Ec*DOS. However, the loss of specific interactions between Arg97 and the heme 6-propionate in the mutant proteins may contribute to an increase in the CO association rate, as suggested by RR spectroscopic findings.[136,137] On the other hand, mutations at Met95 do not significantly change CO association kinetic values, suggesting that Met95 plays a different role in CO association than in O_2 association.

Association rate constants for cyanide binding to the heme Fe(III) complex are significantly lower for Arg97 mutants than for the wild type; as a result, the K_d values of cyanide for Arg97

DOI: 10.1021/acs.chemrev.5b00018
Chem. Rev. 2015, 115, 6491−6533

mutants are substantially higher.[120,134] This suggests that Arg97 also plays a role in the association of cyanide with the heme Fe(III) complex. Furthermore, Ala and Ile mutations at Met95 increase cyanide association with the heme Fe(III) complex, suggesting that Met95 is also involved in negatively regulating the association of cyanide to the heme iron. A study of the pH dependence of cyanide binding to the heme Fe(III) complex of *Ec*DOS provided interesting insights into the protein structural dynamics associated with alkaline denaturation.[138] Cyanide binding to heme Fe(III) complex of *Ec*DOS was found to be strongly affected by the apolar nature of the heme pocket, indicating that cyanide binding to this protein is distinct from cyanide binding to metmyoglobin and other heme enzymes.[138]

2.1.2.5. Reduction Potential. The reduction potential value of the isolated heme-bound domain of *Ec*DOS, at approximately 45−70 mV versus a standard hydrogen electrode (SHE), is similar to that of myoglobin.[54] This implies that the heme Fe(II) complex is more stable than the heme Fe(III) complex, enabling it to exert its oxygen-sensing function. Mutations at heme distal and proximal sides invariably change the reduction potential value to a certain extent.[54,139,140] Notably, mutations at Met95 drastically decrease reduction potential values from −1 to −122 mV versus a SHE.[54,139] Therefore, Met95 appears to be important in keeping the reduction potential in a range suitable for physiological function as an oxygen sensor under aerobic conditions.

2.1.2.6. Resonance Raman (RR) Spectroscopy. RR spectroscopy is a powerful tool for elucidating the structure and ionic characteristics of the environment of the heme iron complex and aromatic amino acid residues of heme proteins.[55,136,137,141−143] It has been successfully used to dissect the structure and function relationships of *Ec*DOS involved in intramolecular signal transduction from the heme-bound domain to the functional domain.

The spin states and coordination structures of the heme Fe(III) and Fe(II) complexes of *Ec*DOS, determined by RR spectra, revealed that complexes without any external ligand form 6-coordinated low-spin complexes.[143,144] The RR spectrum of the heme Fe(II)−CO complex suggested that the Fe−C−O geometry is nearly linear and that the CO environment has a hydrophobic character. RR spectra of the heme Fe(II) complex of His77 and Met95 mutants suggested that these amino acid residues are axial ligands for the heme Fe(II) complex of *Ec*DOS.[143] A His77Ala mutant showed no directing binding between the heme Fe(II) and the proximal side in *Ec*DOS, but time-resolved RR spectra revealed that exogenous imidazole was inserted between the heme Fe(II) complex and the protein surface of the mutant protein.[143]

Ultraviolet and time-resolved RR spectra of *Ec*DOS suggested the following structural features:[136,137,141,142] (1) Upon binding of O_2 to the heme Fe(II) complex, replacement of the distal axial ligand from Met95 with O_2 influences the heme 7-propionate hydrogen-bond network, resulting in profound conformational changes in the FG loop. (2) Interactions of Arg97 with the heme 7-propionate and steric interaction of Phe113 with O_2 are crucial for regulation of competitive axial ligand (Met95 and O_2) binding. (3) The hydrogen-bonding network from the heme 6-propionate to Tyr126 through Asn84 is important in transducing the signal from the PAS domain to the functional domain. (4) Trp53, Trp34, Tyr126, and Tyr80 are located near the 2-vinyl, 4-vinyl, and propionate side changes of heme, respectively. These amino acids then communicate structural changes in the heme side change induced by heme redox changes to the PAS protein surface, resulting in global protein conformational changes that are associated with the redox-dependent catalytic simulation of *Ec*DOS (Figure 5B).

2.1.2.7. Interactions with H_2S. H_2S (hydrogen sulfide) is the fourth most important signal gas molecule after O_2, NO, and CO.[17,145−153] Numerous studies have investigated the role of H_2S in physiology and pathology demonstrating several major mechanisms by which H_2S could affect physiological functions, including (1) reduction/breakage of the S−S bond, (2) formation of persulfide and polysulfide, and (3) interaction with metal cations.[17,145−153] Interactions of H_2S with heme proteins have been extensively studied,[154−157] and the formation of sulfhemoglobin and sulfmyoglobin containing sulfheme, a sulfur-incorporated protoporphyrin IX−iron complex, in the presence of both H_2S and H_2O_2 has been examined.[155−157]

Given that *Ec*DOS accepts NO and CO in addition to O_2 as the catalysis-stimulating gas molecule, it is not surprising that the effects of H_2S on the catalytic function of *Ec*DOS have also been explored. These studies showed that the PDE activity of *Ec*DOS is substantially enhanced by adding H_2S under aerobic conditions.[158] Mutagenesis and pharmacological inhibitor approaches were used to address the possibility that cysteine residue(s) are involved in this catalytic enhancement. Simultaneously mutating all eight cysteine residues to alanine or blocking them by adding *N*-ethylmaleimide completely abolished catalytic activity. However, stepwise mutation of each cysteine residue to alanine failed to yield an individual mutation that completely inhibited *Ec*DOS catalytic activity. Therefore, although one or more cysteine residue(s) clearly is involved in the catalytic enhancement of *Ec*DOS by added H_2S, it was not possible to specifically identify the cysteine residue(s) directly involved in this stimulatory effect.

Changes in the coordination structure of the heme Fe(III) complex induced by adding H_2S under aerobic conditions are complicated.[158] The heme Fe(III) complex is first changed to the heme Fe(III)−SH intermediate, and then the heme iron is reduced and becomes a heme Fe(II) intermediate, which quickly binds O_2. The heme Fe(II)−O_2 complex is autoxidized to yield the heme Fe(III) complex, which is further reduced to the heme Fe(II) intermediate. Absorption spectroscopy revealed that these complicated changes in coordination structure occur within several minutes.

The Arg97Ile and Arg97Ala mutants of *Ec*DOS form verdoheme, an oxygen-incorporated protoporphyrin IX iron complex, after H_2S treatment.[159,160] Mutations at Arg97, the O_2-interacting site in the heme Fe(II)−O_2 complex of *Ec*DOS, would generate considerable amounts of H_2O_2 due to the instability of the heme Fe(II)−O_2 complex in the presence of H_2S. H_2O_2 would likely form a heme Fe(III)−OOH complex that, with the aid of the water molecule near the heme environment, would help to catalyze the verdoheme-formation reaction.[161−163] Contrary to expectations, sulfheme was not formed under these conditions.

2.1.3. *Ax*PDEA1. The phosphodiesterase A1 protein of *Acetobacter xylinum*, *Ax*PDEA1, is a key regulator of bacterial cellulose synthesis.[131] *Ax*PDEA1 linearizes c-di-GMP, an allosteric activator of the bacterial cellulose synthase, to the inactive l-di-GMP (pGpG). This PDE function toward c-di-GMP is the same as that of *Ec*DOS. The domain structure of *Ax*PDEA1, composed of an N-terminal heme-bound PAS domain and a C-terminal PDE domain, is also homologous to

DOI: 10.1021/acs.chemrev.5b00018
Chem. Rev. 2015, 115, 6491−6533

that of *Ec*DOS, although *Ec*DOS has two heme-bound PAS domains, whereas *Ax*PDEA1 has only one.

Characteristic functional features of *Ax*PDEA1 that distinguish it from *Ec*DOS include (1) stimulation of catalysis by dissociation of O_2 from the heme Fe(II) complex in *Ax*PDEA1, in contrast to *Ec*DOS, where O_2 binding to the heme Fe(II) complex stimulates catalysis;[119] (2) loss of activity of the heme-free form, apo-*Ax*PDEA1, in contrast to *Ec*DOS, where the heme-free form, apo-*Ec*DOS, has the same high activity as the O_2-stimulated enzyme;[120,123] and (3) substantial stability of the heme Fe(II)−O_2 complex in *Ax*PDEA1, with an autoxidation rate constant less than 0.001 min^{-1}, which is much lower than that of *Ec*DOS (0.022−0.005 min^{-1}).[134] These specific molecular characteristics would abet the bacterial survival-promoting functions of *Ax*PDEA1. Regarding point (2) above, the heme-free form of the heme-based oxygen sensor adenyl cyclase, HemAC-*Lm*, is inactive, similar to AxPDEA1,[132,133] whereas the heme-free form of another heme-based oxygen sensor, the globin-coupled oxygen sensor YddV, is also active, similar to *Ec*DOS.[116]

2.1.4. Aer2. Aer2 from *Pseudomonas aeruginosa* is a heme-based oxygen sensor containing a heme-bound PAS fold that acts in a microbial aerotaxis control system. This oxygen-sensing system helps bacteria survive by enabling them to move to environments with a high O_2 concentration or away from low O_2 environments.[164,165] The oxygen-sensing characteristics together with methyl-accepting chemotaxis are similar to those observed in the heme-bound globin fold-containing HemAT from *Halobacterium salinarum* and *Bacillus subtilis*, as described in a later section. The crystal structure of the heme Fe(III)−CN complex of a truncated Aer2 consisting of the PAS and di-HAMP domains was determined (Figure 6).[165] The PAS domain is composed of two α-helices and a five-stranded β-sheet. The heme iron complex is accommodated by a hydrophobic pocket in which His234 is the proximal axial ligand, and heme-bound CN^- and Trp283 interact. This arrangement suggests that a hydrogen bond will form between the heme-bound O_2 and Trp283 that stabilizes the heme Fe(II)−O_2 complex. It also revealed that in HAMP (histidine kinases, adenylate cyclases, methyl accepting proteins, and phosphatases), a linker domain composed of a nearly 50-amino-acid α-helical region[166] is disordered for the most part.

Consistent with observations based on the crystal structure of the heme Fe(III)−CN complex, RR spectral data suggest that His251 forms a salt bridge with the 7-propionate in the heme Fe(II)−O_2 complex, similar to the heme Fe(III)−CN complex, implying that His251 is not the direct O_2-binding site in the heme Fe(II)−O_2 complex. The absorption spectrum of the heme Fe(II)−O_2 complex in the His251Ala mutant was the same as that in the wild type, although the autoxidation rate constant of this mutant was 10-fold higher. No stable heme Fe(II)−O_2 complex was observed for a Trp283Leu mutant.

On the basis of these findings, it was proposed[165] that hydrogen-bond formation between Trp283 and O_2 in the heme Fe(II)−O_2 complex causes conformational changes in the β5 strand upon O_2 binding, because Trp283 is located in the C-terminal region of the β5 strand. Once the PAS domain senses O_2 through binding to the heme Fe(II) complex, the O_2-sensing signal is transduced to the C-terminus of the MCP domain. Because the β5 strand is directly linked to the α4 helix, consisting of a linker between the PAS and di-HAMP domains, a conformational change in the di-HAMP domain results in a conformation change in the MCP domain. Unfortunately, however, the predicted O_2-regulated catalytic behavior of Aer2 has not been experimentally confirmed.

A comparison of the crystal structure of the heme-binding PAS domain in the ligand-free heme Fe(III) complex with the previously determined heme Fe(III)−CN complex identified conformational changes induced by ligand binding that are likely essential for the signaling mechanism.[167] Heme pocket alterations share some similarities with those of the heme-based PAS sensors FixL and *Ec*DOS, but propagate to the Iβ strand in a manner predicted to alter PAS-PAS associations and the downstream HAMP junction within full-length Aer2. It was suggested that the Aer2 signaling mechanism differs from that of the *E. coli* Aer paradigm, where direct (side-on) PAS-HAMP contacts are key. An in-line model of Aer2 signaling was proposed in which ligand binding induces alterations in PAS domain structure and subunit association that are relayed through the poly-HAMP junction to downstream domains. The PAS and HAMP domains do not interact directly in the in-line model of Aer2 signaling (Figure 6 [3]).[167]

2.1.5. Gyc-88E. sGC is an NO sensor whose catalysis is activated several hundred fold by binding of NO to the heme Fe(II) complex, as described in detail in a subsequent sGC section. The heme Fe(II) complex of sGC does not bind O_2, thereby allowing sGC to selectively bind NO despite micromolar cellular concentrations of O_2. However, Gyc-88E from *Drosophila* is a DGC containing an O_2-bound heme iron complex in the PAS domain.[168] Gyc-88E is active as a homodimer (5600 nmol min^{-1} mg^{-1}) and is inhibited 3.2-, 2.9-, and 2-fold by O_2, CO, and NO, respectively. Accordingly, absorption spectra revealed that O_2, CO, and NO bind to the heme Fe(II) complex. The K_m for GTP was estimated to be 0.66 mM in air (273 mM O_2) and 0.82 mM under anaerobic conditions, and the K_i for O_2 was calculated to be 51 mM. Thus, it was suggested that Gyc-88E is a DGC that potentially functions as an oxygen sensor in which O_2 dissociation from the heme Fe(II) complex stimulates catalysis, similar to FixL and DosS/DosT.

2.1.6. ThkA. The structure of a histidine kinase (ThkA) complexed with a response regulator (TrrA) in the two-component regulatory system from the hyperthermophile *Thermotoga maritima* was determined by a combination of X-ray crystallography, small-angle X-ray scattering (SAXS), and nuclear magnetic resonance (NMR) (Table 1).[169,170] The PAS sensor domain of ThkA interacts with both the catalytic domain of the same polypeptide chain, through formation of an interdomain β-sheet, and the TrrA molecule. The association interface between ThkA and TrrA contains the phosphotransferring histidine residue in ThkA, indicative of efficient receipt of the phosphoryl group. SAXS experiments also confirmed this association state in solution and showed specific binding between ThkA and TrrA (K_a = 8.2 × 10^{11} M^{-2}). NMR confirmed the specific interaction between ThkA and TrrA and demonstrated that the interaction would be suitable for the intermolecular phosphate group transfer reaction. The observed interdomain and intermolecular interactions clearly reveal a signal transduction pathway in the kinase/regulator complex.

2.2. Heme-Bound GAF Domain-Containing O_2 Sensors

Mycobacterium tuberculosis DosS (DevS) and DosT are oxygen sensor histidine kinases of a two-component signal transduction system that function together with the response regulator, DosR (DevR), which acts to up-regulate downstream genes essential for bacterial survival under hypoxic conditions (Table

DOI: 10.1021/acs.chemrev.5b00018
Chem. Rev. 2015, 115, 6491−6533

1).[37,70−72,171] This two-component signal transduction system is similar to that which includes FixL in that DosS or DosT first undergoes autophosphorylation in response to environmental stimuli. The phosphoryl group of phosphorylated DosS or DosT then is transferred to DosR, a DNA-binding protein that regulates the dormant state of the bacteria (Figure 4A). Similar to FixL, both DosS and DosT are composed of an N-terminal heme-bound domain and C-terminal kinase and ATPase domains. The heme iron complex of both DosS and DosT is bound to one of two tandemly repeated GAF (cGMP-specific and stimulated phosphodiesterases, adenylate cyclases, and *E. coli* formate hydrogen lyase transcriptional activator) domains, forming the oxygen-sensing site.[171] The GAF domains of DosS and DosT are structurally similar to one another.[172−174]

The GAF domain, like the PAS domain, is a ubiquitous cytoplasmic signaling unit in prokaryotic and eukaryotic organisms.[171,172,174,175] The overall topology of the GAF domain resembles that of the PAS domain, consisting of one five-stranded antiparallel β-sheet and four α-helices (Figure 3[C]).[171,172,174,175] The GAF domain has a ligand-binding pocket that accommodates a variety of small molecule ligands, such as flavin, adenine, cGMP, and heme, also similar to the PAS domain. Although the GAF domain is structurally similar to the PAS domain, its heme-binding mode differs from that of the PAS domain.[171,172,174,175] The role of O_2 dissociation from the GAF domain-bound heme Fe(II) complex is in activating the heme-bound histidine kinases. DosS and DosT from *M. tuberculosis* are similar to FixL, an element of the two-component system associated with nitrogen fixation in *B. japonicum* (*Bj*FixL) and *R. meliloti* (*Rm*FixL) described in a previous section.

2.2.1. DosS (or DevS). DosS is a member of the DosS−DosR two-component regulatory system that is thought to mediate the cellular response to anaerobiosis.[71,72,176] UV−vis and RR spectroscopic studies have revealed that His149 is the proximal ligand to both heme Fe(III) and heme Fe(II) complexes and that interactions between the two GAF domains within DosS influence the heme distal pocket environment in the heme-bound GAF domain (Figure 6[4]).[176] It has been found that unliganded, CO-bound, and NO-bound heme Fe(II) complexes are active, whereas the O_2-bound heme Fe(II) complex is inactive.[72] A specific hydrogen-bonding network near the O_2 access channel or the O_2-binding site on the heme distal side of DosS is responsible for discriminating O_2 from NO and CO to the heme Fe(II) complex.[177] Interactions between the two GAF domains are likely responsible for transducing structural changes at the heme domain that accompany ligand binding/dissociation to modulate activity at the kinase domain.[177]

Although DosS has been claimed to function as a redox sensor, spectral findings and analyses of histidine kinase activity under various conditions have shown no evidence of an oxygen or NO sensor.[37,71] However, other groups have argued that DosS is an oxygen (or NO) sensor, but not a redox sensor, based on its very low autoxidation rate constant and low O_2 dissociation rate constant as well as enhancement of the stability of the heme Fe(II)−O_2 complex by interdomain interactions.[176] Results based on RR spectra and autophosphorylation assays of the wild-type and Tyr171Phe mutant of DosS suggest that the hydroxyl group of Tyr171 acts as a relatively poor hydrogen-bond donor to the heme Fe(II) complex-bound O_2 molecule (Figure 6[4]).[177] An examination of DosS and NO interactions showed that, at low concentrations in a reducing environment, NO interacts with the inactive heme Fe(II)−O_2 complex and rapidly converts it into the heme Fe(II)−NO complex. This conversion triggers initiation of dormancy.[178] Ultrafast ligand dynamics of the isolated heme-bound GAF domains of DosS and DosT have also been examined. These studies showed that, despite structural and functional similarities between DosS and DosT, ligand-specific primary dynamics during the initial phases of intraprotein signaling are different between the proteins and predict that the distal tyrosine of both proteins plays an important role in these processes.[179]

Crystal structures of the DosS heme-bound GAF-A domain, the first of the two consecutive N-terminal GAF domains,[172] have been determined (Figure 6[4]). These analyses revealed that the heme is embedded in a hydrophobic cavity in the GAF domain and is roughly perpendicular to the β-sheet of the GAF domain. The heme Fe(III) complex is a 6-coordinated high-spin complex containing a proximal His149 and a water molecule that interacts with Tyr171 at the distal side. Although the heme is isolated inside the GAF domain, the heme Fe(II)−O_2 complex is unstable and rapidly oxidizes to the heme Fe(III) complex, leading to an indeterminable crystal structure of the heme Fe(II)−O_2 complex. Electron transferability through a defined hydrogen-bond network in the heme active site is a mechanism that has been put forward to explain the instability of the heme Fe(II)−O_2 complex. However, again, two other groups have reported that the DosS heme Fe(II)−O_2 complex is very stable,[72,171,176] suggesting that DosS is an oxygen (or NO) sensor. The crystal structure of GAF does not undergo a dramatic conformational change when the inactive heme Fe(III) form is reduced to the active heme Fe(II) form. This heme redox-insensitivity of protein structural changes is in contrast to that of *Ec*DOS, an oxygen sensor containing a heme-bound PAS domain, in which dramatic heme-redox-dependent structural changes occur.[51,85]

The crystal structure of the ATP-binding subdomain of the C-terminal kinase domain of DosS has been determined.[173] This structure suggests that proper positioning of a short ATP "lid" that interacts with a His phosphor-accepting subdomain triggers ATP binding of DosS. Accordingly, ATP binding would function as a structural mechanism for regulating histidine kinase activity.

2.2.2. DosT. The entire protein structure, heme-binding mode, and histidine kinase functions of DosT are similar to those of DosS.[71,72,171,174,179] However, DosT uses Mn^{2+} in addition to Mg^{2+} as the divalent ion for autophosphorylation and transfer of the phosphoryl group from phosphorylated DosT to DosR. Moreover, the phosphoryl transfer rate from DosT to DosR is much slower than that from DosS. In DosT, the heme Fe(II) complex-bound O_2 molecule is stabilized via a hydrogen bond to the OH group of Tyr169 on the distal side.[174] The entire structure of the heme-bound GAF domain of DosT is also similar to that of other heme-based oxygen sensors containing a PAS domain, such as *Ec*DOS and FixL.[51,81−83,85] However, the heme-binding mode in DosT is similar to that of cyclic nucleotide binding in GAF rather than heme binding in the PAS domain, even though DosT contains a five-stranded antiparallel β-sheet instead of the six-stranded sheet found in GAF motifs that bind cyclic nucleotides or linear tetrapyrrole chromophores.[174]

The crystal structure of the isolated ATP binding subdomain in the kinase domain of DosT was found to be similar to that of DosS. Thus, as is the case for DosS, a proper structural

DOI: 10.1021/acs.chemrev.5b00018
Chem. Rev. 2015, 115, 6491−6533

relationship between a short ATP lid and a His phospho-accepting subdomain is crucial for optimal ATP binding.[173]

2.3. Heme-Bound Globin Domain-Containing O_2 Sensors: Globin-Coupled O_2 Sensor (GCS)

The well-known representative heme proteins, myoglobin and hemoglobin, contain a globin fold and are composed of several α-helices.[1,6,8,180−186] In bacterial GCSs, the heme-bound globin domain is located at the N-terminus, whereas the functional domain with activities such as histidine kinase, PDE, DGC, and methyl-accepting chemotaxis is located at the C-terminus (Table 1).[38−40,50,60,185,187] However, the globin domain of GCSs lacks the entire D-helix and part of the E-helix of myoglobin and hemoglobin, which have a common genetic ancestry with sensor globins.[50] The shortened globin fold would thus be expected to have special characteristics that are beneficial for heme-based oxygen sensors. The most characteristic feature of GCSs is that O_2 binding to the heme Fe(II) complex substantially enhances their catalytic activity.[50] This property of GCSs distinguishes them from other heme-based oxygen sensors containing the PAS and GAF domains (with the exception of *Ec*DOS), in which O_2 dissociation from the heme Fe(II) complex enhances catalysis. Another interesting feature of GCSs is that the tyrosine residue at B10 is the O_2-interaction site.[50] This feature is also different from most heme-based oxygen sensors containing a heme-bound PAS domain (FixL and *Ec*DOS), in which an arginine residue is the O_2-interaction site,[81−83,85] although a tyrosine residue is located near the O_2-binding site in DosS and DosT.[174,177]

2.3.1. HemAT. HemAT-*Hs* from the archaeon *Halobacterium salinarum* and HemAT-*Bs* from the Gram-positive bacterium *Bacillus subtilis* have a methyl-accepting chemotaxis function that controls the movement direction of archaea and bacteria in an O_2 gradient.[188,189] The molecular properties of the heme-bound domain of HemATs have been well characterized. However, because no specific substrate/product of a HemAT-mediated reaction has been identified, it has not been possible to definitively establish functional regulation by O_2 association/dissociation and/or heme redox changes in reconstituted systems containing full-length HemATs in vitro. The C-terminal domain interacts with the histidine kinase CheA, which is a component of the CheA/CheY two-component signal transduction system involved in bacterial aerotaxis.

The crystal structures of heme Fe(II) and heme Fe(III)−CN complexes of the isolated heme-bound globin domain of HemAT-*Bs* have been determined (Figures 3[B] and 6[6]).[190] HemAT proteins in crystals were found as dimers, whereas gel filtration chromatography showed that the protein in dilute solution was mostly in a monomeric form. The overall structure of the heme Fe(II)-bound protein was very similar to that of the heme Fe(III)−CN-bound protein, suggesting the absence of profound protein structural changes upon a change in the heme redox state or cyanide binding to the heme Fe(III) complex. Instead, the HemAT sensor is predicted to undergo only small conformational changes within the dimer upon ligand association with or dissociation from the heme iron complex. This relative conformational insensitivity of the HemAT sensor protein structure is in contrast to the global protein structural changes observed in response to the heme redox state and ligand binding in other heme-based oxygen sensors, such as FixL and *Ec*DOS, containing a heme-bound PAS domain.[51,81−83,85] The HemAT sensor domain has low (~15%) sequence homology with myoglobin; however, the proximal His123 (F8) residue is well conserved throughout the globin family.[50]

The cyanide ligand is bound to the heme Fe(III) complex and stabilized by the hydroxyl group of Tyr70 (B10) with a hydrogen bond (Figure 6[6]). Moreover, there is one water molecule within the distal pocket. The distal water molecule is stabilized by a hydrogen bond to the λ oxygen atom of the Thr95 side chain (E-helix).

The O_2 binding equilibrium and kinetic constants for HemAT have high-affinity (K_d = 1−2 μM, k_{O2} = 50−80 s^{-1}) and low-affinity (K_d = 50−100 μM, k_{O2} = 2000 s^{-1}) components.[191] Replacement of Tyr70 (B10) with phenylalanine, leucine, or tryptophan dramatically increases both high- and low-affinity components of k_{O2}, implying that the hydroxyl group of Tyr70 (B10) is the direct/indirect O_2-interacting site within the heme Fe(II)−O_2 complex of HemAT.[191]

RR and ligand binding studies have been conducted on HemAT-*Bs*. These studies, which compared the structural characteristics of this protein with those of other heme proteins, revealed the presence of a unique hydrogen bond between a distal amino acid residue and the proximal atom of O_2 in the heme Fe(II)−O_2 complex.[192] RR spectral studies on Tyr70 and Thr95 mutants of HemAT-*Bs* suggest that the O_2 interaction can take three forms: a closed form, with an interaction between Thr95 and O_2; an open α-form, with interactions between Tyr70 and Thr95 and between Thr95 and O_2; and an open β-form, without interactions between the distal amino acid and O_2.[193] They further suggest the presence of a hydrogen bond between Thr95 and O_2 and between His86 and the heme propionate in the heme Fe(II)−O_2 complex.[194] A Fourier transform infrared spectrometry (FTIR) study emphasized the importance of hydrogen bonds, including Tyr70 and Thr95, on the heme distal side for ligand recognition and discrimination.[195]

Time-resolved ultraviolet RR spectra suggest the presence of hydrogen bonds between Thr95 and O_2 in the heme Fe(II)−O_2 complex and between His86 and the heme 6-propionate,[196] and predict that, upon CO photolysis, a change in heme structure drives displacement of the B- and G-helices.[197]

These spectral studies further suggest that the global protein structural changes caused by association/dissociation of the ligand are critical for signal transduction from the heme-bound domain to the functional domain. Discrepancies in the role of Tyr70 and Thr95 in ligand binding can be partially explained by the involvement of a water molecule in ligand recognition or discrimination.[50]

2.3.2. YddV (or *Ec*DosC). As briefly described above in the section on *Ec*DOS, YddV is a heme-based oxygen sensor DGC composed of an N-terminal heme-bound globin domain and a C-terminal functional domain.[115,116] YddV synthesizes c-di-GMP from GTP in response to O_2 binding to the heme Fe(II) complex bound to the N-terminal sensing domain. YddV is notable in that c-di-GMP is important for various fundamental bacterial physiological functions,[110−114] as described above.

At least in *E. coli*, two heme-based oxygen sensors, YddV, a DGC, and *Ec*DOS, a PDE for c-di-GMP, function synergistically to maintain c-di-GMP homeostasis in response to environmental O_2 concentration. The synthesis of c-di-GMP, subsequent degradation of c-di-GMP, and production of l-di-GMP have been monitored by chromatography in a semi-reconstituted system in which GTP is mixed with both YddV and *Ec*DOS.[115,116] These studies showed that, in the active

DOI: 10.1021/acs.chemrev.5b00018
Chem. Rev. 2015, 115, 6491−6533

heme Fe(II)−O_2 complex form, the DGC activity (0.022 min^{-1}) of YddV is much lower than the PDE activity (61 min^{-1}) of *Ec*DOS.[115,116] Thus, the YddV reaction leading to production of the *Ec*DOS PDE substrate c-di-GMP is the rate-determining step for the two coupled reactions. By extension, O_2 binding and heme redox switching of YddV appear to be critical factors in the regulation of c-di-GMP homeostasis. Because the K_d values for O_2 are significantly different between YddV (14−20 μM) and *Ec*DOS (74−340 μM),[50,115−117,135] the function of the two enzymes in maintaining c-di-GMP in vivo would be dependent on the O_2 concentration. The redox potential and the autoxidation rate constant of the isolated heme-bound domain of YddV are −17 mV and 0.0076 or 0.04 min^{-1}, respectively, whereas the corresponding values for *Ec*DOS are 40−70 mV and 0.0053 min^{-1}.[54,115,116] Thus, the redox environments of YddV and *Ec*DOS would also significantly affect the catalytic activity of these enzymes and thus influence c-di-GMP homeostasis.

Mutations at the Tyr43 residue in the putative heme distal side substantially reduce O_2 affinities, or markedly increase O_2 dissociation rate constants or autoxidation rate constants, suggesting that the hydroxyl group of Tyr43 directly or indirectly interacts with O_2 in the heme Fe(II)−O_2 complex through hydrogen bonding.[115,116] The RR frequency representing ν_{Fe-O2} of the heme Fe(II)−O_2 complex of Tyr43Phe (559 cm^{-1}) differs from that of the wild type (565 cm^{-1}), again corroborating the importance of Tyr43 in stabilization of the heme Fe(II)−O_2 complex or dissociation of the O_2 molecule from the heme Fe(II) complex in YddV.[115,116]

An amino acid sequence alignment of GCSs indicates that Leu65 of YddV is well conserved, and the crystal structure of HemAT suggested that Leu65 is located in the heme distal side.[190,198] Absorption spectra of the heme Fe(III) complex and the pH dependences of Leu65 point mutants are substantially different from those of the wild type, suggesting that a water molecule is the axial ligand of the heme Fe(III) complex in Leu65 mutants. Autoxidation rate constants of the heme Fe(II)−O_2 complex are much higher for Leu65 mutants (>0.10 min^{-1}) than for the wild type (0.011 min^{-1}); O_2 affinities for the heme Fe(II) complex are also markedly higher for the Leu65 mutants. These results suggest that the well-conserved Leu65 located in the heme distal side is critical for restricting water access to the heme distal side and preventing rapid autoxidation of YddV; thus, Leu65 is needed for formation of a stable Fe(II)−O_2 complex with a low autoxidation rate.[198]

Consistent with the purported role of a water molecule as an axial ligand in Leu65 mutants, overexpression of these mutants in *E. coli* tends to result in generation of verdoheme and CO.[199] In particular, the Leu65Asn mutant has strong tendency to exert heme oxygenase activity. Verdoheme and CO are also produced in a reconstituted system composed of Leu65 mutants and NADPH cytochrome P450 reductase. The fact that Leu65 mutations are assumed to allow introduction of a water molecule into the heme distal side of the isolated heme-bound domain of YddV suggests that the water molecule facilitates heme oxygenase reactions in Leu65 mutants. A significant role for a water molecule in the first reaction of the successive heme oxygenase reactions that yield verdoheme has been proposed.[161,162]

2.3.3. *Af*GcHK. *Af*GcHK, a globin-coupled histidine kinase from soil bacterial *Anaeromyxobacter* sp. Fw109-5, functions as part of a two-component signal transduction system.[73] O_2 binding to the heme Fe(II) complex in the N-terminal sensing domain substantially enhances the catalytic activity of this enzyme, including autophosphorylation at a histidine residue within the enzyme and subsequent phospho-transfer from this phosphorylated enzyme to a response regulator. Absorption spectra and functional studies of site-directed mutants suggest that [1] His99 is the proximal heme axial ligand, [2] His183 is the autophosphorylation site, and [3] Asp52 and Asp169 in the response regulator are the phosphorylated sites in this two-component system.[73] On the basis of the amino acid sequences and crystal structures of other GCSs, Tyr45 is predicted to be the O_2-interacting site at the heme distal side. Consistent with this, the O_2 dissociation rate constant (0.10 s^{-1}) is substantially increased (to 8.0 s^{-1}) in the Tyr45Leu mutant. RR frequencies representing ν_{Fe-O2} (559 cm^{-1}) and ν_{O-O} (1149 cm^{-1}) of the heme Fe(II)−O_2 complex of the Tyr45Phe mutant are distinct from the values of ν_{Fe-O2} (557 cm^{-1}) and ν_{O-O} (1141 cm^{-1}) for the wild-type protein. These results suggest that Tyr45 is located at the heme distal side and forms hydrogen bonds with the O_2 molecule in the heme Fe(II)−O_2 complex. Although oxygen sensor histidine kinases with a heme-bound PAS fold (FixL) or GAF fold (DosS, DosT) have been found and are well characterized, *Af*GcHK is the first oxygen sensor histidine kinase in a two-component system that contains a heme-bound globin fold (i.e., a GCS). The mode of O_2-induced catalytic stimulation is also a characteristic feature of *Af*GcHK in that O_2 binding to the heme Fe(II) complex enhances *Af*GcHK catalytic activity, in contrast to FixL and DosS/DosT, where O_2 dissociation from the heme Fe(II) complex enhances catalysis.

2.3.4. HemDGC. Structure and function studies of a heme-containing DGC (HemDGC) from *Desulfotalea psychrophila*[200] have shown that HemDGC has an N-terminal heme-bound sensing domain containing a globin fold and a C-terminal functional domain containing a DDDEF subdomain that is presumed to be involved in DGC activity. O_2 binding to the heme Fe(II) complex in the N-terminal sensing domain of HemDGC substantially enhances its catalytic activity (to 6.9 min^{-1}). Fe−O (ν_{Fe-O}) and O−O (ν_{O-O}) stretching modes of the heme Fe(II)−O_2 complex were observed at 566 and 1138 cm^{-1}, respectively. The ν_{Fe-O} frequency of HemDGC was similar to that of several nonvertebrate hemoglobins, such as *Ascaris suum* Hb (566 cm^{-1}), *M. tuberculosis* HbN (562−566 cm^{-1}), and *Paramecium caudatum* Hb (563 cm^{-1}), suggesting that hydrogen bonds are present between amino acid side chains and both proximal and distal oxygen atoms in the heme Fe(II)−O_2 complex. A Tyr55Phe mutant, containing a substitution at the well-conserved Tyr55 (B10) residue in the putative heme distal side, showed no catalytic activity, partly because it failed to form a stable heme Fe(II)−O_2 complex. Thus, Tyr55 has been suggested to play an important role in stabilization of the heme Fe(II)−O_2 complex.[200]

2.3.5. *Av*GReg. *Av*GReg, a putative GCS from *Azotobacter vinelandii*, was studied by characterizing its heme-binding domain (*Av*GReg178) and the full-length protein.[201] These studies showed that the heme Fe(II)−O_2 complex of *Av*GReg178 is very stable over many hours. Moreover, the heme Fe(III) complex of *Av*GReg was found to be a bis-His coordinated, low-spin complex. This is substantially different from the coordination structures of GCSs hitherto reported for which His has not be observed to be the distal axial ligand for the heme Fe(III) complex; instead, these GCSs are reported to have a vacant site or OH^- as the distal axial ligand.[73,116] O_2 affinities of *Av*GReg178 and *Av*GReg for the heme Fe(II) complex are high, with reported K_d values of 0.025 and 0.12

DOI: 10.1021/acs.chemrev.5b00018
Chem. Rev. 2015, 115, 6491−6533

μM, respectively. An examination of the kinetics of CO binding to both proteins was reported. It was suggested that the heme Fe(II)−O_2 complexes of *Av*GReg178 and *Av*GReg are involved in O_2-mediated NO-detoxification, which yields the heme Fe(III) complex. However, the DGC activity of *Av*GReg was not characterized.

2.3.6. *Bpe*GReg. *Bpe*GReg, a *Bordetella pertussis* GCS, possesses DGC activity that is stimulated ∼10-fold by O_2 binding to the heme Fe(II) complex in a reconstituted system.[202] This enzyme was inferred to consist of three domains: an N-terminal heme-bound globin domain, a middle domain, and a C-terminal DGC domain. The middle domain was suggested to be important for proper folding of the catalytic domain, but not the heme-bound domain. The catalytic activity of *Bpe*GReg is substantially decreased in the presence of the product, c-di-GMP, further suggesting that c-di-GMP binds to inhibitory sites and causes feedback inhibition of enzymatic activity. An examination of catalytic activities for reaction mixtures containing both *Bpe*GReg and a PDE showed that the catalytic rate of the coupled reaction (DGC and PDE) was substantially higher than that of DGC alone, confirming the presence of feedback inhibition of *Bpe*GReg. *Salmonella typhimurium* cell biofilm formation and swimming motility are altered by overexpression of *Bpe*GReg, corroborating that *Bpe*GReg is important for biofilm formation.[202]

2.3.7. *Gs*GCS. *Gs*GCS, a heme-bound globin domain of a GCS from *Geobacter sulfurreducens*, has been crystallized and structurally characterized.[203] The crystal structure of this protein indicates that the heme Fe(III) complex has a bis-His coordinated residue as the axial ligand, consistent with absorption and RR spectral studies. The histidine residue, which was unexpectedly found to be located at the E11 topological site, is the distal axial ligand for the heme Fe(III) complex. This arrangement is distinct from that for the E7 site of Hb, Mb, and other GCSs, although a histidine residue at the F8 site has been observed as a proximal axial ligand for this complex in other GCS and is not unusual.[50] RR and electron paramagnetic resonance (EPR) spectra and ligand (O_2, CO, and NO)-binding kinetic studies were additionally conducted to understand the role of amino acid residues in the heme environment in the ligand binding, recognition, and discrimination. The DGC activity of *Gs*GCS was not assessed. Regarding the unusual heme binding structure of this globin protein, further studies remain to be conducted.

2.3.8. HemAC-*Lm*. The globin-coupled adenylate cyclase, HemAC-*Lm*, in the unicellular eukaryotic organism trypanosomatid parasite *Leishmania major* is the first adenylate cyclase whose function was found to be up-regulated by O_2 binding to the heme Fe(II) complex in the N-terminal sensing domain.[132,133] Gene knockdown and overexpression studies suggest that O_2-dependent cAMP signaling via protein kinase A plays a fundamental role in cell survival through suppression of oxidative stress under hypoxic conditions. In addition, the enzyme-dependent cAMP generation exerts both stimulatory and inhibitory effects on the proliferation of *Leishmania* promastigotes during normoxia. Thus, O_2-dependent cAMP generation by adenylate cyclase likely plays a role in cellular adaptability to varying O_2 tensions.[132]

A homology modeling study suggested that His161 is the axial ligand on the proximal side in the sensing domain.[133] Catalytic studies of H161A revealed that the catalytic activity of the heme-free (apo) form (as confirmed by spectral studies) is very low: 0.5 min^{-1}. This value is lower than that for both inactive, O_2-free (1.2 min^{-1}) and stimulated, O_2-bound (20 min^{-1}) forms. This finding is noteworthy because the catalytic activities of heme-free forms of other heme-based oxygen sensors, such as *Ec*DOS[120,123] and YddV,[116] are high and comparable to those of the O_2-stimulated forms, with the exception of *Ax*PDEA1, in which activity is lost in the heme-free form.[131]

Reconstitution of the heme iron complex with a His161Ala mutant revealed that the dissociation rate constant of O_2 from the heme Fe(II) complex for the heme-reconstituted His161Ala mutant (51 s^{-1}) is significantly higher than that for the wild type (9.1 s^{-1}). The autoxidation rate constant for the heme Fe(II)−O_2 complex of the heme-reconstituted His161Ala mutant (6.1 s^{-1}) is also substantially higher than that of the wild type (<0.0001 s^{-1}). These results suggest that the reconstituted heme iron complex is not properly bound to the heme-binding site in the protein, resulting in characteristics that are different from those of the wild-type protein. Thus, proper binding of the heme iron complex to the protein is essential for O_2 binding to the heme Fe(II) complex to produce structural changes in the sensing domain that are optimal for catalytic enhancement.

2.4. AppA: Heme Sensor Domain with a Central SCHIC Fold

The AppA−PpsR system of *Rhodobacter sphaeroides* plays a key role in up-regulating the expression of numerous photosynthetic genes.[57] PpsR is a transcriptional repressor and AppA is an antirepressor capable of sensing not only O_2 but also light. AppA senses light through a FAD chromophore bound to its N-terminal BLUF (sensors of blue light using FAD) domain. Light causes dissociation of the AppA−PpsR complex, releasing PpsR to repress the transcription of photosynthesis-related genes.[57]

AppA is composed of an N-terminal BLUF domain, a central domain containing a noncovalently attached heme, and a C-terminal cysteine-rich domain. It has been suggested that AppA senses O_2 indirectly through its C-terminal cysteine-rich domain, an approximately 50 amino acid long fragment containing six cysteine residues. These residues are proposed to respond to changes in the cellular redox state by reversible formation of disulfide bonds.[57] The heme-binding domain in AppA is distantly related to the vitamin B_{12}-binding domain and thus has been designated SCHIC, for sensor containing heme instead of cobalamin.[57]

Binding of O_2 to the heme Fe(II) complex in AppA discoordinates the heme, and subsequent O_2 dissociation fully restores heme coordination. In vitro, the extent of heme discoordination increases gradually with rising O_2 levels over a broad concentration range. This response correlates well with the graded decrease in the transcription of photosynthesis-related genes mediated by AppA and its partner repressor PpsR. Taken together, the findings of this previous study suggest that the AppA−PpsR regulatory system functions as an oxygen-dependent transcriptional rheostat via the heme iron complex. However, if heme discoordination occurred in solution in vitro, the heme absorption peak should move to longer or shorter wavelengths, but in this study, the heme discoordination manifested as a decrease in heme absorption intensity. Thus, it is possible that precipitation or degradation of AppA heme, or some other phenomenon, occurred in response to the increase in O_2 concentration. Further studies will be required to elucidate heme iron behavior in AppA in response to changes in O_2 concentration.

DOI: 10.1021/acs.chemrev.5b00018
Chem. Rev. 2015, 115, 6491−6533

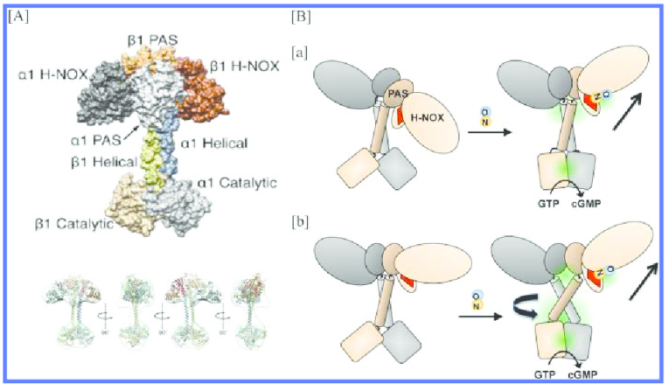


Figure 9. Proposed mechanisms of NO-induced activation of sGC based on both HDX-MA[250] and single-particle EM studies.[251] [A] The higher-order domain architecture is based on a recent single-particle EM study. Homology models of the individual domains could be fit into representative EM maps exhibiting two conformational extremes: the extended conformation [A] and a bent conformation (not shown). [B] NO binding releases and opens the heme-associated helix of the H-NOX domain while condensing and closing the active site pocket of the catalytic domain. Dominant points of conformational articulation are highlighted in green. The allosteric pathway bridging the sensor and output domains may involve two different mechanisms. [a] Large conformational changes at the junction between PAS and helical domains might indicate interdomain pivoting that relieves inhibitory contacts between H-NOX and catalytic domains. [b] Alternatively, the PAS-helical junction might mediate remote allosteric effects via long-range conformational changes propagated through the helical domains. Adapted from Campbell et al.[251] Reproduced with permission from ref 251. Copyright 2014 National Academy of Sciences, U.S.A. [A]. Adapted from Underbakke et al.[250] Adapted with permission from ref 250. Copyright 2014 Elsevier Inc. [B].

3. HEME-BASED NO SENSORS

NO is an important gas molecule involved in a wide range of signal transduction; it also contributes to cytotoxicity associated with numerous and ubiquitous important physiological and pathological functions in mammalian vascular, nervous, and immune systems.[11,12,14,15,18,22,204,205] In mammals, NO is synthesized from L-arginine by nitric oxide synthase (NOS).[11,15,20,21,204] Environmental nitrate (NO_3^-) and nitrite (NO_2^-), present in plants and food, for example, can be reduced and converted into NO, and thus represent a potentially important alternative source of NO.[25−27,206−210]

NO interacts with superoxide or molecular O_2 and is converted to peroxynitrite, which exerts numerous pathological functions, including tyrosine nitration.[28,29,205,211] NO itself interacts directly with cysteine thiolates on the surface of proteins, forming Cys−SNO, which plays an important role in critical functions associated with intermolecular signal transduction.[30−32,205,212−217] NO also interacts with metal centers, including nonheme iron complexes such as nitric oxide reductase, which is important for the biological denitrification process.[33,218−224] It also interacts with SoxR, NorR, iron regulatory protein, and FNR (fumarate and nitrate reduction regulator), which are involved in numerous important physiological functions through modulation of gene expression.[33,218,220,223−226] NO (or HNO) interacts with heme iron complexes, thereby regulating reactions associated with heme proteins, such as myoglobin, hemoglobin, cytochrome, and cytochrome oxidase.[10,58,227−231]

The importance of NO in the functions of heme-based NO sensors warrants particular emphasis. One of the best-known and most important heme-based NO sensors in eukaryotic physiology and pathology is sGC.[9,11,36,204,232−241] Bacterial heme-based NO sensors are also an emerging topic, providing interesting parallels with sGC from the standpoint of structure−function relationships, as detailed below in the section on H-NOX.

3.1. The Eukaryotic NO Sensor sGC

cGMP, a second messenger molecule that is critical for regulating diverse, important physiological functions, including smooth muscle relaxation, platelet inhibition, cell growth, and differentiation, is synthesized by the heme-based NO sensor, sGC (Table 2).[9,11,36,204,232−241] sGC senses picomolar levels of NO (~20 pmol). NO binding to the heme Fe(II) complex in the N-terminal sensing domain triggers guanylate cyclase function in the C-terminal domain, enhancing catalytic activity by ~200-fold. Despite the physiological importance of eukaryotic sGC, the structure of the full-length enzyme, and even that of the isolated heme-bound NO-sensing domain, has not been determined. This is in contrast to bacterial heme-based NO sensors (N-NOXs), which in many cases have been structurally resolved.[242−246] Accordingly, it has been suggested that structure and function relationships among bacterial heme-based NO sensors can provide valuable insight into the mechanisms of action of related eukaryotic proteins.[9,235,243,244,247−250]

3.1.1. Protein Structure. Full-length sGC is a heterodimer consisting of two homologous α1 and β1 subunits, each composed of four domains (Figure 9).[235,249−251] The β1 subunit of sGC is composed of an N-terminal heme Fe-bound, NO-sensing H-NOX (heme-NO and oxygen-binding) domain, central PAS and helix domains, and a C-terminal guanylate cyclase domain. The N-terminal domain of the α1 subunit does not contain a heme iron complex. The PAS and helical/coiled-coil domains are responsible for heterodimer formation and intramolecular, intersubunit, and interdomain signal transmission.[247,252] The C-terminal of both subunits constitute the cyclase active site, which is formed at the subunit interface.[253]

DOI: 10.1021/acs.chemrev.5b00018
Chem. Rev. 2015, 115, 6491−6533

The structure of the full-length, heme-bound heterodimeric form of sGC remains undetermined.[235] However, structures of sGC domain truncations, H-NOX, and homologues have been reported and modeled using diverse approaches, including single-particle electron microscopy (EM)[251] and hydrogen/deuterium exchange mass spectrometry (HDX-MS).[250] Single-particle EM has revealed the following structural features: (1) sGC is separated into two main globular densities and exhibits continuous flexibility; (2) the dimeric catalytic domain corresponds to a smaller, heart-shaped density; (3) the helical coiled-coil domain forms an elongated stalk that provides two points of flexible movement and rotation; (4) PAS and H-NOX domains cluster together in a larger, four-lobed density; and (5) the conformational flexibility of sGC is retained upon NO binding.[251] An HDX-MS analysis of the full-length sGC heterodimer further revealed that NO binding affects several discrete regions. Specifically, NO binding to the H-NOX domain perturbs a signaling surface implicated in PAS domain interactions; it also elicits striking conformational changes in the junction between the PAS and helical domains that propagate as perturbations throughout adjoining helices. Ultimately, NO binding stimulates the catalytic domain by contracting the active site pocket (Figure 9).[250]

Results of a FRET study using endogenous tryptophan residues as donors and the substrate analogue 2′-Mant-3′-dGTP as an acceptor suggested that NO binding to the heme Fe(II) complex drives Trp22 in the αB helix of the β_1 heme binding domain and Trp466 in the second short helix of the α_1 coiled-coil domain closer to the catalytic domain. It was proposed that the respective domains act like "a pair of tongs", forcing the catalytic domain into the NO-activated conformation.[254]

3.1.2. Coordination Structures of the Heme Fe(II) Complex. In general, binding of external ligands such as O_2, NO, CO, cyanide, or imidazole to the heme iron complex of a heme protein forms a 6-coordinated, low-spin complex.[1,6] Catalytic activation of sGC by NO binding to the heme iron complex is unique in that it forms an unusual 5-coordinated heme Fe(II)−NO complex. Importantly, formation of the 5-coordinated NO−heme Fe(II) complex in the β1 subunit of sGC is necessary for catalytic activation (Figure 9).[9,58,59,234,242,255] Rupture of the heme−histidine bond and formation of the 5-coordinated NO-heme Fe(II) complex in sGC have been rationalized on the basis of the crystal structure of the H-NOX protein from *Shewanella oneidensis*,[242] as described later. Time-resolved spectroscopy was used to evaluate the dynamics of heme coordination after NO release and binding.[256] After photodissociation of NO, all heme transitions occurred in the range of 1 ps to 0.2 s, notably the breaking and reformation of the bond between the heme iron and proximal His, considered major events for the activation/deactivation processes. Thus, the structural allosteric transition likely occurred in the time range 1−50 μs.

CO binding results in formation of a 6-coordinated CO−heme (II) complex that only slightly enhances catalysis, whereas O_2 does not bind to the heme Fe(II) complex, probably due to strict steric constraints and/or the hydrophilic environment of the heme distal side, which would repel O_2 binding. A weak Fe(II)−proximal His bond has also been suggested to explain the low O_2 binding to sGC.[257] In addition, the redox potential value is very high (+187 mV); thus the heme Fe(II) complex is very stable and is not prone to be oxidized to the heme Fe(III) complex.[257]

Whereas high-affinity binding of NO to the sGC heme Fe(II) complex stimulates catalytic activity, oxidation of the sGC heme to the heme Fe(III) complex desensitizes the enzyme to NO because of the low affinity of NO for the Fe(III) complex. The heme-oxidized state of sGC has emerged as a potential therapeutic target in the treatment of cardiovascular disease. Reductive nitrosylation of the heme Fe(III) complex in sGC proceeds through 2 equiv of NO. However, the heme Fe(II)−NO complex generated by interaction between heme Fe(III) and NO is not the active form. In the presence of NO, a rat sGC doubly mutated at β_1Cys78 and β_1Cys122 was shown to exhibit catalytic activity comparable to that of the heme Fe(II) complex form of wild-type rat sGC. From these results, it was inferred that sGC undergoes a reductive nitrosylation that is coupled to *S*-nitrosylation of a cysteine residues in sGC, such that heme-assisted β_1Cys78 and β_1Cys122 nitrosothiol formation causes NO desensitization of sGC containing a heme Fe(III) complex.[258] It has also been suggested that both β_1Cys243 and β_1Cys122 of rat sGC are involved in desensitization.[259] For human sGC, it was suggested that interface residues are important in promoting an optimal alignment of the catalytic center and that heterodimerization is required, but not sufficient, for activity.[248]

3.1.3. Catalytic Enhancement of sGC by Chemical Simulators and Activators. In addition to NO donors, nitrate and nitrous, numerous chemicals, including YC-1 and BAY compounds (developed by Bayer), are known to regulate sGC catalysis even in the absence of NO or the heme iron complex.[232,233] These chemicals have potential for use as drugs to treat conditions involving cGMP-related physiology and pathology.

The first compounds developed and advanced to modulate sGC activity were highly specific and potent sGC simulators.[232,233] These simulators exert their effects in a heme-dependent, but NO-independent, manner. YC-1 and BAY 41-2272, and their advanced derivatives, have multiple heteroaromatic rings whose structures are suitable for achieving high potency. A RR spectral study suggested that YC-1 binding substantially activates the heme Fe(II)−CO complex of sGC by causing a protein conformational change in the linker region; additional contributions to activation are provided by allosterically regulated changes in heme geometry and the formation of a 5-coodinated Fe(II)−CO complex.[260,261] This study also suggested that YC-1 and BAY 41-2272 activate sGC through a different mechanism in the presence of excess NO.[260,261] On the basis of linked equilibrium binding measurements, surface plasmon resonance, and domain truncations in *Manduca sexta* and bovine sGC, it was suggested that YC-1 binds near or directly to the H-NOX domain of the β subunit, and this binding overcomes allosteric inhibition by the α subunit.[262] Catalytic and structural studies of sGC and *Nostoc* sp. H-NOX with bound BAY 58-2667 or BAY60-2770 suggested that these compounds displace the heme and act as heme mimetics through both carboxylate-mediated interactions with the conserved YxSxR motif and hydrophobic interactions, as described below (H-NOX section).[263−265]

sGC activators operate on heme-free sGC, which can be formed under oxidative stress conditions that have been causally linked to cardiovascular diseases.[233] In this latter study, the authors used a high-throughput screening method to identify an sGC activator with unprecedented potency. This compound, containing two dicarboxylic acids, acts in a completely different manner from other sGC stimulators,

DOI: 10.1021/acs.chemrev.5b00018
Chem. Rev. 2015, 115, 6491−6533

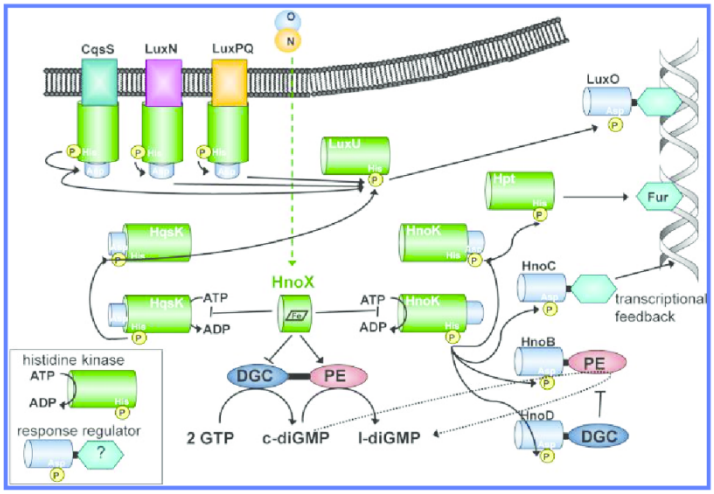


Figure 10. NO-induced regulation involving interactions with stand-alone H-NOX and other functional proteins. H-NOX is a stand-alone, isolated heme-bound protein whose structural changes are caused by NO binding to the heme Fe(II) complex, leading to interactions with other functional proteins and up- or down-regulation of important physiological functions (e.g., DGC, PDE, and histidine kinase in two-component systems) in bacteria. Thus, the NO sensor in this concept is different from other heme-based gas sensors in which the heme-bound gas-sensing site is located at an N-terminal site within the sensor protein that also contains a functional domain at a C-terminal site. Adapted from Plate and Marletta.[56] Note that DNR, a heme-based NO-sensing transcriptional regulator,[282−284] YybT, a heme-based NO sensor PDE,[285,286] and E75, heme-based NO-sensing nuclear receptor with the *c*-type heme,[227] are fused type sensors similar to the heme-based O_2 sensors, but not stand-alone type.

stimulating sGC in both an NO- and a heme-independent fashion. Detailed molecular studies that might enable exploitation of this unique activation mechanism have not yet been done.

3.2. Crystal Structures of the Heme-Bound, NO-Sensing H-NOX Domain of Bacterial NO Sensors: Stand-Alone Type

Crystal structures of bacterial H-NOX NO-sensing domains provide a convenient and effective tool for exploring the molecular mechanism of NO-stimulated catalytic enhancement of sGC. Importantly, many bacterial H-NOXs are stand-alone heme-based NO sensors. Accordingly, an isolated NO-sensing domain alone is capable of exerting its function by association with or dissociation from another isolated, functional protein without being covalently attached to the N-terminus of the full-length protein, as is the case for heme-based O_2 and CO sensors.[56]

3.2.1. *Tt*H-NOX. Bacterial *Tt*H-NOX domains from *Thermoanaerobacter tengcongensis* consist of an N-terminal helical subdomain and a C-terminal subdomain (Table 2).[56,246] The heme cofactor is deeply buried between the two subdomains, and the central iron is coordinated axially to a conserved histidine residue on α-helix F (Figure 6[8]). Furthermore, the propionate groups of the heme form salt bridges with an absolutely conserved YxSxR motif, which is also required for stable heme binding to the protein and activation in sGC. Notably, the structure of the protoporphyrin IX group is distorted from planarity to an extent unprecedented for protein-bound heme groups. A comparison of the structure of two different crystal forms of *Tt*H-NOX suggests a mechanism whereby alteration in the degree of distortion of the heme group is coupled to changes on the molecular surface of the H-NOX domain and potentially to changes in intermolecular interactions.[246]

The isolated heme-bound N-terminal domain of a putative NO sensor from *T. tengcongensis*, TT-SONO$_{HD}$ (heme domain of sensor of NO from *T. tengcongensis*), was independently determined by another group (Figure 6[9]).[245] These studies showed that the tertiary topology of TT-SONO$_{HD}$ is characterized by a proximal domain with an $\alpha\beta\beta\alpha\beta\beta$ motif and an α-helical domain. The heme is sandwiched between the two domains, and its iron atom is coordinated by His102 in the proximal helix. A modeling study suggested that a tyrosine residue is present within hydrogen-bonding distance of the terminal O_2 atom in the heme Fe(II)−O_2 complex. The protein structure of a SONO orthologue from *Clostridium botulinum* (CB-SONO$_{HD}$) was inferred from spectral studies of putative distal mutants. These studies suggested that Tyr139 in the heme distal side interacts with NO in the 5-coordinated heme Fe(II)−NO complex, thereby modulating the bond strength of the proximal Fe−His linkage and subsequently breaking the Fe−His bond.

3.2.2. *Ns*H-NOX. Crystal structures of ligand-free, NO-bound, and CO-bound H-NOX domains of *Ns*H-NOX, a cyanobacterial homologue of sGC from *Nostoc punctiforme*, were used as a platform for considering structure and functional relationships of eukaryotic sGC (Figure 6[10]).[243] A heme pivot-bend mechanism was proposed to explain the difference between the robust activation of sGC induced by NO and the slight activation induced by CO. NO and CO bind to the distal face of the heme and cause the heme to pivot to varying degrees away from Phe74 (Trp74 in *Ns*H-NOX). The larger pivot for CO is likely a result of two features: the limited space adjacent to Phe74 to accommodate the carbon atom, which has

DOI: 10.1021/acs.chemrev.5b00018
Chem. Rev. 2015, 115, 6491−6533

a larger radius than the nitrogen in NO, and the preference of CO to bind perpendicular to the heme. The involvement of residue 145 in NO-related catalytic regulation was also noted. It was further proposed that the second step in the NO activation mechanism involves heme bending and N-subdomain movement. The crystal structure of the activator BAY 60-2770 bound to *Ns*H-NOX revealed that BAY 60-2770 displaces the heme and acts as a heme mimetic through carboxylate-mediated interactions with the conserved YxSxR motif as well as hydrophobic interactions.[263] The hydrophobic phenyl moiety in the BAY 60-2770-bound protein has less flexibility than the BAY 58-2667-bound protein. The more rigid activator, BAY 60-2770, causes the protein region near residue 111, which is suggested to be important for the activation mechanism, to be more ordered as compared to that observed in the BAY 58-2667-bound protein.[263,265]

3.2.3. *So*H-NOX. High-resolution crystal structures of the H-NOX protein from *Shewanella oneidensis* in the unligated, intermediate 6-coordinated and activated 5-coordinated NO-bound states[242] revealed several structural features of the heme pocket of the unligated protein that are necessary for maintaining distortion of the heme from planarity. NO-induced scission of the Fe−His bond elicits a profound conformational change in the protein as the result of structural rearrangements in the heme pocket that permit the heme to relax toward planarity, yielding the signaling-competent, NO-bound conformation.[242] These results are consistent with suggestions based on NMR spectroscopy[266] and crystal structures of a His102Gly mutant[267] that artificial "cleaving" of the Fe−His bond induces a conformational change involving rotation of the distal subdomain relative to the proximal subdomain, centered about the heme cofactor. Paralleling this conformational change, severing the Fe−His bond was found to result in relaxation of the heme toward planarity.

These results are also consistent with a previously reported NO-induced activation model.[242,266−268] In this model, in the basal unligated Fe(II) state, the heme is distorted from planarity due to steric interactions with key conserved residues in the heme pocket. NO binding and subsequent scission of the Fe−His bond relieves the steric strain imparted on the heme, allowing it to relax toward planarity and, through intimate interactions of the protein and heme, to induce a rotation of the distal subdomain with respect to the proximal subdomain. This conformational change is thus hypothesized to communicate NO binding to downstream signaling partners.[242,266−269]

3.3. Functions of Bacterial NO Sensors

It has been well established that bacterial NO sensors that are separated from the functional protein they regulate are fundamentally distinct from other heme-based gas sensors in which the N-terminal heme-bound gas-sensing domain is covalently attached to the C-terminal functional domain (Table 2).[56,67]

A number of recent studies have provided details of the physiological functions of bacterial NO sensors that had previously been studied mainly from a structural and biophysical perspective (Figure 10).[56] On the basis of extensive structural and spectral studies focusing on the heme surrounding the NO-binding site, it was suggested that the heme distal side of bacterial NO sensors adopts a characteristic structure. Specifically, these studies showed that the high ligand specificity of bacterial NO sensors, which strongly favors NO over O_2 binding, prevents O_2 binding to the heme Fe(II) complex. This ligand specificity is dependent on a number of features of the protein, including the hydrophobic heme pocket, hydrogen-bonding networks containing a tyrosine residue as the NO binding site, heme distortion, protein flexibility, and a characteristic ligand access channel.[56,245,270] The crystal structure of the heme Fe(II)−O_2 complex of *Tt*H-NOX shows a hydrogen-bonding network in the distal pocket of the heme, consisting of Tyr140, Trp9, and Asn74. The tyrosine residue forms a direct hydrogen bond with O_2 bound to the heme Fe(II) complex[56,246] (Figure 6 [8]). The hydrogen-bonding network is absent in the distal heme pocket of the NO-selective *Ns*H-NOX protein and is instead replaced by nonhydrogen-bonding, hydrophobic residues[56,243] (Figure 6 [10]). Amino acid sequence alignment shows that the tyrosine and parts of the hydrogen-bonding network are conserved in the O_2-binding H-NOX subfamily, whereas hydrophobic residues occupy the same position in the NO-selective H-NOX proteins, including sGC.[56,243] Mutation of the Tyr to Phe in *Tt*H-NOX weakens the O_2-binding affinity.[271] Introduction of a Tyr into the distal heme pocket of the NO-selective H-NOX of *Legionella pneumophila* and a sGC truncation (β1[1-385]) allows the formation of a weak O_2 complex.[271] Incorporation of a Tyr into full-length sGC heme distal pocket alters NO binding dissociation kinetics, O_2 binding, and specific activity in the presence of NO,[270] confirming that the Tyr residue is a key determinant for O_2 binding and for NO exclusion.[56,271] However, introduction of a Tyr into full-length sGC by another group did not confer O_2 binding,[56,264] suggesting that the mechanism of oxygen exclusion by sGC not only involves the lack of hydrogen bonding in the distal heme pocket, but also depends on structural elements from other domains of sGC. Interestingly, this same tyrosine residue is important for GCSs containing a heme-bound globin or GAF fold,[50] as described above.

3.3.1. *So*H-NOX: Stand-Alone Type. HnoX (or *So*H-NOX), a stand-alone NO sensor from *S. oneidensis*, regulates the separate histidine kinase HnoK as part of a multicomponent signal transduction system (Figure 10). NO-binding to the heme Fe(II) complex in the HnoX protein inhibits autophosphorylation at the histidine residue of HnoK (see Figure 4).[67,272,273] Signal transduction by multicomponent systems plays important roles in numerous physiological functions in bacteria, as described above (see the section on FixL).[67] The phosphoryl group on the phosphorylated histidine of HnoK is transferred to an aspartate residue in multiple response regulators, switching on their output functions. The response regulators of *So*H-NOX include HnoC, which controls transcription, HnoB, which is a PDE toward c-di-GMP, and HnoD, which regulates the function of HnoB. NO-controlled repression of HnoB PDE activity leads to an increase in c-di-GMP levels, which results in a switch to a lower-motility pattern and "stickier" bacteria.[272,273]

3.3.2. *Sw*H-NOX: Stand-Alone Type. *Sw*H-NOX, from the biofilm-dwelling bacterium *S. woodyi*, mediates NO-induced biofilm dispersal (Figures 7 and 10).[274,275] *Sw*H-NOX is cocistronic with a gene encoding a dual-functioning DGC/PDE enzyme, designated HaCE (H-NOX-associated cyclic-di-GMP processing enzyme). In the absence of NO, *Sw*HaCE stimulates DGC activity, while PDE activity remains at basal levels. In the presence of NO-bound *Sw*H-NOX, however, *Sw*HaCE PDE activity is up-regulated, while cyclase activity remains at basal levels.

DOI: 10.1021/acs.chemrev.5b00018
Chem. Rev. 2015, 115, 6491−6533

The H-NOX-associated protein Lpg1057 (*Lp* HaCE) from *Legionella pneumophila* exhibits in vitro DGC activity that is inhibited by NO-bound H-NOX.[276]

3.3.3. H-NOX from *Pseudoalteromonas atlantica*: Stand-Alone Type. A stand-alone H-NOX from *P. atlantica* regulates the histidine kinase activity of a separate HahK protein as part of a two-component signal transduction system (Figures 4 and 10).[277] The autophosphorylation activity at the histidine residue in the HahK protein is inhibited by NO binding to the heme Fe(II) complex in the isolated H-NOX protein. A phosphoryl transfer reaction links HahK to a cognate response regulator, a protein annotated as a c-di-GMP-degrading enzyme termed HarR (H-NOX-associated response regulator). The resulting decrease in c-di-GMP levels modulates biofilm formation. Thus, biofilm formation is regulated, in part, by NO through the HahK−HarR two-component signal transduction system.

3.3.4. H-NOX from *Vibrio fischeri*: Stand-Alone Type. Many genes are involved specifically in hemin uptake as a source of iron, linking NO-H-NOX signaling to repression of hemin acquisition and utilization.[56,278] The NO-bound, stand-alone H-NOX in *V. fischeri* down-regulates expression of hemin-specific ferric uptake regulator (Fur)-associated genes through a two-component signaling pathway containing an isolated histidine kinase protein (HnoK) and a response regulator attached to its own HnoK protein (Figures 4 and 10).[278]

3.3.5. H-NOX in *Vibrio harveyi*: Stand-Alone Type. Bacteria use small molecules to signal their presence and gauge their surroundings, or to assess the density and identity of nearby organisms and formulate a response.[279−281] This process, called quorum sensing, regulates bioluminescence, biofilm formation, and virulence, and plays a role in communication and competition between different bacterial species. *V. harveyi* has four quorum-sensing pathways. In one, an NO-bound, stand-alone H-NOX regulates autophosphorylation of a separate kinase named HqsK that transfers a phosphoryl group to a common phospho-relay protein, LuxU, which ultimately regulates bacterial bioluminescence (Figures 4 and 10). Thus, phosphorylated LuxU transfers a phosphoryl group to LuxO, a transcription factor that, when phosphorylated, indirectly represses the master regulator of quorum sensing, LuxR, through activation of quorum regulatory RNAs (Qrrs).[56,279,280]

3.3.6. DNR: Fused Type. Heme-containing DNR (dissimilative nitrate-respiration regulator) of *Pseudomonas aeruginosa* is an NO sensor involved in regulating transcription of genes associated with nitrate respiration (denitrification).[282,283] DNR contains an N-terminal H-NOX domain and a C-terminal functional domain within a single protein molecule (fused type) (Figure 10), distinguishing it from the prototypal bacterial NO sensor described in the preceding sections, in which the H-NOX protein exists as an isolated form (stand-alone type). DNR belongs to the CRP-FNR (cAMP receptor protein/fumarate and nitrate reductase regulators) superfamily, whose members sense a wide variety of stimuli, such as O_2, NO, and redox state due to their ability to bind various cofactors. Generally speaking, CRP-FNRs are homodimers in which each monomer is composed of (1) an N-terminal sensing domain containing a fold typical of the cAMP-binding domain of CRP; (2) a dimerization-mediating α-helix recruited to form the dimer interface; and (3) a C-terminal DNA-binding domain containing a helix-turn-helix motif. The heme iron complex in DNR is presumably located at the dimerization helix containing the axial ligands, His139 and His187. NO binding to the heme iron complex forms a 5-coordinated NO−heme Fe(II) complex and triggers its DNA binding. Protein flexibility and dynamics are key structural features essential for explaining the evolutionary success and adaptability of CRP-FNRs, and may represent a common strategy employed by heme-based redox sensors, features fundamentally different from those of canonical heme proteins. Furthermore, fluorescence anisotropy studies have shown that high-affinity, sequence-specific DNA binding of DNR occurs only when the heme is nitrosylated, consistent with the proposed function of DNR as an NO sensor and transcriptional activator. This role is further supported by the NO "trapping" properties revealed by ultrafast spectroscopy, which are similar to those of other heme-based NO-sensor proteins.[284] Further studies will be required to elucidate the structure and function relationships of DNR.

3.3.7. YybT: Fused Type. YybT family proteins (COG3887) are proteins of generally unknown function that are widely distributed among the firmicutes, including the human pathogens *Staphylococcus aureus* and *Listeria monocytogenes*.[285,286] YybT family proteins contain an N-terminal domain that shares minimum sequence homology with the PAS domains. *Bs*YybT and *Gf*YybT, two representative YybT family proteins from *B. subtilis* and *Geobacillus thermodenitrificans*, respectively, are found to bind *b*-type heme with 1:1 stoichiometry. YybT is composed of an N-terminal heme-bound NO-sensing domain and a C-terminal PDE domain (fused type), but the domain arrangement is different from that of prototypical bacterial NO sensors in which the NO sensor protein, H-NOX, exists as a separate protein that interacts with a separate functional protein to exert its regulatory effects. The coordination of NO to the heme iron complex creates a 5-coordinated heme Fe(II)−NO complex that stimulates PDE activity toward c-di-GMP, suggesting that YybT family proteins function as stress-signaling proteins involved in monitoring cellular heme or NO levels (Figures 7 and 10).[285] The heme-free form, apoYybT, has significantly higher catalytic activity than that of the Fe(II)−NO-bound form, suggesting that binding of the heme iron complex to the enzyme serves to suppress catalysis, similar to the heme-based oxygen sensors *Ec*DOS and YddV, described above. An NMR study revealed that YybT possesses a PAS domain containing a potential ligand-binding pocket, reinforcing the view that the PAS domain of this enzyme functions as a regulatory domain in modulating cellular cyclic di-AMP concentrations in response to NO.[286]

3.4. Insect E75: Fused Type

Extensive biochemical and physicochemical studies, including ligand binding kinetics analyses, have been conducted on E75 family nuclear receptors from the insects *Oncopeltus fasciatus* and *Blattella germanica*.[227] These studies have shown that E75 proteins contain a heme iron complex in their ligand-binding domain. Their homologous nuclear receptors, Rev-erbα and Rev-erbβ, have been implicated as heme-responsive heme sensors, in which association of the heme iron complex with the ligand-binding domain, or dissociation from it, regulates transcriptional activity. However, the E75 protein from *O. fasciatus* was shown to exhibit covalent heme binding via heme methyl group, strongly suggesting that this protein is an NO sensor or diatomic gas sensor. It is not clear if the E75 protein acts as a redox sensor, although redox sensor proteins

DOI: 10.1021/acs.chemrev.5b00018
Chem. Rev. 2015, 115, 6491−6533

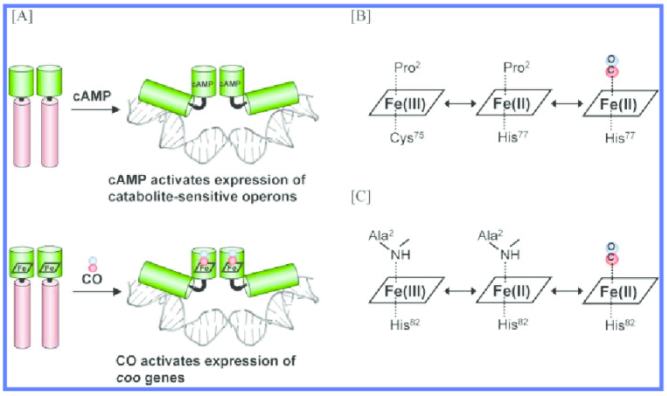


Figure 11. Heme coordination and protein structural changes that occur upon CO binding to the heme Fe(II) complex in *Rr*CooA ([A], lower)[310,312] as compared to the protein structural changes caused by binding of cAMP to the catabolite gene activator protein (CAP) family ([A], upper). CO binding to the heme Fe(II) complex in the dimeric *Rr*CooA protein induces profound structural changes that enable the C-terminal domain to interact with DNA in the promoter region of the *coo* gene. This CO-induced activation of *Rr*CooA is similar to cAMP-induced activation of CAP. Note that the proposed changes in coordination structure induced by redox changes and CO binding for *Rr*CooA [B] are different from those of *Ch*CooA [C].[54,332,333]

containing a covalent *c*-type heme iron complex (e.g., DcrA, GSU0582, GSU0935, and MA4561) have been characterized, as described below (see heme redox sensor with *c*-type heme).

3.5. Human Cystathionine β-Synthase: Fused Type

Mammalian cystathionine β-synthase (CBS) is a heme-bound enzyme that catalyzes the condensation of serine and homocysteine to produce cystathionine; it also generates H_2S by catalyzing the β-replacement of cysteine with homocysteine.[145−147,287−291] Catalysis is regulated by heme redox and CO binding to the heme Fe(II) complex, as described below in the CO-sensor section. However, human CBS is inhibited by NO, which binds more rapidly and tightly to the heme Fe(II) complex than CO.[292] Thus, it is possible that human CBS is an NO sensor.

4. HEME-BASED CO SENSORS

Atmospheric CO is generated by numerous natural and industrial processes, such as volcanic activity and incomplete combustion (biotic and abiotic) of organic matter.[13,293] The concentration of CO is held below toxic levels by microorganisms that utilize it. In a number of aerobic and anaerobic bacteria, and also in certain archaea, CO can serve as a source of energy and/or cell carbon.[13,293]

CO is a key metabolite and signaling molecule for many species of CO-utilizing bacteria and archaea.[13,293−295] Numerous prokaryotes express distinct CO-regulated systems that catalyze catabolically productive aerobic and anaerobic CO oxidation. Aerobic organisms employ a high-affinity, oxygen-tolerant, molybdo-flavoprotein complex to effect CO oxidation. This system is encoded by *cox* genes and has been shown to be transcriptionally regulated.[13,294]

The pathways to anaerobic CO oxidation mechanisms that employ variants of the enzyme carbon monoxide dehydrogenase (CODH), the oxygen-sensitive Ni-containing protein complex that enables anaerobic CO utilization, encoded by *coo* genes, are distinct from CO oxidation in aerobes mediated by *cox* genes.[13,293−295] Anaerobic CO metabolism is usually controlled by the transcriptional regulator, CooA.[52,294−296] CooA is a heme-based CO sensor whose transcription of CO-associated metabolism in bacteria is triggered by CO binding to its heme Fe(II) complex. An additional prokaryotic CO-dependent transcriptional regulator is RcoM (regulator of CO metabolism), a heme-bound CO sensor that represents a one-component CO-sensing transcriptional factor (Table 3).[52,294]

CO gas is generated by heme oxygenase in pathogenic bacteria.[161−163,297−301] Pathogenic bacteria degrade the heme iron complex, which is biologically extracted from hemoglobin in the host cells. This degradation of the heme iron complex by heme oxygenase generates free iron, biliverdin, and CO as the enzymatic products. The main purpose of pathobacterial heme degradation is to use the heme-released iron as a nutrient. However, the various CO utilizing systems indicated above may oxidize the CO generated by heme oxygenase. Notable in this context, however, are the heme oxygenases MhuD from *M. tuberculosis* and IsdG/IsdI from *S. aureus*, which degrade the heme iron complex without forming CO; instead, they generate aldehyde-bound tetrapyrrole (mycobilin) and formaldehyde.[299]

CO is also an important signaling molecule in eukaryotes (Table 3). The physiological and pathological effects of CO in mammals, acting in part as an antioxidant, have been well documented.[12,13,16−19,302−305] In eukaryotes, CO is synthesized by heme oxygenase with the aid of NADPH cytochrome P450 reductase.[161−163,300−307] Unlike O_2 and NO, which are easily converted into reactive oxygen and nitrogen species, CO is a stable molecule that is difficult for eukaryotes to convert into other species. CO also interacts only with metal complexes, such as heme iron complexes or nonheme iron or molybdenum iron complexes,[308,309] and not with intracellular compounds or amino acid residues on the surface of proteins. This chemical behavior of CO is different from that of O_2, which interacts with amino acid residues and metal ion complexes directly and as reactive oxygen species (such as hydroxyl radical, superoxide anion, and H_2O_2). It also differs from that of NO, which interacts with amino acids on the protein surface directly and in its derived forms, such as peroxynitrite. Thus, probably most

DOI: 10.1021/acs.chemrev.5b00018
Chem. Rev. 2015, 115, 6491−6533

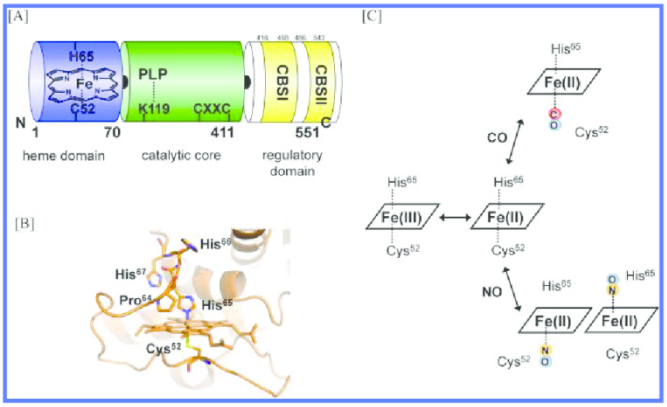


Figure 12. Domain organization [A] and close-up view of the heme Fe(III) complex surroundings [B] and the changes in coordination structure of the heme iron complex caused by CO and NO binding [C] in human CBS.[287,289]

(or all) eukaryotic physiological reactions associated with CO are caused by binding of CO with a heme iron complex or other metal cation complex.

4.1. CooA

*Rr*CooA from *Rhodospirillum rubrum* belongs to the catabolite activator protein (CAP) family of transcription regulators, whose members activate the expression of specific genes in response to distinct external signals.[52,310,311] *Rr*CooA is a homodimeric protein in which each monomer consists of an N-terminal effector-binding domain with a *b*-type heme and a C-terminal DNA-binding domain containing a classical helix-turn-helix motif (Figures 6[12] and 11A).[312] The two domains are connected via a long helix (the C-helix) that serves as the dimerization interface. For the heme Fe(II) complex of *Rr*CooA, His77 in both subunits provides one axial heme ligand, whereas the N-terminal nitrogen of Pro2 residues from the opposite subunit provides the other axial ligand. Binding of cAMP substantially changes the structure of homodimeric CAP proteins such that the C-terminal domain interacts with DNA.[310] CO binding to the heme Fe(II) complex activates *Rr*CooA, initiating the transcription of a series of genes encoding the CO oxidation system in *R. rubrum*.[34,52,296,313−317] On the basis of its overall structure and general comparison with CAP proteins, it is assumed that CO binding to the heme Fe(II) complex in the N-terminus of *Rr*CooA allosterically promotes adoption of similar profound structural changes in the C-terminus, enabling DNA interactions.[312]

The axial ligands for the heme Fe(III) complex of *Rr*CooA are Pro2, supplied by the other subunit in the homodimer, and Cys75 in the N-terminus.[312] Reduction of the heme Fe(III) complex to the heme Fe(II) complex causes dissociation of Cys75 from the heme Fe(II) complex, making His77 the axial ligand trans to Pro2 (Figure 11B).[318−324] Binding of CO to the heme Fe(II) complex in *Rr*CooA displaces Pro-2, which moves away from the heme, leading to substantial structural changes in the heme-bound domain that allosterically trigger C-terminal transcriptional or DNA binding activity (Figure 11).[55,325−330] Mapping of CooA-RNA polymerase interactions identified activating regions 2 and 3 in CooA.[331]

In *Ch*CooA from *Carboxydothermus hydrogenoformans*, a homologue of *Rr*CooA,[332] the axial ligands for the heme Fe(III) complex are His82 and the main chain NH of Ala2. Importantly, redox-dependent axial ligand switching does not occur for *Ch*CooA, resulting in CO binding to the heme Fe(II) complex trans to His82 (Figures 6[13] and 11C). This redox-insensitive axial ligand behavior is different from that of *Rr*CooA, in which the axial ligand Cys75 for the heme Fe(III) complex is replaced by His77 upon heme reduction to an Fe(II) complex. Thus, subtle and minute protein structural changes upon heme reduction that occur for *Ch*CooA are different from those of *Rr*CooA, as reflected in differences in these proteins' absorption and RR spectra and redox potential values. Nevertheless, the crystal structure of imidazole-bound *Ch*CooA suggests that the structural changes in *Ch*CooA caused by adding CO are similar to the profound changes in protein structure observed for *Rr*CooA.[333] Interestingly, adding NO promotes formation of a 6-coordinated heme Fe(II)−NO, yielding the DNA-binding, active form of *Ch*CooA.[334] This is in contrast to *Rr*CooA, in which adding NO causes formation of a 5-coordinated heme Fe(II)−NO complex that is inactive. However, whether *Ch*CooA is a heme-based NO sensor remains unclear.

RR spectral studies suggest that displacement of the C-helix by CO ligation is associated with DNA binding.[335,336] Additionally, it has been suggested that, once CO displaces the Pro2 ligand, the displacement of the heme into an adjacent hydrophobic cavity initiates the conformational change required for DNA binding.[337]

The low-frequency vibrational dynamics of the heme of *Ch*CooA have been investigated using vibrational coherence spectroscopy.[316] These studies suggested that distortion of the heme in the form of "doming" or "saddling" upon CO binding in *Ch*CooA is associated with the heme environmental and geometry changes that lead to activation of the DNA-binding domain. DNA binding to the *Rr*CooA heme Fe(II)−CO complex changes CO rebinding behavior, suggesting the presence of an allosteric transition in *Rr*CooA.[315]

DOI: 10.1021/acs.chemrev.5b00018
Chem. Rev. 2015, 115, 6491−6533

4.2. RcoM

RcoM is a single-component, CO-dependent transcriptional regulator that appears to regulate the expression of *coo* and *cox* genes involved in CO metabolism in different bacteria.[294] The RcoM proteins from *Burkholderia xenonorans*, $RcoM_{Bx}$-1 and $RcoM_{Bx}$-2, are composed of an N-terminal heme-bound PAS domain containing a 6-coordinated *b*-type heme Fe(II) complex and a C-terminal LytTR transcriptional/DNA-binding domain.[294,338] CO binding to the heme Fe(II) complex substantially enhances the transcriptional activity of $RcoM_{Bx}$.[294] $RcoM_{Bx}$-2 undergoes heme redox-dependent ligand switching in which the axial ligands in the heme Fe(III) complex, His74 and Cys94, change to His74 and Met104 in the heme Fe(II) complex and to His74 and CO in the heme Fe(II)−CO complex.[339,340] The ligand switching events caused by redox changes and/or CO binding induce profound structural changes in the heme-bound domain of the enzyme. $RcoM_{Bx}$-1 has a high CO affinity and multiple low-affinity DNA-binding states, suggesting a transcriptional "accumulating switch" that senses low but persistent CO levels.[341] Thus, the CO-dependent regulation of RcoM is significantly different from that of CooA, another CO-dependent transcriptional regulator.

4.3. Cystathionine *β*-Synthase

Mammalian CBS is a pyridoxal phosphate-dependent heme-binding enzyme that catalyzes the condensation of serine and homocysteine to yield cystathionine; in yeast and the protozoan *Trypanosoma cruzi*, the corresponding enzymes do not contain heme.[145−147,287−291] CBS also catalyzes the *β*-replacement of cysteine with homocysteine to generate H_2S and the corresponding thiol ether.[145−147,287−291,342]

Mammalian CBS is composed of an N-terminal heme-bound domain, a central catalytic core, and a C-terminal regulatory domain, which consists of two CBS domains (Figure 12).[287,289−291,343−347] Pyridoxal phosphate is bound to Lys119 in the catalytic core, and *S*-adenosylmethionine is bound to the CBS domain, where it acts as an allosteric activator to exert intrasteric regulation.

For mammalian CBS, catalysis is regulated by heme redox and CO binding such that CBS containing a heme Fe(III) complex is active, whereas CO (or NO) binding to the heme Fe(II) complex inhibits catalysis.[287,289−291,348] In these enzymes, the role of the heme iron complex in catalysis is similar to that of heme-based oxygen sensors such as *Ec*DOS and YddV, in which the heme-free forms exhibit optimal catalytic activity and changes in the heme-redox state or O_2 binding regulate (switch on or off) catalysis. This suggests that supplying the heme iron complex to the enzyme serves to suppress catalysis, and changes in heme redox status or O_2 binding to or dissociation from the heme iron complex release this suppression.[50,116,120] Therefore, the role of the heme iron complex in catalysis of mammalian CBS appears critical for its functional role in mammalian cells. Considering that yeast and protozoan CBS enzymes have no heme, the heme-containing CBS enzyme would appear to represent an evolutionarily advanced, more sophisticated form that is particularly suited for mammalian survival in response to environmental stimuli.

CO binding to the heme Fe(II) complex of human CBS inhibits catalysis. The axial ligands for both heme Fe(III) and Fe(II) complexes of human CBS are Cys52 and His65 (Figures 6[14] and 12B]). CO binding to the heme Fe(II) complex displaces Cys52, and the axial ligands of the heme Fe(II) complex become CO and His65 (Figure 12C).[343−345,348] CO binding to the heme Fe(II) complex inhibits catalysis, probably because CO binding breaks the salt bridge between Arg266 and Cys52.[147,287,289−291,349]

The redox potential of the heme iron complex of human CBS is low (−350 mV), suggesting that the heme Fe(III) complex is extremely stable as compared to the heme Fe(II) complex. Because CO binds only to the Fe(II) complex and not to the heme Fe(III) complex, this raises questions about the feasibility of forming a heme Fe(II)−CO complex under physiological conditions. Human methionine synthase reductase, an NADPH-dependent diflavin oxidoreductase, is suggested to play a significant role as a CBS reductase, providing a possible resolution of this apparent conundrum.[147,350]

NO binding to the heme Fe(II) complex of CBS inhibits catalysis.[287,289,290] NO has been shown to bind to the heme Fe(II) complex of human CBS more rapidly and tightly than CO, with a k_{on} value of $\sim 10^4$ M^{-1} s^{-1} and a K_d value ≤ 0.23 μM.[292] Therefore, NO may act together with CO and H_2S as a gasotransmitter in CBS function to play a critical (patho)-physiological role in cell signaling.

4.4. BK (Slo1) and Kv1.4 K^+ Channels, Nav1.5 Na^+ Channel, and Connexin Hemichannels

The heme Fe(III) complex binds to the Ca^{2+}-dependent large-conductance K^+ (BK) channel, also known as Slo1,[351] and the voltage-dependent K^+ channel Kv1.4,[352] and regulates their functions. Heme oxygenase-2 is part of the BK/Slo1 channel complex, and CO, a product of heme oxygenase, significantly regulates BK/Slo1 channel function.[353−356] CO also mediates the antiapoptotic effects of heme oxygenase-1 in medulloblastoma DAOY cells via K^+ channel inhibition,[357] and inhibits the function of the cardiac Na^+ channel, Nav1.5.[358] CO inhibits connexin hemichannel opening as well.[359]

Interestingly, it has been suggested that the heme Fe(II) complex is a CO receptor in Ca^{2+}-dependent K^+ channels.[360] Domain structure and function relationships involving CO generated from human heme oxygenase-2 and the heme iron complex and BK/Slo1 channel under both hypoxic and normoxic conditions have been proposed.[361,362] However, notable in this context, CO binds only to the heme Fe(II) complex and not to the heme Fe(III) complex. Thus, it is not clear how the heme Fe(III) complex bound to those channel proteins and reduced to the heme Fe(II) complex, the CO acceptor. The molecular mechanisms underlying heme-induced functional regulation, notably including how CO engages this function to form a heme Fe(II)−CO complex, remain unresolved.

4.5. NPAS2, CLOCK, Rev-erb*α*, Rev-erb*β*, E75, Per1, and Per2

CO appears to significantly contribute to the transcription regulation associated with circadian rhythms, and the heme iron complex, in particular the heme Fe(II) complex, is clearly an acceptor of CO in this system. In fact, transcriptional regulatory factors associated with circadian rhythms, including NPAS2,[363−368] CLOCK,[369,370] Rev-erb*α*,[371−373] Rev-erb*β*[371,374−376] (Figure 6[15]), E75,[227,375,377] Per1,[378] and Per2,[379−384] are heme-binding proteins. It has been suggested that these proteins are heme-based CO or NO sensors, because either CO or NO binds to the heme Fe(II) complex bound to those transcriptional regulatory proteins. Importantly, the transcription regulatory activity of the heme-bound NPAS2-bMAL1 dimer is inhibited by CO binding to the heme Fe(II)

DOI: 10.1021/acs.chemrev.5b00018
Chem. Rev. 2015, 115, 6491−6533

complex.[363] It has also been suggested that heme oxygenase is involved in the transcriptional regulation by NPAS2 and bMAL, and subsequent action of mouse Per2. This implies that CO contributes to the transcription mediated by heme-bound transcriptional factors.[382] It has also been suggested that these proteins are heme sensors in which Cys serves as the axial ligand for the heme Fe(III) complex; thus, association/dissociation of the heme iron complex regulates transcription associated with circadian rhythms.[7,46,362,385]

E75 from *O. fasciatus* has been suggested to be an NO or CO sensor, because both NO and CO bind to the heme Fe(II) complex in this protein. However, a heme iron complex in this protein is covalently attached to the protein with the heme methyl group; this contrasts with E75 from *Drosophila melanogaster* and *Bombyx mori*, where the heme iron complex is bound to the protein with coordination bonds acting as axial ligands to the heme iron complex.[227,375,377]

However, it is not clear how the heme Fe(III) complex, which reportedly binds to the above-mentioned transcriptional regulatory factors, is reduced to the CO-binding heme Fe(II) complex. One possibility is that NO reduces the heme iron complex; in this scenario, the heme Fe(III) complex bound to CLOCK undergoes reductive nitrosylation in the presence of NO to generate the heme Fe(II)−NO complex.[369] CO might then substitute with NO and form the heme Fe(II)−CO complex. Clearly, however, additional research will be required to establish the molecular mechanism by which the heme Fe(II)−CO complex is involved in transcription associated with circadian rhythms.

5. HEME REDOX SENSORS WITH *c*-Type AND Non-*c*-Type HEME IRON COMPLEXES

Various regulatory sensors continually monitor the redox state of the internal and external environments and control the processes that work to maintain redox homeostasis.[386] Apart from its gas (O_2, NO, and CO) sensor role, the redox state of the heme iron complex is critical for the regulation of various functions in bacteria (Table 4). Heme-based redox sensors with *c*-type (covalently attached: Figure 1E) heme have been reported.[387−389] Importantly, autophosphorylation, perhaps as part of a two-component signal transduction system, is regulated by heme redox changes in MA4561, a heme-based sensor with a *c*-type heme.[387] Among other heme-based sensors with *c*-type heme, including GSU582/GSU935,[388,390−393] DcrA has been extensively studied with respect to structural and physicochemical properties of the isolated heme domain.[389] Unfortunately, catalytic and functional regulation of DcrA by heme redox changes has not been examined. A defining characteristic of sensors with *c*-type heme is their low reduction potential values, from −85 to −250 mV. This property suggests that the heme Fe(II) complex is more stable than the heme Fe(III) complex and that redox-dependent ligand switching occurs, probably accompanied by profound structural changes in the heme-bound site. Redox-dependent ligand switching and/or protein structural changes induced by gas binding to the heme were observed for most heme-based gas sensors whose crystal structures were determined. In addition, these changes in the coordination and/or protein structures appear to be tightly linked to the signal transduction from the heme-bound domain to the functional domain.

Cytochrome *c* is not a gas-binding heme protein and does not undergo redox-dependent ligand switching, but it is involved in electron transfer reactions.[8] Thus, heme sensors with a *c*-type heme should act as redox sensors in response to environmental redox changes. Global protein structural alterations in the heme-bound site accompanied by changes in coordination structure also appear to occur upon ligand (NO, CO) binding, suggesting the additional possibility that heme-based sensors with a *c*-type heme could act as gas (NO, CO) sensors.[227,389,390] The covalently attached "non-*c*-type " heme proteins are formed under various conditions, suggesting possibilities of emerging and new functions of heme proteins.[394−396] Furthermore, a heme redox sensor with non-*c*-type heme (NtrY) has been reported for the NtrY/NtrX two-component signal transduction system.[74] Other heme proteins that mediate heme redox-dependent catalysis and putative heme redox sensors are described below.

Table 4. Functions of Heme Redox Sensors[a]

	functions	refs
Bacterial		
MA4561	histidine kinase/autophosphorylation	387
GSU582 and GSU935	MCP	388, 391−393
DcrA	MCP	389
NtrY	TC with NtrX	74
phenylacetaldoxime dehydratase (OxdB)	dehydration of acetaldoxime	397
Insect		
E-75	transcription regulator	227

[a]DcrA, heme redox sensor from *Desulfovibrio vulgaris* Hildenborough; E-75, a putative heme redox sensor or NO sensor from *Oncopeltus fasciatus*; GSU582 and GSU935, heme redox sensors from *Geobacter sulfurreducens*; MA4561, heme redox sensor from the methanogenic archaeon *Methanosarcina acetivorans*; MCP, methyl-accepting chemotaxis protein; NtrY, histidine kinase with the heme-bound PAS domain and a part of the NtrY/NtrX two-component system from *Brucella* spp.; phenylacetaldoxime dehydratase, phenylacetaldoxime dehydratase from *Bacillus* sp. strain OxB-1 (OxdB) that catalyzes the dehydration reaction of *Z*-phenylacetaldoxime to produce phenylacetonitrile; TC, two-component system.

5.1. MA4561

MA4561 of *Methanosarcina acetivorans* is a multidomain sensory kinase composed (in N- to C-terminal order) of PAS, GAF, PAS, GAF, and histidine kinase-like ATP domains.[387] The heme iron complex is covalently attached to Cys656 via a vinyl side chain in the second GAF domain of MA4561. The reduction potential value of MA4561 is −85 mV. MA4561 proteins containing a heme Fe(III) or heme Fe(III)−DMS (dimethyl sulfide) complex autophosphorylate, whereas those containing heme Fe(II), heme Fe(II)−CO, or heme Fe(II)−DMS do not, suggesting that this kinase is a redox sensor. MA4561 appears to be a sensor kinase in a two-component signal transduction system that regulates methyl sulfide metabolism. Notably, MA4561 is the only one heme redox sensor with a *c*-type heme whose catalytic or functional activity has been clearly demonstrated.

5.2. GSU582 and GSU935

The crystal structures and physicochemical properties of periplasmic sensor domains from two methyl-accepting chemotaxis proteins, GSU582 and GSU935, from *Geobacter sulfurreducens* have been characterized.[388] These studies showed that the sensor domains of both proteins form a swapped dimer and exhibit a PAS-type fold. Structural analysis of these heme

DOI: 10.1021/acs.chemrev.5b00018
Chem. Rev. 2015, 115, 6491−6533

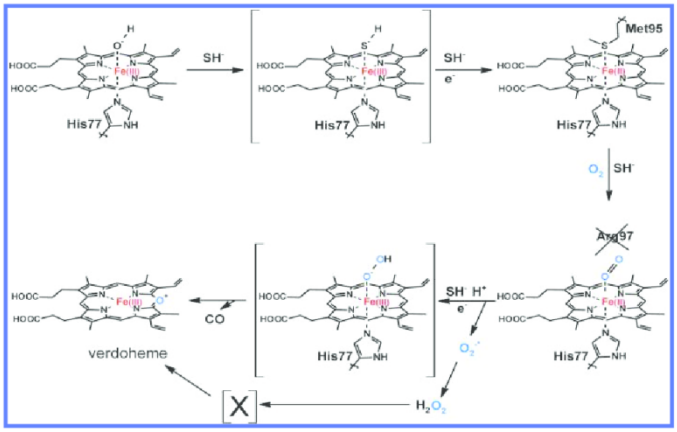


Figure 13. H_2S-induced heme modification. The mutations Arg97Ala and Arg97Ile, corresponding to the direct O_2-binding residues on the heme distal side, modify the porphyrin ring and cause formation of verdoheme, an oxygen-incorporated porphyrin, in the presence of excess H_2S.[159,160] Sulfheme, a well-known sulfur-incorporating porphyrin, is not formed under these conditions, unlike the case for hemoglobin and myoglobin.

Fe(III)-bound sensor domains revealed that the heme iron complex is covalently bound to the protein. His143-Fe(III)-water coordination was observed for GSU582, whereas His144-Fe(III)-Met260 and His344-Fe(III)-water coordination were observed for monomers A and B of GSU935, respectively. The redox potentials of both proteins are very low: −156 mV for GSU582 and −251 mV for GSU935. Although the structures of the heme Fe(II) complex-bound forms were not determined, redox-dependent ligand switching of the heme iron complex accompanied by profound protein structural changes were predicted for both proteins. These molecular characteristics may be related to the signal transduction mechanism of those chemotaxis-regulating proteins. Biochemical reactions in a reconstituted system have not been reported.

5.3. DcrA

The chemotaxis signal-transducing protein DcrA from *Desulfovibrio vulgaris* Hildenborough contains a *c*-type heme in its periplasmic domain that senses redox changes and/or O_2.[389] Physicochemical studies, including absorption and RR spectroscopy, and kinetic analyses of CO association/dissociation were performed on the heme-bound domain of DcrA. These studies showed that the CO affinity of the DcrA-bound heme Fe(II) complex ($K_d \approx 138\ \mu M$) and redox potential of the protein (−250 mV) are both extremely low. Similar to the heme-sensors GSU582 and GS0935 containing a *c*-type heme, DcrA exhibits redox-dependent ligand switching. Again, biochemical reactions in a reconstituted system have not been reported.

5.4. NtrY/NtrX

NtrY, a histidine kinase containing a heme-bound PAS domain, is one component of the *B. abortus* NtrY/NitrX two-component signal transduction system.[74] The O_2-bound Fe(II) complex is very unstable, showing rapid oxidation to the heme Fe(III) complex in the presence of O_2. Under low O_2 tension, the active NtrY form containing a heme Fe(II) complex is formed, executing autophosphorylation and phosphoryl transfer reactions to the cognate response regulator NtrX. The phosphorylated form of NtrX binds to specific promoter regions and thereby controls the expression of genes encoding nitrogen respiration enzymes.

5.5. OxdB

Phenylacetaldoxime dehydratase from *Bacillus* sp. strain OxB-1 (OxdB) catalyzes the dehydration of *Z*-phenylacetaldoxime (PAOx) to yield phenylacetonitrile. OxdB contains a heme iron complex that serves as the active center of the dehydration reaction.[397] The enzymatic activity of the heme Fe(II) complex form of OxdB is ∼1150-fold higher than that of the heme Fe(III) complex form, indicating that the heme Fe(II) complex is the active form in OxdB catalysis. The catalytic mechanism has been suggested to include the following features: (1) the aldoxime residue in the substrate, PAOx, binds directly to the heme Fe(II) complex in the heme distal side; (2) dehydration proceeds through a general acid catalysis mechanism involving the heme Fe(II) complex with the aid of His306; and (3) phenylacetonitrile and water are generated as the final products. The affinity of the substrate, PAOx, for the heme Fe(III) complex in OxdB is much lower than that for the heme Fe(II) complex. Therefore, OxdB catalysis is regulated by the heme redox state. This suggests that OxdB is a heme-redox sensor, although the heme iron complex is directly involved in catalysis, but does not act as signaling receptor/sensor.

5.6. Insect E75

Insect E75 from *O. fasciatus* has an N-terminal covalently bound heme.[227] This heme is not a typical *c*-type heme that binds via a thiol-vinyl link, thus strongly altering the properties of the iron moiety. Rather, the heme in insect E75 is bound covalently to the heme methyl groups,[227] making it unlikely that insect E75 is the redox sensor. On the basis of spectral studies, it was suggested that insect E75 is a heme-based NO sensor, as described above.

5.7. *Ec*DOS

*Ec*DOS is a heme-based oxygen sensor PDE that acts on the substrate c-di-GMP as described above in the O_2 sensor section.[115,117,119,120] In *Ec*DOS, the heme iron complex is bound to the PAS domain through coordination bonds with

DOI: 10.1021/acs.chemrev.5b00018
Chem. Rev. 2015, 115, 6491−6533

amino acids of the protein, as the axial ligands, and through ionic bonds between the heme propionate and an arginine residue of the protein, but no *c*-type (covalently attached) heme is formed.[51,85] The *Ec*DOS-associated PDE activity toward cAMP is regulated by the heme redox state of the enzyme[53,121−123,125] such that the heme Fe(II) complex form of *Ec*DOS is active toward c-AMP, whereas the heme Fe(III) complex form is inactive toward the same substrate. A gene knockout of *Ec*DOS in *E. coli* results in high intracellular concentrations of cAMP, suggesting that cAMP is an alternative substrate of *Ec*DOS, although the activity of *Ec*DOS toward cAMP is very low as compared to that toward c-di-GMP.[54,124,125]

6. HEME-BASED H_2S SENSORS

No heme-based H_2S sensors have been reported to date. Notably, however, catalytic activity of the heme-based oxygen-sensing *Ec*DOS PDE is substantially enhanced by the addition of H_2S under aerobic conditions as already shown in the *Ec*DOS section (Figure 13).[158,160] Although this enhancement is mainly caused by changes in the coordination structure of the heme iron complex in the enzyme, it is unlikely that *Ec*DOS is a heme-based H_2S sensor, because the H_2S concentration needed to stimulate catalysis is in a physiologically irrelevant (~100 μM) range. However, it is assumed that deep-sea marine organisms living near volcanic hypothermal vents use H_2S-associated biochemistry and physiology. Thus, it is possible that future studies will identify heme-based or non heme-based H_2S sensors.

7. COMMON CHARACTERISTICS OF HEME-BASED GAS SENSORS

(1) Ligand binding and heme redox change induce profound structural changes in most heme-based gas sensors. Such profound protein structural changes are not observed for prototypical heme proteins, such as hemoglobin, myoglobin, cytochrome *c*, and P450.

(2) The rank order of affinity for gas binding to the heme Fe(II) complex is $O_2 \ll CO \ll NO$. A "sliding scale rule" was proposed to explain differences in affinity between these three gas molecules.[58,59,398] Accordingly, for heme-based gas sensors, structural deformation of the heme plane, the protein structure surrounding the gas binding channel, and/or the distal structure of the gas-bound heme complex in the protein significantly affects the specificity of gas binding to the heme Fe(II) complex.

(3) Heme sensors, but not heme-based gas sensors, in which association/dissociation of the heme Fe(III) complex to the protein per se regulates functions, can also be gas sensors. However, these gas molecules bind only to the heme Fe(II) complex; thus, changes in heme redox status must occur to convert them from heme sensor to gas sensor. In addition to reductases, NO might act as a reducing agent. Yet, the molecular mechanism by which a small molecule reductant or reductase might facilitate reduction of the heme Fe(III) complex to the heme Fe(II) complex remains elusive.

(4) Heme-based gas sensors can also be converted into heme sensors when the heme Fe(II) complex is changed to the heme Fe(III) complex under oxidative stress conditions through (auto)oxidation, the converse of characteristic (3). NO might act as the oxidizing agent under nitrosive/oxidative conditions.

(5) Results obtained for *Ec*DOS and YddV suggest that incorporation of a heme iron complex in heme-based gas sensors may serve to suppress catalysis, with gas binding acting to release catalytic suppression.[116,120,123] However, this is not always the case because the heme-free forms of *Ax*PEA1[131] and HemAC-*Lm*[133] have very low catalytic activities. It is possible that binding of the heme iron complex is needed to form a protein structure appropriate for optimal signal transduction or catalytic functions.

8. CONCERNS THAT NEED TO BE ADDRESSED

There is considerable confusion in understanding the differences between heme-responsive heme sensors and heme-based gas sensors. For heme-responsive heme sensors, the association/dissociation of the heme iron complex to/from the protein regulate(s) its functions, including catalytic reactions (such as kinase and proteolysis) or DNA binding. Indeed, the association/dissociation of the "heme Fe(III) complex" to/from the protein has been studied in several cases. In contrast, gas molecules such as O_2 and CO bind only to the "heme Fe(II) complex". Therefore, under reducing conditions, a heme-responsive heme sensor can be converted into a heme-based gas sensor. However, it is not clear which reductase or reductant (substance or chemical) is involved in the reduction of the heme Fe(III) complex to the heme Fe(II) complex present in some heme-based gas sensors. For example, NPAS2 was first reported to be a heme-based CO sensor.[363] Later, however, NPAS2 was found to have an additional function as a heme-responsive heme sensor, in that the association/dissociation of the heme Fe(III) complex regulates DNA binding of this protein,[366] but the reductase or reductant of the heme-bound protein has not been identified. For many sensors, this point is elusive and requires exploration in greater detail.

Similar confusion is present for heme-redox sensors, because it is not clear whether the redox sensor is an actual redox sensor or a heme-based oxygen sensor. It is not practical for many laboratories to take advantage of anaerobic conditions, making it difficult to isolate and separate the heme Fe(II) or Fe(II)−O_2 complex as the active species under aerobic conditions. In addition, some heme Fe(II)−O_2 complexes are unstable, resulting in rapid conversion to the heme Fe(III) complex except when the heme iron complex has a high redox potential. Thus, it is only possible to determine the real active heme species (heme Fe(II), Fe(II)−O_2, or Fe(III) complex) of the redox sensor when the reconstituted system can be used under anaerobic conditions.

Many more careful studies of systems reconstituted from purified proteins are needed to unequivocally understand the molecular mechanisms of heme-responsive heme sensors and heme-based gas sensors. Solid and reliable conclusions require combined studies conducted from both biological and chemical points of view.

9. PERSPECTIVES

The molecular mechanisms of heme-based gas sensors have attracted considerable research attention from microbiologists, biophysicists, biochemists, and bioinorganic chemists. Crystal structures for some bacterial and archeae heme-based gas sensors have been solved, reflecting the relative ease of overexpressing and purifying bacterial gas-sensing proteins in *E. coli* as compared to related proteins from eukaryotic systems. However, medical professionals often ask, what are the heme-

DOI: 10.1021/acs.chemrev.5b00018
Chem. Rev. 2015, 115, 6491−6533

based gas sensors in humans or higher organisms and how do they act to regulate important physiological functions? This interest is natural and reflects a desire to solve clinical problems of unknown cause combined with a sense that some serious diseases might be associated with heme iron complexes and gaseous molecules. This is in fact a valid perspective because human sGC and CBS are really heme-based NO or CO sensors whose impairment can cause serious diseases associated with their enzymatic functions.[399] Because new heme proteins with novel features are continuously being discovered, it is expected that future studies will reveal additional important heme-based, disease-associated gas sensors. However, bacterial heme-containing sensor proteins are also important subjects of investigation in a clinical context because they represent interesting targets for the generation of new antibacterial and antimicrobial drugs with minimal side effects on eukaryotic organisms.

AUTHOR INFORMATION

Corresponding Authors

*Tel./fax: +81-22-378-3985. E-mail: shimizu@tagen.tohoku.ac.jp.
*Tel.: +420-22-195-1242. Fax: +420-22-195-1283. E-mail: marketa.martinkova@natur.cuni.cz.

Notes

The authors declare no competing financial interest.

Biographies



Toru Shimizu received his B.S., M.S., and Ph.D. degrees in chemistry from Tohoku University, Sendai, Japan. After several years as a postdoctoral researcher at Albert Einstein College of Medicine, New York, with Jack Peisach, and Keio University School of Medicine, Tokyo, with Yuzuru Ishimura, he returned to Tohoku University where he held the positions of Associate Professor and Professor before retiring in 2012. He is now a Professor Emeritus of Tohoku University, Professor of Shantou University Medical College, Visiting Professor of Charles University in Prague, and Visiting Researcher of AIST. He won the Academic Award from the Chemical Society of Japan in 1991. His main research interest is the structure and function relationships of heme-sensor proteins.



Donyang Huang received a B.S. in clinical medicine from China Medical University, Shenyang, China, in 1984 and a Ph.D. in biochemistry from Kagawa Medical University, Takamatsu, Japan, in 1997. While at Kagawa Medical University, he received a fellowship from the Japan Society for the Promotion Science (JSPS). After several years working as an Assistant Lecturer, Lecturer, and Professor at China Medical University, he became a faculty member of Shantou University Medical College in 2002. He is now Chairperson and Professor of Cell Biology and Genetics and Executive Associate Dean of Shantou University Medical College, China. In cooperation with Toru Shimizu, he is conducting research in the field of heme-based O_2 sensors.



Fan Yang received a B.S. in pharmacy from Henan University, Kaifeng, China, in 2012. She is now undertaking a Master's degree at Shantou University Medical College. Her main research interests are the H_2S-induced structural and catalytic changes of the heme-based O_2 sensor phosphodiesterase, *Ec*DOS.



Martin Stranava received a M.S. in biochemistry from Charles University in Prague. His diploma thesis was dedicated to the

DOI: 10.1021/acs.chemrev.5b00018
Chem. Rev. 2015, 115, 6491−6533

preparation, purification, and enzymatic characterization of cytochrome P450 reductase, a protein involved in xenobiotic metabolism. Currently he is a Ph.D. student in the laboratory of Markéta Martínková and, in cooperation with Toru Shimizu, is investigating the heme sensor proteins YddV and *Af*GcHK.



Martina Bartosova studied the properties of medicinal plants during her Bachelor studies. She focused on the NADP/dehydrogenase activity and contents of phenolic compounds and flavonoids in medicinal plants. During her Master's studies, she focused on the heme sensor protein *Af*GcHK and its interaction with sodium sulfide. She now works at SOTIO, a Czech biotechnological company.



Veronika Fojtíková completed a Master's Degree in Science at Charles University in Prague in 2014, specializing in clinical and toxicological analysis. During her studies, she focused on the biochemistry of regulation and influence of exogenous conditions, applied analytical chemistry, toxicokinetics, and pharmacology. The aim of her Master's studies was to determine the kinetics parameters of the reaction catalyzed by the globin coupled histidine kinase, *Af*GcHK. Currently she is a Ph.D. student in the Department of Biochemistry, Charles University in Prague. She is interested in heme-containing gas sensing proteins and their properties.



Markéta Martínková received a Ph.D. degree in 2003 from Charles University in Prague for her work on cytochromes P450 and peroxidases from an enzymology perspective. In 2004, she was awarded a postdoctoral fellowship by the Japan Society for the Promotion of Science (JSPS) to work on heme-containing sensor proteins at the laboratory of Toru Shimizu (Tohoku University, Sendai). Currently, she is an Associate Professor of Biochemistry at the Department of Biochemistry, Faculty of Science, Charles University in Prague, and a Vice-Dean of the same faculty. Her professional interests lie in the characterization of various hemoproteins, including heme-based gas sensors.

ACKNOWLEDGMENTS

This work was supported in part by Grants-in-Aid from Shantou University Medical College, National Natural Science Foundation of China (NSFC) (no. 31170736, no. 31371333), Guangdong Natural Science Foundation (no. S2012030006289), Charles University in Prague (UNCE 204025/2012), Grant Agency of the Czech Republic (grant 15-19883S), and Grant Agency of Charles University in Prague (grants 756214 and 362115).

ABBREVIATIONS

Aer2	aerotaxis transducer
AppA	antirepressor of PpsR from *Rhodobacter sphaeroides*
BLUF	sensors of blue light using FAD
CAP	catabolite activator protein
CBS	cystathionine β-synthase
c-di-GMP	cyclic-di-GMP or bis(3′-5′)-cyclic dimeric guanosine monophosphate
CheA/CheY	two-component signal transduction system involved in bacterial aerotaxis
CODH	carbon monoxide dehydrogenase
CooA	a heme-regulated CO-sensing transcriptional factor (e.g., *Rr*CooA from *Rhodospirillum rubrum* and *Ch*CooA from *Carboxydothermus hydrogenoformans*)
CRP	cAMP receptor protein (a cAMP-dependent transcriptional regulator)
CRP-FNR	cAMP receptor protein/fumarate and nitrate reductase regulator
DGC	diguanylate cyclase
DNR	dissimilative nitrate respiration regulator
DosS/DosT	O_2 sensor histidine kinases
DosR	DNA-binding transcriptional regulator (effector of DosS/DosT)

DOI: 10.1021/acs.chemrev.5b00018
Chem. Rev. 2015, 115, 6491−6533

*Ec*DOS	*E. coli* direct oxygen sensor (heme-regulated O_2 sensor phosphodiesterase), also designated *Ec*DosP
*Ec*DosC	heme-based oxygen sensor diguanylate cyclase from *E. coli*, also designated YddV
*Ec*DosP	heme-regulated O_2 sensor phosphodiesterase from *E. coli*, also designated *Ec*DOS
EM	single-particle electron microscopy
EPR	electron paramagnetic resonance
EXAFS	extended X-ray absorption fine structure
FixL	two-component O_2-sensor histidine kinase, for example, from *R. meliloti* (*Rm*FixL) or *B. japonicum* (*Bj*FixL)
FixJ	cognate response regulator of FixL
FRET	Förster (or fluorescence) resonance energy transfer
FTIR	Fourier transform infrared spectroscopy
GAF	cGMP-specific and -stimulated phosphodiesterase, adenylate cyclase, and *E. coli* formate hydrogen lyase transcriptional activator
GcHK	globin-coupled histidine kinase (e.g., *Af*GcHK from *Anaeromyxobacter* sp. Fw109-5)
GCS	globin-coupled O_2 sensor
GReg	globin-coupled regulator (O_2-sensor with DGC activity; e.g., *Av*GReg from *Azotobacter vinelandii* and *Bpe*GReg from *Bordetella pertussis*)
HaCE	H-NOX-associated cyclic-di-GMP processing enzyme
HAMP	histidine kinase, adenylate cyclase, methyl accepting protein, and phosphatase
Hb	hemoglobin
HDX-MS	hydrogen/deuterium exchange mass spectrometry
HemAC-*Lm*	a globin-coupled O_2-sensor adenylate cyclase from *Leishmania major*
HemAT	a globin-coupled O_2-sensor MCP from *Halobacterium salinarum* and *Bacillus subtilis*
HemDGC	heme-containing DGC
heme Fe(III)	protoporphyrin IX-ferric complex (hemin)
heme Fe(II)	protoporphyrin IX-ferrous complex
HK	histidine kinase
H-NOX	heme-nitric oxide/oxygen binding domain/protein
K_a	equilibrium association constant
K_d	equilibrium dissociation constant
k_{ox}	autoxidation rate constant
k_{off}	dissociation rate constant
k_{on}	association rate constant
l-di-GMP	linear-di-GMP (pGpG)
MALDI-TOF	matrix-assisted laser desorption/ionization-time of flight
Mant-NTP	(*N*-methyl)anthraniloyl-substituted nucleotide
*Ma*Pgb	protoglobin from *Methanosarcina acetivorans* C2A
Mb	myoglobin
MCP	methyl-accepting chemotaxis protein
NMR	nuclear magnetic resonance
NtrY/NtrX	nitrogen regulation proteins
PAS	Per (*Drosophila* period clock protein), Arnt (vertebrate aryl hydrocarbon receptor nuclear translocator), and Sim (*Drosophila* single-minded protein)
PDE	phosphodiesterase
RcoM	a prokaryotic regulator of CO metabolism
PDEA1	phosphodiesterase A1 (e.g., *Ax*PDEA1 from *Acetobacter xylinum*)
RR	resonance Raman spectroscopy
SAXS	small-angle X-ray scattering
SCHIC	sensor containing heme instead of cobalamin
$SONO_{HD}$	sensor of NO heme domain (e.g., TT-$SONO_{HD}$ from *T. tengcongensis* and CB-$SONO_{HD}$ from *Clostridium botulinum*)
SW Mb	sperm whale myoglobin
sGC	soluble guanylate cyclase
YddV	see *Ec* DosC

REFERENCES

(1) Antonini, E. B.; Brunori, M. *Hemoglobin and Myoglobin in Their Reactions with Ligands*; North-Holland: Amsterdam, 1971.
(2) Guengerich, F. P. New Trends in Cytochrome P450 Research at the Half-Century Mark. *J. Biol. Chem.* **2013**, *288*, 17063−17064.
(3) Guengerich, F. P.; Munro, A. W. Unusual Cytochrome P450 Enzymes and Reactions. *J. Biol. Chem.* **2013**, *288*, 17065−17073.
(4) Ortiz de Montellano, P. R. Hydrocarbon Hydroxylation by Cytochrome P450 Enzymes. *Chem. Rev.* **2010**, *110*, 932−948.
(5) Ortiz de Montellano, P. R., Ed. *Cytochrome P450: Structure, Mechanism, and Biochemistry*, 3rd ed.; Kluwer Academic/Plenum: New York, 2005.
(6) Poulos, T. L. Heme Enzyme Structure and Function. *Chem. Rev.* **2014**, *114*, 3919−3962.
(7) Smith, A. T.; Pazicni, S.; Marvin, K. A.; Stevens, D. J.; Paulsen, K. M.; Burstyn, J. N. Functional Divergence of Heme-Thiolate Proteins: A Classification Based on Spectroscopic Attributes. *Chem. Rev.* **2015**, *115*, 2532−2558.
(8) Voet, D.; Voet, J. G. *Biochemistry*, 4th ed.; John Wiley & Sons: New York, 2011.
(9) Cary, S. P. L.; Winger, J. A.; Derbyshire, E. R.; Marletta, M. A. Nitric Oxide Signaling: No Longer Simply on or off. *Trends Biochem. Sci.* **2006**, *31*, 231−239.
(10) Cooper, C. E. Nitric Oxide and Cytochrome Oxidase: Substrate, Inhibitor or Effector? *Trends Biochem. Sci.* **2002**, *27*, 33−39.
(11) De Mel, A.; Murad, F.; Seifalian, A. M. Nitric Oxide: A Guardian for Vascular Grafts? *Chem. Rev.* **2011**, *111*, 5742−5767.
(12) Fukuto, J. M.; Carrington, S. J.; Tantillo, D. J.; Harrison, J. G.; Ignarro, L. J.; Freeman, B. A.; Chen, A.; Wink, D. A. Small Molecule Signaling Agents: The Integrated Chemistry and Biochemistry of Nitrogen Oxides, Oxides of Carbon, Dioxygen, Hydrogen Sulfide, and Their Derived Species. *Chem. Res. Toxicol.* **2012**, *25*, 769−793.
(13) Gullotta, F.; di Masi, A.; Coletta, M.; Ascenzi, P. CO Metabolism, Sensing, and Signaling. *BioFactors* **2012**, *38*, 1−13.
(14) Hill, B. G.; Dranka, B. P.; Bailey, S. M.; Lancaster, J. R., Jr.; Darley-Usmar, V. M. What Part of NO Don't You Understand? Some Answers to the Cardinal Questions in Nitric Oxide Biology. *J. Biol. Chem.* **2010**, *285*, 19699−19704.
(15) Leiper, J.; Nandi, M. The Therapeutic Potential of Targeting Endogenous Inhibitors of Nitric Oxide Synthesis. *Nat. Rev. Drug Discovery* **2011**, *10*, 277−291.
(16) Motterlini, R.; Otterbein, L. E. The Therapeutic Potential of Carbon Monoxide. *Nat. Rev. Drug Discovery* **2010**, *9*, 728−743.
(17) Mustafa, A. K.; Gadalla, M. M.; Snyder, S. H. Signaling by Gasotransmitters. *Sci. Signaling* **2009**, *2*, re2.
(18) Prabhakar, N. R.; Semenza, G. L. Gaseous Messengers in Oxygen Sensing. *J. Mol. Med.* **2012**, *90*, 265−272.
(19) Rochette, L.; Cottin, Y.; Zeller, M.; Vergely, C. Carbon Monoxide: Mechanisms of Action and Potential Clinical Implications. *Pharmacol. Ther.* **2013**, *137*, 133−152.
(20) Stuehr, D. J.; Tejero, J.; Haque, M. M. Structural and Mechanistic Aspects of Flavoproteins: Electron Transfer through the Nitric Oxide Synthase Flavoprotein Domain. *FEBS J.* **2009**, *276*, 3959−3974.

DOI: 10.1021/acs.chemrev.5b00018
Chem. Rev. 2015, 115, 6491−6533

(21) Tejero, J.; Stuehr, D. Tetrahydrobiopterin in Nitric Oxide Synthase. *IUBMB Life* **2013**, *65*, 358−365.
(22) Toledo, J. C., Jr.; Augusto, O. Connecting the Chemical and Biological Properties of Nitric Oxide. *Chem. Res. Toxicol.* **2012**, *25*, 975−989.
(23) Gardner, P. R.; Gardner, A. M.; Brashear, W. T.; Suzuki, T.; Hvitved, A. N.; Setchell, K. D. R.; Olson, J. S. Hemoglobins Dioxygenate Nitric Oxide with High Fidelity. *J. Inorg. Biochem.* **2006**, *100*, 542−550.
(24) Yukl, E. T.; de Vries, S.; Moënne-Loccoz, P. The Millisecond Intermediate in the Reaction of Nitric Oxide with Oxymyoglobin Is an Iron(III)-Nitrate Complex, Not a Peroxynitrite. *J. Am. Chem. Soc.* **2009**, *131*, 7234−7235.
(25) Gladwin, M. T.; Grubina, R.; Doyle, M. P. The New Chemical Biology of Nitrite Reactions with Hemoglobin: R-State Catalysis, Oxidative Denitrosylation, and Nitrite Reductase/anhydrase. *Acc. Chem. Res.* **2009**, *42*, 157−167.
(26) Gladwin, M. T.; Kim-Shapiro, D. B. The Functional Nitrite Reductase Activity of the Heme-Globins. *Blood* **2008**, *112*, 2636−2647.
(27) Lundberg, J. O.; Weitzberg, E.; Gladwin, M. T. The Nitrate-Nitrite-Nitric Oxide Pathway in Physiology and Therapeutics. *Nat. Rev. Drug Discovery* **2008**, *7*, 156−167.
(28) Carballal, S.; Bartesaghi, S.; Radi, R. Kinetic and Mechanistic Considerations to Assess the Biological Fate of Peroxynitrite. *Biochim. Biophys. Acta* **2014**, *1840*, 768−780.
(29) Szabo, C.; Ischiropoulos, H.; Radi, R. Peroxynitrite: Biochemistry, Pathophysiology and Development of Therapeutics. *Nat. Rev. Drug Discovery* **2007**, *6*, 662−680.
(30) Haldar, S. M.; Stamler, J. S. S-Nitrosylation: Integrator of Cardiovascular Performance and Oxygen Delivery. *J. Clin. Invest.* **2013**, *123*, 101−110.
(31) Hess, D. T.; Stamler, J. S. Regulation by S-Nitrosylation of Protein Post-Translational Modification. *J. Biol. Chem.* **2012**, *287*, 4411−4418.
(32) Seth, D.; Stamler, J. S. The SNO-Proteome: Causation and Classifications. *Curr. Opin. Chem. Biol.* **2011**, *15*, 129−136.
(33) Crack, J. C.; Green, J.; Thomson, A. J.; Le Brun, N. E. Iron-Sulfur Clusters as Biological Sensors: The Chemistry of Reactions with Molecular Oxygen and Nitric Oxide. *Acc. Chem. Res.* **2014**, *47*, 3196−3205.
(34) Aono, S. Metal-Containing Sensor Proteins Sensing Diatomic Gas Molecules. *Dalton Trans.* **2008**, *24*, 3137−3146.
(35) Aono, S. Novel Bacterial Gas Sensor Proteins with Transition Metal-Containing Prosthetic Groups as Active Sites. *Antioxid. Redox Signaling* **2012**, *16*, 678−686.
(36) Derbyshire, E. R.; Marletta, M. A. Structure and Regulation of Soluble Guanylate Cyclase. *Annu. Rev. Biochem.* **2012**, *81*, 533−559.
(37) Farhana, A.; Saini, V.; Kumar, A.; Lancaster, J. R., Jr.; Steyn, A. J. C. Environmental Heme-Based Sensor Proteins: Implications for Understanding Bacterial Pathogenesis. *Antioxid. Redox Signaling* **2012**, *17*, 1232−1245.
(38) Freitas, T. A. K.; Hou, S.; Alam, M. The Diversity of Globin-Coupled Sensors. *FEBS Lett.* **2003**, *552*, 99−104.
(39) Freitas, T. A. K.; Saito, J. A.; Hou, S.; Alam, M. Globin-Coupled Sensors, Protoglobins, and the Last Universal Common Ancestor. *J. Inorg. Biochem.* **2005**, *99*, 23−33.
(40) Germani, F.; Moens, L.; Dewilde, S. Haem-Based Sensors: A Still Growing Old Superfamily. *Adv. Microb. Physiol.* **2013**, *63*, 1−47.
(41) Gilles-Gonzalez, M. A. Oxygen Signal Transduction. *IUBMB Life* **2001**, *51*, 165−173.
(42) Gilles-Gonzalez, M. A.; Gonzalez, G. Signal Transduction by Heme-Containing PAS-Domain Proteins. *J. Appl. Physiol.* **2004**, *96*, 774−783.
(43) Gilles-Gonzalez, M. A.; Gonzalez, G. Heme-Based Sensors: Defining Characteristics, Recent Developments, and Regulatory Hypotheses. *J. Inorg. Biochem.* **2005**, *99*, 1−22.
(44) Girvan, H. M.; Munro, A. W. Heme Sensor Proteins. *J. Biol. Chem.* **2013**, *288*, 13194−13203.
(45) Green, J.; Crack, J. C.; Thomson, A. J.; LeBrun, N. E. Bacterial Sensors of Oxygen. *Curr. Opin. Microbiol.* **2009**, *12*, 145−151.
(46) Igarashi, J.; Kitanishi, K.; Shimizu, T. Emerging Roles of Heme as a Signal and a Gas-Sensing Site: Heme-Sending and Gas-Sending Proteins. In *Handbook of Porphyrin Science*; Kadish, K. M., Smith, K. M., Guilard, R., Eds.; World Scientific Publishing: Hackensack, 2011; Vol. *15*, pp 399−460.
(47) Jain, R.; Chan, M. K. Mechanisms of Ligand Discrimination by Heme Proteins. *J. Biol. Inorg. Chem.* **2003**, *8*, 1−11.
(48) Liebl, U.; Lambry, J. C.; Vos, M. H. Primary Processes in Heme-Based Sensor Proteins. *Biochim. Biophys. Acta* **2013**, *1834*, 1684−1692.
(49) Henry, J. T.; Crosson, S. Ligand-Binding PAS Domains in a Genomic, Cellular, and Structural Context. *Annu. Rev. Microbiol.* **2011**, *65*, 261−286.
(50) Martínková, M.; Kitanishi, K.; Shimizu, T. Heme-Based Globin-Coupled Oxygen Sensors: Linking Oxygen Binding to Functional Regulation of Diguanylate Cyclase, Histidine Kinase, and Methyl-Accepting Chemotaxis. *J. Biol. Chem.* **2013**, *288*, 27702−27711.
(51) Kurokawa, H.; Lee, D. S.; Watanabe, M.; Sagami, I.; Mikami, B.; Raman, C. S.; Shimizu, T. A Redox-Controlled Molecular Switch Revealed by the Crystal Structure of a Bacterial Heme PAS Sensor. *J. Biol. Chem.* **2004**, *279*, 20186−20193.
(52) Roberts, G. P.; Youn, H.; Kerby, R. L. CO-Sensing Mechanisms. *Microbiol. Mol. Biol. Rev.* **2004**, *68*, 453−473.
(53) Sasakura, Y.; Yoshimura-Suzuki, T.; Kurokawa, H.; Shimizu, T. Structure-Function Relationships of *Ec*DOS, a Heme-Regulated Phosphodiesterase from *Escherichia coli*. *Acc. Chem. Res.* **2006**, *39*, 37−43.
(54) Shimizu, T. The Heme-Based Oxygen-Sensor Phosphodiesterase *Ec* DOS (DosP): Structure-Function Relationships. *Biosensors* **2013**, *3*, 211−237.
(55) Uchida, T.; Kitagawa, T. Mechanism for Transduction of the Ligand-Binding Signal in Heme-Based Gas Sensory Proteins Revealed by Resonance Raman Spectroscopy. *Acc. Chem. Res.* **2005**, *38*, 662−670.
(56) Plate, L.; Marletta, M. A. Nitric Oxide-Sensing H-NOX Proteins Govern Bacterial Communal Behavior. *Trends Biochem. Sci.* **2013**, *38*, 566−575.
(57) Moskvin, O. V.; Kaplan, S.; Gilles-Gonzalez, M. A.; Gomelsky, M. Novel Heme-Based Oxygen Sensor with a Revealing Evolutionary History. *J. Biol. Chem.* **2007**, *282*, 28740−28748.
(58) Tsai, A. L.; Martin, E.; Berka, V.; Olson, J. S. How Do Heme-Protein Sensors Exclude Oxygen? Lessons Learned from Cytochrome c′, *Nostoc puntiforme* Heme Nitric Oxide/oxygen-Binding Domain, and Soluble Guanylyl Cyclase. *Antioxid. Redox Signaling* **2012**, *17*, 1246−1263.
(59) Wu, G.; Liu, W.; Berka, V.; Tsai, A. L. The Selectivity of *Vibrio cholerae* H-NOX for Gaseous Ligands Follows the "Sliding Scale Rule" Hypothesis. Ligand Interactions with Both Ferrous and Ferric *Vc* H-NOX. *Biochemistry* **2013**, *52*, 9432−9446.
(60) Aono, S. The Dos Family of Globin-Related Sensors Using PAS Domains to Accommodate Haem Acting as the Active Site for Sensing External Signals. *Adv. Microb. Physiol.* **2013**, *63*, 273−327.
(61) DeMille, D.; Grose, J. H. PAS Kinase: A Nutrient Sensing Regulator of Glucose Homeostasis. *IUBMB Life* **2013**, *65*, 921−929.
(62) Grose, J. H.; Rutter, J. The Role of PAS Kinase in PASsing the Glucose Signal. *Sensors* **2010**, *10*, 5668−5682.
(63) Haase, V. H. Regulation of Erythropoiesis by Hypoxia-Inducible Factors. *Blood Rev.* **2013**, *27*, 41−53.
(64) McIntosh, B. E.; Hogenesch, J. B.; Bradfield, C. A. Mammalian Per-Arnt-Sim Proteins in Environmental Adaptation. *Annu. Rev. Physiol.* **2010**, *72*, 625−645.
(65) Taylor, B. L.; Zhulin, I. B. PAS Domains: Internal Sensors of Oxygen, Redox Potential, and Light. *Microbiol. Mol. Biol. Rev.* **1999**, *63*, 479−506.
(66) Gilles-Gonzalez, M. A.; Ditta, G. S.; Helinski, D. R. A Haemoprotein with Kinase Activity Encoded by the Oxygen Sensor of *Rhizobium meliloti*. *Nature* **1991**, *350*, 170−172.

DOI: 10.1021/acs.chemrev.5b00018
Chem. Rev. 2015, 115, 6491−6533

(67) Casino, P.; Rubio, V.; Marina, A. The Mechanism of Signal Transduction by Two-Component Systems. *Curr. Opin. Struct. Biol.* **2010**, *20*, 763−771.
(68) Cheng, R. R.; Morcos, F.; Levine, H.; Onuchic, J. N. Toward Rationally Redesigning Bacterial Two-Component Signaling Systems Using Coevolutionary Information. *Proc. Natl. Acad. Sci. U.S.A.* **2014**, *111*, E563−E571.
(69) Crosson, S.; McGrath, P. T.; Stephens, C.; McAdams, H. H.; Shapiro, L. Conserved Modular Design of an Oxygen Sensory/signaling Network with Species-Specific Output. *Proc. Natl. Acad. Sci. U.S.A.* **2005**, *102*, 8018−8023.
(70) Ioanoviciu, A.; Yukl, E. T.; Moënne-Loccoz, P.; Ortiz de Montellano, P. R. DevS, a Heme-Containing Two-Component Oxygen Sensor of *Mycobacterium tuberculosis*. *Biochemistry* **2007**, *46*, 4250−4260.
(71) Kumar, A.; Toledo, J. C., Jr.; Patel, R. P.; Lancaster, J. R., Jr.; Steyn, A. J. C. *Mycobacterium tuberculosis* DosS Is a Redox Sensor and DosT Is a Hypoxia Sensor. *Proc. Natl. Acad. Sci. U.S.A.* **2007**, *104*, 11568−11573.
(72) Sousa, E. H. S.; Tuckerman, J. R.; Gonzalez, G.; Gilles-Gonzalez, M. A. DosT and DevS Are Oxygen-Switched Kinases in *Mycobacterium tuberculosis*. *Protein Sci.* **2007**, *16*, 1708−1719.
(73) Kitanishi, K.; Kobayashi, K.; Uchida, T.; Ishimori, K.; Igarashi, J.; Shimizu, T. Identification and Functional and Spectral Characterization of a Globin-Coupled Histidine Kinase from *Anaeromyxobacter* sp. Fw109−5. *J. Biol. Chem.* **2011**, *286*, 35522−35534.
(74) Carrica, M. C.; Fernandez, I.; Martí, M. A.; Paris, G.; Goldbaum, F. A. The NtrY/X Two-Component System of *Brucella* spp. Acts as a Redox Sensor and Regulates the Expression of Nitrogen Respiration Enzymes. *Mol. Microbiol.* **2012**, *85*, 39−50.
(75) Kurashima-Ito, K.; Kasai, Y.; Hosono, K.; Tamura, K.; Oue, S.; Isogai, M.; Ito, Y.; Nakamura, H.; Shiro, Y. Solution Structure of the C-Terminal Transcriptional Activator Domain of FixJ from *Sinorhizobium meliloti* and Its Recognition of the fixK Promoter. *Biochemistry* **2005**, *44*, 14835−14844.
(76) Saito, K.; Ito, E.; Hosono, K.; Nakamura, K.; Imai, K.; Iizuka, T.; Shiro, Y.; Nakamura, H. The Uncoupling of Oxygen Sensing, Phosphorylation Signalling and Transcriptional Activation in Oxygen Sensor FixL and FixJ Mutants. *Mol. Microbiol.* **2003**, *48*, 373−383.
(77) Sousa, E. H. S.; Gonzalez, G.; Gilles-Gonzalez, M. A. Oxygen Blocks the Reaction of the FixL-FixJ Complex with ATP but Does Not Influence Binding of FixJ or ATP to FixL. *Biochemistry* **2005**, *44*, 15359−15365.
(78) Tuckerman, J. R.; Gonzalez, G.; Gilles-Gonzalez, M. A. Complexation Precedes Phosphorylation for Two-Component Regulatory System FixL/FixJ of *Sinorhizobium meliloti*. *J. Mol. Biol.* **2001**, *308*, 449−455.
(79) Sousa, E. H. S.; Tuckerman, J. R.; Gonzalez, G.; Gilles-Gonzalez, M. A. A Memory of Oxygen Binding Explains the Dose Response of the Heme-Based Sensor FixL. *Biochemistry* **2007**, *46*, 6249−6257.
(80) Nakamura, H.; Kumita, H.; Imai, K.; Iizuka, T.; Shiro, Y. ADP Reduces the Oxygen-Binding Affinity of a Sensory Histidine Kinase, FixL: The Possibility of an Enhanced Reciprocating Kinase Reaction. *Proc. Natl. Acad. Sci. U.S.A.* **2004**, *101*, 2742−2746.
(81) Gong, W.; Hao, B.; Mansy, S. S.; Gonzalez, G.; Gilles-Gonzalez, M. A.; Chan, M. K. Structure of a Biological Oxygen Sensor: A New Mechanism for Heme-Driven Signal Transduction. *Proc. Natl. Acad. Sci. U.S.A.* **1998**, *95*, 15177−15182.
(82) Gong, W.; Hao, B.; Chan, M. K. New Mechanistic Insights from Structural Studies of the Oxygen-Sensing Domain of *Bradyrhizobium japonicum* FixL. *Biochemistry* **2000**, *39*, 3955−3962.
(83) Hao, B.; Isaza, C.; Arndt, J.; Soltis, M.; Chan, M. K. Structure-Based Mechanism of O_2 Sensing and Ligand Discrimination by the FixL Heme Domain of *Bradyrhizobium japonicum*. *Biochemistry* **2002**, *41*, 12952−12958.
(84) Miyatake, H.; Mukai, M.; Park, S. Y.; Adachi, S.; Tamura, K.; Nakamura, H.; Nakamura, K.; Tsuchiya, T.; Iizuka, T.; Shiro, Y. Sensory Mechanism of Oxygen Sensor FixL from *Rhizobium meliloti*: Crystallographic, Mutagenesis and Resonance Raman Spectroscopic Studies. *J. Mol. Biol.* **2000**, *301*, 415−431.
(85) Park, H.; Suquet, C.; Satterlee, J. D.; Kang, C. Insights into Signal Transduction Involving PAS Domain Oxygen-Sensing Heme Proteins from the X-Ray Crystal Structure of *Escherichia coli* Dos Heme Domain (*Ec* DosH). *Biochemistry* **2004**, *43*, 2738−2746.
(86) Mukai, M.; Nakamura, K.; Nakamura, H.; Iizuka, T.; Shiro, Y. Roles of Ile209 and Ile210 on the Heme Pocket Structure and Regulation of Histidine Kinase Activity of Oxygen Sensor FixL from *Rhizobium meliloti*. *Biochemistry* **2000**, *39*, 13810−13816.
(87) Key, J.; Moffat, K. Crystal Structures of Deoxy and CO-Bound *bj*FixLH Reveal Details of Ligand Recognition and Signaling. *Biochemistry* **2005**, *44*, 4627−4635.
(88) Key, J.; Srajer, V.; Pahl, R.; Moffat, K. Time-Resolved Crystallographic Studies of the Heme Domain of the Oxygen Sensor FixL: Structural Dynamics of Ligand Rebinding and Their Relation to Signal Transduction. *Biochemistry* **2007**, *46*, 4706−4715.
(89) Miyatake, H.; Mukai, M.; Adachi, S.; Nakamura, H.; Tamura, K.; Iizuka, T.; Shiro, Y.; Strange, R. W.; Hasnain, S. S. Iron Coordination Structures of Oxygen Sensor FixL Characterized by Fe K-Edge Extended X-Ray Absorption Fine Structure and Resonance Raman Spectroscopy. *J. Biol. Chem.* **1999**, *274*, 23176−23184.
(90) Hiruma, Y.; Kikuchi, A.; Tanaka, A.; Shiro, Y.; Mizutani, Y. Resonance Raman Observation of the Structural Dynamics of FixL on Signal Transduction and Ligand Discrimination. *Biochemistry* **2007**, *46*, 6086−6096.
(91) Jasaitis, A.; Hola, K.; Bouzhir-Sima, L.; Lambry, J. C.; Balland, V.; Vos, M. H.; Liebl, U. Role of Distal Arginine in Early Sensing Intermediates in the Heme Domain of the Oxygen Sensor FixL. *Biochemistry* **2006**, *45*, 6018−6026.
(92) Kruglik, S. G.; Jasaitis, A.; Hola, K.; Yamashita, T.; Liebl, U.; Martin, J. L.; Vos, M. H. Subpicosecond Oxygen Trapping in the Heme Pocket of the Oxygen Sensor FixL Observed by Time-Resolved Resonance Raman Spectroscopy. *Proc. Natl. Acad. Sci. U.S.A.* **2007**, *104*, 7408−7413.
(93) Balland, V.; Bouzhir-Sima, L.; Kiger, L.; Marden, M. C.; Vos, M. H.; Liebl, U.; Mattioli, T. A. Role of Arginine 220 in the Oxygen Sensor FixL from *Bradyrhizobium japonicum*. *J. Biol. Chem.* **2005**, *280*, 15279−15288.
(94) Nuernberger, P.; Lee, K. F.; Bonvalet, A.; Bouzhir-Sima, L.; Lambry, J. C.; Liebl, U.; Joffre, M.; Vos, M. H. Strong Ligand-Protein Interactions Revealed by Ultrafast Infrared Spectroscopy of CO in the Heme Pocket of the Oxygen Sensor FixL. *J. Am. Chem. Soc.* **2011**, *133*, 17110−17113.
(95) Balland, V.; Bouzhir-Sima, L.; Anxolabéhère-Mallart, E.; Boussac, A.; Vos, M. H.; Liebl, U.; Mattioli, T. A. Functional Implications of the Propionate 7-Arginine 220 Interaction in the FixLH Oxygen Sensor from *Bradyrhizobium japonicum*. *Biochemistry* **2006**, *45*, 2072−2084.
(96) Miksovská, J.; Suquet, C.; Satterlee, J. D.; Larsen, R. W. Characterization of Conformational Changes Coupled to Ligand Photodissociation from the Heme Binding Domain of FixL. *Biochemistry* **2005**, *44*, 10028−10036.
(97) Tanaka, A.; Nakamura, H.; Shiro, Y.; Fujii, H. Roles of the Heme Distal Residues of FixL in O_2 Sensing: A Single Convergent Structure of the Heme Moiety Is Relevant to the Downregulation of Kinase Activity. *Biochemistry* **2006**, *45*, 2515−2523.
(98) Gilles-Gonzalez, M. A.; Caceres, A. I.; Sousa, E. H. S.; Tomchick, D. R.; Brautigam, C.; Gonzalez, C.; Machius, M. A Proximal Arginine R206 Participates in Switching of the *Bradyrhizobium japonicum* FixL Oxygen Sensor. *J. Mol. Biol.* **2006**, *360*, 80−89.
(99) Akimoto, S.; Tanaka, A.; Nakamura, K.; Shiro, Y.; Nakamura, H. O_2-Specific Regulation of the Ferrous Heme-Based Sensor Kinase FixL from *Sinorhizobium meliloti* and Its Aberrant Inactivation in the Ferric Form. *Biochem. Biophys. Res. Commun.* **2003**, *304*, 136−142.
(100) Satterlee, J. D.; Suquet, C.; Bidwai, A. K.; Erman, J. E.; Schwall, L.; Jimenez, R. Mass Instability in Isolated Recombinant FixL Heme Domains of *Bradyrhizobium japonicum*. *Biochemistry* **2008**, *47*, 1540−1553.

DOI: 10.1021/acs.chemrev.5b00018
Chem. Rev. 2015, 115, 6491−6533

(101) Shikama, K. The Molecular Mechanism of Autoxidation for Myoglobin and Hemoglobin: A Venerable Puzzle. *Chem. Rev.* **1998**, *98*, 1357−1374.
(102) Springer, B. A.; Sligar, S. G.; Olson, J. S.; Phillips, G. N., Jr. Mechanisms of Ligand Recognition in Myoglobin. *Chem. Rev.* **1994**, *94*, 699−714.
(103) Dunham, C. M.; Dioum, E. M.; Tuckerman, J. R.; Gonzalez, G.; Scott, W. G.; Gilles-Gonzalez, M. A. A Distal Arginine in Oxygen-Sensing Heme-PAS Domains Is Essential to Ligand Binding, Signal Transduction, and Structure. *Biochemistry* **2003**, *42*, 7701−7708.
(104) Gonzalez, G.; Gilles-Gonzalez, M. A.; Rybak-Akimova, E. V.; Buchalova, M.; Busch, D. H. Mechanisms of Autoxidation of the Oxygen Sensor FixL and *Aplysia* Myoglobin: Implications for Oxygen-Binding Heme Proteins. *Biochemistry* **1998**, *37*, 10188−10194.
(105) Rodgers, K. R.; Lukat-Rodgers, G. S.; Tang, L. Spectroscopic Observation of a FixL Switching Intermediate. *J. Am. Chem. Soc.* **1999**, *121*, 11241−11242.
(106) Rodgers, K. R.; Tang, L.; Lukat-Rodgers, G. S.; Wengenack, N. L. Insights into the Signal Transduction Mechanism of *Rm*FixL Provided by Carbon Monoxide Recombination Kinetics. *Biochemistry* **2001**, *40*, 12932−12942.
(107) Lukat-Rodgers, G. S.; Rodgers, K. R. Characterization of Ferrous FixL-Nitric Oxide Adducts by Resonance Raman Spectroscopy. *Biochemistry* **1997**, *36*, 4178−4187.
(108) Lukat-Rodgers, G. S.; Rexine, J. L.; Rodgers, K. R. Heme Speciation in Alkaline Ferric FixL and Possible Tyrosine Involvement in the Signal Transduction Pathway for Regulation of Nitrogen Fixation. *Biochemistry* **1998**, *37*, 13543−13552.
(109) Kumita, H.; Yamada, S.; Nakamura, H.; Shiro, Y. Chimeric Sensory Kinases Containing O_2 Sensor Domain of FixL and Histidine Kinase Domain from Thermophile. *Biochim. Biophys. Acta* **2003**, *1646*, 136−144.
(110) Hengge, R. Principles of c-di-GMP Signalling in Bacteria. *Nat. Rev. Microbiol.* **2009**, *7*, 263−273.
(111) Malone, J. Bacterial Signalling Mechanisms-Checking out the Neighbourhood. *Biochemist* **2014**, *36*, 20−24.
(112) Römling, U.; Gomelsky, M.; Galperin, M. Y. C-di-GMP: The Dawning of a Novel Bacterial Signalling System. *Mol. Microbiol.* **2005**, *57*, 629−639.
(113) Schirmer, T.; Jenal, U. Structural and Mechanistic Determinants of c-di-GMP Signalling. *Nat. Rev. Microbiol.* **2009**, *7*, 724−735.
(114) Tuckerman, J. R.; Gonzalez, G.; Gilles-Gonzalez, M. A. Cyclic di-GMP Activation of Polynucleotide Phosphorylase Signal-Dependent RNA Processing. *J. Mol. Biol.* **2011**, *407*, 633−639.
(115) Tuckerman, J. R.; Gonzalez, G.; Sousa, E. H. S.; Wan, X.; Saito, J. A.; Alam, M.; Gilles-Gonzalez, M. A. An Oxygen-Sensing Diguanylate Cyclase and Phosphodiesterase Couple for c-di-GMP Control. *Biochemistry* **2009**, *48*, 9764−9774.
(116) Kitanishi, K.; Kobayashi, K.; Kawamura, Y.; Ishigami, I.; Ogura, T.; Nakajima, K.; Igarashi, J.; Tanaka, A.; Shimizu, T. Important Roles of Tyr43 at the Putative Heme Distal Side in the Oxygen Recognition and Stability of the Fe(II)-O_2 Complex of YddV, a Globin-Coupled Heme-Based Oxygen Sensor Diguanylate Cyclase. *Biochemistry* **2010**, *49*, 10381−10393.
(117) Delgado-Nixon, V. M.; Gonzalez, G.; Gilles-Gonzalez, M. A. Dos, a Heme-Binding PAS Protein from *Escherichia coli*, Is a Direct Oxygen Sensor. *Biochemistry* **2000**, *39*, 2685−2691.
(118) Takahashi, H.; Shimizu, T. Phosphodiesterase Activity of *Ec* DOS, a Heme-Regulated Enzyme from *Escherichia coli*, toward 3′, 5′-Cyclic Diguanylic Acid Is Obviously Enhanced by O_2 and CO Binding. *Chem. Lett.* **2006**, *35*, 970−971.
(119) Tanaka, A.; Takahashi, H.; Shimizu, T. Critical Role of the Heme Axial Ligand, Met95, in Locking Catalysis of the Phosphodiesterase from *Escherichia coli* (*Ec* DOS) toward Cyclic diGMP. *J. Biol. Chem.* **2007**, *282*, 21301−21307.
(120) Tanaka, A.; Shimizu, T. Ligand Binding to the Fe(III)-Protoporphyrin IX Complex of Phosphodiesterase from *Escherichia coli* (*Ec* DOS) Markedly Enhances Catalysis of Cyclic di-GMP: Roles of Met95, Arg97, and Phe113 of the Putative Heme Distal Side in Catalytic Regulation and Ligand Binding. *Biochemistry* **2008**, *47*, 13438−13446.
(121) Sasakura, Y.; Hirata, S.; Sugiyama, S.; Suzuki, S.; Taguchi, S.; Watanabe, M.; Matsui, T.; Sagami, I.; Shimizu, T. Characterization of a Direct Oxygen Sensor Heme Protein from *Escherichia coli*. Effects of the Heme Redox States and Mutations at the Heme-Binding Site on Catalysis and Structure. *J. Biol. Chem.* **2002**, *277*, 23821−23827.
(122) Sasakura, Y.; Kanda, K.; Yoshimura-Suzuki, T.; Matsui, T.; Fukuzono, S.; Shimizu, T. Investigation of the Relationship between Protein-Protein Interaction and Catalytic Activity of a Heme-Regulated Phosphodiesterase from *Escherichia coli* (*Ec* DOS) by Protein Microarray. *Biochemistry* **2005**, *44*, 9598−9605.
(123) Yoshimura, T.; Sagami, I.; Sasakura, Y.; Shimizu, T. Relationships between Heme Incorporation, Tetramer Formation, and Catalysis of a Heme-Regulated Phosphodiesterase from *Escherichia coli*: A Study of Deletion and Site-Directed Mutants. *J. Biol. Chem.* **2003**, *278*, 53105−53111.
(124) Imamura, R.; Yamanaka, K.; Ogura, T.; Hiraga, S.; Fujita, N.; Ishihama, A.; Niki, H. Identification of the *cpdA* Gene Encoding Cyclic 3′,5′-Adenosine Monophosphate Phosphodiesterase in *Escherichia coli*. *J. Biol. Chem.* **1996**, *271*, 25423−25429.
(125) Yoshimura-Suzuki, T.; Sagami, I.; Yokota, N.; Kurokawa, H.; Shimizu, T. DOS(*Ec*), a Heme-Regulated Phosphodiesterase, Plays an Important Role in the Regulation of the Cyclic AMP Level in *Escherichia coli*. *J. Bacteriol.* **2005**, *187*, 6678−6682.
(126) Cowan, J. A. *Inorganic Biochemistry, An Introduction*, 2nd ed.; Wiley-VCH: Weinheim, 1997.
(127) Lippard, S. J.; Berg, J. M. *Principles of Bioinorganic Chemistry*; University Science Books: Mill Valley, CA, 1994.
(128) Roat-Malone, R. M. *Bioinorganic Chemistry, A Short Course*, 2nd ed.; John Wiley and Sons: Hoboken, 2007.
(129) Honjo, A.; Takahashi, H.; Sekimoto, M.; Igarashi, J.; Shimizu, T. Novel Effects of Mn^{2+} on Catalytic Enhancement of the Inactive Form of Fe(III) Heme-Bound *Ec*DOS, a Heme-Regulated Phosphodiesterase from *Escherichia coli*. In *Gas Sensors: Developments, Efficacy and Safety*; Qiu, X., Ed.; Nova Science: Hauppauge, 2012; pp 251−261.
(130) Anzenbacher, P.; Marchal, S.; Palacký, J.; Anzenbacherová, E.; Domaschke, T.; Lange, R.; Shimizu, T.; Kitanishi, K.; Stranava, M.; Stiborová, M.; Martinkova, M. Pressure Effects Reveal That Changes in the Redox States of the Heme Iron Complexes in the Sensor Domains of Two Heme-Based Oxygen Sensor Proteins, *Ec*DOS and YddV, Have Profound Effects on Their Flexibility. *FEBS J.* **2014**, *281*, 5208−5219.
(131) Chang, A. L.; Tuckerman, J. R.; Gonzalez, G.; Mayer, R.; Weinhouse, H.; Volman, G.; Amikam, D.; Benziman, M.; Gilles-Gonzalez, M. A. Phosphodiesterase A1, a Regulator of Cellulose Synthesis in *Acetobacter xylinum*, Is a Heme-Based Sensor. *Biochemistry* **2001**, *40*, 3420−3426.
(132) Sen Santara, S.; Roy, J.; Mukherjee, S.; Bose, M.; Saha, R.; Adak, S. Globin-Coupled Heme Containing Oxygen Sensor Soluble Adenylate Cyclase in *Leishmania* Prevents Cell Death during Hypoxia. *Proc. Natl. Acad. Sci. U.S.A.* **2013**, *110*, 16790−16795.
(133) Roy, J.; Sen Santara, S.; Bose, M.; Mukherjee, S.; Saha, R.; Adak, S. The Ferrous-Dioxy Complex of *Leishmania major* Globin Coupled Heme Containing Adenylate Cyclase: The Role of Proximal Histidine on Its Stability. *Biochim. Biophys. Acta* **2014**, *1844*, 615−622.
(134) Ishitsuka, Y.; Araki, Y.; Tanaka, A.; Igarashi, J.; Ito, O.; Shimizu, T. Arg97 at the Heme-Distal Side of the Isolated Heme-Bound PAS Domain of a Heme-Based Oxygen Sensor from *Escherichia coli* (*Ec* DOS) Plays Critical Roles in Autoxidation and Binding to Gases, Particularly O_2. *Biochemistry* **2008**, *47*, 8874−8884.
(135) Taguchi, S.; Matsui, T.; Igarashi, J.; Sasakura, Y.; Araki, Y.; Ito, O.; Sugiyama, S.; Sagami, I.; Shimizu, T. Binding of Oxygen and Carbon Monoxide to a Heme-Regulated Phosphodiesterase from *Escherichia coli*. Kinetics and Infrared Spectra of the Full-Length Wild-Type Enzyme, Isolated PAS Domain, and Met-95 Mutants. *J. Biol. Chem.* **2004**, *279*, 3340−3347.

DOI: 10.1021/acs.chemrev.5b00018
Chem. Rev. 2015, 115, 6491−6533

(136) El-Mashtoly, S. F.; Takahashi, H.; Shimizu, T.; Kitagawa, T. Ultraviolet Resonance Raman Evidence for Utilization of the Heme 6-Propionate Hydrogen-Bond Network in Signal Transmission from Heme to Protein in *Ec* DOS Protein. *J. Am. Chem. Soc.* **2007**, *129*, 3556−3563.
(137) El-Mashtoly, S. F.; Nakashima, S.; Tanaka, A.; Shimizu, T.; Kitagawa, T. Roles of Arg-97 and Phe-113 in Regulation of Distal Ligand Binding to Heme in the Sensor Domain of *Ec* DOS Protein. Resonance Raman and Mutation Study. *J. Biol. Chem.* **2008**, *283*, 19000−19010.
(138) Bidwai, A. K.; Ok, E. Y.; Erman, J. E. pH Dependence of Cyanide Binding to the Ferric Heme Domain of the Direct Oxygen Sensor from *Escherichia coli* and the Effect of Alkaline Denaturation. *Biochemistry* **2008**, *47*, 10458−10470.
(139) Hirata, S.; Matsui, T.; Sasakura, Y.; Sugiyama, S.; Yoshimura, T.; Sagami, I.; Shimizu, T. Characterization of Met95 Mutants of a Heme-Regulated Phosphodiesterase from *Escherichia coli*. Optical Absorption, Magnetic Circular Dichroism, Circular Dichroism, and Redox Potentials. *Eur. J. Biochem.* **2003**, *270*, 4771−4779.
(140) Watanabe, M.; Kurokawa, H.; Yoshimura-Suzuki, T.; Sagami, I.; Shimizu, T. Critical Roles of Asp40 at the Haem Proximal Side of Haem-Regulated Phosphodiesterase from *Escherichia coli* in Redox Potential, Auto-Oxidation and Catalytic Control. *Eur. J. Biochem.* **2004**, *271*, 3937−3942.
(141) El-Mashtoly, S. F.; Takahashi, H.; Kurokawa, H.; Sato, A.; Shimizu, T.; Kitagawa, T. Resonance Raman Investigation of Redox-Induced Structural Changes of Protein and Heme in the Sensor Domain of *Ec* DOS Protein. *J. Raman Spectrosc.* **2008**, *39*, 1614−1626.
(142) El-Mashtoly, S. F.; Kubo, M.; Nakashima, S.; Shimizu, T.; Kitagawa, T. Structural Dynamics of *Ec*DOS Heme Domain Revealed by Time-Resolved Ultraviolet Resonance Raman Spectroscopy. *J. Phys. Chem. Lett.* **2011**, *2*, 2212−2217.
(143) Sato, A.; Sasakura, Y.; Sugiyama, S.; Sagami, I.; Shimizu, T.; Mizutani, Y.; Kitagawa, T. Stationary and Time-Resolved Resonance Raman Spectra of His77 and Met95 Mutants of the Isolated Heme Domain of a Direct Oxygen Sensor from *Escherichia coli*. *J. Biol. Chem.* **2002**, *277*, 32650−32658.
(144) Tomita, T.; Gonzalez, G.; Chang, A. L.; Ikeda-Saito, M.; Gilles-Gonzalez, M. A. A Comparative Resonance Raman Analysis of Heme-Binding PAS Domains: Heme Iron Coordination Structures of the *Bj*FixL, *Ax*PDEA1, *Ec*Dos, and *Mt*Dos Proteins. *Biochemistry* **2002**, *41*, 4819−4826.
(145) Banerjee, R. Hydrogen Sulfide: Redox Metabolism and Signaling. *Antioxid. Redox Signaling* **2011**, *15*, 339−341.
(146) Kabil, O.; Banerjee, R. Redox Biochemistry of Hydrogen Sulfide. *J. Biol. Chem.* **2010**, *285*, 21903−21907.
(147) Kabil, O.; Motl, N.; Banerjee, R. H_2S and Its Role in Redox Signaling. *Biochim. Biophys. Acta* **2014**, *1844*, 1355−1366.
(148) Kimura, H.; Shibuya, N.; Kimura, Y. Hydrogen Sulfide Is a Signaling Molecule and a Cytoprotectant. *Antioxid. Redox Signaling* **2012**, *17*, 45−57.
(149) Kimura, H. Hydrogen Sulfide and Polysulfides as Biological Mediators. *Molecules* **2014**, *19*, 16146−16157.
(150) Szabo, C. Hydrogen Sulphide and Its Therapeutic Potential. *Nat. Rev. Drug Discovery* **2007**, *6*, 917−935.
(151) Szabo, C. Gaseotransmitters: New Frontiers for Translational Science. *Sci. Transl. Med.* **2010**, *2*, ps54.
(152) Wang, R. Hydrogen Sulfide: The Third Gasotransmitter in Biology and Medicine. *Antioxid. Redox Signaling* **2010**, *12*, 1061−1064.
(153) Paul, B. D.; Snyder, S. H. H_2S Signalling through Protein Sulfhydration and beyond. *Nat. Rev. Mol. Cell Biol.* **2012**, *13*, 499−507.
(154) Ramos-Alvarez, C.; Yoo, B. K.; Pietri, R.; Lamarre, I.; Martin, J. L.; Lopez-Garriga, J.; Negrerie, M. Reactivity and Dynamics of H_2S, NO, and O_2 Interacting with Hemoglobins from *Lucina pectinata*. *Biochemistry* **2013**, *52*, 7007−7021.
(155) Pietri, R.; Román-Morales, E.; López-Garriga, J. Hydrogen Sulfide and Hemeproteins: Knowledge and Mysteries. *Antioxid. Redox Signaling* **2011**, *15*, 393−404.
(156) Ríos-González, B. B.; Román-Morales, E. M.; Pietri, R.; López-Garriga, J. Hydrogen Sulfide Activation in Hemeproteins: The Sulfheme Scenario. *J. Inorg. Biochem.* **2014**, *133*, 78−86.
(157) Shimizu, T. Revisit of the Interactions between Hydrogen Sulfide and Heme Proteins. *Curr. Chem. Biol.* **2013**, *7*, 207−212.
(158) Takahashi, H.; Sekimoto, M.; Tanaka, M.; Tanaka, A.; Igarashi, J.; Shimizu, T. Hydrogen Sulfide Stimulates the Catalytic Activity of a Heme-Regulated Phosphodiesterase from *Escherichia coli* (*Ec* DOS). *J. Inorg. Biochem.* **2012**, *109*, 66−71.
(159) Du, Y.; Liu, G.; Yan, Y.; Huang, D.; Luo, W.; Martinkova, M.; Man, P.; Shimizu, T. Conversion of a Heme-Based Oxygen Sensor to a Heme Oxygenase by Hydrogen Sulfide: Effects of Mutations in the Heme Distal Side of a Heme-Based Oxygen Sensor Phosphodiesterase (*Ec* DOS). *BioMetals* **2013**, *26*, 839−852.
(160) Yan, F.; Fojtikova, V.; Man, P.; Stranava, M.; Martínková, M.; Du, Y.; Huang, D.; Shimizu, T. Catalytic Enhancement of the Heme-Based Oxygen-Sensing Phosphodiesterase *Ec*DOS by Hydrogen Sulfide Is Caused by Changes in Heme Coordination Structure. *BioMetals* **2015**, in press, DOI: 10.1007/s10534-015-9847-7.
(161) Matsui, T.; Iwasaki, M.; Sugiyama, R.; Unno, M.; Ikeda-Saito, M. Dioxygen Activation for the Self-Degradation of Heme: Reaction Mechanism and Regulation of Heme Oxygenase. *Inorg. Chem.* **2010**, *49*, 3602−3609.
(162) Matsui, T.; Unno, M.; Ikeda-Saito, M. Heme Oxygenase Reveals Its Strategy for Catalyzing Three Successive Oxygenation Reactions. *Acc. Chem. Res.* **2010**, *43*, 240−247.
(163) Ortiz de Montellano, P. R. Heme Oxygenase Mechanism: Evidence for an Electrophilic, Ferric Peroxide Species. *Acc. Chem. Res.* **1998**, *31*, 543−549.
(164) Watts, K. J.; Taylor, B. L.; Johnson, M. S. PAS/poly-HAMP Signalling in Aer-2, a Soluble Haem-Based Sensor. *Mol. Microbiol.* **2011**, *79*, 686−699.
(165) Sawai, H.; Sugimoto, H.; Shiro, Y.; Ishikawa, H.; Mizutani, Y.; Aono, S. Structural Basis for Oxygen Sensing and Signal Transduction of the Heme-Based Sensor Protein Aer2 from *Pseudomonas aeruginosa*. *Chem. Commun.* **2012**, *48*, 6523−6525.
(166) Parkinson, J. S. Signaling Mechanisms of HAMP Domains in Chemoreceptors and Sensor Kinases. *Annu. Rev. Microbiol.* **2010**, *64*, 101−122.
(167) Airola, M. V.; Huh, D.; Sukomon, N.; Widom, J.; Sircar, R.; Borbat, P. P.; Freed, J. H.; Watts, K. J.; Crane, B. R. Architecture of the Soluble Receptor Aer2 Indicates an In-Line Mechanism for PAS and HAMP Domain Signaling. *J. Mol. Biol.* **2013**, *425*, 886−901.
(168) Huang, S. H.; Rio, D. C.; Marletta, M. A. Ligand Binding and Inhibition of an Oxygen-Sensitive Soluble Guanylate Cyclase, Gyc-88E, from *Drosophila*. *Biochemistry* **2007**, *46*, 15115−15122.
(169) Yamada, S.; Akiyama, S.; Sugimoto, H.; Kumita, H.; Ito, K.; Fujisawa, T.; Nakamura, H.; Shiro, Y. The Signaling Pathway in Histidine Kinase and the Response Regulator Complex Revealed by X-Ray Crystallography and Solution Scattering. *J. Mol. Biol.* **2006**, *362*, 123−139.
(170) Yamada, S.; Sugimoto, H.; Kobayashi, M.; Ohno, A.; Nakamura, H.; Shiro, Y. Structure of PAS-Linked Histidine Kinase and the Response Regulator Complex. *Structure* **2009**, *17*, 1333−1344.
(171) Sivaramakrishnan, S.; Ortiz de Montellano, P. R. The DosS-DosT/DosR Mycobacterial Sensor System. *Biosensors* **2013**, *3*, 259−282.
(172) Cho, H. Y.; Cho, H. J.; Kim, Y. M.; Oh, J. I.; Kang, B. S. Structural Insight into the Heme-Based Redox Sensing by DosS from *Mycobacterium tuberculosis*. *J. Biol. Chem.* **2009**, *284*, 13057−13067.
(173) Cho, H. Y.; Lee, Y. H.; Bae, Y. S.; Kim, E.; Kang, B. S. Activation of ATP Binding for the Autophosphorylation of DosS, a *Mycobacterium tuberculosis* Histidine Kinase Lacking an ATP Lid Motif. *J. Biol. Chem.* **2013**, *288*, 12437−12447.
(174) Podust, L. M.; Ioanoviciu, A.; Ortiz de Montellano, P. R. 2.3 A X-Ray Structure of the Heme-Bound GAF Domain of Sensory Histidine Kinase DosT of *Mycobacterium tuberculosis*. *Biochemistry* **2008**, *47*, 12523−12531.

DOI: 10.1021/acs.chemrev.5b00018
Chem. Rev. 2015, 115, 6491−6533

(175) Ho, Y. S.; Burden, L. M.; Hurley, J. H. Structure of the GAF Domain, a Ubiquitous Signaling Motif and a New Class of Cyclic GMP Receptor. *EMBO J.* **2000**, *19*, 5288−5299.
(176) Ioanoviciu, A.; Meharenna, Y. T.; Poulos, T. L.; Ortiz de Montellano, P. R. DevS Oxy Complex Stability Identifies This Heme Protein as a Gas Sensor in *Mycobacterium tuberculosis* Dormancy. *Biochemistry* **2009**, *48*, 5839−5848.
(177) Yukl, E. T.; Ioanoviciu, A.; Nakano, M. M.; de Montellano, P. R. O.; Moënne-Loccoz, P. A Distal Tyrosine Residue Is Required for Ligand Discrimination in DevS from *Mycobacterium tuberculosis*. *Biochemistry* **2008**, *47*, 12532−12539.
(178) Yukl, E. T.; Ioanoviciu, A.; Sivaramakrishnan, S.; Nakano, M. M.; Ortiz de Montellano, P. R.; Moënne-Loccoz, P. Nitric Oxide Dioxygenation Reaction in DevS and the Initial Response to Nitric Oxide in *Mycobacterium tuberculosis*. *Biochemistry* **2011**, *50*, 1023−1028.
(179) Vos, M. H.; Bouzhir-Sima, L.; Lambry, J. C.; Luo, H.; Eaton-Rye, J. J.; Ioanoviciu, A.; Ortiz de Montellano, P. R.; Liebl, U. Ultrafast Ligand Dynamics in the Heme-Based GAF Sensor Domains of the Histidine Kinases DosS and DosT from *Mycobacterium tuberculosis*. *Biochemistry* **2012**, *51*, 159−166.
(180) Davidge, K. S.; Dikshit, K. L. Haemoglobins of Mycobacteria: Structural Features and Biological Functions. *Adv. Microb. Physiol.* **2013**, *63*, 147−194.
(181) Johnson, E. A.; Lecomte, J. T. J. The Globins of Cyanobacteria and Algae. *Adv. Microb. Physiol.* **2013**, *63*, 195−272.
(182) Pesce, A.; Bolognesi, M.; Nardini, M. The Diversity of 2/2 (truncated) Globins. *Adv. Microb. Physiol.* **2013**, *63*, 49−78.
(183) Vinogradov, S. N.; Moens, L. Diversity of Globin Function: Enzymatic, Transport, Storage, and Sensing. *J. Biol. Chem.* **2008**, *283*, 8773−8777.
(184) Vinogradov, S. N.; Bailly, X.; Smith, D. R.; Tinajero-Trejo, M.; Poole, R. K.; Hoogewijs, D. Microbial Eukaryote Globins. *Adv. Microb. Physiol.* **2013**, *63*, 391−446.
(185) Vinogradov, S. N.; Tinajero-Trejo, M.; Poole, R. K.; Hoogewijs, D. Bacterial and Archaeal Globins - a Revised Perspective. *Biochim. Biophys. Acta* **2013**, *1834*, 1789−1800.
(186) Wittenberg, J. B.; Bolognesi, M.; Wittenberg, B. A.; Guertin, M. Truncated Hemoglobins: A New Family of Hemoglobins Widely Distributed in Bacteria, Unicellular Eukaryotes, and Plants. *J. Biol. Chem.* **2002**, *277*, 871−874.
(187) Freitas, T. A.; Saito, J. A.; Wan, X.; Hou, S.; Alam, M. Protoglobin and Globin-Coupled Sensors. In *The Smallest Biomolecules, Diatomics and Their Interactions with Heme Proteins*; Ghosh, A., Ed.; Elsevier B.V.: Amsterdam, 2008; pp 175−202.
(188) Hou, S.; Larsen, R. W.; Boudko, D.; Riley, C. W.; Karatan, E.; Zimmer, M.; Ordal, G. W.; Alam, M. Myoglobin-like Aerotaxis Transducers in Archaea and Bacteria. *Nature* **2000**, *403*, 540−544.
(189) Hou, S.; Freitas, T.; Larsen, R. W.; Piatibratov, M.; Sivozhelezov, V.; Yamamoto, A.; Meleshkevitch, E. A.; Zimmer, M.; Ordal, G. W.; Alam, M. Globin-Coupled Sensors: A Class of Heme-Containing Sensors in Archaea and Bacteria. *Proc. Natl. Acad. Sci. U.S.A.* **2001**, *98*, 9353−9358.
(190) Zhang, W.; Phillips, G. N., Jr. Structure of the Oxygen Sensor in *Bacillus subtilis*: Signal Transduction of Chemotaxis by Control of Symmetry. *Structure* **2003**, *11*, 1097−1110.
(191) Zhang, W.; Olson, J. S.; Phillips, G. N., Jr. Biophysical and Kinetic Characterization of HemAT, an Aerotaxis Receptor from *Bacillus subtilis*. *Biophys. J.* **2005**, *88*, 2801−2814.
(192) Aono, S.; Kato, T.; Matsuki, M.; Nakajima, H.; Ohta, T.; Uchida, T.; Kitagawa, T. Resonance Raman and Ligand Binding Studies of the Oxygen-Sensing Signal Transducer Protein HemAT from *Bacillus subtilis*. *J. Biol. Chem.* **2002**, *277*, 13528−13538.
(193) Ohta, T.; Yoshimura, H.; Yoshioka, S.; Aono, S.; Kitagawa, T. Oxygen-Sensing Mechanism of HemAT from *Bacillus subtilis*: A Resonance Raman Spectroscopic Study. *J. Am. Chem. Soc.* **2004**, *126*, 15000−15001.
(194) Yoshimura, H.; Yoshioka, S.; Kobayashi, K.; Ohta, T.; Uchida, T.; Kubo, M.; Kitagawa, T.; Aono, S. Specific Hydrogen-Bonding Networks Responsible for Selective O_2 Sensing of the Oxygen Sensor Protein HemAT from *Bacillus subtilis*. *Biochemistry* **2006**, *45*, 8301−8307.
(195) Pinakoulaki, E.; Yoshimura, H.; Daskalakis, V.; Yoshioka, S.; Aono, S.; Varotsis, C. Two Ligand-Binding Sites in the O_2-Sensing Signal Transducer HemAT: Implications for Ligand Recognition/discrimination and Signaling. *Proc. Natl. Acad. Sci. U.S.A.* **2006**, *103*, 14796−14801.
(196) El-Mashtoly, S. F.; Gu, Y.; Yoshimura, H.; Yoshioka, S.; Aono, S.; Kitagawa, T. Protein Conformation Changes of HemAT-Bs upon Ligand Binding Probed by Ultraviolet Resonance Raman Spectroscopy. *J. Biol. Chem.* **2008**, *283*, 6942−6949.
(197) El-Mashtoly, S. F.; Kubo, M.; Gu, Y.; Sawai, H.; Nakashima, S.; Ogura, T.; Aono, S.; Kitagawa, T. Site-Specific Protein Dynamics in Communication Pathway from Sensor to Signaling Domain of Oxygen Sensor Protein, HemAT-Bs: Time-Resolved Ultraviolet Resonance Raman Study. *J. Biol. Chem.* **2012**, *287*, 19973−19984.
(198) Nakajima, K.; Kitanishi, K.; Kobayashi, K.; Kobayashi, N.; Igarashi, J.; Shimizu, T. Leu65 in the Heme Distal Side Is Critical for the Stability of the Fe(II)-O_2 Complex of YddV, a Globin-Coupled Oxygen Sensor Diguanylate Cyclase. *J. Inorg. Biochem.* **2012**, *108*, 163−170.
(199) Stranava, M.; Martínková, M.; Stiborová, M.; Man, P.; Kitanishi, K.; Muchová, L.; Vítek, L.; Martínek, V.; Shimizu, T. Introduction of Water into the Heme Distal Side by Leu65 Mutations of an Oxygen Sensor, YddV, Generates Verdoheme and Carbon Monoxide, Exerting the Heme Oxygenase Reaction. *J. Inorg. Biochem.* **2014**, *140*, 29−38.
(200) Sawai, H.; Yoshioka, S.; Uchida, T.; Hyodo, M.; Hayakawa, Y.; Ishimori, K.; Aono, S. Molecular Oxygen Regulates the Enzymatic Activity of a Heme-Containing Diguanylate Cyclase (HemDGC) for the Synthesis of Cyclic di-GMP. *Biochim. Biophys. Acta* **2010**, *1804*, 166−172.
(201) Thijs, L.; Vinck, E.; Bolli, A.; Trandafir, F.; Wan, X.; Hoogewijs, D.; Coletta, M.; Fago, A.; Weber, R. E.; Van Doorslaer, S.; et al. Characterization of a Globin-Coupled Oxygen Sensor with a Gene-Regulating Function. *J. Biol. Chem.* **2007**, *282*, 37325−37340.
(202) Wan, X.; Tuckerman, J. R.; Saito, J. A.; Freitas, T. A. K.; Newhouse, J. S.; Denery, J. R.; Galperin, M. Y.; Gonzalez, G.; Gilles-Gonzalez, M. A.; Alam, M. Globins Synthesize the Second Messenger Bis-(3′-5′)-Cyclic Diguanosine Monophosphate in Bacteria. *J. Mol. Biol.* **2009**, *388*, 262−270.
(203) Pesce, A.; Thijs, L.; Nardini, M.; Desmet, F.; Sisinni, L.; Gourlay, L.; Bolli, A.; Coletta, M.; Van Doorslaer, S.; Wan, X.; et al. HisE11 and HisF8 Provide Bis-Histidyl Heme Hexa-Coordination in the Globin Domain of *Geobacter sulfurreducens* Globin-Coupled Sensor. *J. Mol. Biol.* **2009**, *386*, 246−260.
(204) Bian, K.; Ghassemi, F.; Sotolongo, A.; Siu, A.; Shauger, L.; Kots, A.; Murad, F. NOS-2 Signaling and Cancer Therapy. *IUBMB Life* **2012**, *64*, 676−683.
(205) Martínez-Ruiz, A.; Cadenas, S.; Lamas, S. Nitric Oxide Signaling: Classical, Less Classical, and Nonclassical Mechanisms. *Free Radical Biol. Med.* **2011**, *51*, 17−29.
(206) Castiglione, N.; Rinaldo, S.; Giardina, G.; Stelitano, V.; Cutruzzolà, F. Nitrite and Nitrite Reductases: From Molecular Mechanisms to Significance in Human Health and Disease. *Antioxid. Redox Signaling* **2012**, *17*, 684−716.
(207) Sparacino-Watkins, C. E.; Tejero, J.; Sun, B.; Gauthier, M. C.; Thomas, J.; Ragireddy, V.; Merchant, B. A.; Wang, J.; Azarov, I.; Basu, P.; et al. Nitrite Reductase and Nitric-Oxide Synthase Activity of the Mitochondrial Molybdopterin Enzymes mARC1 and mARC2. *J. Biol. Chem.* **2014**, *289*, 10345−10358.
(208) Liu, C.; Wajih, N.; Liu, X.; Basu, S.; Janes, J.; Marvel, M.; Keggi, C.; Helms, C. C.; Lee, A. N.; Belanger, A. M.; et al. Mechanisms of Human Erythrocytic Bioactivation of Nitrite. *J. Biol. Chem.* **2015**, *290*, 1281−1294.
(209) Maia, L. B.; Pereira, V.; Mira, L.; Moura, J. J. G. Nitrite Reductase Activity of Rat and Human Xanthine Oxidase, Xanthine Dehydrogenase, and Aldehyde Oxidase: Evaluation of Their

DOI: 10.1021/acs.chemrev.5b00018
Chem. Rev. 2015, 115, 6491−6533

Contribution to NO Formation in Vivo. *Biochemistry* **2015**, *54*, 685−710.
(210) He, C.; Howes, B. D.; Smulevich, G.; Rumpel, S.; Reijerse, E. J.; Lubitz, W.; Cox, N.; Knipp, M. Nitrite Dismutase Reaction Mechanism: Kinetic and Spectroscopic Investigation of the Interaction between Nitrophorin and Nitrite. *J. Am. Chem. Soc.* **2015**, *137*, 4141−4150.
(211) Smulik, R.; Dębski, D.; Zielonka, J.; Michałowski, B.; Adamus, J.; Marcinek, A.; Kalyanaraman, B.; Sikora, A. Nitroxyl (HNO) Reacts with Molecular Oxygen and Forms Peroxynitrite at Physiological pH: Biological Implications. *J. Biol. Chem.* **2014**, *289*, 35570−35581.
(212) Diers, A. R.; Keszler, A.; Hogg, N. Detection of S-Nitrosothiols. *Biochim. Biophys. Acta* **2014**, *1840*, 892−900.
(213) Gusarov, I.; Nudler, E. S-Nitrosylation Signaling in *Escherichia coli*. *Sci. Signaling* **2012**, *5*, pe26.
(214) Nakamura, T.; Tu, S.; Akhtar, M. W.; Sunico, C. R.; Okamoto, S. I.; Lipton, S. A. Aberrant Protein S-Nitrosylation in Neurodegenerative Diseases. *Neuron* **2013**, *78*, 596−614.
(215) Marozkina, N. V.; Gaston, B. S-Nitrosylation Signaling Regulates Cellular Protein Interactions. *Biochim. Biophys. Acta* **2012**, *1820*, 722−729.
(216) Smith, B. C.; Marletta, M. A. Mechanisms of S-Nitrosothiol Formation and Selectivity in Nitric Oxide Signaling. *Curr. Opin. Chem. Biol.* **2012**, *16*, 498−506.
(217) Jia, J.; Arif, A.; Terenzi, F.; Willard, B.; Plow, E. F.; Hazen, S. L.; Fox, P. L. Target-Selective Protein S-Nitrosylation by Sequence Motif Recognition. *Cell* **2014**, *159*, 623−634.
(218) Bellota-Antón, C.; Munnoch, J.; Robb, K.; Adamczyk, K.; Candelaresi, M.; Parker, A. W.; Dixon, R.; Hutchings, M. I.; Hunt, N. T.; Tucker, N. P. Spectroscopic Analysis of Protein Fe-NO Complexes. *Biochem. Soc. Trans.* **2011**, *39*, 1293−1298.
(219) Caranto, J. D.; Weitz, A.; Hendrich, M. P.; Kurtz, D. M., Jr. The Nitric Oxide Reductase Mechanism of a Flavo-Diiron Protein: Identification of Active-Site Intermediates and Products. *J. Am. Chem. Soc.* **2014**, *136*, 7981−7992.
(220) Chakraborty, S.; Reed, J.; Ross, M.; Nilges, M. J.; Petrik, I. D.; Ghosh, S.; Hammes-Schiffer, S.; Sage, J. T.; Zhang, Y.; Schulz, C. E.; et al. Spectroscopic and Computational Study of a Nonheme Iron Nitrosyl Center in a Biosynthetic Model of Nitric Oxide Reductase. *Angew. Chem., Int. Ed.* **2014**, *53*, 2417−2421.
(221) Fitzpatrick, J.; Kalyvas, H.; Filipovic, M. R.; Ivanović-Burmazović, I.; MacDonald, J. C.; Shearer, J.; Kim, E. Transformation of a Mononitrosyl Iron Complex to a [2Fe-2S] Cluster by a Cysteine Analogue. *J. Am. Chem. Soc.* **2014**, *136*, 7229−7232.
(222) Li, Q.; Li, C.; Mahtani, H. K.; Du, J.; Patel, A. R.; Lancaster, J. R., Jr. Nitrosothiol Formation and Protection against Fenton Chemistry by Nitric Oxide-Induced Dinitrosyliron Complex Formation from Anoxia-Initiated Cellular Chelatable Iron Increase. *J. Biol. Chem.* **2014**, *289*, 19917−19927.
(223) Speelman, A. L.; Lehnert, N. Heme versus Non-Heme Iron-Nitroxyl {FeN(H)O}^{8} Complexes: Electronic Structure and Biologically Relevant Reactivity. *Acc. Chem. Res.* **2014**, *47*, 1106−1116.
(224) Tucker, N. P.; D'Autréaux, B.; Yousafzai, F. K.; Fairhurst, S. A.; Spiro, S.; Dixon, R. Analysis of the Nitric Oxide-Sensing Non-Heme Iron Center in the NorR Regulatory Protein. *J. Biol. Chem.* **2008**, *283*, 908−918.
(225) Butler, A. R.; Megson, I. L. Non-Heme Iron Nitrosyls in Biology. *Chem. Rev.* **2002**, *102*, 1155−1166.
(226) D'Autréaux, B.; Tucker, N. P.; Dixon, R.; Spiro, S. A Non-Haem Iron Centre in the Transcription Factor NorR Senses Nitric Oxide. *Nature* **2005**, *437*, 769−772.
(227) Aicart-Ramos, C.; Valhondo Falcón, M.; Ortiz de Montellano, P. R.; Rodriguez-Crespo, I. Covalent Attachment of Heme to the Protein Moiety in an Insect E75 Nitric Oxide Sensor. *Biochemistry* **2012**, *51*, 7403−7416.
(228) Doctorovich, F.; Bikiel, D. E.; Pellegrino, J.; Suárez, S. A.; Martí, M. A. Reactions of HNO with Metal Porphyrins: Underscoring the Biological Relevance of HNO. *Acc. Chem. Res.* **2014**, *47*, 2907−2916.
(229) Liu, X.; Follmer, D.; Zweier, J. R.; Huang, X.; Hemann, C.; Liu, K.; Druhan, L. J.; Zweier, J. L. Characterization of the Function of Cytoglobin as an Oxygen-Dependent Regulator of Nitric Oxide Concentration. *Biochemistry* **2012**, *51*, 5072−5082.
(230) Purwar, N.; McGarry, J. M.; Kostera, J.; Pacheco, A. A.; Schmidt, M. Interaction of Nitric Oxide with Catalase: Structural and Kinetic Analysis. *Biochemistry* **2011**, *50*, 4491−4503.
(231) Silkstone, G.; Kapetanaki, S. M.; Husu, I.; Vos, M. H.; Wilson, M. T. Nitric Oxide Binding to the Cardiolipin Complex of Ferric Cytochrome c. *Biochemistry* **2012**, *51*, 6760−6766.
(232) Evgenov, O. V.; Pacher, P.; Schmidt, P. M.; Haskó, G.; Schmidt, H. H. H. W.; Stasch, J. P. NO-Independent Stimulators and Activators of Soluble Guanylate Cyclase: Discovery and Therapeutic Potential. *Nat. Rev. Drug Discovery* **2006**, *5*, 755−768.
(233) Follmann, M.; Griebenow, N.; Hahn, M. G.; Hartung, I.; Mais, F. J.; Mittendorf, J.; Schäfer, M.; Schirok, H.; Stasch, J. P.; Stoll, F.; et al. The Chemistry and Biology of Soluble Guanylate Cyclase Stimulators and Activators. *Angew. Chem., Int. Ed.* **2013**, *52*, 9442−9462.
(234) Garthwaite, J. New Insight into the Functioning of Nitric Oxide-Receptive Guanylyl Cyclase: Physiological and Pharmacological Implications. *Mol. Cell. Biochem.* **2010**, *334*, 221−232.
(235) Gileadi, O. Structures of Soluble Guanylate Cyclase: Implications for Regulatory Mechanisms and Drug Development. *Biochem. Soc. Trans.* **2014**, *42*, 108−113.
(236) Potter, L. R. Guanylyl Cyclase Structure, Function and Regulation. *Cell. Signaling* **2011**, *23*, 1921−1926.
(237) Rogers, N. M.; Seeger, F.; Garcin, E. D.; Roberts, D. D.; Isenberg, J. S. Regulation of Soluble Guanylate Cyclase by Matricellular Thrombospondins: Implications for Blood Flow. *Front. Physiol.* **2014**, *5*, 134.
(238) Gheorghiade, M.; Marti, C. N.; Sabbah, H. N.; Roessig, L.; Greene, S. J.; Böhm, M.; Burnett, J. C.; Campia, U.; Cleland, J. G. F.; Collins, S. P.; et al. Soluble Guanylate Cyclase: A Potential Therapeutic Target for Heart Failure. *Heart Failure Rev.* **2013**, *18*, 123−134.
(239) Nossaman, B.; Pankey, E.; Kadowitz, P. Stimulators and Activators of Soluble Guanylate Cyclase: Review and Potential Therapeutic Indications. *Crit. Care Res. Pract.* **2012**, *2012*, 290805.
(240) Stasch, J. P.; Pacher, P.; Evgenov, O. V. Soluble Guanylate Cyclase as an Emerging Therapeutic Target in Cardiopulmonary Disease. *Circulation* **2011**, *123*, 2263−2273.
(241) Ellis, D. Z. Guanylate Cyclase Activators, Cell Volume Changes and IOP Reduction. *Cell. Physiol. Biochem.* **2011**, *28*, 1145−1154.
(242) Herzik, M. A., Jr.; Jonnalagadda, R.; Kuriyan, J.; Marletta, M. A. Structural Insights into the Role of Iron-Histidine Bond Cleavage in Nitric Oxide-Induced Activation of H-NOX Gas Sensor Proteins. *Proc. Natl. Acad. Sci. U.S.A.* **2014**, *111*, E4156−E4164.
(243) Ma, X.; Sayed, N.; Beuve, A.; van den Akker, F. NO and CO Differentially Activate Soluble Guanylyl Cyclase via a Heme Pivot-Bend Mechanism. *EMBO J.* **2007**, *26*, 578−588.
(244) Ma, X.; Sayed, N.; Baskaran, P.; Beuve, A.; van den Akker, F. PAS-Mediated Dimerization of Soluble Guanylyl Cyclase Revealed by Signal Transduction Histidine Kinase Domain Crystal Structure. *J. Biol. Chem.* **2008**, *283*, 1167−1178.
(245) Nioche, P.; Berka, V.; Vipond, J.; Minton, N.; Tsai, A. L.; Raman, C. S. Femtomolar Sensitivity of a NO Sensor from *Clostridium botulinum*. *Science* **2004**, *306*, 1550−1553.
(246) Pellicena, P.; Karow, D. S.; Boon, E. M.; Marletta, M. A.; Kuriyan, J. Crystal Structure of an Oxygen-Binding Heme Domain Related to Soluble Guanylate Cyclases. *Proc. Natl. Acad. Sci. U.S.A.* **2004**, *101*, 12854−12859.
(247) Fritz, B. G.; Roberts, S. A.; Ahmed, A.; Breci, L.; Li, W.; Weichsel, A.; Brailey, J. L.; Wysocki, V. H.; Tama, F.; Montfort, W. R. Molecular Model of a Soluble Guanylyl Cyclase Fragment Determined by Small-Angle X-Ray Scattering and Chemical Cross-Linking. *Biochemistry* **2013**, *52*, 1568−1582.

DOI: 10.1021/acs.chemrev.5b00018
Chem. Rev. 2015, 115, 6491−6533

(248) Seeger, F.; Quintyn, R.; Tanimoto, A.; Williams, G. J.; Tainer, J. A.; Wysocki, V. H.; Garcin, E. D. Interfacial Residues Promote an Optimal Alignment of the Catalytic Center in Human Soluble Guanylate Cyclase: Heterodimerization Is Required but Not Sufficient for Activity. *Biochemistry* **2014**, *53*, 2153−2165.
(249) Underbakke, E. S.; Iavarone, A. T.; Marletta, M. A. Higher-Order Interactions Bridge the Nitric Oxide Receptor and Catalytic Domains of Soluble Guanylate Cyclase. *Proc. Natl. Acad. Sci. U.S.A.* **2013**, *110*, 6777−6782.
(250) Underbakke, E. S.; Iavarone, A. T.; Chalmers, M. J.; Pascal, B. D.; Novick, S.; Griffin, P. R.; Marletta, M. A. Nitric Oxide-Induced Conformational Changes in Soluble Guanylate Cyclase. *Structure* **2014**, *22*, 602−611.
(251) Campbell, M. G.; Underbakke, E. S.; Potter, C. S.; Carragher, B.; Marletta, M. A.; Single-Particle, E. M. Reveals the Higher-Order Domain Architecture of Soluble Guanylate Cyclase. *Proc. Natl. Acad. Sci. U.S.A.* **2014**, *111*, 2960−2965.
(252) Purohit, R.; Weichsel, A.; Montfort, W. R. Crystal Structure of the Alpha Subunit PAS Domain from Soluble Guanylyl Cyclase. *Protein Sci.* **2013**, *22*, 1439−1444.
(253) Allerston, C. K.; von Delft, F.; Gileadi, O. Crystal Structures of the Catalytic Domain of Human Soluble Guanylate Cyclase. *PloS One* **2013**, *8*, e57644.
(254) Busker, M.; Neidhardt, I.; Behrends, S. Nitric Oxide Activation of Guanylate Cyclase Pushes the α1 Signaling Helix and the β1 Heme-Binding Domain Closer to the Substrate-Binding Site. *J. Biol. Chem.* **2014**, *289*, 476−484.
(255) Gunn, A.; Derbyshire, E. R.; Marletta, M. A.; Britt, R. D. Conformationally Distinct Five-Coordinate Heme-NO Complexes of Soluble Guanylate Cyclase Elucidated by Multifrequency Electron Paramagnetic Resonance (EPR). *Biochemistry* **2012**, *51*, 8384−8390.
(256) Yoo, B. K.; Lamarre, I.; Martin, J. L.; Rappaport, F.; Negrerie, M. Motion of Proximal Histidine and Structural Allosteric Transition in Soluble Guanylate Cyclase. *Proc. Natl. Acad. Sci. U.S.A.* **2015**, *112*, E1697−E1704.
(257) Makino, R.; Park, S.; Obayashi, E.; Iizuka, T.; Hori, H.; Shiro, Y. Oxygen Binding and Redox Properties of the Heme in Soluble Guanylate Cyclase: Implications for the Mechanism of Ligand Discrimination. *J. Biol. Chem.* **2011**, *286*, 15678−15687.
(258) Fernhoff, N. B.; Derbyshire, E. R.; Underbakke, E. S.; Marletta, M. A. Heme-Assisted S-Nitrosation Desensitizes Ferric Soluble Guanylate Cyclase to Nitric Oxide. *J. Biol. Chem.* **2012**, *287*, 43053−43062.
(259) Sayed, N.; Baskaran, P.; Ma, X.; van den Akker, F.; Beuve, A. Desensitization of Soluble Guanylyl Cyclase, the NO Receptor, by S-Nitrosylation. *Proc. Natl. Acad. Sci. U.S.A.* **2007**, *104*, 12312−12317.
(260) Ibrahim, M.; Derbyshire, E. R.; Marletta, M. A.; Spiro, T. G. Probing Soluble Guanylate Cyclase Activation by CO and YC-1 Using Resonance Raman Spectroscopy. *Biochemistry* **2010**, *49*, 3815−3823.
(261) Ibrahim, M.; Derbyshire, E. R.; Soldatova, A. V.; Marletta, M. A.; Spiro, T. G. Soluble Guanylate Cyclase Is Activated Differently by Excess NO and by YC-1: Resonance Raman Spectroscopic Evidence. *Biochemistry* **2010**, *49*, 4864−4871.
(262) Purohit, R.; Fritz, B. G.; The, J.; Issaian, A.; Weichsel, A.; David, C. L.; Campbell, E.; Hausrath, A. C.; Rassouli-Taylor, L.; Garcin, E. D.; et al. YC-1 Binding to the B Subunit of Soluble Guanylyl Cyclase Overcomes Allosteric Inhibition by the A Subunit. *Biochemistry* **2014**, *53*, 101−114.
(263) Kumar, V.; Martin, F.; Hahn, M. G.; Schaefer, M.; Stamler, J. S.; Stasch, J. P.; van den Akker, F. Insights into BAY 60−2770 Activation and S-Nitrosylation-Dependent Desensitization of Soluble Guanylyl Cyclase via Crystal Structures of Homologous Nostoc H-NOX Domain Complexes. *Biochemistry* **2013**, *52*, 3601−3608.
(264) Martin, F.; Baskaran, P.; Ma, X.; Dunten, P. W.; Schaefer, M.; Stasch, J. P.; Beuve, A.; van den Akker, F. Structure of Cinaciguat (BAY 58−2667) Bound to Nostoc H-NOX Domain Reveals Insights into Heme-Mimetic Activation of the Soluble Guanylyl Cyclase. *J. Biol. Chem.* **2010**, *285*, 22651−22657.
(265) Von Wantoch Rekowski, M.; Kumar, V.; Zhou, Z.; Moschner, J.; Marazioti, A.; Bantzi, M.; Spyroulias, G. A.; van den Akker, F.; Giannis, A.; Papapetropoulos, A. Insights into Soluble Guanylyl Cyclase Activation Derived from Improved Heme-Mimetics. *J. Med. Chem.* **2013**, *56*, 8948−8952.
(266) Erbil, W. K.; Price, M. S.; Wemmer, D. E.; Marletta, M. A. A Structural Basis for H-NOX Signaling in Shewanella Oneidensis by Trapping a Histidine Kinase Inhibitory Conformation. *Proc. Natl. Acad. Sci. U.S.A.* **2009**, *106*, 19753−19760.
(267) Olea, C., Jr.; Herzik, M. A., Jr.; Kuriyan, J.; Marletta, M. A. Structural Insights into the Molecular Mechanism of H-NOX Activation. *Protein Sci.* **2010**, *19*, 881−887.
(268) Olea, C., Jr.; Kuriyan, J.; Marletta, M. A. Modulating Heme Redox Potential through Protein-Induced Porphyrin Distortion. *J. Am. Chem. Soc.* **2010**, *132*, 12794−12795.
(269) Muralidharan, S.; Boon, E. M. Heme Flattening Is Sufficient for Signal Transduction in the H-NOX Family. *J. Am. Chem. Soc.* **2012**, *134*, 2044−2046.
(270) Derbyshire, E. R.; Deng, S.; Marletta, M. A. Incorporation of Tyrosine and Glutamine Residues into the Soluble Guanylate Cyclase Heme Distal Pocket Alters NO and O_2 Binding. *J. Biol. Chem.* **2010**, *285*, 17471−17478.
(271) Boon, E. M.; Huang, S. H.; Marletta, M. A. A Molecular Basis for NO Selectivity in Soluble Guanylate Cyclase. *Nat. Chem. Biol.* **2005**, *1*, 53−59.
(272) Plate, L.; Marletta, M. A. Nitric Oxide Modulates Bacterial Biofilm Formation through a Multicomponent Cyclic-di-GMP Signaling Network. *Mol. Cell* **2012**, *46*, 449−460.
(273) Plate, L.; Marletta, M. A. Phosphorylation-Dependent Derepression by the Response Regulator HnoC in the *Shewanella oneidensis* Nitric Oxide Signaling Network. *Proc. Natl. Acad. Sci. U.S.A.* **2013**, *110*, E4648−E4657.
(274) Lahiri, T.; Luan, B.; Raleigh, D. P.; Boon, E. M. A Structural Basis for the Regulation of an H-NOX-Associated Cyclic-di-GMP Synthase/phosphodiesterase Enzyme by Nitric Oxide-Bound H-NOX. *Biochemistry* **2014**, *53*, 2126−2135.
(275) Liu, N.; Xu, Y.; Hossain, S.; Huang, N.; Coursolle, D.; Gralnick, J. A.; Boon, E. M. Nitric Oxide Regulation of Cyclic di-GMP Synthesis and Hydrolysis in *Shewanella woodyi*. *Biochemistry* **2012**, *51*, 2087−2099.
(276) Carlson, H. K.; Vance, R. E.; Marletta, M. A. H-NOX Regulation of c-di-GMP Metabolism and Biofilm Formation in *Legionella pneumophila*. *Mol. Microbiol.* **2010**, *77*, 930−942.
(277) Arora, D. P.; Boon, E. M. Nitric Oxide Regulated Two-Component Signaling in *Pseudoalteromonas atlantica*. *Biochem. Biophys. Res. Commun.* **2012**, *421*, 521−526.
(278) Wang, Y.; Dufour, Y. S.; Carlson, H. K.; Donohue, T. J.; Marletta, M. A.; Ruby, E. G. H-NOX-Mediated Nitric Oxide Sensing Modulates Symbiotic Colonization by *Vibrio fischeri*. *Proc. Natl. Acad. Sci. U.S.A.* **2010**, *107*, 8375−8380.
(279) Henares, B. M.; Higgins, K. E.; Boon, E. M. Discovery of a Nitric Oxide Responsive Quorum Sensing Circuit in *Vibrio harveyi*. *ACS Chem. Biol.* **2012**, *7*, 1331−1336.
(280) Henares, B. M.; Xu, Y.; Boon, E. M. A Nitric Oxide-Responsive Quorum Sensing Circuit in *Vibrio harveyi* Regulates Flagella Production and Biofilm Formation. *Int. J. Mol. Sci.* **2013**, *14*, 16473−16484.
(281) Miller, M. B.; Bassler, B. L. Quorum Sensing in Bacteria. *Annu. Rev. Microbiol.* **2001**, *55*, 165−199.
(282) Giardina, G.; Rinaldo, S.; Johnson, K. A.; Di Matteo, A.; Brunori, M.; Cutruzzolà, F. NO Sensing in *Pseudomonas aeruginosa*: Structure of the Transcriptional Regulator DNR. *J. Mol. Biol.* **2008**, *378*, 1002−1015.
(283) Rinaldo, S.; Castiglione, N.; Giardina, G.; Caruso, M.; Arcovito, A.; Longa, S. D.; D'Angelo, P.; Cutruzzolà, F. Unusual Heme Binding Properties of the Dissimilative Nitrate Respiration Regulator, a Bacterial Nitric Oxide Sensor. *Antioxid. Redox Signaling* **2012**, *17*, 1178−1189.

DOI: 10.1021/acs.chemrev.5b00018
Chem. Rev. 2015, 115, 6491−6533

(284) Lobato, L.; Bouzhir-Sima, L.; Yamashita, T.; Wilson, M. T.; Vos, M. H.; Liebl, U. Dynamics of the Heme-Binding Bacterial Gas-Sensing Dissimilative Nitrate Respiration Regulator (DNR) and Activation Barriers for Ligand Binding and Escape. *J. Biol. Chem.* **2014**, *289*, 26514−26524.
(285) Rao, F.; Ji, Q.; Soehano, I.; Liang, Z. X. Unusual Heme-Binding PAS Domain from YybT Family Proteins. *J. Bacteriol.* **2011**, *193*, 1543−1551.
(286) Tan, E.; Rao, F.; Pasunooti, S.; Pham, T. H.; Soehano, I.; Turner, M. S.; Liew, C. W.; Lescar, J.; Pervushin, K.; Liang, Z. X. Solution Structure of the PAS Domain of a Thermophilic YybT Protein Homolog Reveals a Potential Ligand-Binding Site. *J. Biol. Chem.* **2013**, *288*, 11949−11959.
(287) Banerjee, R.; Zou, C. G. Redox Regulation and Reaction Mechanism of Human Cystathionine-β-Synthase: A PLP-Dependent Hemesensor Protein. *Arch. Biochem. Biophys.* **2005**, *433*, 144−156.
(288) McCorvie, T. J.; Kopec, J.; Hyung, S. J.; Fitzpatrick, F.; Feng, X.; Termine, D.; Strain-Damerell, C.; Vollmar, M.; Fleming, J.; Janz, J. M.; et al. Inter-Domain Communication of Human Cystathionine β-Synthase: Structural Basis of S-Adenosyl-L-Methionine Activation. *J. Biol. Chem.* **2014**, *289*, 36018−36030.
(289) Singh, S.; Madzelan, P.; Banerjee, R. Properties of an Unusual Heme Cofactor in PLP-Dependent Cystathionine β-Synthase. *Nat. Prod. Rep.* **2007**, *24*, 631−639.
(290) Singh, S.; Ballou, D. P.; Banerjee, R. Pre-Steady-State Kinetic Analysis of Enzyme-Monitored Turnover during Cystathionine β-Synthase-Catalyzed H_2S Generation. *Biochemistry* **2011**, *50*, 419−425.
(291) Singh, S.; Banerjee, R. PLP-Dependent H_2S Biogenesis. *Biochim. Biophys. Acta* **2011**, *1814*, 1518−1527.
(292) Vicente, J. B.; Colaço, H. G.; Mendes, M. I. S.; Sarti, P.; Leandro, P.; Giuffrè, A. NO* Binds Human Cystathionine β-Synthase Quickly and Tightly. *J. Biol. Chem.* **2014**, *289*, 8579−8587.
(293) Oelgeschläger, E.; Rother, M. Carbon Monoxide-Dependent Energy Metabolism in Anaerobic Bacteria and Archaea. *Arch. Microbiol.* **2008**, *190*, 257−269.
(294) Kerby, R. L.; Youn, H.; Roberts, G. P. RcoM: A New Single-Component Transcriptional Regulator of CO Metabolism in Bacteria. *J. Bacteriol.* **2008**, *190*, 3336−3343.
(295) Techtmann, S. M.; Colman, A. S.; Murphy, M. B.; Schackwitz, W. S.; Goodwin, L. A.; Robb, F. T. Regulation of Multiple Carbon Monoxide Consumption Pathways in Anaerobic Bacteria. *Front. Microbiol.* **2011**, *2*, 147.
(296) Aono, S. Biochemical and Biophysical Properties of the CO-Sensing Transcriptional Activator CooA. *Acc. Chem. Res.* **2003**, *36*, 825−831.
(297) Ogura, H.; Evans, J. P.; Peng, D.; Satterlee, J. D.; Ortiz de Montellano, P. R.; La Mar, G. N. The Orbital Ground State of the Azide-Substrate Complex of Human Heme Oxygenase Is an Indicator of Distal H-Bonding: Implications for the Enzyme Mechanism. *Biochemistry* **2009**, *48*, 3127−3137.
(298) Peng, D.; Ogura, H.; Zhu, W.; Ma, L. H.; Evans, J. P.; Ortiz de Montellano, P. R.; La Mar, G. N. Coupling of the Distal Hydrogen Bond Network to the Exogenous Ligand in Substrate-Bound, Resting State Human Heme Oxygenase. *Biochemistry* **2009**, *48*, 11231−11242.
(299) Wilks, A.; Ikeda-Saito, M. Heme Utilization by Pathogenic Bacteria: Not All Pathways Lead to Biliverdin. *Acc. Chem. Res.* **2014**, *47*, 2291−2298.
(300) Unno, M.; Matsui, T.; Ikeda-Saito, M. Structure and Catalytic Mechanism of Heme Oxygenase. *Nat. Prod. Rep.* **2007**, *24*, 553−570.
(301) Yoshida, T.; Migita, C. T. Mechanism of Heme Degradation by Heme Oxygenase. *J. Inorg. Biochem.* **2000**, *82*, 33−41.
(302) Fujita, T.; Toda, K.; Karimova, A.; Yan, S. F.; Naka, Y.; Yet, S. F.; Pinsky, D. J. Paradoxical Rescue from Ischemic Lung Injury by Inhaled Carbon Monoxide Driven by Derepression of Fibrinolysis. *Nat. Med.* **2001**, *7*, 598−604.
(303) Lancel, S.; Montaigne, D.; Marechal, X.; Marciniak, C.; Hassoun, S. M.; Decoster, B.; Ballot, C.; Blazejewski, C.; Corseaux, D.; Lescure, B.; et al. Carbon Monoxide Improves Cardiac Function and Mitochondrial Population Quality in a Mouse Model of Metabolic Syndrome. *PLoS One* **2012**, *7*, e41836.
(304) Otterbein, L. E.; Zuckerbraun, B. S.; Haga, M.; Liu, F.; Song, R.; Usheva, A.; Stachulak, C.; Bodyak, N.; Smith, R. N.; Csizmadia, E.; et al. Carbon Monoxide Suppresses Arteriosclerotic Lesions Associated with Chronic Graft Rejection and with Balloon Injury. *Nat. Med.* **2003**, *9*, 183−190.
(305) Almeida, A. S.; Queiroga, C. S. F.; Sousa, M. F. Q.; Alves, P. M.; Vieira, H. L. A. Carbon Monoxide Modulates Apoptosis by Reinforcing Oxidative Metabolism in Astrocytes: Role of Bcl-2. *J. Biol. Chem.* **2012**, *287*, 10761−10770.
(306) Sugishima, M.; Moffat, K.; Noguchi, M. Discrimination between CO and O_2 in Heme Oxygenase: Comparison of Static Structures and Dynamic Conformation Changes Following CO Photolysis. *Biochemistry* **2012**, *51*, 8554−8562.
(307) Varfaj, F.; Lampe, J. N.; Ortiz de Montellano, P. R. Role of Cysteine Residues in Heme Binding to Human Heme Oxygenase-2 Elucidated by Two-Dimensional NMR Spectroscopy. *J. Biol. Chem.* **2012**, *287*, 35181−35191.
(308) Fisher, K.; Hare, N. D.; Newton, W. E. Another Role for CO with Nitrogenase? CO Stimulates Hydrogen Evolution Catalyzed by Variant *Azotobacter vinelandii* Mo-Nitrogenases. *Biochemistry* **2014**, *53*, 6151−6160.
(309) Spatzal, T.; Perez, K. A.; Einsle, O.; Howard, J. B.; Rees, D. C. Ligand Binding to the FeMo-Cofactor: Structures of CO-Bound and Reactivated Nitrogenase. *Science* **2014**, *345*, 1620−1623.
(310) Chan, M. K. CooA, CAP and Allostery. *Nat. Struct. Biol.* **2000**, *7*, 822−824.
(311) Roberts, G. P.; Kerby, R. L.; Youn, H.; Conrad, M. CooA, a Paradigm for Gas Sensing Regulatory Proteins. *J. Inorg. Biochem.* **2005**, *99*, 280−292.
(312) Lanzilotta, W. N.; Schuller, D. J.; Thorsteinsson, M. V.; Kerby, R. L.; Roberts, G. P.; Poulos, T. L. Structure of the CO Sensing Transcription Activator CooA. *Nat. Struct. Biol.* **2000**, *7*, 876−880.
(313) Aono, S.; Nakajima, H.; Saito, K.; Okada, M. A Novel Heme Protein That Acts as a Carbon Monoxide-Dependent Transcriptional Activator in *Rhodospirillum rubrum*. *Biochem. Biophys. Res. Commun.* **1996**, *228*, 752−756.
(314) Aono, S.; Matsuo, T.; Shimono, T.; Ohkubo, K.; Takasaki, H.; Nakajima, H. Single Transduction in the Transcriptional Activator CooA Containing a Heme-Based CO Sensor: Isolation of a Dominant Positive Mutant Which Is Active as the Transcriptional Activator Even in the Absence of CO. *Biochem. Biophys. Res. Commun.* **1997**, *240*, 783−786.
(315) Benabbas, A.; Karunakaran, V.; Youn, H.; Poulos, T. L.; Champion, P. M. Effect of DNA Binding on Geminate CO Recombination Kinetics in CO-Sensing Transcription Factor CooA. *J. Biol. Chem.* **2012**, *287*, 21729−21740.
(316) Karunakaran, V.; Benabbas, A.; Youn, H.; Champion, P. M. Vibrational Coherence Spectroscopy of the Heme Domain in the CO-Sensing Transcriptional Activator CooA. *J. Am. Chem. Soc.* **2011**, *133*, 18816−18827.
(317) Shelver, D.; Kerby, R. L.; He, Y.; Roberts, G. P. CooA, a CO-Sensing Transcription Factor from *Rhodospirillum rubrum*, Is a CO-Binding Heme Protein. *Proc. Natl. Acad. Sci. U.S.A.* **1997**, *94*, 11216−11220.
(318) Aono, S.; Ohkubo, K.; Matsuo, T.; Nakajima, H. Redox-Controlled Ligand Exchange of the Heme in the CO-Sensing Transcriptional Activator CooA. *J. Biol. Chem.* **1998**, *273*, 25757−25764.
(319) Nakajima, H.; Honma, Y.; Tawara, T.; Kato, T.; Park, S. Y.; Miyatake, H.; Shiro, Y.; Aono, S. Redox Properties and Coordination Structure of the Heme in the CO-Sensing Transcriptional Activator CooA. *J. Biol. Chem.* **2001**, *276*, 7055−7061.
(320) Nakajima, H.; Nakagawa, E.; Kobayashi, K.; Tagawa, S.; Aono, S. Ligand-Switching Intermediates for the CO-Sensing Transcriptional Activator CooA Measured by Pulse Radiolysis. *J. Biol. Chem.* **2001**, *276*, 37895−37899.

DOI: 10.1021/acs.chemrev.5b00018
Chem. Rev. 2015, 115, 6491−6533

(321) Shelver, D.; Thorsteinsson, M. V.; Kerby, R. L.; Chung, S. Y.; Roberts, G. P.; Reynolds, M. F.; Parks, R. B.; Burstyn, J. N. Identification of Two Important Heme Site Residues (Cysteine75 and Histidine77) in CooA, the CO-Sensing Transcription Factor of *Rhodospirillum rubrum*. *Biochemistry* **1999**, *38*, 2669−2678.
(322) Thorsteinsson, M. V.; Kerby, R. L.; Youn, H.; Conrad, M.; Serate, J.; Staples, C. R.; Roberts, G. P. Redox-Mediated Transcriptional Activation in a CooA Variant. *J. Biol. Chem.* **2001**, *276*, 26807−26813.
(323) Youn, H.; Kerby, R. L.; Roberts, G. P. Changing the Ligand Specificity of CooA, a Highly Specific Heme-Based CO Sensor. *J. Biol. Chem.* **2004**, *279*, 45744−45752.
(324) Youn, H.; Conrad, M.; Chung, S. Y.; Roberts, G. P. Roles of the Heme and Heme Ligands in the Activation of CooA, the CO-Sensing Transcriptional Activator. *Biochem. Biophys. Res. Commun.* **2006**, *348*, 345−350.
(325) Clark, R. W.; Youn, H.; Parks, R. B.; Cherney, M. M.; Roberts, G. P.; Burstyn, J. N. Investigation of the Role of the N-Terminal Proline, the Distal Heme Ligand in the CO Sensor CooA. *Biochemistry* **2004**, *43*, 14149−14160.
(326) Thorsteinsson, M. V.; Kerby, R. L.; Conrad, M.; Youn, H.; Staples, C. R.; Lanzilotta, W. N.; Poulos, T. J.; Serate, J.; Roberts, G. P. Characterization of Variants Altered at the N-Terminal Proline, a Novel Heme-Axial Ligand in CooA, the CO-Sensing Transcriptional Activator. *J. Biol. Chem.* **2000**, *275*, 39332−39338.
(327) Thorsteinsson, M. V.; Kerby, R. L.; Roberts, G. P. Altering the Specificity of CooA, the Carbon Monoxide-Sensing Transcriptional Activator: Characterization of CooA Variants That Bind Cyanide in the Fe(II) Form with High Affinity. *Biochemistry* **2000**, *39*, 8284−8290.
(328) Uchida, T.; Ishikawa, H.; Ishimori, K.; Morishima, I.; Nakajima, H.; Aono, S.; Mizutani, Y.; Kitagawa, T. Identification of Histidine 77 as the Axial Heme Ligand of Carbonmonoxy CooA by Picosecond Time-Resolved Resonance Raman Spectroscopy. *Biochemistry* **2000**, *39*, 12747−12752.
(329) Yamamoto, K.; Ishikawa, H.; Takahashi, S.; Ishimori, K.; Morishima, I.; Nakajima, H.; Aono, S. Binding of CO at the Pro2 Side Is Crucial for the Activation of CO-Sensing Transcriptional Activator CooA. ^{1}H NMR Spectroscopic Studies. *J. Biol. Chem.* **2001**, *276*, 11473−11476.
(330) Yamashita, T.; Hoashi, Y.; Watanabe, K.; Tomisugi, Y.; Ishikawa, Y.; Uno, T. Roles of Heme Axial Ligands in the Regulation of CO Binding to CooA. *J. Biol. Chem.* **2004**, *279*, 21394−21400.
(331) Leduc, J.; Thorsteinsson, M. V.; Gaal, T.; Roberts, G. P. Mapping CooA.RNA Polymerase Interactions. Identification of Activating Regions 2 and 3 in CooA, the Co-Sensing Transcriptional Activator. *J. Biol. Chem.* **2001**, *276*, 39968−39973.
(332) Inagaki, S.; Masuda, C.; Akaishi, T.; Nakajima, H.; Yoshioka, S.; Ohta, T.; Pal, B.; Kitagawa, T.; Aono, S. Spectroscopic and Redox Properties of a CooA Homologue from *Carboxydothermus hydrogenoformans*. *J. Biol. Chem.* **2005**, *280*, 3269−3274.
(333) Komori, H.; Inagaki, S.; Yoshioka, S.; Aono, S.; Higuchi, Y. Crystal Structure of CO-Sensing Transcription Activator CooA Bound to Exogenous Ligand Imidazole. *J. Mol. Biol.* **2007**, *367*, 864−871.
(334) Clark, R. W.; Lanz, N. D.; Lee, A. J.; Kerby, R. L.; Roberts, G. P.; Burstyn, J. N. Unexpected NO-Dependent DNA Binding by the CooA Homolog from *Carboxydothermus hydrogenoformans*. *Proc. Natl. Acad. Sci. U.S.A.* **2006**, *103*, 891−896.
(335) Kubo, M.; Inagaki, S.; Yoshioka, S.; Uchida, T.; Mizutani, Y.; Aono, S.; Kitagawa, T. Evidence for Displacements of the C-Helix by CO Ligation and DNA Binding to CooA Revealed by UV Resonance Raman Spectroscopy. *J. Biol. Chem.* **2006**, *281*, 11271−11278.
(336) Yamashita, T.; Hoashi, Y.; Tomisugi, Y.; Ishikawa, Y.; Uno, T. The C-Helix in CooA Rolls upon CO Binding to Ferrous Heme. *J. Biol. Chem.* **2004**, *279*, 47320−47325.
(337) Ibrahim, M.; Kerby, R. L.; Puranik, M.; Wasbotten, I. H.; Youn, H.; Roberts, G. P.; Spiro, T. G. Heme Displacement Mechanism of CooA Activation: Mutational and Raman Spectroscopic Evidence. *J. Biol. Chem.* **2006**, *281*, 29165−29173.
(338) Kerby, R. L.; Roberts, G. P. Sustaining N_2-Dependent Growth in the Presence of CO. *J. Bacteriol.* **2011**, *193*, 774−777.
(339) Marvin, K. A.; Kerby, R. L.; Youn, H.; Roberts, G. P.; Burstyn, J. N. The Transcription Regulator RcoM-2 from *Burkholderia xenovorans* Is a Cysteine-Ligated Hemoprotein That Undergoes a Redox-Mediated Ligand Switch. *Biochemistry* **2008**, *47*, 9016−9028.
(340) Smith, A. T.; Marvin, K. A.; Freeman, K. M.; Kerby, R. L.; Roberts, G. P.; Burstyn, J. N. Identification of Cys94 as the Distal Ligand to the Fe(III) Heme in the Transcriptional Regulator RcoM-2 from *Burkholderia xenovorans*. *J. Biol. Inorg. Chem.* **2012**, *17*, 1071−1082.
(341) Kerby, R. L.; Roberts, G. P. *Burkholderia Xenovorans* $RcoM_{Bx}$-1, a Transcriptional Regulator System for Sensing Low and Persistent Levels of Carbon Monoxide. *J. Bacteriol.* **2012**, *194*, 5803−5816.
(342) Vandiver, M. S.; Snyder, S. H. Hydrogen Sulfide: A Gasotransmitter of Clinical Relevance. *J. Mol. Med.* **2012**, *90*, 255−263.
(343) Ereño-Orbea, J.; Oyenarte, I.; Martínez-Cruz, L. A. CBS Domains: Ligand Binding Sites and Conformational Variability. *Arch. Biochem. Biophys.* **2013**, *540*, 70−81.
(344) Ereño-Orbea, J.; Majtan, T.; Oyenarte, I.; Kraus, J. P.; Martínez-Cruz, L. A. Structural Basis of Regulation and Oligomerization of Human Cystathionine β-Synthase, the Central Enzyme of Transsulfuration. *Proc. Natl. Acad. Sci. U.S.A.* **2013**, *110*, E3790−E3799.
(345) Ereño-Orbea, J.; Majtan, T.; Oyenarte, I.; Kraus, J. P.; Martínez-Cruz, L. A. Structural Insight into the Molecular Mechanism of Allosteric Activation of Human Cystathionine β-Synthase by S-Adenosylmethionine. *Proc. Natl. Acad. Sci. U.S.A.* **2014**, *111*, E3845−E3852.
(346) Su, Y.; Majtan, T.; Freeman, K. M.; Linck, R.; Ponter, S.; Kraus, J. P.; Burstyn, J. N. Comparative Study of Enzyme Activity and Heme Reactivity in *Drosophila melanogaster* and *Homo sapiens* Cystathionine β-Synthases. *Biochemistry* **2013**, *52*, 741−751.
(347) Smith, A. T.; Su, Y.; Stevens, D. J.; Majtan, T.; Kraus, J. P.; Burstyn, J. N. Effect of the Disease-Causing R266K Mutation on the Heme and PLP Environments of Human Cystathionine β-Synthase. *Biochemistry* **2012**, *51*, 6360−6370.
(348) Taoka, S.; Lepore, B. W.; Kabil, O.; Ojha, S.; Ringe, D.; Banerjee, R. Human Cystathionine β-Synthase Is a Heme Sensor Protein. Evidence That the Redox Sensor Is Heme and Not the Vicinal Cysteines in the CXXC Motif Seen in the Crystal Structure of the Truncated Enzyme. *Biochemistry* **2002**, *41*, 10454−10461.
(349) Yadav, P. K.; Xie, P.; Banerjee, R. Allosteric Communication between the Pyridoxal 5′-Phosphate (PLP) and Heme Sites in the H_2S Generator Human Cystathionine β-Synthase. *J. Biol. Chem.* **2012**, *287*, 37611−37620.
(350) Kabil, O.; Weeks, C. L.; Carballal, S.; Gherasim, C.; Alvarez, B.; Spiro, T. G.; Banerjee, R. Reversible Heme-Dependent Regulation of Human Cystathionine β-Synthase by a Flavoprotein Oxidoreductase. *Biochemistry* **2011**, *50*, 8261−8263.
(351) Tang, X. D.; Xu, R.; Reynolds, M. F.; Garcia, M. L.; Heinemann, S. H.; Hoshi, T. Haem Can Bind to and Inhibit Mammalian Calcium-Dependent Slo1 BK Channels. *Nature* **2003**, *425*, 531−535.
(352) Sahoo, N.; Goradia, N.; Ohlenschläger, O.; Schönherr, R.; Friedrich, M.; Plass, W.; Kappl, R.; Hoshi, T.; Heinemann, S. H. Heme Impairs the Ball-and-Chain Inactivation of Potassium Channels. *Proc. Natl. Acad. Sci. U.S.A.* **2013**, *110*, E4036−E4044.
(353) Hoshi, T.; Lahiri, S. Cell Biology. Oxygen Sensing: It's a Gas! *Science* **2004**, *306*, 2050−2051.
(354) Hou, S.; Reynolds, M. F.; Horrigan, F. T.; Heinemann, S. H.; Hoshi, T. Reversible Binding of Heme to Proteins in Cellular Signal Transduction. *Acc. Chem. Res.* **2006**, *39*, 918−924.
(355) Hou, S.; Xu, R.; Heinemann, S. H.; Hoshi, T. The RCK1 High-Affinity Ca^{2+} Sensor Confers Carbon Monoxide Sensitivity to Slo1 BK Channels. *Proc. Natl. Acad. Sci. U.S.A.* **2008**, *105*, 4039−4043.
(356) Williams, S. E. J.; Wootton, P.; Mason, H. S.; Bould, J.; Iles, D. E.; Riccardi, D.; Peers, C.; Kemp, P. J. Hemoxygenase-2 Is an Oxygen

DOI: 10.1021/acs.chemrev.5b00018
Chem. Rev. 2015, 115, 6491−6533

Sensor for a Calcium-Sensitive Potassium Channel. *Science* **2004**, *306*, 2093−2097.
(357) Al-Owais, M. M. A.; Scragg, J. L.; Dallas, M. L.; Boycott, H. E.; Warburton, P.; Chakrabarty, A.; Boyle, J. P.; Peers, C. Carbon Monoxide Mediates the Anti-Apoptotic Effects of Heme Oxygenase-1 in Medulloblastoma DAOY Cells via K^+ Channel Inhibition. *J. Biol. Chem.* **2012**, *287*, 24754−24764.
(358) Elies, J.; Dallas, M. L.; Boyle, J. P.; Scragg, J. L.; Duke, A.; Steele, D. S.; Peers, C. Inhibition of the Cardiac Na^+ Channel Nav1.5 by Carbon Monoxide. *J. Biol. Chem.* **2014**, *289*, 16421−16429.
(359) León-Paravic, C. G.; Figueroa, V. A.; Guzmán, D. J.; Valderrama, C. F.; Vallejos, A. A.; Fiori, M. C.; Altenberg, G. A.; Reuss, L.; Retamal, M. A. Carbon Monoxide (CO) Is a Novel Inhibitor of Connexin Hemichannels. *J. Biol. Chem.* **2014**, *289*, 36150−36157.
(360) Jaggar, J. H.; Li, A.; Parfenova, H.; Liu, J.; Umstot, E. S.; Dopico, A. M.; Leffler, C. W. Heme Is a Carbon Monoxide Receptor for Large-Conductance Ca^{2+}-Activated K^+ Channels. *Circ. Res.* **2005**, *97*, 805−812.
(361) Yi, L.; Morgan, J. T.; Ragsdale, S. W. Identification of a Thiol/disulfide Redox Switch in the Human BK Channel That Controls Its Affinity for Heme and CO. *J. Biol. Chem.* **2010**, *285*, 20117−20127.
(362) Ragsdale, S. W.; Yi, L.; Bender, G.; Gupta, N.; Kung, Y.; Yan, L.; Stich, T. A.; Doukov, T.; Leichert, L.; Jenkins, P. M.; et al. Redox, Haem and CO in Enzymatic Catalysis and Regulation. *Biochem. Soc. Trans.* **2012**, *40*, 501−507.
(363) Dioum, E. M.; Rutter, J.; Tuckerman, J. R.; Gonzalez, G.; Gilles-Gonzalez, M. A.; McKnight, S. L. PAS2: A Gas-Responsive Transcription Factor. *Science* **2002**, *298*, 2385−2387.
(364) Ishida, M.; Ueha, T.; Sagami, I. Effects of Mutations in the Heme Domain on the Transcriptional Activity and DNA-Binding Activity of NPAS2. *Biochem. Biophys. Res. Commun.* **2008**, *368*, 292−297.
(365) Koudo, R.; Kurokawa, H.; Sato, E.; Igarashi, J.; Uchida, T.; Sagami, I.; Kitagawa, T.; Shimizu, T. Spectroscopic Characterization of the Isolated Heme-Bound PAS-B Domain of Neuronal PAS Domain Protein 2 Associated with Circadian Rhythms. *FEBS J.* **2005**, *272*, 4153−4162.
(366) Mukaiyama, Y.; Uchida, T.; Sato, E.; Sasaki, A.; Sato, Y.; Igarashi, J.; Kurokawa, H.; Sagami, I.; Kitagawa, T.; Shimizu, T. Spectroscopic and DNA-Binding Characterization of the Isolated Heme-Bound Basic Helix-Loop-Helix-PAS-A Domain of Neuronal PAS Protein 2 (NPAS2), a Transcription Activator Protein Associated with Circadian Rhythms. *FEBS J.* **2006**, *273*, 2528−2539.
(367) Uchida, T.; Sato, E.; Sato, A.; Sagami, I.; Shimizu, T.; Kitagawa, T. CO-Dependent Activity-Controlling Mechanism of Heme-Containing CO-Sensor Protein, Neuronal PAS Domain Protein 2. *J. Biol. Chem.* **2005**, *280*, 21358−21368.
(368) Uchida, T.; Sagami, I.; Shimizu, T.; Ishimori, K.; Kitagawa, T. Effects of the bHLH Domain on Axial Coordination of Heme in the PAS-A Domain of Neuronal PAS Domain Protein 2 (NPAS2): Conversion from His119/Cys170 Coordination to His119/His171 Coordination. *J. Inorg. Biochem.* **2012**, *108*, 188−195.
(369) Lukat-Rodgers, G. S.; Correia, C.; Botuyan, M. V.; Mer, G.; Rodgers, K. R. Heme-Based Sensing by the Mammalian Circadian Protein CLOCK. *Inorg. Chem.* **2010**, *49*, 6349−6365.
(370) Asher, G.; Schibler, U. A CLOCK-Less Clock. *Trends Cell Biol.* **2006**, *16*, 547−549.
(371) Raghuram, S.; Stayrook, K. R.; Huang, P.; Rogers, P. M.; Nosie, A. K.; McClure, D. B.; Burris, L. L.; Khorasanizadeh, S.; Burris, T. P.; Rastinejad, F. Identification of Heme as the Ligand for the Orphan Nuclear Receptors REV-ERBα and REV-ERBβ. *Nat. Struct. Mol. Biol.* **2007**, *14*, 1207−1213.
(372) Rogers, P. M.; Ying, L.; Burris, T. P. Relationship between Circadian Oscillations of Rev-Erbα Expression and Intracellular Levels of Its Ligand, Heme. *Biochem. Biophys. Res. Commun.* **2008**, *368*, 955−958.
(373) Yin, L.; Wu, N.; Curtin, J. C.; Qatanani, M.; Szwergold, N. R.; Reid, R. A.; Waitt, G. M.; Parks, D. J.; Pearce, K. H.; Wisely, G. B.; et al. Rev-Erbα, a Heme Sensor That Coordinates Metabolic and Circadian Pathways. *Science* **2007**, *318*, 1786−1789.
(374) Gupta, N.; Ragsdale, S. W. Thiol-Disulfide Redox Dependence of Heme Binding and Heme Ligand Switching in Nuclear Hormone Receptor Rev-Erbβ. *J. Biol. Chem.* **2011**, *286*, 4392−4403.
(375) Marvin, K. A.; Reinking, J. L.; Lee, A. J.; Pardee, K.; Krause, H. M.; Burstyn, J. N. Nuclear Receptors *Homo sapiens* Rev-Erbβ and *Drosophila melanogaster* E75 Are Thiolate-Ligated Heme Proteins Which Undergo Redox-Mediated Ligand Switching and Bind CO and NO. *Biochemistry* **2009**, *48*, 7056−7071.
(376) Pardee, K. I.; Xu, X.; Reinking, J.; Schuetz, A.; Dong, A.; Liu, S.; Zhang, R.; Tiefenbach, J.; Lajoie, G.; Plotnikov, A. N.; et al. The Structural Basis of Gas-Responsive Transcription by the Human Nuclear Hormone Receptor REV-ERBβ. *PLoS Biol.* **2009**, *7*, e43.
(377) Reinking, J.; Lam, M. M. S.; Pardee, K.; Sampson, H. M.; Liu, S.; Yang, P.; Williams, S.; White, W.; Lajoie, G.; Edwards, A.; et al. The Drosophila Nuclear Receptor E75 Contains Heme and Is Gas Responsive. *Cell* **2005**, *122*, 195−207.
(378) Nagata, R.; Harada, M.; Kitanishi, K.; Igarashi, J.; Uchida, T.; Ishimori, K.; Shimizu, T. Heme Binding Characteristics of Mouse PER1, A Transcriptional Regulatory Factor Associated with Circadian Rhythms. In *Circadian Rhythms: Biology, Cognition and Disorders*; Golovkin, L., Maliszkewicz, A., Eds.; Nova Science: Hauppauge, 2011; Chapter VI, pp 133−160.
(379) Guenthner, C. J.; Bickar, D.; Harrington, M. E. Heme Reversibly Damps PERIOD2 Rhythms in Mouse Suprachiasmatic Nucleus Explants. *Neuroscience* **2009**, *164*, 832−841.
(380) Kitanishi, K.; Igarashi, J.; Hayasaka, K.; Hikage, N.; Saiful, I.; Yamauchi, S.; Uchida, T.; Ishimori, K.; Shimizu, T. Heme-Binding Characteristics of the Isolated PAS-A Domain of Mouse Per2, a Transcriptional Regulatory Factor Associated with Circadian Rhythms. *Biochemistry* **2008**, *47*, 6157−6168.
(381) Kitanishi, K.; Hayasaka, K.; Harada, M.; Nagata, R.; Igarashi, J.; Shimizu, T. Emerging Functions of Heme in Transcription Associated with Circadian Rhythms. In *Circadian Rhythms: Biology, Cognition and Disorders, Chapter X*; Golovkin, L., Maliszkewicz, A., Eds.; Nova Science: Hauppauge, 2011; pp 225−245.
(382) Kaasik, K.; Lee, C. C. Reciprocal Regulation of Haem Biosynthesis and the Circadian Clock in Mammals. *Nature* **2004**, *430*, 467−471.
(383) Yang, J.; Kim, K. D.; Lucas, A.; Drahos, K. E.; Santos, C. S.; Mury, S. P.; Capelluto, D. G. S.; Finkielstein, C. V. A Novel Heme-Regulatory Motif Mediates Heme-Dependent Degradation of the Circadian Factor Period 2. *Mol. Cell. Biol.* **2008**, *28*, 4697−4711.
(384) Hayasaka, K.; Kitanishi, K.; Igarashi, J.; Shimizu, T. Heme-Binding Characteristics of the Isolated PAS-B Domain of Mouse Per2, a Transcriptional Regulatory Factor Associated with Circadian Rhythms. *Biochim. Biophys. Acta* **2011**, *1814*, 326−333.
(385) Shimizu, T. Binding of Cysteine Thiolate to the Fe(III) Heme Complex Is Critical for the Function of Heme Sensor Proteins. *J. Inorg. Biochem.* **2012**, *108*, 171−177.
(386) Green, J.; Paget, M. S. Bacterial Redox Sensors. *Nat. Rev. Microbiol.* **2004**, *2*, 954−966.
(387) Molitor, B.; Stassen, M.; Modi, A.; El-Mashtoly, S. F.; Laurich, C.; Lubitz, W.; Dawson, J. H.; Rother, M.; Frankenberg-Dinkel, N. A Heme-Based Redox Sensor in the Methanogenic Archaeon *Methanosarcina acetivorans*. *J. Biol. Chem.* **2013**, *288*, 18458−18472.
(388) Pokkuluri, P. R.; Pessanha, M.; Londer, Y. Y.; Wood, S. J.; Duke, N. E. C.; Wilton, R.; Catarino, T.; Salgueiro, C. A.; Schiffer, M. Structures and Solution Properties of Two Novel Periplasmic Sensor Domains with *c*-Type Heme from Chemotaxis Proteins of *Geobacter sulfurreducens*: Implications for Signal Transduction. *J. Mol. Biol.* **2008**, *377*, 1498−1517.
(389) Yoshioka, S.; Kobayashi, K.; Yoshimura, H.; Uchida, T.; Kitagawa, T.; Aono, S. Biophysical Properties of a *c*-Type Heme in Chemotaxis Signal Transducer Protein DcrA. *Biochemistry* **2005**, *44*, 15406−15413.
(390) Catarino, T.; Pessanha, M.; De Candia, A. G.; Gouveia, Z.; Fernandes, A. P.; Pokkuluri, P. R.; Murgida, D.; Marti, M. A.;

DOI: 10.1021/acs.chemrev.5b00018
Chem. Rev. 2015, 115, 6491−6533

Todorovic, S.; Salgueiro, C. A. Probing the Chemotaxis Periplasmic Sensor Domains from *Geobacter sulfurreducens* by Combined Resonance Raman and Molecular Dynamic Approaches: NO and CO Sensing. *J. Phys. Chem. B* **2010**, *114*, 11251−11260.
(391) Freeman, T. L.; Hong, Y.; Schiavoni, K. H.; Bandara, D. M. I.; Pletneva, E. V. Changes in the Heme Ligation during Folding of a *Geobacter sulfurreducens* Sensor GSU0935. *Dalton Trans.* **2012**, *41*, 8022−8030.
(392) Silva, M. A.; Lucas, T. G.; Salgueiro, C. A.; Gomes, C. M. Protein Folding Modulates the Swapped Dimerization Mechanism of Methyl-Accepting Chemotaxis Heme Sensors. *PLoS One* **2012**, *7*, e46328.
(393) Silva, M. A.; Valente, R. C.; Pokkuluri, P. R.; Turner, D. L.; Salgueiro, C. A.; Catarino, T. Thermodynamic and Kinetic Characterization of Two Methyl-Accepting Chemotaxis Heme Sensors from *Geobacter sulfurreducens* Reveals the Structural Origin of Their Functional Difference. *Biochim. Biophys. Acta* **2014**, *1837*, 920−928.
(394) Colas, C.; Ortiz de Montellano, P. R. Autocatalytic Radical Reactions in Physiological Prosthetic Heme Modification. *Chem. Rev.* **2003**, *103*, 2305−2332.
(395) Huang, L.; Wojciechowski, G.; Ortiz de Montellano, P. R. Role of Heme-Protein Covalent Bonds in Mammalian Peroxidases. Protection of the Heme by a Single Engineered Heme-Protein Link in Horseradish Peroxidase. *J. Biol. Chem.* **2006**, *281*, 18983−18988.
(396) Wojciechowski, G.; Huang, L.; Ortiz de Montellano, P. R. Autocatalytic Modification of the Prosthetic Heme of Horseradish but Not Lactoperoxidase by Thiocyanate Oxidation Products. A Role for Heme-Protein Covalent Cross-Linking. *J. Am. Chem. Soc.* **2005**, *127*, 15871−15879.
(397) Kobayashi, K.; Yoshioka, S.; Kato, Y.; Asano, Y.; Aono, S. Regulation of Aldoxime Dehydratase Activity by Redox-Dependent Change in the Coordination Structure of the Aldoxime-Heme Complex. *J. Biol. Chem.* **2005**, *280*, 5486−5490.
(398) Tsai, A. L.; Berka, V.; Martin, E.; Olson, J. S. A "Sliding Scale Rule" for Selectivity among NO, CO and O_2 by Heme Protein Sensors. *Biochemistry* **2012**, *51*, 172−186.
(399) Yuan, G.; Vasavda, C.; Peng, Y. J.; Makarenko, V. V.; Raghuraman, G.; Nanduri, J.; Gadalla, M. M.; Semenza, G. L.; Kumar, G. K.; Snyder, S. H.; et al. Protein Kinase G-Regulated Production of H_2S Governs Oxygen Sensing. *Sci. Signaling* **2015**, *8*, ra37 DOI: 10.1126/scisignal.2005846.
(400) Meier, M.; Janosik, M.; Kery, V.; Kraus, J. P.; Burkhard, P. Structure of Human Cystathionine β-Synthase: A Unique Pyridoxal 5′-Phosphate-Dependent Heme Protein. *EMBO J.* **2001**, *20*, 3910−3916.

DOI: 10.1021/acs.chemrev.5b00018
Chem. Rev. 2015, 115, 6491−6533

3.2 Kinetic analysis of a globin-coupled histidine kinase, *Af*GcHK: effects of the heme iron complex, response regulator, and metal cations on autophosphorylation activity

Fojtikova V., Stranava M., Vos M. H., Liebl U., Hranicek J., Kitanishi K., Shimizu T., Martinkova M. *Biochemistry* (2015) 54, 5017 **(IF$_{2016}$ 2,9)**.

Podíl předkladatelky na této práci: 75 % (plánování experimentů, exprese a purifikace proteinů, kinetické analýzy, vyhodnocení a zpracování výsledků)

potvrzeno korespondujícím autorem, doc. RNDr. Markéta Martínková, Ph.D.

BIOCHEMISTRY
including biophysical chemistry & molecular biology

Article

pubs.acs.org/biochemistry

Kinetic Analysis of a Globin-Coupled Histidine Kinase, *Af*GcHK: Effects of the Heme Iron Complex, Response Regulator, and Metal Cations on Autophosphorylation Activity

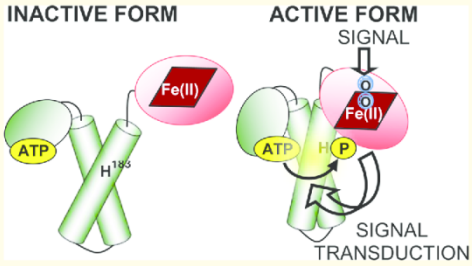
Veronika Fojtikova,[†] Martin Stranava,[†] Marten H. Vos,[§] Ursula Liebl,[§] Jakub Hranicek,[‡] Kenichi Kitanishi,[†] Toru Shimizu,[†] and Marketa Martinkova*[,†]

[†]Department of Biochemistry and [‡]Department of Analytical Chemistry, Faculty of Science, Charles University in Prague, Hlavova (Albertov) 2030-8, Prague 2, Czech Republic

[§]Laboratoire d'Optique et Biosciences, INSERM U1182-CNRS UMR7645, Ecole Polytechnique, 91128 Palaiseau Cedex, France

Supporting Information

ABSTRACT: The globin-coupled histidine kinase, *Af*GcHK, is a part of the two-component signal transduction system from the soil bacterium *Anaeromyxobacter* sp. Fw109-5. Activation of its sensor domain significantly increases its autophosphorylation activity, which targets the His183 residue of its functional domain. The phosphate group of phosphorylated *Af*GcHK is then transferred to the cognate response regulator. We investigated the effects of selected variables on the autophosphorylation reaction's kinetics. The k_{cat} values of the heme Fe(III)-OH^-, Fe(III)-cyanide, Fe(III)-imidazole, and Fe(II)-O_2 bound active *Af*GcHK forms were 1.1−1.2 min^{-1}, and their K_m^{ATP} values were 18.9−35.4 μM. However, the active form bearing a CO-bound Fe(II) heme had a k_{cat} of 1.0 min^{-1} but a very high K_m^{ATP} value of 357 μM, suggesting that its active site structure differs strongly from the other active forms. The Fe(II) heme-bound inactive form had k_{cat} and K_m^{ATP} values of 0.4 min^{-1} and 78 μM, respectively, suggesting that its low activity reflects a low affinity for ATP relative to that of the Fe(III) form. The heme-free form exhibited low activity, with k_{cat} and K_m^{ATP} values of 0.3 min^{-1} and 33.6 μM, respectively, suggesting that the heme iron complex is essential for high catalytic activity. Overall, our results indicate that the coordination and oxidation state of the sensor domain heme iron profoundly affect the enzyme's catalytic activity because they modulate its ATP binding affinity and thus change its k_{cat}/K_m^{ATP} value. The effects of the response regulator and different divalent metal cations on the autophosphorylation reaction are also discussed.



The ability to sense environmental changes is important for all organisms. In particular, it is important to detect changes in the concentration of the physiologically most important gas, O_2, and other gases such as CO and NO, as well. Heme iron complexes have been shown to play central roles in gas sensing.[1] Heme-containing sensor proteins generally consist of two domains: an N-terminal sensor domain containing the heme-based gas-sensing site and a C-terminal functional domain. The structure−function relationship and mechanisms of communication between these domains have not yet been resolved in detail. DNA sequencing has revealed thousands of heme-binding domains (motifs and proteins) in the genomes of various organisms,[2] demonstrating their physiological importance and emphasizing the need for a detailed understanding of their mechanisms of action and the structure−function relationships of their domains.

One subgroup of heme-containing oxygen sensor proteins features functional domains that exhibit histidine kinase activity. Several such proteins have recently been characterized.[3−14] Histidine kinases are the first components of the two-component signal transduction systems found in bacteria; the second components are the response regulator (RR) proteins.[15−17] In general, sensor kinases are multidomain proteins containing a nonconserved sensory input domain responsible for detecting a particular stimulus or ligand and a conserved kinase domain.[15−18] RRs are also multidomain proteins with a conserved receiver domain and a variable output domain.[19−21] Once the sensor domain of a histidine kinase is activated by the first signal, the functional domain is stimulated and the autophosphorylation of a conserved His residue in the functional domain can be observed. This phosphate group is subsequently transferred to a conserved Asp residue in the receiver domain of the cognate RR, activating its output domain.

The most extensively characterized heme-containing oxygen sensor histidine kinases are FixL,[5,6] DosT,[8−11] and DevS (DosS).[8−11] FixL is involved in regulating the expression of

Received: May 11, 2015
Revised: July 2, 2015
Published: July 25, 2015

ACS Publications © 2015 American Chemical Society

DOI: 10.1021/acs.biochem.5b00517
Biochemistry 2015, 54, 5017−5029

genes essential for nitrogen fixation and the anaerobic respiratory chain in root nodule bacteria such as *Rhizobium meliloti*.[5,6] DosT and DevS are enzymes from *Mycobacterium tuberculosis* that regulate the expression of genes necessary for survival under hypoxic conditions.[8−11] A new member of the heme-containing oxygen sensor histidine kinase family was recently discovered, a globin-coupled histidine kinase known as *Af*GcHK from the soil bacterium *Anaeromyxobacter* sp. Fw109-5.[14] Although oxygen sensor histidine kinases with heme-bound PAS folds (FixL) or GAF folds (DosS, DosT) are known and have been well-characterized, *Af*GcHK is the first oxygen sensor histidine kinase that contains a heme-bound globin fold and is involved in a two-component signaling system. *Af*GcHK is also distinctive in that its catalytic activity is stimulated by the binding of O_2 to its heme Fe(II) complex, whereas the catalytic activity of FixL and DosS/DosT is stimulated by the dissociation of O_2 from the heme Fe(II) complex.[22] *Af*GcHK has already been partially characterized,[14] but many questions regarding its function and mechanism of action remain unresolved. In particular, its mechanism of action is poorly understood because it is not clear how signals are transduced between the sensor and functional domains. Two-component signaling has been linked to biofilm formation and virulence in certain pathogenic bacteria, making the components of these signaling systems attractive targets for controlling and suppressing these pathological processes. However, to control the function of these proteins, we must understand molecular mechanisms of their action. This work sheds new light on the process of signal transduction between the sensor and functional domains of a model heme-containing sensor protein.

It has been suggested that unlike well-known oxygen storage hemoproteins such as myoglobin, the heme-containing sensor proteins require a degree of structural flexibility to be functional.[23−25] However, their structures and the global conformational changes induced by changes in the redox state or coordination of the heme iron have been characterized using only indirect experimental methods, while X-ray crystallographic data for only a few isolated sensor and/or functional domains of certain heme-based gas sensor proteins have been obtained, there are currently no X-ray crystal structures for any full-length heme-based oxygen sensor protein[26,27] and only one such structure for a full-length heme-based CO sensor protein.[27] The lack of robust structural data makes it challenging to explain the general relationships among signal transduction, protein conformation, and the functional state of these sensor proteins. However, an understanding of these relationships is required to effectively manipulate their behavior.

To address this knowledge gap, we investigated the full-length heme-based gas sensor protein *Af*GcHK. The interactions between its sensor and functional domains were probed by performing kinetic analyses of its autophosphorylation activity under diverse conditions. Specifically, we studied the impact of changes in the heme iron's redox state as well as the effects of various ligands, the RR protein, and different metal cations on the autophosphorylation activity of the *Af*GcHK functional domain.

EXPERIMENTAL PROCEDURES

Materials. Ampicillin was obtained from P-lab (Prague, Czech Republic). Isopropyl β-D-thiogalactopyranoside, hemin, and acrylamide were obtained from Sigma-Aldrich (St. Louis, MO). Water, doubly distilled over quartz, was purified using a Milli-Q Plus system (EMD Millipore, Billerica, MA). All glassware used for sample preparation was conditioned in advance by being allowed to stand for 24 h in 10% HCl suprapur (Merck, Darmstadt, Germany). Phos-tag was from the Phos-tag consortium Wako Pure Chemical Industries (Osaka, Japan). All chemicals used were of the highest purity grade available from commercial sources and used without further purification.

Overexpression and Purification of the Wild-Type and Mutant Proteins. Cloning, site-directed mutagenesis, overexpression in *Escherichia coli*, and purification of His tagged-*Af*GcHK were performed in a manner slightly different from that of the experiments previously described.[14] The full-length wild-type and His99Ala proteins were prepared as described below. Briefly, *E. coli* BL21(DE3) (Novagen) was transformed with the appropriate pET 21c(+) plasmid, plated on LB agar containing 100 μg mL^{-1} ampicillin, and incubated at 37 °C overnight. The following day, a single colony was inoculated in LB medium containing 100 μg mL^{-1} ampicillin and shaken overnight at 250 rpm and 37 °C. The culture medium was then added to fresh Terrific Broth (1:1000 dilution) containing the same antibiotic concentration, and the mixture was again shaken at 250 rpm and 37 °C for 4 h. Subsequently, the medium was cooled to 15 °C, and protein expression was induced by the addition of 0.1 mM isopropyl β-D-thiogalactopyranoside followed by further shaking for 20 h. The *E. coli* cells were harvested by centrifugation for 30 min at 5000*g* and 4 °C, frozen in liquid nitrogen, and stored at −80 °C until the protein was purified. Frozen pellet cells were resuspended in buffer A [50 mM Tris-HCl (pH 8.0) and 100 mM NaCl] containing 1 mM phenylmethanesulfonyl fluoride and 1 mM ethylenediaminetetraacetic acid and lysed with 0.2 mg mL^{-1} lysozyme. The crude extract was sonicated six times for 1 min each (with 1 min intervals between sonications) on ice and then centrifuged at 50000*g* for 60 min at 4 °C. The resulting supernatant was incubated for 20 min with or without (in the case of the His99Ala mutant) hemin in dimethyl sulfoxide (300 μM) and then applied to a TALON Metal Affinity Resin column (Clontech Laboratories) that had been pre-equilibrated with buffer A. The column was then washed with buffer A containing 20 mM imidazole, and *Af*GcHK fractions were eluted with a linear gradient from 20 to 200 mM imidazole in buffer A. Protein fractions were pooled and applied to a Superdex 200 10/300 GL column (GE Healthcare) equilibrated with 20 mM Tris-HCl pH 8.0 buffer containing 150 mM NaCl. The desired eluates (identified by monitoring at 280 nm) were collected and concentrated with Amicon Ultra Centrifugal Filters (Millipore). Finally, the purified proteins were quickly frozen in liquid nitrogen and stored at −80 °C. Protein and heme concentrations were determined using the bicinchoninic acid assay with bovine serum albumin as a standard (Sunrise Absorbance Reader, TECAN) and the pyridine hemochromogen assay, respectively.[28] Purified proteins were >90% homogeneous, as confirmed by polyacrylamide gel electrophoresis in the presence of sodium dodecyl sulfate (SDS−PAGE).

The apo form of the WT *Af*GcHK protein was prepared by omitting the incubation with hemin during the purification process and by removing the residual heme iron complex from the expression process using the previously reported procedure.[29]

Cloning, site-directed mutagenesis, overexpression in *E. coli*, and purification of GST-tagged RR were performed in a

DOI: 10.1021/acs.biochem.5b00517
Biochemistry 2015, 54, 5017−5029

manner slightly different from that of the experiments previously described.[14] The full-length wild-type and Asp52/169Ala mutant RR were prepared as described below. Briefly, *E. coli* BL21(DE3) cells (Novagen) were transformed with the corresponding pGEX-6P-2 expression vector, plated on LB agar containing 100 μg mL^{-1} ampicillin, and incubated at 37 °C overnight. The following day, a single colony was inoculated in LB medium containing 100 μg mL^{-1} ampicillin and shaken overnight at 250 rpm and 37 °C. The culture medium was then added to fresh Terrific Broth (1:1000 dilution) containing the antibiotic mentioned above, and the mixture was again shaken at 250 rpm and 37 °C for 4 h. Subsequently, the medium was cooled to 15 °C, and protein expression was induced by the addition of 0.1 mM isopropyl β-D-thiogalactopyranoside followed by further shaking for 20 h. The *E. coli* cells were harvested by centrifugation for 30 min at 5000*g* and 4 °C, frozen in liquid nitrogen, and stored at −80 °C until the protein was purified. *E. coli* cells were resuspended in buffer B [10 mM Na_2HPO_4, 1.8 mM KH_2PO_4 (pH 7.5), 140 mM NaCl, and 2.7 mM KCl] with 1 mM ethylenediaminetetraacetic acid, 1 mM phenylmethanesulfonyl fluoride, and 0.2 mg mL^{-1} lysozyme. Cells were crushed via pulsed sonication six times for 1 min each (with 1 min intervals between sonications) on ice and then centrifuged at 50000*g* for 60 min at 4 °C. The supernatant fractions were applied to a glutathione-Sepharose 4B column (GE Healthcare). The column was then washed with buffer B, and protein fractions were eluted with 10 mM reduced glutathione in 50 mM Tris-HCl (pH 8.0). Protein fractions were pooled and applied to a Superdex 200 10/300 GL column (GE Healthcare) equilibrated with 50 mM Tris-HCl (pH 8.0) buffer containing 150 mM NaCl. The desired eluates (identified by monitoring at 280 nm) were collected and concentrated with Amicon Ultra Centrifugal Filters (Millipore). Purified proteins were immediately frozen in liquid nitrogen and stored at −80 °C until they were used. Purified GST-RR was more than 97% homogeneous as determined by SDS−PAGE followed by staining with Coomassie Brilliant Blue. Protein concentrations were determined using the bicinchoninic acid assay with bovine serum albumin as a standard (Sunrise Absorbance Reader, TECAN).

Optical Absorption Spectroscopy. Optical absorption spectral data were obtained using an HP 8453 UV−vis spectrophotometer (Agilent Technologies, Santa Clara, CA) at 20 °C under aerobic conditions as previously described.[14] Anaerobic spectral experiments were conducted on a DeNovix DS-11 spectrophotometer in a gastight plastic box (Sigma-Aldrich, Schnelldorf, Germany) with 99.998% Ar (O_2 concentrations of <3 ppm). To ensure that the solution was maintained at an appropriate temperature (20 °C), the reaction mixture was incubated for 5 min prior to spectroscopic measurement. The Fe(II) complex was prepared in N_2-saturated buffer [50 mM Tris-HCl (pH 8.0)].

Femtosecond Spectroscopy. Ultrafast pump−probe spectroscopy with pump pulses centered at 570 nm and continuum broadband probe pulses was performed using a 500 Hz repetition rate setup as described previously.[30] Samples were prepared in gastight 1 mm optical path-length cells in 20 mM Tris (pH 8.0) with a heme concentration of 40 μM for CO experiments or 50 μM for O_2 experiments. The CO complex was prepared by exposing dithionite-reduced degassed *Af*GcHK to 1 atm of CO. For some experiments, an equimolar quantity of a degassed RR solution was also added. The O_2 complex was prepared by reducing the degassed protein with a minimal amount of dithionite and subsequently exposing it to air. This complex has a very low autoxidation rate,[14] making it amenable to characterization and experimental study.

Kinetic Analysis of *Af*GcHK Autophosphorylation. The autophosphorylation activity of *Af*GcHK was assayed under various conditions. Unless stated otherwise, the experiments were conducted at 20 °C in a reaction mixture containing 10 μM *Af*GcHK, 50 mM Tris-HCl (pH 8.0), 50 mM KCl, and 5 mM $MgCl_2$. The reaction mixture was preincubated for 5 min at 20 °C, and the reaction was initiated by adding 1 mM ATP. The reaction time was usually 60 s.

The effect of pH on *Af*GcHK autophosphorylation was tested in reaction mixtures containing various buffers. Reactions at pH 5.5, 6.0, and 6.5 were performed using 100 mM phosphate buffer (Na_2HPO_4 + NaH_2PO_4); incubations at pH 7.0, 7.5, 8.0, 8.5, and 9.0 were performed in 100 mM Tris buffer (Tris-HCl), and incubations at pH 9.5 and 10.0 were performed using 100 mM glycine buffer. The *Af*GcHK autophosphorylation assay was also performed in 50 mM NaOH (pH 12.7) and 100 mM NaOH (pH 13.0) with no buffer.

The time course of the autophosphorylation reaction catalyzed by WT and His99Ala *Af*GcHK was assayed at 20 °C in a reaction mixture containing 10 μM *Af*GcHK (WT or His99Ala), 50 mM Tris-HCl (pH 8.0), 50 mM KCl, and 5 mM $MgCl_2$. The reaction mixture was preincubated for 5 min, and then the reaction was initiated by adding 1 mM ATP at 20 °C. The state of the reaction was determined at the following time points after its initiation: 0, 0.5, 1, 2, 5, 10, 15, 20, 30, 40, 50, 60, and 180 min.

To estimate the kinetic parameters of the autophosphorylation of *Af*GcHK, a reaction mixture containing 10 μM *Af*GcHK, 5−5000 μM ATP, 50 mM Tris-HCl (pH 8.0), 50 mM KCl, and 5 mM $MgCl_2$ in a total volume of 100 μL was used. The reaction was started by the addition of ATP. The product of the autophosphorylation reaction was the His^{183}-phosphorylated form of *Af*GcHK, i.e., P-*Af*GcHK, and its rate of formation was determined by Phos-tag electrophoresis (see below). On the basis of the previously determined (see the preceding paragraph) time course for the autophosphorylation reaction catalyzed by WT *Af*GcHK, the amount of reaction product formed per minute over the first minute of the reaction was taken to be equivalent to the initial velocity of the autophosphorylation. Therefore, the reaction mixtures for determination of kinetic parameters were incubated at 20 °C for 30 s; the reaction during this period was assumed to proceed under initial velocity conditions because of the reaction's linearity over the first 1 min. The *Af*GcHK autophosphorylation reaction is a pseudobisubstrate process (the two substrates being ATP and the enzyme itself). However, the kinetic study focused on the apparent kinetics observed when the concentration of the enzyme is invariant while that of ATP is varied. Kinetic constants were determined by nonlinear least-squares regression using the Michaelis−Menten equation. The results obtained in this way were consistent with those obtained from a Lineweaver−Burk plot (Figure S1). At least three replicate experiments were performed for each set of reaction conditions, and the results obtained for each replicate performed under a given set of conditions were usually within 10% of those for the other replicates. The standard deviations over all experimental replicates performed under each set of experimental conditions are reported in the figures and tables.

DOI: 10.1021/acs.biochem.5b00517
Biochemistry 2015, 54, 5017−5029

The effects of the sensor domain's heme iron as well as its redox and coordination state on the Michaelis−Menten kinetics of the autophosphorylation reaction were investigated by varying the configuration of the sensor domain heme. The sensor domain of the isolated protein was in the Fe(III)-OH^- state. The heme Fe(II) species were prepared by placing a 20 μM solution of the Fe(III)-OH^- protein in a quartz cuvette and reducing it using 10 mM sodium dithionite. Fe(II)-CO complexes were then prepared by gently bubbling gaseous carbon monoxide (Linde, Wiesbaden, Germany) through the cuvette for 15 min. No spectral changes indicative of heme oxidation over time were detected in the spectral recordings. Sodium dithionite, which was used to reduce the Fe(III) complex, was kept in the solution throughout the experiments with the Fe(II) and Fe(II)-CO complexes to prevent Fe(II)-O_2 complex formation. Separate experiments demonstrated that the presence of sodium dithionite did not affect the measured kinetic parameters. The Fe(II)-O_2 complex was prepared by removing sodium dithionite and exposing the Fe(II) species to air for 10 min. After the kinetic experiments, we characterized the samples by UV−vis spectroscopy to verify that the heme iron species remained in the Fe(II)-O_2 form. These studies revealed no evidence of heme iron autoxidation. The Fe(III)-CN^- and Fe(III)-imidazole forms of *Af*GcHK were produced by mixing a 20 μM solution of the Fe(III)-OH^- protein with 0.1 M KCN and 0.1 M imidazole, respectively. The KCN was used in 100 mM Tris buffer (pH 8.0), and the solution's pH was monitored. Heme-free experiments were performed using the His99Ala *Af*GcHK mutant instead of the WT protein.

The effect of the RR on *Af*GcHK autophosphorylation was tested in reaction mixtures containing 10 μM GST-RR and no $MgCl_2$. The lack of Mg^{2+} was necessary to suppress the phosphotransfer reaction to GST-RR, which competes with the autophosphorylation of *Af*GcHK. To investigate the effect of the RR on the autophosphorylation reaction in the presence of 5 mM Mg^{2+}, experiments were conducted using a mutated RR variant (10 μM Asp52/169Ala GST-RR). The mutant cannot undergo the phosphotransfer reaction because it lacks the necessary active aspartic acid residues.

The effects of divalent metal ions on *Af*GcHK autophosphorylation were investigated using reaction mixtures containing solutions of different metal salts instead of $MgCl_2$. Specifically, the $MgCl_2$ was replaced with 5 mM $MnCl_2$, 5 mM $CaCl_2$, 5 mM $CoCl_2$, 5 mM $NiCl_2$, 5 mM $ZnSO_4$, or 5 mM $CdCl_2$ as appropriate. To assess the enzyme's activity in the absence of divalent metal cations, reactions were performed with no added metal salt; these reaction mixtures were analyzed by atomic absorption spectroscopy (see below) to verify that they contained no divalent metal ions.

Identification of the P-*Af*GcHK by Phos-tag Electrophoresis. At the designated times, the *Af*GcHK autophosphorylation assay reaction was terminated by adding 100 μL aliquots of termination buffer [125 mM Tris-HCl (pH 6.8), 4% SDS, 10% 2-mercaptoethanol, 20% glycerol, and 0.004% bromophenol blue]. Samples of the quenched reaction mixtures were then loaded on a 10% SDS−polyacrylamide gel containing 75 μM Phos-tag acrylamide and 0.2 mM $MnCl_2$. Each lane was loaded with a quantity of quenched reaction mixture containing 0.5 μg of *Af*GcHK. Phosphorylated proteins in the sample interacted with the Phos-tag manganese complex in the gel, reducing their mobility relative to those of phosphate-free proteins.[14,24,31] After electrophoresis, the proteins were visualized by staining with Coomassie Brilliant Blue R350 and the stained gels were imaged using a Scanjet G3010 (HP) scanner. The protein loadings were then quantified by analyzing the scanned images using ImageJ.

Atomic Absorption Spectroscopy. Reference measurements of magnesium, manganese, and calcium concentrations were acquired using an AAS 3 (Zeiss, Jena, Germany) atomic absorption spectrometer with a flame atomization unit. The spectrometer was operated using predefined optimal settings. Varian Mn, Mg, and Ca hollow cathode lamps were operated at 279.5, 285.2, and 422.7 nm, respectively, with 0.2, 0.5, and 0.5 nm spectral bandpasses, respectively. A lamp current of 5 mA was used in all cases. Atomization was performed with an air−acetylene flame for Mn and Mg or a nitrous oxide−acetylene flame for Ca. The concentration of manganese was determined without adding any chemical agents. To suppress common interference during magnesium determination, a small amount of strontium nitrate (releasing agent) was added to all samples at a final concentration of 1000 mg L^{-1}. To avoid calcium ionization during its measurement, a small amount of potassium chloride was added to all samples at a final concentration of 3000 mg L^{-1}. All reagents used were of analytical reagent grade or higher purity. Deionized water (<0.1 mS cm^{-1}, Milli-QPLUS, Millipore) was used to prepare all solutions. Working standards were prepared by diluting standard 1.000 g L^{-1} stock solutions of Mn^{2+}, Mg^{2+}, and Ca^{2+} (Merck).

RESULTS

Optimization of the Autophosphorylation Activity of *Af*GcHK in Its Native Form. Purified preparations of *Af*GcHK were phosphorylated under conditions typical for histidine kinases with ATP, KCl, and $MgCl_2$ after incubations at 20 °C for 0.5−180 min, as previously reported.[14,32] Using UV−vis spectroscopy, we investigated the previous suggestion that the heme iron in the native protein obtained after purification forms a six-coordinate low-spin Fe(III) complex with an axial hydroxyl ligand on the heme-distal side (data not shown).[14] To further characterize the autophosphorylation of the Fe(III)-OH^--bound *Af*GcHK in its native form, its kinetics were examined.

The autophosphorylation reaction catalyzed by the Fe(III)-OH^--bound *Af*GcHK is a pseudobisubstrate reaction with the first substrate being ATP and the second the enzyme itself. The initial rate of autophosphorylation was determined at various *Af*GcHK concentrations and found to increase linearly with enzyme concentration (data not shown). The apparent Michaelis constant (K_m) with respect to *Af*GcHK could not be evaluated because the enzyme is both substrate and catalyst, and the catalyst concentration must be held constant to obtain a Michaelis constant with respect to a substrate. Therefore, kinetic analyses were performed only with respect to ATP, keeping the enzyme concentration constant at 10 μM. The time course of the autophosphorylation reaction catalyzed by *Af*GcHK revealed that its progress was linear during at least the first minute (Figure 1). That is to say, the amount of reaction product (the His^{183}-phosphorylated form of *Af*GcHK, henceforth termed P-*Af*GcHK) formed per minute during the first minute of the reaction was equivalent to the initial velocity of the kinase reaction. The initial velocities of autophosphorylation were measured at various ATP concentrations (0−1000 μM) at pH 8.0 in the presence of 50 mM K^+ and 5 mM Mg^{2+} (Figure 2). The reaction follows Michaelis−Menten kinetics with an apparent K_m^{ATP} value of 18.9 ± 2.3 μM and an maximal apparent enzyme velocity with respect to ATP (V_{max}^{ATP}) of

DOI: 10.1021/acs.biochem.5b00517
Biochemistry 2015, 54, 5017−5029

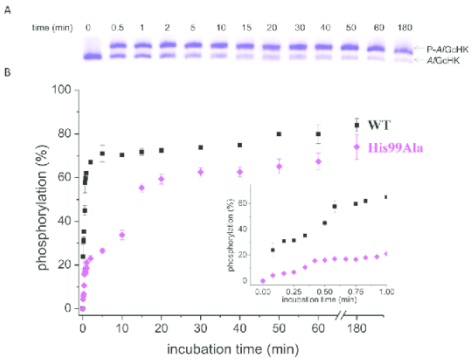


Figure 1. Time course of the histidine kinase reactions catalyzed by the WT *Af*GcHK [in its Fe(III)-OH^- form] and the His99Ala mutant of *Af*GcHK. (A) Phos-tag SDS−PAGE gel patterns demonstrating separation of *Af*GcHK and P-*Af*GcHK formed by WT *Af*GcHK at different time periods and (B) a graphical representation of the results: WT *Af*GcHK (■) and His99Ala (pink diamonds). In each run, a reaction mixture containing 10 μM *Af*GcHK (WT or His99Ala), 1 mM ATP, 50 mM Tris-HCl (pH 8.0), 50 mM KCl, and 5 mM $MgCl_2$ in a total volume of 100 μL was incubated for various time periods (for further details, see Experimental Procedures). The inset shows the expansion of initial time points of the time course plot.

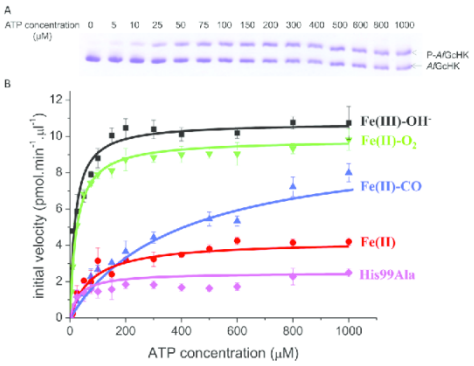


Figure 2. Effect of the heme iron redox states, heme iron ligand states, and the presence of heme iron in the sensor domain on the Michaelis−Menten kinetics of the autophosphorylation reaction catalyzed by WT *Af*GcHK. (A) Phos-tag SDS−PAGE gel patterns demonstrating separation of *Af*GcHK and P-*Af*GcHK formed by Fe(II)-O_2-bound *Af*GcHK at different ATP concentrations and (B) graphical representation of results for each of the different *Af*GcHK forms: Fe(III)-OH^- (native form, black line and squares), Fe(II)-O_2 (green line and triangles), Fe(II)-CO (blue line and triangles), Fe(II) (red line and circles), and heme-free form (His99Ala) (pink line and diamonds). In each run, a reaction mixture containing 10 μM *Af*GcHK, 0−1000 μM ATP, 50 mM Tris-HCl (pH 8.0), 50 mM KCl, and 5 mM $MgCl_2$ in a total volume of 100 μL was incubated for 30 s (for further details, see Experimental Procedures).

10.8 ± 0.3 pmol of P-*Af*GcHK min^{-1} μL^{-1}. The k_{cat} and k_{cat}/K_m^{ATP} values were determined to be 1.1 min^{-1} and 1000 M^{-1} s^{-1}, respectively (Table 1 and Figure S1).

Table 1. Effect of the Heme Iron Oxidation State, Ligand Coordination in the Sensor Domain, and the Presence of RRs (WT and Asp52/169Ala) on the Kinetic Parameters of the Autophosphorylation Reaction Catalyzed by *Af*GcHK

heme iron state in the sensor domain of *Af*GcHK or the presence of RR	K_m^{ATP} (μM)	V_{max}^{ATP} (pmol of P-*Af*GcHK min^{-1} μL^{-1})	k_{cat} (min^{-1})	k_{cat}/K_m^{ATP} (M^{-1} s^{-1})
Fe(III)-OH^- (WT, native form)	18.9 ± 2.3	10.8 ± 0.3	1.1	1000
Fe(III)-CN^-	35.4 ± 9.7	11.8 ± 0.6	1.2	600
Fe(III)-imidazole	23.8 ± 4.1	11.2 ± 0.3	1.1	800
Fe(II)-O_2	23.0 ± 1.3	9.6 ± 0.1	1.0	700
Fe(II)-CO	357.0 ± 28.0	10.4 ± 0.3	1.0	50
Fe(II)	78.0 ± 4.7	4.2 ± 0.2	0.4	90
no heme (His99Ala *Af*GcHK)	33.6 ± 1.7	2.5 ± 0.1	0.3	120
Fe(III)-OH^- and Asp52/169Ala RR	47.7 ± 1.4	10.0 ± 0.3	1.0	300
Fe(III)-OH^- and WT RR (in the absence of Mg^{2+})	152.0 ± 10.6	1.8 ± 0.2	0.16	20

Effect of pH on the Autophosphorylation Reaction Catalyzed by the Fe(III)-OH^--Bound *Af*GcHK. The efficiency of the autophosphorylation of the Fe(III)-OH^--bound *Af*GcHK was examined by measuring the amount of P-*Af*GcHK formed over an experimental period of 1 min using reaction mixtures containing 50 mM K^+ and 5 mM Mg^{2+} at pH values ranging from 5.5 to 13 (Figure 3). The enzyme was

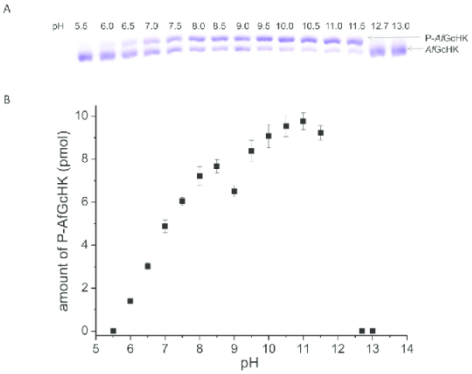


Figure 3. Effect of pH on the autophosphorylation reaction catalyzed by WT *Af*GcHK [in its Fe(III)-OH^- form]. (A) Phos-tag SDS−PAGE gel patterns demonstrating separation of *Af*GcHK and P-*Af*GcHK formed by Fe(III)-OH^--bound *Af*GcHK at different pH values and (B) a graphical representation of the results. In each run, a reaction mixture containing 10 μM *Af*GcHK, 1 mM ATP, 50 mM KCl, 5 mM $MgCl_2$, and an appropriate pH buffer (100 mM) in a total volume of 100 μL was incubated for 60 s (for further details, see Experimental Procedures). Note that the discontinuity at pH 9.0 is reproducible and may be due to a change in the axial ligand from OH^- to Tyr-O^-.

inactive below pH 5.5 or above pH 12.7 but exhibited discernible activity at between pH 6.0 and 11.5. Within this range, its activity exhibited an asymmetric bell-shaped dependence upon pH. Its optimal pH was around 11.0; the rate of autophosphorylation at pH 7.0 was around half that observed at

DOI: 10.1021/acs.biochem.5b00517
Biochemistry 2015, 54, 5017−5029

the optimal pH, while at pH 8.0, it was around 75% of the optimal rate. We conducted our subsequent experiments at pH 8.0 because these mildly alkaline conditions are optimal for preserving the conformation and stability of *Af*GcHK.[14] Moreover, pH 8.0 is more physiologically relevant than pH 11.0.

AfGcHK Retains Catalytic Activity When the Native Hydroxyl Ligand of the Sensor Domain Heme Iron Is Replaced with Cyanide or Imidazole (Figure 4). As

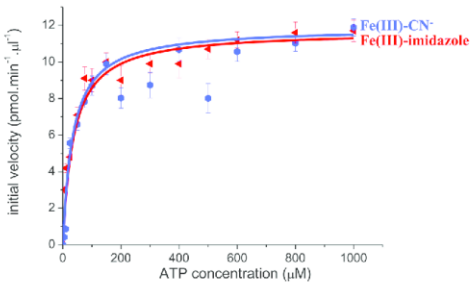


Figure 4. Effects of binding of cyanide and imidazole to the heme iron in the sensor domain on the Michaelis−Menten kinetics of the autophosphorylation reaction catalyzed by Fe(III)-bound *Af*GcHK: Fe(III)-CN^- (blue line and hexagons) and Fe(III)-imidazole (red line and triangles). In each run, a reaction mixture containing 10 μM *Af*GcHK, 0−1000 μM ATP, 50 mM Tris-HCl (pH 8.0), 50 mM KCl, and 5 mM $MgCl_2$ in a total volume of 100 μL was incubated for 30 s (for further details, see Experimental Procedures).

mentioned previously, the six-coordinate low-spin Fe(III) complex with an axial hydroxyl ligand at the heme-distal side of *Af*GcHK, Fe(III)-OH^-, is fully enzymatically active (Figure 2 and Table 1). Experiments were performed to determine how the coordination of alternative external ligands to the Fe(III) complex affected the functional domain's catalytic activity (Table 1 and Figure 4). Both the Fe(III)-CN^- and Fe(III)-imidazole forms of *Af*GcHK were enzymatically active with kinetic parameters that were very similar to those for the Fe(III)-OH^- complex (Table 1 and Figure 4).

The Heme Fe(II) Complex of *Af*GcHK Exhibits Low Activity but Is Activated by the Coordination of CO or O_2. While the six-coordinate low-spin Fe(III) complexes [Fe(III)-OH^-, Fe(III)-CN^-, and Fe(III)-imidazole] of *Af*GcHK are fully catalytically active (Figures 2 and 4 and Table 1), the five-coordinate high-spin Fe(II) complex of the same enzyme was significantly less active (Figure 2 and Table 1). While a detailed kinetic analysis of the reaction catalyzed by the Fe(II) complex of *Af*GcHK revealed that it followed Michaelis−Menten kinetics (Figure 2), its K_m^{ATP} value (78 μM) was more than 4 times greater than that for the Fe(III) complexes of *Af*GcHK, and its V_{max}^{ATP} value (4.2 pmol of P-*Af*GcHK min^{-1} μL^{-1}) was around half that for the Fe(III) complexes. The latter of these findings shows that the low activity of the five-coordinate high-spin Fe(II) complex is due to its low basal autophosphorylation activity compared to those of the Fe(III) complexes of *Af*GcHK. The effect of reducing the sensor domain heme iron on the autophosphorylation reaction is similar to that of removing the heme iron altogether, as discussed below (Figure 2 and Table 1).

When the Fe(II) complex of *Af*GcHK was exposed to either O_2 or CO, its catalytic activity was dramatically enhanced. The enzyme kinetics of the Fe(II)-O_2 complex closely resemble those of the Fe(III)-OH^- complex (Figure 2). Likewise, the kinetic parameters (K_m^{ATP} and V_{max}^{ATP}) of the Fe(III)-OH^- and Fe(II)-O_2 complexes are also very similar (Table 1).

The coordination of CO to the Fe(II) complex had remarkable effects: the K_m^{ATP} value of the resulting Fe(II)-CO complex was ~20 times higher than that of the parent Fe(II) complex, and its V_{max}^{ATP} value was similar to those for the Fe(III)-OH^- and Fe(II)-O_2 complexes. The strong increase in K_m^{ATP} caused by the coordination of CO suggests a dramatic reduction in the enzyme's affinity for ATP (Figure 2 and Table 1).

The Heme-Free Enzyme Has Low Activity. Two different strategies were used to study the effect of the heme's presence in the sensor domain on the autophosphorylation activity of *Af*GcHK. Experiments were performed using either (i) the apo form of WT *Af*GcHK or (ii) His99Ala *Af*GcHK. It was difficult to obtain pure samples of the apo WT *Af*GcHK protein because the prepared material always contained some traces of heme (data not shown), which hampered the interpretation of the kinetic analyses. Consequently, the second approach using the His99Ala mutant was adopted. It has been shown that the histidine residue at position 99 is the proximal axial ligand of the heme iron;[14] when this ligand is replaced with alanine, the protein loses its heme binding ability. This makes it straightforward to prepare the His99Ala mutant in a pure heme-free form.

Figure 2 shows the effect of the absence of the sensor domain heme on the Michaelis−Menten kinetics of the autophosphorylation reaction catalyzed by the heme-free apo form of *Af*GcHK His99Ala. The results obtained indicate that the heme's presence was essential for effective autophosphorylation by the functional domain. The V_{max}^{ATP} value for the autophosphorylation of *Af*GcHK without the sensor domain heme (His99Ala) was approximately 4 times lower than that of WT (Table 1). The absence of the heme in the sensor domain also reduced the mutant apo form's affinity for ATP: its K_m^{ATP} value was approximately twice that of the heme-containing WT *Af*GcHK enzyme (Table 1).

To determine whether coordination of the heme iron in the sensor domain was required for the autophosphorylation of the functional domain of *Af*GcHK, it was necessary to prove that the His99Ala mutation does not hinder the correct folding of the kinase domain. The time course of the autophosphorylation of the His99Ala mutant was monitored (Figure 1B) for that purpose.

The time course of the His99Ala autophosphorylation (Figure 1B) differed from that for WT *Af*GcHK. The reaction of His99Ala was significantly slower than that of the WT: the autophosphorylation of the WT went to completion within 5 min, but that of His99Ala took >60 min. Consequently, experiments conducted over longer periods of time (>60 min) would misleadingly suggest that the WT and His99Ala mutant have very similar activity. This may be why Kitanishi et al.[14] suggested that the presence of the heme iron in the sensor domain does not affect the activity of the functional domain; they examined the outcome of the autophosphorylation reaction only after an extended incubation period and did not investigate the enzyme's kinetics. The results indicate that the His99Ala mutant's functional domain is folded correctly and capable of autophosphorylation.

RR Binding Reduces the Affinity of *Af*GcHK for ATP. An abortive RR double mutant (Asp52/169Ala) in which the aspartate residues of the phosphorylation sites were replaced

DOI: 10.1021/acs.biochem.5b00517
Biochemistry 2015, 54, 5017−5029

with alanine residues that cannot be phosphorylated was used to investigate the effect of the RR on *Af*GcHK autophosphorylation. It was necessary to use the double mutant because the WT RR induces a phosphotransfer reaction from phosphorylated *Af*GcHK that interferes with the autophosphorylation of *Af*GcHK. The K_m^{ATP} value (47.7 μM) for autophosphorylation of *Af*GcHK in the presence of Asp52/169Ala RR was 2.5-fold higher than that in the absence of RR [18.9 μM (Table 1 and Figure 5)]. This finding suggests that the presence of the RR

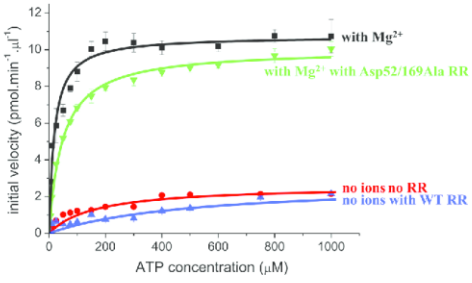


Figure 5. Effects of WT and Asp52/169Ala RR on the autophosphorylation of native *Af*GcHK. Note that WT RR in the presence of Mg^{2+} also catalyzes its autophosphorylation reaction, which competes with the studied process (autophosphorylation of *Af*GcHK): in the presence of Mg^{2+} and Asp52/169Ala RR (green line and triangles), in the presence of Mg^{2+} and in the absence of Asp52/169Ala RR (black line and squares), in the absence of both Mg^{2+} and RR (red line and circles), and in the absence of Mg^{2+} and in the presence of RR (blue line and triangles). In each run, a reaction mixture containing 10 μM *Af*GcHK and 0 or 10 μM RR (WT or Asp52/169Ala), 5−1000 μM ATP, 50 mM Tris-HCl (pH 8.0), 50 mM KCl, and 0 or 5 mM $MgCl_2$ in a total volume of 100 μL was incubated for 30 s (for further details, see Experimental Procedures).

mutant protein significantly reduces the affinity of *Af*GcHK for ATP. The RR-binding site of *Af*GcHK is probably located close to the ATP-binding site such that the binding of the RR interferes with that of ATP. Interestingly, the V_{max}^{ATP} value of *Af*GcHK was not significantly affected by the presence of the RR mutant (Table 1).

As an alternative way of eliminating the competing phosphotransfer reaction to the Asp52 and Asp169 residues of the RR, we studied the effect of the wild-type RR protein on the autophosphorylation activity of *Af*GcHK in the absence of Mg^{2+} ions. The WT RR protein did not affect the V_{max}^{ATP} value (1.8−2.2 pmol of P-*Af*GcHK min^{-1} μL^{-1}) associated with the very low basal autophosphorylation activity of *Af*GcHK under these conditions (Table 2), but the K_m^{ATP} value for *Af*GcHK in the presence of WT RR (152.0 μM) was 2.7 times greater than that in the absence of RR (55.9 μM) under the same conditions (Figure 5 and Tables 1 and 2). These results are consistent with those obtained in the experiments using the double mutant: both suggest that the presence of the RR protein significantly reduces the affinity of *Af*GcHK for ATP because the RR protein-binding site is probably situated close to the ATP-binding site.

Characterization of Ultrafast CO and O_2 Dissociation and Binding Kinetics. We examined the kinetics of CO and O_2 binding to and dissociation from the heme iron of *Af*GcHK on the femto- to nanosecond time scales using transient

Table 2. Effect of Divalent Metal Ions (Mg^{2+}, Mn^{2+}, Ca^{2+}, Co^{2+}, Ni^{2+}, Zn^{2+}, and Cd^{2+}) on the Kinetic Parameters of the Autophosphorylation Reaction Catalyzed by Fe(III)-Bound *Af*GcHK

ion for incubation of Fe(III)-bound *Af*GcHK	K_m^{ATP} (μM)	V_{max}^{ATP} (pmol of P-*Af*GcHK min^{-1} μL^{-1})	k_{cat} (min^{-1})	k_{cat}/K_m^{ATP} (M^{-1} s^{-1})
Mg^{2+}	18.9 ± 2.3	10.8 ± 0.3	1.1	1000
Mn^{2+}	93.2 ± 9.5	13.1 ± 0.3	1.3	233
Ca^{2+}	403.9 ± 105.4	6.9 ± 0.8	0.7	30
Co^{2+}	no reaction			
Ni^{2+}	no reaction			
Zn^{2+}	no reaction			
Cd^{2+}	no reaction			
no ions	55.9 ± 4.1	2.2 ± 0.1	0.2	60

absorption spectroscopy. The Fe(II)-CO and Fe(II)-O_2 forms of *Af*GcHK represent two extremes of catalytic efficiency, with the former complex's affinity for ATP being more than 1 order of magnitude lower than the latter's (Table 1). Selected transient spectra in the Soret region for the dissociation from the WT Fe(II)-CO complex are shown in Figure 6A. The difference spectra show the red shift that is typical for transitions from a six-coordinate state to a five-coordinate one. After spectral relaxations due to photophysical processes (not shown), which mainly occur over time scales of up to a few picoseconds,[33] the spectra become almost identical in shape but with diminished amplitudes, reflecting substantial geminate heme-CO recombination on the pico- to nanosecond time scale. A global analysis assuming multiexponential decay revealed rebinding phases of 170 ps (24%), 1.5 ns (49%), and >4 ns (27%). Such multiphasic rebinding behavior is observed in many heme proteins[30,34−39] and may reflect a process whereby CO samples a distribution of heme environments prior to rebinding, in competition with escape from the heme pocket.

This kinetic behavior is markedly different from that observed for myoglobin, mammalian hemoglobin, and the globin-coupled oxygen sensor YddV (unpublished results), where virtually no geminate rebinding occurs. However, it is qualitatively similar to that of truncated bacterial hemoglobins.[37,38]

Analyses of the kinetics of CO dissociation can be used to sensitively probe the heme environment, as demonstrated by experiments on genetically modified proteins.[36,38−41] This is also the case for *Af*GcHK (Figure S2). The inset of Figure 6A shows that in contrast to the results obtained for other enzymes, the kinetics of CO rebinding are not affected by the presence of the RR protein. This suggests that whereas the coordination state of the heme domain affects the catalytic efficiency of the enzymatic domain by modulating its ATP affinity, there is no significant reverse effect. In general terms, this finding is consistent with the observation that the CO rebinding kinetics of the heme domain of *Ec* Dos do not depend on the catalytic domain's presence.[42]

Excitation of the Fe(II)-O_2 complex of *Af*GcHK yielded a signal that was far weaker than the CO dissociation signal and featured a small red-shift that evolved on the time scale of hundreds of femtoseconds to a few picoseconds (Figure 6B). These findings are similar to those achieved for other sensor complexes and presumably reflect heme photophysics, including cooling of the heme. The quantum yield (QY) of

DOI: 10.1021/acs.biochem.5b00517
Biochemistry 2015, 54, 5017−5029

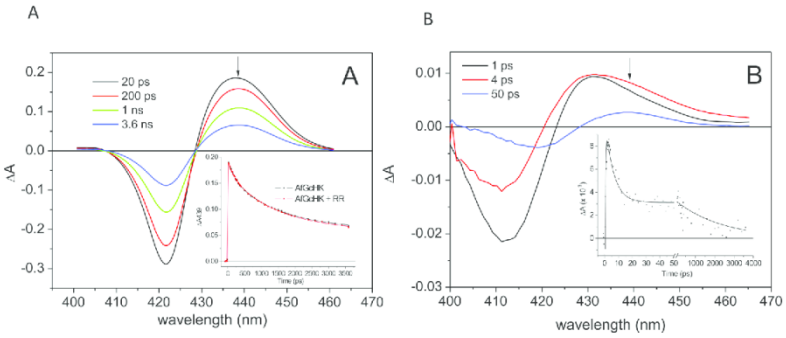


Figure 6. Selected transient spectra of WT *Af*GcHK upon (A) CO and (B) O_2 dissociation. The insets show kinetics at (A) 439 and (B) 440 nm, for panel A in the presence and absence of stoichiometric amounts of the response regulator. Note the difference in signal amplitude in the two panels.

dissociated O_2 after these phases can be estimated by comparing the signal's amplitude to that of the steady-state difference spectrum and using MbCO dissociation (100% QY) under the same experimental conditions as a reference.[43,44] In this way, the QY at 50 ps was estimated to be ~1.8%. This very low value (for comparative purposes, the QY of MbO_2 is ~30%) is similar to those reported for other O_2 sensor and heme proteins (~5% for FixL-O_2[43] and ~1% for HbO from *M. tuberculosis*[38]). The effective O_2 escape yield was lower still because the majority of the dissociated O_2 rebound on a time scale of a few nanoseconds (Figure 6B, inset). Thus, *Af*GcHK appears to act as a highly efficient O_2 trap.

Effects of Divalent Metal Cations on *Af*GcHK Autophosphorylation. We tested the effect of several divalent metal cations (Mg^{2+}, Mn^{2+}, Ca^{2+}, Co^{2+}, Ni^{2+}, Zn^{2+}, and Cd^{2+}) on the autophosphorylation activity of *Af*GcHK (Figure 7 and Table 2). It was confirmed by atomic absorption spectroscopy that there were no traces of the aforementioned divalent ions in the isolated *Af*GcHK sample (Figure S3).

Of the divalent cations investigated, Mg^{2+} ions were by far the most effective at stimulating autophosphorylation in terms of k_{cat}/K_m^{ATP} values (Figure 7 and Table 2). Moreover, the K_m^{ATP} value (93.2 μM) in the presence of Mn^{2+} was approximately 5 times higher than that (18.9 μM) in the presence of Mg^{2+}. The V_{max}^{ATP} value (13.1 pmol of P-*Af*GcHK min^{-1} μL^{-1}) in the presence of Mn^{2+} was slightly higher than that (10.8 pmol of P-*Af*GcHK min^{-1} μL^{-1}) in the presence of Mg^{2+}. Considering that both Mg^{2+} and Mn^{2+} form the metal-ATP complex, these results suggest that the enzyme's affinity for the Mn^{2+}-ATP complex and the orientation of ATP in its active site are different from those of the Mg^{2+}-ATP complex.

It was also found that Ca^{2+} ions can serve as divalent ion cofactors that facilitate the autophosphorylation of *Af*GcHK. However, they are less effective in this role than Mg^{2+}, which is reflected by the significantly higher K_m^{ATP} value (403.9 μM) observed in the presence of Ca^{2+} compared to that with either Mg^{2+} or Mn^{2+} (Figure 7 and Table 2).

It should be emphasized that while the V_{max}^{ATP} value observed in the presence of Mg^{2+} ions (10.8 pmol of P-*Af*GcHK min^{-1} μL^{-1}) is >4 times greater than that observed in the absence of divalent metal ions (2.2 pmol of P-*Af*GcHK min^{-1} μL^{-1}), the enzyme retains a low basal level of activity even when no divalent metal ion is present. It is therefore interesting that the presence of Co^{2+}, Ni^{2+}, Zn^{2+}, or Cd^{2+} completely suppresses even the metal-free basal autophosphorylation activity. Presumably, these divalent metal ions cause the formation of a metal-ATP complex that is incapable of undergoing the phosphate−phosphate bond cleavage required for the autophosphorylation reaction.

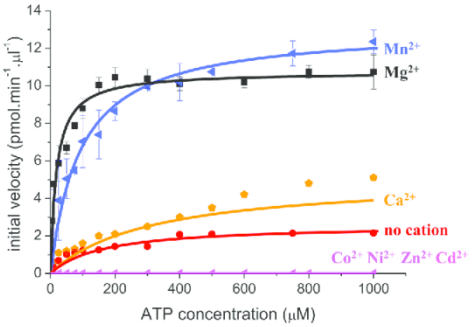


Figure 7. Effect of divalent metal ions on the autophosphorylation reaction catalyzed by the native form of *Af*GcHK: Mg^{2+} (black line and squares), Mn^{2+} (blue line and triangles), Ca^{2+} (orange line and pentagons), Co^{2+}, Ni^{2+}, Zn^{2+}, and Cd^{2+} (pink line and triangles), and no divalent cations (red line and circles). In each run, a reaction mixture containing 10 μM *Af*GcHK, 5−1000 μM ATP, 50 mM Tris-HCl (pH 8.0), 50 mM KCl, and 0 or 5 mM $MgCl_2$, 5 mM $MnCl_2$, 5 mM $CaCl_2$, 5 mM $CoCl_2$, 5 mM $NiCl_2$, 5 mM $ZnSO_4$, or 5 mM $CdCl_2$ in a total volume of 100 μL was incubated for 30 s (for further details, see Experimental Procedures).

DISCUSSION

The results presented herein demonstrate for the first time that the initial velocity of the autophosphorylation reaction catalyzed by the heme Fe(III)-OH^--bound form of *Af*GcHK follows Michaelis−Menten kinetics with respect to the concentration of ATP (Figure 2). Furthermore, it was found that the catalytically optimal pH value for *Af*GcHK autophosphorylation is in the alkaline region, around pH 10.0−11.0 (Figure 3). The UV−vis spectrum of the Fe(III) complex was stable over a pH range of 7.0−10.0.[14] The pK_a values for water coordinated to sperm whale myoglobin and human hemoglobin are 8.99 and 8.05, respectively, whereas

DOI: 10.1021/acs.biochem.5b00517
Biochemistry 2015, 54, 5017−5029

that of Tyr-OH is 10.9.[28] It is therefore possible that the OH^- axial ligand would be replaced by Tyr-O^- at pH >8 or >9, and this process may be linked to the catalytic enhancement observed under alkaline conditions, although it should be noted that such conditions would also affect the properties of the phosphorylatable histidine residue. The histidine kinase reaction involved in most enzymatic autophosphorylations occurs under mildly alkaline conditions.[32,45−47] For example, it was shown that CheA autophosphorylation has an optimal pH of approximately 8.4.[46] In contrast, FixL autophosphorylation is relatively insensitive to variation in pH over a wide range but has an optimum close to pH 7.5.[32]

We have previously shown that the heme Fe(III)-OH^--, Fe(II)-O_2-, and Fe(II)-CO-bound forms of *Af*GcHK are active whereas the heme Fe(II)-bound form is inactive.[14] Furthermore, it was shown that the heme-free His99Ala mutant is active but shows unusual catalytic behavior. In this work, we determined the values of kinetic parameters such as K_m^{ATP}, V_{max}^{ATP}, and k_{cat} for the catalytic autophosphorylation of *Af*GcHK under various conditions, taking into consideration the effects of the heme iron's redox and coordination states as well as the presence of the enzyme's response regulator on its catalytic behavior.

The kinetic parameters (V_{max}^{ATP} and k_{cat}) determined for the catalytic autophosphorylation of the Fe(III)-OH^-, Fe(II)-O_2, and Fe(II)-CO heme complexes of the *Af*GcHK histidine kinase were consistent with previous reports (Figures 2 and 4 and Table 1).[14] This work also showed for the first time that the heme Fe(III)-CN^-- and Fe(III)-imidazole-bound forms are also active and have kinetic parameters that differ only slightly from those for the Fe(III)-OH^- complex (Figure 4 and Table 1). The V_{max}^{ATP} and k_{cat} values of these active forms were 9.6−11.8 pmol of P-*Af*GcHK min^{-1} μL^{-1} and 1.0−1.2 min^{-1}, respectively, suggesting that all of the active complexes have similar active site structures that support optimal activity (Figure 8). In all of the enzyme's active forms, the heme iron complex exists in a six-coordinate low-spin state. On the basis of the known structures of hemoglobin and myoglobin, the heme iron in such complexes lies in the heme plane. Conversely, the inactive Fe(II) complex exists in a five-coordinate high-spin state. On the basis of the structures of the corresponding hemoglobin and myoglobin complexes, the iron cation in such species will lie outside the heme plane. This difference in the heme coordination structures of the active and inactive forms may partially explain the heme structure-dependent catalytic regulation of *Af*GcHK.

The conformational changes associated with changes in the coordination or oxidation state of the heme iron in the sensor domain could result in either substantial rearrangements of the catalytic domain or simply an unmasking of the active site. The experiments presented herein are not adequate to characterize these conformational changes in any detail. However, as mentioned above, we suggest that the activation of the functional domain is dependent on the formation of a six-coordinate low-spin heme iron complex. Very similar results have been reported for another heme-based oxygen sensor, *Ec* DOS, which forms active low-spin complexes such as heme Fe(III)-CN^-, Fe(III)-imidazole, Fe(II)-O_2, and Fe(II)-CO.[48,49] Low-spin complexes of other heme-based sensor proteins such as the Fe(II)-O_2 and Fe(II)-CO complexes of globin-coupled diguanylate cyclase (YddV) are also active.[50,51]

In contrast to their V_{max}^{ATP} and k_{cat} values, the K_m^{ATP} values of these heme-bound active forms (18.9−357 μM) varied over more than 1 order of magnitude (Table 1). This suggests that the redox and/or coordination state of the heme iron in the oxygen sensing domain has profound effects on the ATP affinity of the active site in the functional domain. However, it should be remembered that all of these active forms have very similar k_{cat} values of 1.0−1.2 min^{-1}. It is noteworthy that the K_m^{ATP} value (357 μM) of the heme Fe(II)-CO complex is substantially higher than those of the Fe(III)-OH^- and Fe(II)-O_2 complexes (18.9−23.0 μM). The binding of CO to the heme Fe(II) complex in the oxygen-sensing domain presumably induces significant structural changes in the ATP-binding site that differ from those induced by alternative axial ligands such as cyanide, imidazole, and O_2. In terms of k_{cat}/K_m^{ATP}, the catalytic efficiency of the enzyme with the heme Fe(II)-O_2 complex (700 M^{-1} s^{-1}) is significantly greater than that with the heme Fe(II)-CO complex (50 M^{-1} s^{-1}) (Table 1), implying that O_2 binding and CO binding have different effects on catalytic regulation (Figure 8). Spectroscopic data on the heme Fe(II)-CO and Fe(II)-O_2 enzymes did not provide useful insights into the structure of the functional domain's active site because the spectra provided information about only the structure in the vicinity of the heme-binding site in the oxygen-sensing domain.[14] Nevertheless, the binding mode of CO differs from that of O_2 because the k_{off} and K_d values of CO among the Tyr45 mutants did not differ substantially from those for the WT enzyme even though these mutants exhibited dramatic differences in their O_2 binding. Tyr45 is believed to play an important role in binding O_2 within the Fe(II)-O_2 complex.[14] Moreover, it seems that O_2 binding occurs more rapidly than that of CO.[14]

Conversely, the data for the dissociation (and subsequent ultrafast rebinding) of CO and O_2 from the Fe(II) complexes examined in this study do provide new insights into the functional properties of the sensing domain when considered in conjunction with previously determined ligand binding and

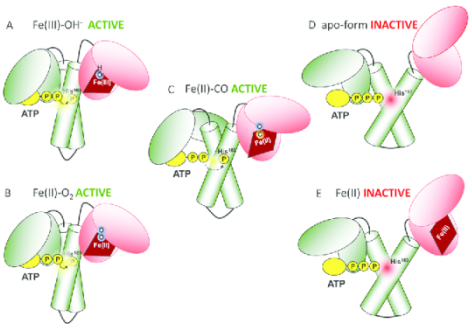


Figure 8. Schematic representation of the sensor domain's effect on the functional domain's activity for various sensor domain heme iron redox and coordination states. *Af*GcHKs with (A) Fe(III)-OH^-, (B) Fe(II)-O_2, and (C) Fe(II)-CO complexes are active in autophosphorylation, whereas (D) heme-free *Af*GcHK and (E) *Af*GcHK with Fe(II) have low activities. Presumably, the autophosphorylation reaction of dimeric *Af*GcHK would occur in a "crosswise" fashion, with a phosphate moiety being transferred from an ATP molecule bound to one subunit to the His183 residue of the other. It is also likely that the RR-binding site is close to the ATP-binding site. To avoid confusion, the figure shows autophosphorylation occurring on only one subunit of the dimeric protein.

DOI: 10.1021/acs.biochem.5b00517
Biochemistry 2015, 54, 5017−5029

dissociation data.[14] Upon dissociation, the Fe(II)-CO complex of *Af*GcHK displays a high fraction of geminate heme-CO recombination, which is unusual in hemoglobins and presumably contributes significantly to the relatively low rate of overall dissociation of CO from the protein.[14] Interestingly, qualitatively similar CO rebinding properties are observed in truncated bacterial hemoglobins[37,38] that have similar hydrophobic heme pockets featuring close-lying tyrosine and leucine residues.

The ligand dynamics of the O_2 complex are of more direct functional relevance to the enzyme's behavior *in vivo*. We found that, as for other heme-based oxygen sensors such as FixL, *Ec* DOS, and *M. tuberculosis* DosT,[52,53] the effective photodissociation yield (on the picosecond time scale) of the Fe(II)-O_2 *Af*GcHK complex was very low (1.8%, which is more than 1 order of magnitude lower than the corresponding value for Mb). On the basis of the assumption that the intrinsic thermal Fe-O_2 complex dissociation rate is similar to those of other heme proteins, we previously interpreted this behavior in terms of strain on the bound O_2, which would force its rebinding to the heme following the breaking of the heme−O_2 bond even prior to heme doming, i.e., within ∼100 fs.[43] In the case of *Af*GcHK, this strain may be induced by interactions with the proximal tyrosine residue.[14] The effective rate of dissociation is further reduced by substantial recombination on a time scale of a few nanoseconds. Overall, the *Af*GcHK heme pocket acts as a highly efficient O_2 trap, which may explain the enzyme's low O_2 dissociation rate.[14] Although *Af*GcHK is different from other O_2 sensors in that its O_2 affinity is surprisingly high and its catalytic activity is increased rather than decreased by O_2 binding,[14] the "O_2 trap" property demonstrated here is present in a variety of O_2 sensor proteins.[54] This property effectively makes the sensor a bistable switch, which helps to ensure that its reaction time is well-matched to physiologically relevant response times.

The heme-free form of *Af*GcHK, His99Ala, is relatively inactive as demonstrated by its k_{cat} value of 0.3 min^{-1} (Figure 2 and Table 1). This finding is similar to results obtained for a heme-based oxygen sensor phosphodiesterase of *Acetobacter xylinum*, *Ax*PDEA1,[55] and a heme-based oxygen sensor adenylate cyclase of *Leishmania*, HemAC-Lm;[56] in both cases, the heme-free forms had very low activities. The binding of heme to the sensor domain presumably causes significant and profound structural changes in the active site that allow the efficient functioning of these heme-based oxygen sensors (Figure 8). However, the results obtained for *Af*GcHK differ from those for heme-based oxygen sensors such as the phosphodiesterase *Ec* DOS and the diguanylate cyclase YddV from *E. coli*, whose heme-free forms have appreciable catalytic activity. It was suggested that the heme iron complexes of *Ec* DOS and YddV suppress catalysis when bound to the oxygen-sensing domain, and that O_2 binding relieves this suppression.

The addition of the abortive RR double mutant Asp52/169Ala to the heme Fe(III)-OH^- complex of *Af*GcHK significantly increased the K_m^{ATP} value of the latter protein from 18.9 to 47.7 μM without affecting its k_{cat} value (Figure 5 and Table 1). This strongly suggests that RR binds in the proximity of the enzyme's catalytic site and hampers the binding of ATP to the active site. Our finding that the presence of the RR does not influence the ligand dynamics in the sensor domain (Figure 6A, inset) is consistent with the notion that it binds specifically to the catalytic domain. Moreover, given the sensitivity of the CO binding kinetics to the details of the heme pocket's composition, this finding implies that RR binding does not induce a significant structural change in the sensor domain. Thus, whereas the heme configuration affects the functional properties of the catalytic domain, the reverse appears not to be the case.

The kinetic parameters for the active form of another histidine kinase, CheA (K_m^{ATP} = 0.26 mM; k_{cat} = 17 min^{-1}),[57] are strikingly different from those for *Af*GcHK. This is unsurprising because CheA belongs to a different family of histidine kinases. However, as shown in Table 1, the kinetic parameters determined for *Af*GcHK are quite similar to those for other heme-containing oxygen sensor histidine kinases from two-component signal transduction systems such as *Bj*FixL (K_m^{ATP} = 47 μM; k_{cat} = 0.006 min^{-1}),[58,59] DevS (K_m^{ATP} = 73 μM; k_{cat} not determined),[10] DosT (K_m^{ATP} = 39 μM; k_{cat} not determined),[10] and HpkA (K_m^{ATP} = 25 μM; k_{cat} = 0.025 min^{-1}).[60] We therefore suggest that these histidine kinases have a common molecular mechanism of action that allows them to regulate various processes in bacterial cells. Note that the k_{cat} value of the active form of *Af*GcHK is around 1 min^{-1} (Table 1). This value is comparable to those determined for an artificial light-regulated histidine kinase (0.9 min^{-1})[61] and the hemoprotein CYP1B1 (0.3−4.4 min^{-1}), both of which belong to different groups of heme-containing enzymes.[62]

The intracellular ATP concentration in bacteria is generally predicted to be between 2 and 10 mM.[63−65] Because the highest K_m^{ATP} value determined for the different *Af*GcHK complexes considered in this work was 357 μM, the k_{cat} values obtained for *Af*GcHK probably reflect its actual catalytic activity in cells (Table 1). This suggests that heme-free *Af*GcHK and the heme Fe(II) complex are less active forms whereas the heme Fe(III)-OH^-, Fe(III)-CN^-, Fe(III)-imidazole, Fe(II)-CO, and Fe(II)-O_2 complexes are active forms. Because the autoxidation rate of the heme Fe(II)-O_2 complex is very slow,[14] it is suggested that the heme Fe(II) and Fe(II)-O_2 complexes exist in equilibrium *in vivo*, that the position of this equilibrium will depend on the local O_2 concentration, and that it regulates the enzyme's catalytic activity in response to external stimuli. This is reflected in the different catalytic efficiencies of these two complexes: the k_{cat}/K_m^{ATP} values determined for the less active heme Fe(II) and the active heme Fe(II)-O_2 species were 90 and 700 M^{-1} s^{-1}, respectively (Table 1).

It was also found that Mg^{2+} and Mn^{2+} ions substantially enhanced the autophosphorylation activity of *Af*GcHK, although the presence of a divalent metal ion does not appear to be essential for the reaction (Figure 7 and Table 2). Mg^{2+} (or Mn^{2+}) is often important for phosphate-, nucleic acid-, or nucleotide-associated reactions because it can form ionic bonds with phosphate groups, which greatly facilitates their transfer.[66−68]

In contrast to our findings in the case of FixL catalysis, the most effective divalent cation was a Mn^{2+}, causing a 20-fold increase in the initial rate of autophosphorylation compared to that with Mg^{2+}.[32] Conversely, Mg^{2+} was the most effective divalent cation at enhancing the histidine kinase activity of DosT, whereas Mg^{2+} and Mn^{2+} were comparable in their ability to enhance the histidine kinase activity of DevS.[10] It should be noted that the phosphodiesterase activity of the heme-based oxygen sensor *Ec* DOS was substantially enhanced when external axial ligands such as O_2, CO, cyanide, and imidazole were bound to the heme in the presence of Mg^{2+}.[48,49] Importantly, however, the enzyme's activity was quite high

DOI: 10.1021/acs.biochem.5b00517
Biochemistry 2015, 54, 5017−5029

even in the absence of those external axial ligands when Mn^{2+} was used instead of Mg^{2+}.[1,69,70] This was taken to imply that Mn^{2+} may be bound or coordinated within the active site, and that the Mn^{2+}-bound form of *Ec* DOS without exogenous ligands mimics the Mg^{2+}-bound form with those ligands. Thus, one plausible explanation for the gas sensing function of *Ec* DOS and other heme-based oxygen sensor proteins is that binding of O_2 (or NO/CO) to the heme enhances the active site's affinity for Mg^{2+} and/or creates a Mg^{2+} coordination structure that is optimal for efficient phosphodiesterase catalysis.[69,70] However, the results presented herein for *Af*GcHK raise another possibility: the affinity of ATP for the active site or the orientation of the metal-ATP complex in the active site can be modulated by the binding of oxygen to the heme. This is supported by the observation that the K_m^{ATP} values measured for *Af*GcHK varied strongly with the heme's oxidation and coordination states, the presence of the RR, and the binding of divalent cations other than Mg^{2+} (Table 2).

We also tested the effects of other divalent metal ions such as Ca^{2+}, Co^{2+}, Ni^{2+}, Zn^{2+}, and Cd^{2+}. While Ca^{2+} ions can partly reproduce the effects of Mg^{2+} and Mn^{2+} on the *Af*GcHK autophosphorylation reaction, the other tested ions totally inhibit the process. The deviation from the Michaelis−Menten hyperbola obtained with calcium ions can be explained by at least two mechanisms. First, it is possible that both free ATP and ATP-Ca^{2+} complexes are present in these reaction mixtures, whereas in the presence of Mg^{2+} or Mn^{2+}, all of the ATP would be coordinated to a divalent metal ion. The presence of multiple ATP species in the Ca^{2+} mixtures could influence the reaction's course. Second, Ca^{2+} ions may bind to a unique (specific) site in the *Af*GcHK protein that regulates the autophosphorylation reaction. Autophosphorylation in the absence of divalent cations is slower, but the enzyme retains a degree of basal activity under such conditions, suggesting that the absence of a metal cation reduces but does not eliminate its affinity for ATP. The inhibitory divalent metal cations probably bind to sites that are important for catalysis in addition to the enzyme-bound ATP moiety.

SUMMARY

In summary, our results suggest that the heme configuration of *Af*GcHK plays a vital role in regulating its histidine kinase autophosphorylation activity by changing its affinity for ATP, as revealed by changes in its K_m^{ATP} value. This in turn affects the enzyme's catalytic activity, which was quantified in terms of its k_{cat}/K_m^{ATP} value. Figure 8 shows a schematic representation illustrating the effects of changes in the sensor domain heme's redox and coordination states on the activity of the functional domain. It was also shown that the RR-binding site is probably located close to the ATP-binding site of the full-length *Af*GcHK protein because the presence of the RR protein affected the enzyme's K_m^{ATP} value. The results of our kinetic investigations have thus shed new light on the molecular mechanism of the heme-regulated histidine kinase autophosphorylation reaction of *Af*GcHK.

ASSOCIATED CONTENT

Supporting Information

Double reciprocal plots used to determine the enzyme's Michaelis−Menten kinetic parameters, kinetics of CO rebinding in *Af*GcHK proteins and atomic absorption spectroscopy results for WT *Af*GcHK (in its native form). The Supporting Information is available free of charge on the ACS Publications website at DOI: 10.1021/acs.biochem.5b00517.

(PDF)

AUTHOR INFORMATION

Corresponding Author

*Department of Biochemistry, Faculty of Science, Charles University in Prague, Hlavova (Albertov) 2030-8, Prague 2, Czech Republic. Telephone: +420 2 21951242. Fax: +420 2 21951283. E-mail: marketa.martinkova@natur.cuni.cz.

Funding

This work was supported in part by Charles University in Prague (UNCE 204025/2012), by the Grant Agency of the Czech Republic (Grant 15-19883S), and by the Grant Agency of Charles University in Prague (Grants 756214 and 362115).

Notes

The authors declare no competing financial interest.

Dedication

Dedicated to the 65th birthday of Prof. Marie Stiborová.

ABBREVIATIONS

*Af*GcHK, globin-coupled histidine kinase from *Anaeromyxobacter* sp. Fw109-5; P-*Af*GcHK, phosphoform of *Af*GcHK; *Ec* DOS, *E. coli* direct oxygen sensor or heme-regulated phosphodiesterase from *E. coli* or *Ec* DosP; Fe(III), Fe(III)-protoporphyrin IX complex, or hemin; Fe(II), Fe(II)-protoporphyrin IX complex; FixL, oxygen sensor histidine kinase with the heme-bound PAS domain that regulates nitrogen fixation in *R. meliloti* or *Bradyrhizobium japonicum*; GAF, domain conserved in cyclic GMP-specific and stimulated phosphodiesterases, adenylate cyclases, and *E. coli* formate hydrogenlyase transcriptional activator; PAS, acronym from Per (*Drosophila* period clock protein)-Arnt (vertebrate aryl hydrocarbon receptor nuclear translocator)-Sim (*Drosophila* single-minded protein); RR, response regulator; YddV, heme-bound diguanylate cyclase from *E. coli* or *Ec* DosC; WT, wild type.

REFERENCES

(1) Shimizu, T., Huang, D., Yan, F., Stranava, M., Bartosova, M., Fojtíková, V., and Martínková, M. (2015) Gaseous O_2, NO, and CO in signal transduction: Structure and function relationships of heme-based gas sensors and heme-redox sensors. *Chem. Rev. 115*, 6491−6533.

(2) Igarashi, J., Kitanishi, K., and Shimizu, T. (2011) Emerging roles of heme as a signal and a gas-sending site: Heme-sensing and gas-sending proteins. In *Handbook of Porphyrin Science* (Kadish, K. M., Smith, K. M., and Guilard, R., Eds.) Vol. *15*, pp 399−460, World Scientific Publishing, Hackensack, NJ.

(3) Green, J., Crack, J. C., Thomson, A. J., and LeBrun, N. E. (2009) Bacterial sensors of oxygen. *Curr. Opin. Microbiol. 12*, 145−151.

(4) Gilles-Gonzalez, M.-A., and Gonzalez, G. (2005) Heme-based sensors: defining characteristics, recent developments, and regulatory hypotheses. *J. Inorg. Biochem. 99*, 1−22.

(5) Gilles-Gonzalez, M.-A., and Gonzalez, G. (2004) Signal transduction by heme-containing PAS-domain proteins. *J. Appl. Physiol. 96*, 774−783.

(6) Nakamura, H., Kumita, H., Imai, K., Iizuka, T., and Shiro, Y. (2004) ADP reduces the oxygen-binding affinity of a sensory histidine kinase, FixL: the possibility of an enhanced reciprocating kinase reaction. *Proc. Natl. Acad. Sci. U. S. A. 101*, 2742−2746.

(7) Uchida, T., and Kitagawa, T. (2005) Mechanism for transduction of the ligand-binding signal in heme-based gas sensory proteins revealed by resonance Raman spectroscopy. *Acc. Chem. Res. 38*, 662−670.

DOI: 10.1021/acs.biochem.5b00517
Biochemistry 2015, 54, 5017−5029

(8) Sardiwal, S., Kendall, S. L., Movahedzadeh, F., Rison, S. C. G., Stoker, N. G., and Djordjevic, S. (2005) A GAF domain in the hypoxia/NO-inducible *Mycobacterium tuberculosis* DosS protein binds haem. *J. Mol. Biol. 353*, 929−936.
(9) Ioanoviciu, A., Yukl, E. T., Moënne-Loccoz, P., and Ortiz de Montellano, P. R. (2007) DevS, a heme-containing two-component oxygen sensor of *Mycobacterium tuberculosis*. *Biochemistry 46*, 4250−4260.
(10) Sousa, E. H. S., Tuckerman, J. R., Gonzalez, G., and Gilles-Gonzalez, M.-A. (2007) DosT and DevS are oxygen-switched kinases in *Mycobacterium tuberculosis*. *Protein Sci. 16*, 1708−1719.
(11) Kumar, A., Toledo, J. C., Patel, R. P., Lancaster, J. R., and Steyn, A. J. C. (2007) *Mycobacterium tuberculosis* DosS is a redox sensor and DosT is a hypoxia sensor. *Proc. Natl. Acad. Sci. U. S. A. 104*, 11568−11573.
(12) Boon, E. M., and Marletta, M. A. (2005) Ligand specificity of H-NOX domains: from sGC to bacterial NO sensors. *J. Inorg. Biochem. 99*, 892−902.
(13) Ito, Y., Nakagawa, S., Komagata, A., Ikeda-Saito, M., Shiro, Y., and Nakamura, H. (2009) Heme-dependent autophosphorylation of a heme sensor kinase, ChrS, from *Corynebacterium diphtheriae* reconstituted in proteoliposomes. *FEBS Lett. 583*, 2244−2248.
(14) Kitanishi, K., Kobayashi, K., Uchida, T., Ishimori, K., Igarashi, J., and Shimizu, T. (2011) Identification and functional and spectral characterization of a globin-coupled histidine kinase from *Anaeromyxobacter* sp. Fw109−5. *J. Biol. Chem. 286*, 35522−35534.
(15) Inouye, M., and Dutta, R. (2003) *Histidine Kinases in Signal Transduction*, Academic Press, Inc., San Diego.
(16) Kramer, R., and Jung, K. (2010) *Bacterial Signaling*, Wiley-VCH, Weinheim, Germany.
(17) Casino, P., Rubio, V., and Marina, A. (2010) The mechanism of signal transduction by two-component systems. *Curr. Opin. Struct. Biol. 20*, 763−771.
(18) Cheung, J., and Hendrickson, W. A. (2010) Sensor domains of two-component regulatory systems. *Curr. Opin. Microbiol. 13*, 116−123.
(19) Gao, R., Mack, T. R., and Stock, A. M. (2007) Bacterial response regulators: versatile regulatory strategies from common domains. *Trends Biochem. Sci. 32*, 225−234.
(20) Galperin, M. Y. (2010) Diversity of structure and function of response regulator output domains. *Curr. Opin. Microbiol. 13*, 150−159.
(21) Jenal, U., and Galperin, M. Y. (2009) Single domain response regulators: molecular switches with emerging roles in cell organization and dynamics. *Curr. Opin. Microbiol. 12*, 152−160.
(22) Martínková, M., Kitanishi, K., and Shimizu, T. (2013) Heme-based globin-coupled oxygen sensors: linking oxygen binding to functional regulation of diguanylate cyclase, histidine kinase, and methyl-accepting chemotaxis. *J. Biol. Chem. 288*, 27702−27711.
(23) Igarashi, J., Kitanishi, K., Martinkova, M., Murase, M., Iizuka, A., and Shimizu, T. (2008) The roles of thiolate-heme proteins, other than the P450 cytochromes, in the regulation of heme-sensor proteins. *Acta Chim. Slov. 55*, 67−74.
(24) Igarashi, J., Murase, M., Iizuka, A., Pichierri, F., Martinkova, M., and Shimizu, T. (2008) Elucidation of the heme binding site of heme-regulated eukaryotic initiation factor 2alpha kinase and the role of the regulatory motif in heme sensing by spectroscopic and catalytic studies of mutant proteins. *J. Biol. Chem. 283*, 18782−18791.
(25) Anzenbacher, P., Marchal, S., Palacký, J., Anzenbacherová, E., Domaschke, T., Lange, R., Shimizu, T., Kitanishi, K., Stranava, M., Stiborová, M., and Martinkova, M. (2014) Pressure effects reveal that changes in the redox states of the heme iron complexes in the sensor domains of two heme-based oxygen sensor proteins, *Ec*DOS and YddV, have profound effects on their flexibility. *FEBS J. 281*, 5208−5219.
(26) Zhang, W., and Phillips, G. N. (2003) Structure of the oxygen sensor in *Bacillus subtilis*: signal transduction of chemotaxis by control of symmetry. *Structure 11*, 1097−1110.
(27) Yamada, S., Sugimoto, H., Kobayashi, M., Ohno, A., Nakamura, H., and Shiro, Y. (2009) Structure of PAS-linked histidine kinase and the response regulator complex. *Structure 17*, 1333−1344.
(28) Antonini, E., and Brunori, M. (1971) *Hemoglobin and Myoglobin in Their Reactions with Ligands*, North-Holland Publishing Co., Amsterdam.
(29) Fanelli, A. R., Antonini, E., and Caputo, A. (1958) Studies on the structure of hemoglobin. I. Physicochemical properties of human globin. *Biochim. Biophys. Acta 30*, 608−615.
(30) Lobato, L., Bouzhir-Sima, L., Yamashita, T., Wilson, M. T., Vos, M. H., and Liebl, U. (2014) Dynamics of the heme-binding bacterial gas-sensing dissimilative nitrate respiration regulator (DNR) and activation barriers for ligand binding and escape. *J. Biol. Chem. 289*, 26514−26524.
(31) Yamada, S., Nakamura, H., Kinoshita, E., Kinoshita-Kikuta, E., Koike, T., and Shiro, Y. (2007) Separation of a phosphorylated histidine protein using phosphate affinity polyacrylamide gel electrophoresis. *Anal. Biochem. 360*, 160−162.
(32) Gilles-Gonzalez, M. A., and Gonzalez, G. (1993) Regulation of the kinase activity of heme protein FixL from the two-component system FixL/FixJ of *Rhizobium meliloti*. *J. Biol. Chem. 268*, 16293−16297.
(33) Vos, M. H. (2008) Ultrafast dynamics of ligands within heme proteins. *Biochim. Biophys. Acta, Bioenerg. 1777*, 15−31.
(34) Kumazaki, S., Nakajima, H., Sakaguchi, T., Nakagawa, E., Shinohara, H., Yoshihara, K., and Aono, S. (2000) Dissociation and recombination between ligands and heme in a CO-sensing transcriptional activator CooA. A flash photolysis study. *J. Biol. Chem. 275*, 38378−38383.
(35) Kapetanaki, S. M., Field, S. J., Hughes, R. J. L., Watmough, N. J., Liebl, U., and Vos, M. H. (2008) Ultrafast ligand binding dynamics in the active site of native bacterial nitric oxide reductase. *Biochim. Biophys. Acta, Bioenerg. 1777*, 919−924.
(36) Vos, M. H., Bouzhir-Sima, L., Lambry, J.-C., Luo, H., Eaton-Rye, J. J., Ioanoviciu, A., Ortiz de Montellano, P. R., and Liebl, U. (2012) Ultrafast ligand dynamics in the heme-based GAF sensor domains of the histidine kinases DosS and DosT from *Mycobacterium tuberculosis*. *Biochemistry 51*, 159−166.
(37) Feis, A., Lapini, A., Catacchio, B., Brogioni, S., Foggi, P., Chiancone, E., Boffi, A., and Smulevich, G. (2008) Unusually strong H-bonding to the heme ligand and fast geminate recombination dynamics of the carbon monoxide complex of *Bacillus subtilis* truncated hemoglobin. *Biochemistry 47*, 902−910.
(38) Jasaitis, A., Ouellet, H., Lambry, J. C., Martin, J. L., Friedman, J. M., Guertin, M., and Vos, M. H. (2012) Ultrafast heme-ligand recombination in a truncated hemoglobin: a ligand cage. *Chem. Phys. 396*, 10−16.
(39) Silkstone, G., Jasaitis, A., Wilson, M. T., and Vos, M. H. (2007) Ligand dynamics in an electron transfer protein. Picosecond geminate recombination of carbon monoxide to heme in mutant forms of cytochrome *c*. *J. Biol. Chem. 282*, 1638−1649.
(40) Jasaitis, A., Hola, K., Bouzhir-Sima, L., Lambry, J.-C., Balland, V., Vos, M. H., and Liebl, U. (2006) Role of distal arginine in early sensing intermediates in the heme domain of the oxygen sensor FixL. *Biochemistry 45*, 6018−6026.
(41) Yamashita, T., Bouzhir-Sima, L., Lambry, J.-C., Liebl, U., and Vos, M. H. (2008) Ligand dynamics and early signaling events in the heme domain of the sensor protein Dos from *Escherichia coli*. *J. Biol. Chem. 283*, 2344−2352.
(42) Lechauve, C., Bouzhir-Sima, L., Yamashita, T., Marden, M. C., Vos, M. H., Liebl, U., and Kiger, L. (2009) Heme ligand binding properties and intradimer interactions in the full-length sensor protein Dos from *Escherichia coli* and its isolated heme domain. *J. Biol. Chem. 284*, 36146−36159.
(43) Kruglik, S. G., Jasaitis, A., Hola, K., Yamashita, T., Liebl, U., Martin, J.-L., and Vos, M. H. (2007) Subpicosecond oxygen trapping in the heme pocket of the oxygen sensor FixL observed by time-resolved resonance Raman spectroscopy. *Proc. Natl. Acad. Sci. U. S. A. 104*, 7408−7413.

DOI: 10.1021/acs.biochem.5b00517
Biochemistry 2015, 54, 5017−5029

(44) Ye, X., Demidov, A., and Champion, P. M. (2002) Measurements of the photodissociation quantum yields of MbNO and MbO_2 and the vibrational relaxation of the six-coordinate heme species. *J. Am. Chem. Soc. 124*, 5914−5924.
(45) Huang, J. M., Wei, Y. F., Kim, Y. H., Osterberg, L., and Matthews, H. R. (1991) Purification of a protein histidine kinase from the yeast *Saccharomyces cerevisiae*. The first member of this class of protein kinases. *J. Biol. Chem. 266*, 9023−9031.
(46) Conley, M. P., Berg, H. C., Tawa, P., Stewart, R. C., Ellefson, D. D., and Wolfe, A. J. (1994) pH dependence of CheA autophosphorylation in *Escherichia coli*. *J. Bacteriol. 176*, 3870−3877.
(47) Casino, P., Miguel-Romero, L., and Marina, A. (2014) Visualizing autophosphorylation in histidine kinases. *Nat. Commun. 5*, 3258.
(48) Tanaka, A., Takahashi, H., and Shimizu, T. (2007) Critical role of the heme axial ligand, Met95, in locking catalysis of the phosphodiesterase from *Escherichia coli* (*Ec* DOS) toward cyclic diGMP. *J. Biol. Chem. 282*, 21301−21307.
(49) Tanaka, A., and Shimizu, T. (2008) Ligand binding to the Fe(III)-protoporphyrin IX complex of phosphodiesterase from *Escherichia coli* (*Ec* DOS) markedly enhances catalysis of cyclic di-GMP: roles of Met95, Arg97, and Phe113 of the putative heme distal side in catalytic regulation and ligand binding. *Biochemistry 47*, 13438−13446.
(50) Nakajima, K., Kitanishi, K., Kobayashi, K., Kobayashi, N., Igarashi, J., and Shimizu, T. (2012) Leu65 in the heme distal side is critical for the stability of the Fe(II)-O_2 complex of YddV, a globin-coupled oxygen sensor diguanylate cyclase. *J. Inorg. Biochem. 108*, 163−170.
(51) Kitanishi, K., Kobayashi, K., Kawamura, Y., Ishigami, I., Ogura, T., Nakajima, K., Igarashi, J., Tanaka, A., and Shimizu, T. (2010) Important roles of Tyr43 at the putative heme distal side in the oxygen recognition and stability of the Fe(II)-O_2 complex of YddV, a globin-coupled heme-based oxygen sensor diguanylate cyclase. *Biochemistry 49*, 10381−10393.
(52) Liebl, U., Bouzhir-Sima, L., Kiger, L., Marden, M. C., Lambry, J.-C., Négrerie, M., and Vos, M. H. (2003) Ligand binding dynamics to the heme domain of the oxygen sensor Dos from *Escherichia coli*. *Biochemistry 42*, 6527−6535.
(53) Liebl, U., Bouzhir-Sima, L., Negrerie, M., Martin, J.-L., and Vos, M. H. (2002) Ultrafast ligand rebinding in the heme domain of the oxygen sensors FixL and Dos: general regulatory implications for heme-based sensors. *Proc. Natl. Acad. Sci. U. S. A. 99*, 12771−12776.
(54) Liebl, U., Lambry, J.-C., and Vos, M. H. (2013) Primary processes in heme-based sensor proteins. *Biochim. Biophys. Acta, Proteins Proteomics 1834*, 1684−1692.
(55) Chang, A. L., Tuckerman, J. R., Gonzalez, G., Mayer, R., Weinhouse, H., Volman, G., Amikam, D., Benziman, M., and Gilles-Gonzalez, M. A. (2001) Phosphodiesterase A1, a regulator of cellulose synthesis in *Acetobacter xylinum*, is a heme-based sensor. *Biochemistry 40*, 3420−3426.
(56) Roy, J., Sen Santara, S., Bose, M., Mukherjee, S., Saha, R., and Adak, S. (2014) The ferrous-dioxy complex of *Leishmania major* globin coupled heme containing adenylate cyclase: the role of proximal histidine on its stability. *Biochim. Biophys. Acta, Proteins Proteomics 1844*, 615−622.
(57) Levit, M., Liu, Y., Surette, M., and Stock, J. (1996) Active site interference and asymmetric activation in the chemotaxis protein histidine kinase CheA. *J. Biol. Chem. 271*, 32057−32063.
(58) Gilles-Gonzalez, M. A., Gonzalez, G., Perutz, M. F., Kiger, L., Marden, M. C., and Poyart, C. (1994) Heme-based sensors, exemplified by the kinase FixL, are a new class of heme protein with distinctive ligand binding and autoxidation. *Biochemistry 33*, 8067−8073.
(59) Gilles-González, M. A., González, G., and Perutz, M. F. (1995) Kinase activity of oxygen sensor FixL depends on the spin state of its heme iron. *Biochemistry 34*, 232−236.
(60) Foster, J. E., Sheng, Q., McClain, J. R., Bures, M., Nicas, T. I., Henry, K., Winkler, M. E., and Gilmour, R. (2004) Kinetic and mechanistic analyses of new classes of inhibitors of two-component signal transduction systems using a coupled assay containing HpkA-DrrA from *Thermotoga maritima*. *Microbiology 150*, 885−896.
(61) Möglich, A., Ayers, R. A., and Moffat, K. (2009) Design and signaling mechanism of light-regulated histidine kinases. *J. Mol. Biol. 385*, 1433−1444.
(62) Hanna, I. H., Dawling, S., Roodi, N., Guengerich, F. P., and Parl, F. F. (2000) Cytochrome P450 1B1 (CYP1B1) pharmacogenetics: association of polymorphisms with functional differences in estrogen hydroxylation activity. *Cancer Res. 60*, 3440−3444.
(63) Bennett, B. D., Kimball, E. H., Gao, M., Osterhout, R., Van Dien, S. J., and Rabinowitz, J. D. (2009) Absolute metabolite concentrations and implied enzyme active site occupancy in *Escherichia coli*. *Nat. Chem. Biol. 5*, 593−599.
(64) Lowry, O. H., Carter, J., Ward, J. B., and Glaser, L. (1971) The effect of carbon and nitrogen sources on the level of metabolic intermediates in *Escherichia coli*. *J. Biol. Chem. 246*, 6511−6521.
(65) Koç, A., Wheeler, L. J., Mathews, C. K., and Merrill, G. F. (2004) Hydroxyurea arrests DNA replication by a mechanism that preserves basal dNTP pools. *J. Biol. Chem. 279*, 223−230.
(66) Cohen, P. (2000) The regulation of protein function by multisite phosphorylation–a 25 year update. *Trends Biochem. Sci. 25*, 596−601.
(67) Gani, D., and Wilkie, J. (1997) Metal ions in the mechanism of enzyme-catalyzed phosphate monoester hydrolysis. In *Metal Sites in Proteins and Models: Phosphatases, Lewis Acids and Vanadium* (Hill, H. A. O., Sadler, P. J., and Thomson, A. J., Eds.) pp 133−175, Springer-Verlag, Berlin.
(68) Johnson, L. N., and Lewis, R. J. (2001) Structural basis for control by phosphorylation. *Chem. Rev. 101*, 2209−2242.
(69) Shimizu, T. (2013) The heme-based oxygen-sensor phosphodiesterase *Ec* DOS (DosP): Structure-function relationships. *Biosensors 3*, 211−237.
(70) Honjo, A., Takahashi, H., Sekimoto, M., Igarashi, J., and Shimizu, T. (2012) Novel effects of Mn^{2+} on the catalytic enhancement of the inactive form of the Fe(III) heme-bound *Ec* DOS, a heme-regulated phosphodiesterase from *Escherichia coli*. In *Gas Sensors: Developments, Efficacy and Safety* (Qin, X., Ed.) pp 251−261, Nova Science, Hauppauge, NY.

DOI: 10.1021/acs.biochem.5b00517
Biochemistry 2015, 54, 5017−5029

4. Publikace BLOKU II

4.1 Catalytic enhancement of the heme-based oxygen sensing phosphodiesterase *Ec*DOS by hydrogen sulfide is caused by changes in heme coordination structure

Yan F., **Fojtikova V**., Man P., Stranava M., Martínková M., Du Y., Huang D., Shimizu T. *Biometals* (2015) 28, 637 (**IF$_{2016}$ 2,2**).

Podíl předkladatelky na této práci: 65 % (exprese a purifikace proteinu *Ec*DOS v jeho přirozené a mutantních formách, spektroskopická měření, enzymové analýzy, zpracování a vyhodnocení výsledků)

potvrzeno korespondujícím autorem, doc. RNDr. Markéta Martínková, Ph.D., v.z.

Biometals (2015) 28:637–652
DOI 10.1007/s10534-015-9847-7

Catalytic enhancement of the heme-based oxygen-sensing phosphodiesterase *Ec*DOS by hydrogen sulfide is caused by changes in heme coordination structure

Fang Yan · Veronika Fojtikova · Petr Man · Martin Stranava · Markéta Martínková · Yongming Du · Dongyang Huang · Toru Shimizu

Received: 7 March 2015 / Accepted: 13 March 2015 / Published online: 25 March 2015
© Springer Science+Business Media New York 2015

Abstract *Ec*DOS is a heme-based O_2-sensing phosphodiesterase in which O_2 binding to the heme iron complex in the N-terminal domain substantially enhances catalysis toward cyclic-di-GMP, which occurs in the C-terminal domain. Here, we found that hydrogen sulfide enhances the catalytic activity of full-length *Ec*DOS, possibly owing to the admixture of 6-coordinated heme Fe(III)–SH^- and Fe(II)–O_2 complexes generated during the reaction. Alanine substitution at Met95, the axial ligand for the heme Fe(II) complex, converted the heme Fe(III) complex into the heme Fe(III)–SH^- complex, but the addition of Na_2S did not further reduce it to the heme Fe(II) complex of the Met95Ala mutant, and no subsequent formation of the heme Fe(II)–O_2 complex was observed. In contrast, a Met95His mutant formed a stable heme Fe(II)–O_2 complex in response to the same treatment. An Arg97Glu mutant, containing a glutamate substitution at the amino acid that interacts with O_2 in the heme Fe(II)–O_2 complex, formed a stable heme Fe(II) complex in response to Na_2S, but this complex failed to bind O_2. Interestingly, the addition of Na_2S promoted formation of verdoheme (oxygen-incorporated, modified protoporphyrin IX) in an Arg97Ile mutant. Catalytic enhancement by Na_2S was similar for Met95 mutants and the wild type, but significantly lower for the Arg97 mutants. Thus, this study shows the first isolation of spectrometrically separated, stable heme Fe(III)–SH^-, heme Fe(II) and heme Fe(II)–O_2 complexes of full-length *Ec*DOS with Na_2S, and confirms that external-ligand–bound, 6-coordinated heme Fe(III)–SH^- or heme Fe(II)–O_2 complexes critically contribute to the Na_2S-induced catalytic enhancement of *Ec*DOS.

Keywords Heme · O_2 sensor · Phosphodiesterase · c-di-GMP · Hydrogen sulfide

Fang Yan and Veronika Fojtikova have contributed equally to this work.

Electronic supplementary material The online version of this article (doi:10.1007/s10534-015-9847-7) contains supplementary material, which is available to authorized users.

F. Yan · Y. Du · D. Huang · T. Shimizu (✉)
Department of Cell Biology and Genetics and Key Laboratory of Molecular Biology in High Cancer Incidence Coastal Chaoshan Area of Guangdong Higher Education Institutes, Shantou University Medical College, Shantou 515041, Guangdong, China
e-mail: shimizu@tagen.tohoku.ac.jp

V. Fojtikova · P. Man · M. Stranava · M. Martínková · T. Shimizu
Department of Biochemistry, Faculty of Science, Charles University in Prague, 128 43 Prague 2, Czech Republic

P. Man
Institute of Microbiology, Academy of Sciences of the Czech Republic, v.v.i., Videnska 1083, 140 00 Prague 4, Czech Republic

Abbreviations

c-di-GMP	Cyclic dinucleotide-GMP, bis(3′,5′)-cyclic dimeric guanosine monophosphate
*Ec*DOS	A heme-based O_2-sensor phosphodiesterase from *E. coli* (also called DosP)
Heme Fe(II)	Protoporphyrin IX ferrous complex
Heme Fe(III)	Protoporphyrin IX ferric complex, hemin
HPLC	High-pressure (performance) liquid chromatography
l-di-GMP	Linear dinucleotide-GMP (also called pGpG)
MALDI	Matrix-assisted laser desorption/ionization
FT-ICR	Fourier transform-ion cyclotron resonance
PDE	Phosphodiesterase
P450	Cytochromes P450
YddV	A heme-based O_2 sensor diguanylate cyclase from *E. coli* (also called DosC)

Introduction

In heme-based O_2-sensing proteins, which are composed of a heme-bound N-terminal domain and a functional C-terminal domain, the O_2-sensing function of the heme iron complex is different from that of other well-known heme proteins, such as hemoglobin, myoglobin, cytochrome *c* and P450, in which the heme iron complex acts as the functional center (Guengerich 2013; Ortiz de Montellano 2010; Poulos 2014; Voet and Voet 2011). This distinctly different role of the heme iron complex is important in bacterial physiology (Aono 2012; Germani et al. 2013; Gilles-Gonzalez and Gonzalez 2005; Girvan and Munro 2013; Green et al. 2009; Igarashi et al. 2011; Martínková et al. 2013; Uchida and Kitagawa 2005). Another interesting feature of heme-based O_2 sensors that distinguishes them from the well-known heme proteins in which O_2 plays a role in metabolism is that O_2 acts as the first signaling molecule in intramolecular signal transduction.

Cyclic-di-GMP (c-di-GMP) is an important second messenger for numerous important functions of bacteria, such as cell motility, virulence, biofilm formation, and many more (Hengge 2009; Römling et al. 2005; Schirmer and Jenal 2009). *Ec*DOS (also known as *Ec*DosP) is an O_2-sensing phosphodiesterase (PDE) of *Escherichia coli* that linearizes c-di-GMP and generates linear di-GMP (Fig. 1a) (Delgado-Nixon et al. 2000; Gilles-Gonzalez and Gonzalez 2005; Sasakura et al. 2002, 2006; Shimizu 2013a; Takahashi and Shimizu 2006; Tanaka et al. 2007). Binding of O_2 to the heme Fe(II) complex in the N-terminal sensing domain of *Ec*DOS substantially enhances the PDE catalytic activity of the C-terminal functional domain (Fig. 1b). Regulation of c-di-GMP concentration in response to external stimuli through degradation by *Ec*DOS and synthesis by diguanylate cyclase YddV (also known as DosC) (Kitanishi et al. 2010; Tuckerman et al. 2009), another heme-based O_2 sensor in *E. coli*, is crucial for bacterial survival. The PDE reaction of *Ec*DOS is regulated by the coordination state of the heme iron complex, such that formation of a 6-coordinated complex bound to external axial ligands substantially stimulates catalysis. This formation of a 6-coordinated complex and enhancement of catalytic activity reflects binding of cyanide anion or imidazole to the heme Fe(III) complex, or binding of O_2, NO or CO to the heme Fe(II) complex (Fig. 2a) (Takahashi and Shimizu 2006; Tanaka et al. 2007; Tanaka and Shimizu 2008).

Hydrogen sulfide (H_2S) is the fourth-most important gaseous signaling molecule after O_2, NO and CO. Most H_2S-mediated functional regulation is attributable to oxidative stress-dependent formation or breakage of –S–S bonds on a protein's surface (Banerjee 2011; Kabil et al. 2014; Kimura 2014; Paul and Snyder 2012; Szabo 2010; Wang 2010). Importantly, it has been reported that SH^- is bound to the heme iron complex of hemoglobin and myoglobin (Nicoletti et al. 2010; Pietri et al. 2011; Ríos-González et al. 2014; Ramos-Alvarez et al. 2013; Shimizu 2013b). In addition, H_2S has been reported to modify the porphyrin IX ring of hemoglobin and myoglobin when added in the presence of H_2O_2, resulting in formation of a sulfheme complex, a sulfur-incorporated porphyrin iron complex (Ríos-González et al. 2014; Pietri et al. 2011; Ramos-Alvarez et al. 2013; Shimizu 2013a, b).

Addition of Na_2S to heme Fe(III) complex-bound *Ec*DOS under aerobic conditions substantially enhances PDE activity (Takahashi et al. 2012). It has

Biometals (2015) 28:637–652 639

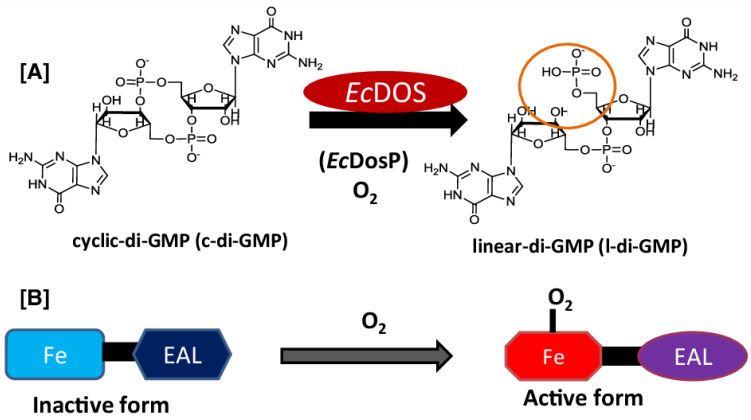


Fig. 1 **a** PDE reaction toward c-di-GMP catalyzed by *Ec*DOS. **b** Binding of O_2 to the heme Fe(II) complex of the sensing domain (*left*) of full-length *Ec*DOS substantially enhances the catalytic activity of the functional domain (*right*) via intramolecular signal transduction. The Glu-Ala-Leu (EAL) sequence of the functional domain is involved in PDE activity (Delgado-Nixon et al. 2000; Gilles-Gonzalez and Gonzalez 2005; Sasakura et al. 2002, 2006; Shimizu 2013a; Takahashi and Shimizu 2006; Tanaka et al. 2007)

been suggested that the admixture of 6-coordinated heme Fe(III)–SH^- and Fe(II)–O_2 complexed with external axial ligands (SH^- and O_2) formed during the reaction significantly contributes to the H_2S-induced catalytic enhancement of *Ec*DOS, although the separation of each species formed during the fast consecutive reactions was not feasible (Fig. 2b). It was also suggested that eight cysteine residues of *Ec*DOS are involved in the H_2S-induced catalytic enhancement, although none of the eight residues was singled out as being unequivocally or directly involved (Takahashi et al. 2012).

To understand the role of the heme environment in the changes in coordination structure and redox state of the heme iron complex caused by the addition of Na_2S, we prepared mutations at Met95, the distal axial ligand for the heme Fe(II) complex, and Arg97, the site that interacts with O_2 bound to the heme Fe(II) complex (Fig. 3) (Kurokawa et al. 2004; Park et al. 2004), and examined their effects on the absorption and mass spectra of the isolated heme-bound domain of *Ec*DOS in the presence of Na_2S (Du et al. 2013). For Met95Ala and Met95Leu mutants, the addition of Na_2S resulted in formation of a heme Fe(III)–SH^- complex. However, for the Met95Leu mutant, there was no further reduction to form the heme Fe(II) complex, and thus no subsequent O_2 binding to the heme Fe(II) complex was observed. For the Met95His mutant, the addition of Na_2S caused no spectral changes. In contrast, the addition of Na_2S to Arg97Ala and Arg97Ile mutants partially converted the porphyrin IX ring into verdoheme (oxygen-incorporated porphyrin IX), but caused no spectral changes in the Arg97Glu mutant. Thus, Met95 and Arg97 appear to play crucial roles in the changes in coordination structure and redox state, as well as heme modification of the isolated heme-bound domain of *Ec*DOS, caused by Na_2S.

In the present study, we further examined the role of these critical amino acid residues in the heme status of wild-type and Met95 and Arg97 mutant full-length *Ec*DOS in the presence of Na_2S using absorption spectroscopy and mass spectrometry. We also studied the catalytic activities of wild-type and mutant enzymes in the presence of H_2S using high-performance liquid chromatography (HPLC). Importantly, we isolated spectrometrically separated, stable heme Fe(III)–SH^-, Fe(II) and Fe(II)–O_2 complexes of full-length *Ec*DOS mutants with Na_2S for the first time and examined the catalytic activities of individual complexes. The catalytic activity of the verdoheme-bound Arg97Ile mutant was also examined. Taken together, our results strongly suggest that H_2S-induced enhancement of the catalytic activity of full-length

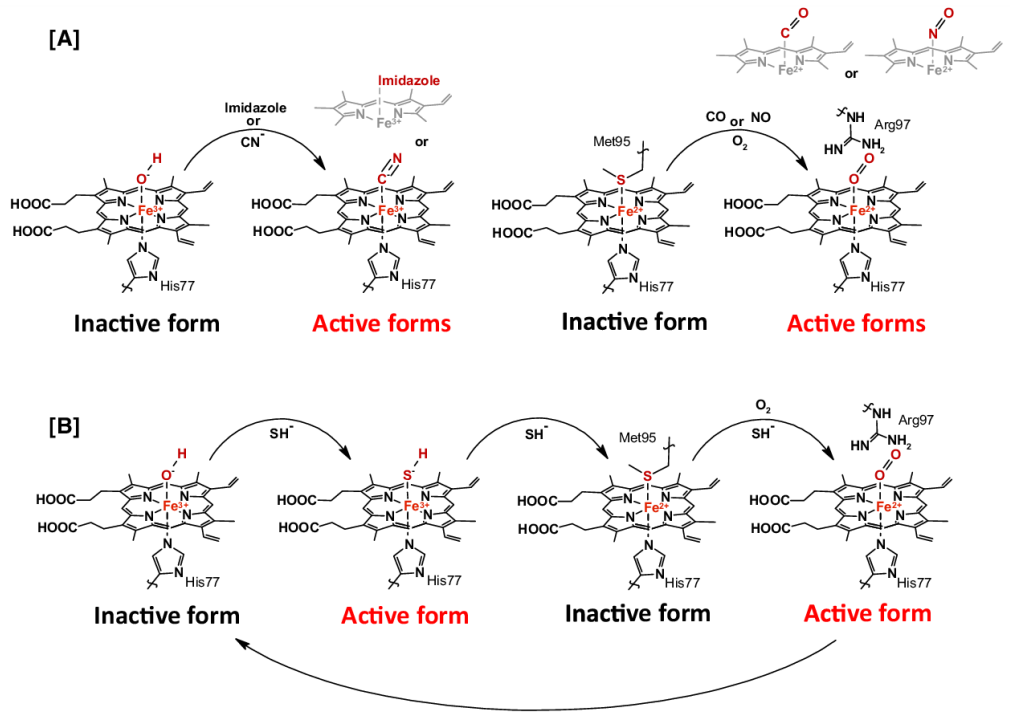


Fig. 2 **a** Binding of external axial ligands cyanide anion and imidazole to the heme Fe(III) and O_2, NO, and CO to the heme Fe(II) complex of the sensing domain of full-length *Ec*DOS substantially enhances the catalytic activity of the functional domain (Takahashi and Shimizu 2006; Tanaka et al. 2007; Tanaka and Shimizu 2008). **b** The catalytic activity of heme Fe(III) complex-bound, wild-type, full-length *Ec*DOS was markedly enhanced by adding Na_2S under aerobic conditions (Takahashi et al. 2012). This suggests that the catalytic enhancement caused by Na_2S is related to changes in heme coordination structure and redox state of the heme Fe(III) complex in *Ec*DOS, reflecting the critical contribution of the external-axial-ligand bound heme Fe(III)–SH^- and Fe(II)-O_2 complexes formed during the reaction. However, validation of the proposed active species has remained elusive because consecutive reactions that rapidly change heme coordination structure and redox status take place after the addition of Na_2S, making separation of the respective complexes challenging

*Ec*DOS is closely associated with changes in the heme iron complex coordination structure.

Experimental procedures

Materials

c-di-GMP and linear di-GMP (pGpG) were purchased from BIOLOG (Bremen, Germany). Other chemicals of the highest guaranteed grade available were purchased from Sigma-Aldrich China (Shanghai, China or St. Louis, MO, USA) and used without further purification.

Construction of expression plasmids, and protein expression and purification

Cloning of full-length *Ec*DOS, site-directed mutagenesis, and construction of the pET28a(+)-*Ec*DOS expression plasmid were conducted as previously described (Tanaka et al. 2007; Tanaka and Shimizu 2008). The *Ec*DOS protein was overexpressed in the *E. coli* strain, BL21(DE3), transformed with the pET28a(+)-*Ec*DOS plasmid expressing an N-terminally His_6-tagged *Ec*DOS. Culture conditions for *E. coli* and protein purification procedures were as previously described (Tanaka et al. 2007; Tanaka and Shimizu 2008). Proteins were purified to homogeneity,

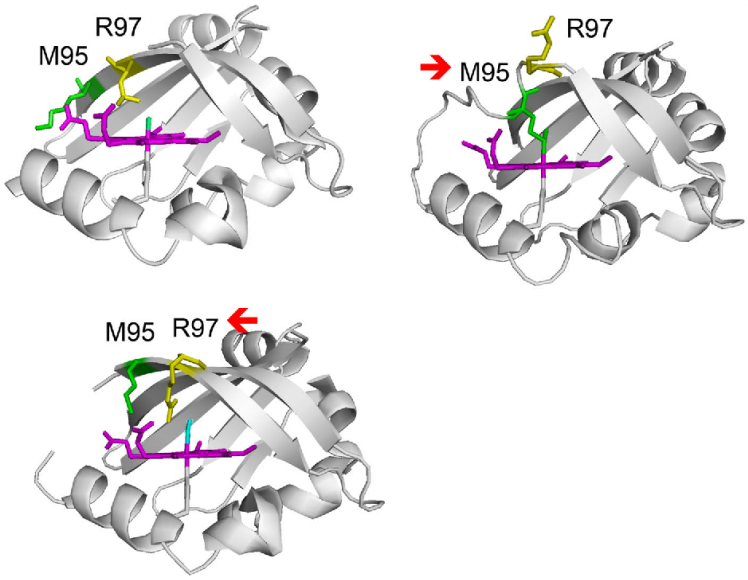


Fig. 3 X-ray crystal structures of the isolated heme-bound domain of wild-type *Ec*DOS (Kurokawa et al. 2004; Park et al. 2004). **a** Heme Fe(III) complex (PDB code, IV9Y); low activity. The hydroxyl anion is the axial ligand on the distal side. **b** Heme Fe(II) complex (PDB code, IV9Z); low activity. Met95 is the axial ligand on the distal side. **c** Heme Fe(II)-O_2 complex (PDB code, IVB6); high activity. The Arg97 side chain interacts with the O_2 molecule bound to the heme Fe(II) complex

as demonstrated by sodium dodecyl sulfate–polyacrylamide gel electrophoresis (SDS-PAGE). After dialysis against 20 mM Tris–HCl (pH 8.0) containing 5 % glycerol, oxidized (heme Fe(III)-bound) proteins were concentrated with an Amicon Centriprep (Millipore, Billerica, MA). Samples were stored at −20 °C in the presence of 30 % glycerol.

Optical absorption spectroscopy

Optical absorption spectral data were obtained using UV-2550PC (Shimadzu-China, Suzhou, China) and HP 8453 (Agilent Technologies, CA, USA) UV–Vis spectrophotometers at 20 °C under aerobic conditions, as previously described (Du et al. 2013; Kitanishi et al. 2010, 2011; Takahashi et al. 2012). Aliquots of 200 mM Na_2S stock solution in 500 mM Tris–HCl buffer (pH 8.0) were added to the protein solution (2–5 μM) to yield final Na_2S concentrations of 200 μM to 5 mM in the cell. To examine whether a heme Fe(II) complex formed as the final product, we added a CO solution to the mixture, since CO binds only the heme Fe(II) complex and not the heme Fe(III) complex. Sodium dithionate ($Na_2S_2O_4$) was further added to determine whether treatment with Na_2S converted the heme Fe(III) complex to the heme Fe(II) complex. A stock solution saturated with CO (~1 mM), made by bubbling CO gas into the buffer, was used to achieve a final CO concentration of ~10 μM in the protein solution. Spectra of full-length *Ec*DOS proteins were obtained in 50 mM Tris–HCl (pH 8.0). We confirmed that addition of chemical reagents caused essentially no change in the pH value of the full-length *Ec*DOS solution under the experimental conditions used.

Mass spectrometry

After spectral changes of the full-length *Ec*DOS solutions were completed, 0.5 μL of each solution was spotted on a MALDI (matrix-assisted laser desorption/ionization) plate and overlaid with 0.5 μL of a saturated solution of α-cyano-4-hydroxycinnamic acid in methanol/water, as described previously (Du et al. 2013). Mass spectra were acquired on a hybrid 12T Fourier transform ion cyclotron resonance mass

spectrometer (FT-ICR; SolariX, Bruker Daltonics, Bremen, Germany) equipped with MALDI source and operating in positive ion mode. Data were collected in a positive ion mode over the mass range 350–1000 *m/z* at 1 M data points, resulting in a maximum resolution of 250,000 at 400 *m/z*. The instrument was externally calibrated using singly charged arginine clusters, resulting in sub–parts-per-million accuracy. Spectra were processed for possible elemental compositions of detected compounds, and their fragment ions were generated in Data Analysis 4.2 (Bruker Daltonics).

Assay of PDE activity by HPLC

*Ec*DOS (0.3 μM) in 50 mM Tris–HCl (pH 8.0), 50 mM NaCl, and 5 mM $MgCl_2$ was incubated with 1 mM Na_2S or buffer (control) at 25 °C for 10 min. The enzyme solution was mixed with 100 μM c-di-GMP and further incubated at 25 °C for 5 min. The catalytic reaction was terminated by adding $CaCl_2$ (final concentration, 10 mM). The solution was applied to a chromatography column (LUNA 5 μC18 (2) column, 15 × 4.6 cm; Phenomenex Torrance, CA, USA) and analyzed using an HPLC system (Agilent). A gradient was applied using Buffer A (100 mM KH_2PO_4 with 4 mM tetrabutyl ammonium hydrogen sulfate, pH 6.0) and Buffer B (75 % buffer A/25 % methanol), delivered at a flow rate of 0.7 ml/min under the following conditions: 0.0 min, 40 % B/60 % A; 15.0 min, 100 % B; 20.0 min, 100 % B, and 21.0 min, 40 % B/60 % A. Absorption changes were monitored at 254 nm and are presented as described previously (Honjo et al. 2012; Takahashi et al. 2012). Catalytic activities of *Ec*DOS were obtained by evaluating either the decrease in the substrate (c-di-GMP) or increase in the product (l-di-GMP) by reference to calibration curves prepared using purified chemicals. Experiments were repeated at least four times; experimental errors were calculated and are shown in the results.

Results and discussion

Optical absorption spectra of full-length *Ec*DOS in the presence of Na_2S

The pK_a value of H_2S is near 6.9; thus, a significant amount of SH^- should be available to interact with heme Fe(III) complexes and form a heme Fe(III)–SH^- complex under physiological conditions (Banerjee 2011; Kabil et al. 2014; Kimura 2014; Nicoletti et al. 2010; Paul and Snyder 2012; Pietri et al. 2011; Ramos-Alvarez et al. 2013; Ríos-González et al. 2014; Shimizu 2013b; Szabo 2010; Wang 2010). In our experiments, Na_2S was used as a source of SH^- since it forms SH^- during the dissolution process, according to the relationship $Na_2S + H_2O \rightarrow NaHS + NaOH$. All experiments were performed in buffer systems, and the pH was always monitoring to prevent possible side effects due to alkalization of the reaction mixture. Our previous study showed that addition of Na_2S to the wild-type isolated heme-bound domain of *Ec*DOS converts the heme Fe(III) complex into the heme Fe(III)–SH^- complex, which is subsequently reduced to the heme Fe(II) complex, to which O_2 binds to form the heme Fe(II)–O_2 complex; the heme Fe(II)–O_2 complex ultimately is gradually autooxidized to the heme Fe(III)–OH complex (Fig. 2b) (Takahashi et al. 2012).

Met95 is the axial ligand for the heme Fe(II) complex, and Arg97 interacts with the O_2 molecule bound to the heme Fe(II) complex and stabilizes the heme Fe(II)–O_2 complex (Fig. 3) (Kurokawa et al. 2004; Park et al. 2004). Mutations at these residues dramatically alter a number of physicochemical characteristics, including resonance Raman spectra (Sato et al. 2002), autooxidation rate constants (Ishitsuka et al. 2008; Taguchi et al. 2004), ligand-binding kinetic values (Ishitsuka et al. 2008; Kobayashi et al. 2010; Taguchi et al. 2004; Watanabe et al. 2002; Yamashita et al. 2008) and reduction-potential values (Hirata et al. 2003; Ishitsuka et al. 2008), suggesting that these amino acid residues are important for the structure and function of the heme iron complex in *Ec*DOS. For the isolated heme-bound domain of *Ec*DOS containing mutations at Met95 or Arg97 residues, changes in coordination and redox state of the heme Fe(III) complex caused by Na_2S were significantly different compared with those of the wild type (Supplementary Table S1) (Du et al. 2013; Takahashi et al. 2012). For the Met95Leu mutant in particular, the addition of Na_2S led to formation of the heme Fe(III)–SH^- complex, but further reduction to the heme Fe(II) complex was not observed. Importantly, the addition of excess Na_2S to the Arg97Ala and Arg97Ile mutants modified protoporphyrin IX, causing partial formation of verdoheme (oxygen-incorporated protoporphyrin IX derivative), whereas

the same procedure caused no spectral change in the Met95His and Arg97Glu mutants.

Analyses of spectral changes upon addition of Na_2S revealed distinctive features of wild-type, full-length *Ec*DOS and the corresponding Met95 and Arg97 mutants

Wild type

Absorption spectral changes in the heme Fe(III) complex of full-length wild-type *Ec*DOS caused by Na_2S were the same as those observed for the isolated heme-bound domain of *Ec*DOS (Fig. 4a; Tables 1, S1–S3). Specifically, upon addition of Na_2S, the Soret peak at 418 nm of wild-type, heme Fe(III)–OH complex-containing *Ec*DOS shifted to the 422–425 nm position characteristic of the heme Fe(III)–SH^- complex, and then gradually returned to 417–418 nm, reflecting an admixture of the heme Fe(II)–O_2 complex and its autooxidized species, heme Fe(III)–OH.

Met95 mutants

For the full-length Met95Ala mutant, on the other hand, the Soret peak at 415 nm quickly moved to 425 nm upon addition of Na_2S, and the intensity of the Soret band increased (Fig. 4b; Tables 1, S2). The final spectrum is likely attributable to the heme Fe(III)–SH^- complex, since addition of CO to this species did not change the spectra in Soret or visible regions, suggesting that the complex is stable enough to resist reduction to heme Fe(II) or heme Fe(II)–O_2 complexes in the presence of Na_2S (Fig. 4b). This final spectrum corresponds to a pure, stable heme Fe(III)–SH^- complex of *Ec*DOS obtained for the first time (Table S2), although separating this spectrum has proven difficult because of the readiness of the heme Fe(III)–SH^- complex of *Ec*DOS to become reduced to the heme Fe(II) complex (Fig. 2).

For the full-length Met95His mutant, the intensity of the Soret peak at 416 nm increased slightly upon addition of Na_2S with the concomitant appearance of

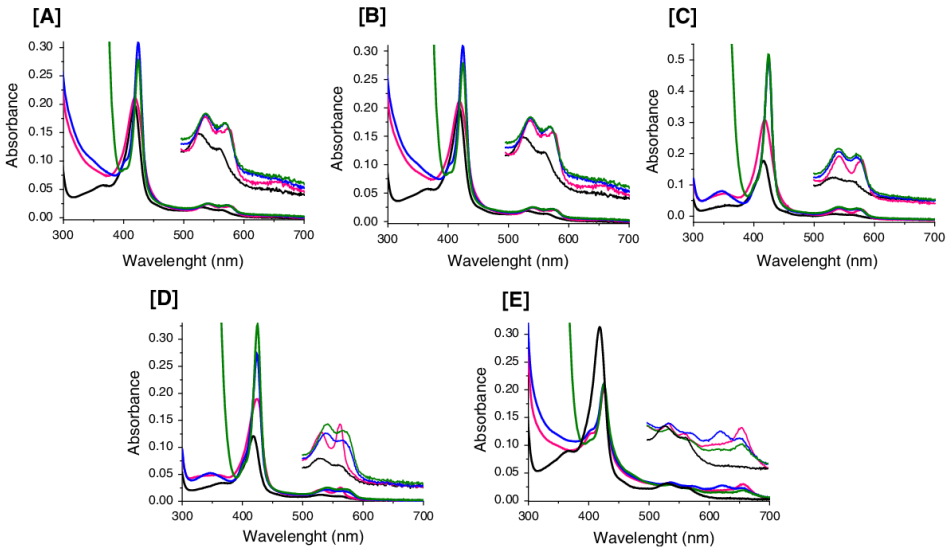


Fig. 4 Absorption spectral changes of wild-type and Met95 and Arg97 mutants of the heme Fe(III) complex of full-length *Ec*DOS (2–5 μM) caused by the addition of Na_2S (5 mM). **a** Wild type; **b** Met95Ala; **c** Met95His; **d** Arg97Glu; **e** Arg97Ile. *Black line* spectrum of the heme Fe(III) complex without Na_2S; *pink line* spectrum 2 h after the addition of H_2S; *green line* addition of CO to the reaction mixture; *blue line* addition of $Na_2S_2O_4$ to the CO-treated reaction mixture. (Color figure online)

Table 1 Proposed changes in coordination structure and redox state of the heme Fe(III) complexes of wild-type and Met95 and Arg97 mutants of full-length *Ec*DOS caused by the addition of Na_2S

Proteins	Proposed intermediate species		Proposed final species
Wild type	His–Fe(III)–OH	→His–Fe(III)–SH^-	→His–Fe(II)–O_2 + His–Fe(III)–OH
	418 nm	422–425 nm	418, 539, 579 + 417 nm
Met95Ala	His–Fe(III)–OH		→His–Fe(III)–SH^-
	415 nm		425, 543, 578 nm
Met95His	His–Fe(III)–His	→His–Fe(III)–SH^-	→His–Fe(II)–O_2
	416 nm	425 nm	416, 542, 580 nm
Arg97Glu	His–Fe(III)–Glu	→His–Fe(III)–SH^-	→His–Fe(II)–Met
	418 nm	424 nm	429, 532, 563 nm
Arg97Ile	His–Fe(III)–OH		→Verdoheme–Fe(II)
	418 nm		425, 533, 657 nm

two distinct bands at 542 and 580 nm (Fig. 4c; Tables 1, S2). The addition of CO changed the spectrum of this complex, moving the Soret band to 424 nm and increasing the breadth of the visible bands at ~573 nm and slightly increasing their intensity, suggesting that this species is the heme Fe(II) complex. This spectrum is attributable to the heme Fe(II)–O_2 complex, based on previously reported spectral bands (Table S3), and was stable enough to resist autoxidation to the heme Fe(III) complex for more than 2 h. These results demonstrate formation of a stable heme Fe(II)–O_2 complex upon addition of H_2S to *Ec*DOS in the absence of an admixture of both heme Fe(III)–SH^- and heme Fe(III)–OH complexes.

The spectral changes observed upon addition of Na_2S to the Met95Ala and Met95His mutants of full-length *Ec*DOS were different from those of the isolated heme-bound PAS domain of *Ec*DOS, where spectral changes were comparable for the Met95Ala mutant and the wild type and no spectral change was observed for the Met95His mutant (Supplementary Table S1) (Du et al. 2013). The present findings for the full-length Met95Ala mutant are reasonable since the reduction potential of the Met95Ala mutant (−26 mV vs. a standard hydrogen electrode [SHE]) is significantly lower than that of the wild type (45 mV vs. SHE) (Table S4). However, it is not clear why the heme iron complex for the full-length Met95His mutant was reduced to an extent similar to that of the wild type, even though its reduction potential (−122 mV vs. SHE) is much lower than that of the wild type. It is possible that the ionic character of HS^- does not favor interactions with the hydrophobic Met95Ala mutant, whereas it might accommodate interactions with imidazole in the Met95His mutant. Stereochemical factors could also explain the differences in the heme-reducing ability of H_2S towards Met95 mutants.

In addition, the Met95His mutant of full-length *Ec*DOS formed a stable heme Fe(II)–O_2 complex upon addition of Na_2S (Tables 1, S2), but the autooxidation rate constant of the corresponding Met95His mutant of the isolated heme-bound PAS domain of *Ec*DOS was higher than that of the wild type (Supplementary Table S4). Two possible explanations might be invoked to account for the difference in the stability of the heme Fe(II)–O_2 complex between the full-length *Ec*DOS and isolated heme-bound PAS domain of *Ec*DOS. First, there may be a difference in the protein structure surrounding the heme between the full-length *Ec*DOS and the isolated heme-bound PAS domain of *Ec*DOS. Alternatively, the changes in protein structure and coordination/redox status caused by SH^- are subtly different from those caused by other chemicals lacking an SH^- group. Further studies will be required to resolve this issue.

Arg97 mutants

For the full-length Arg97Glu mutant, the Soret band at 418 nm of the heme Fe(III) complex was shifted to 429 nm concomitantly with the appearance of two sharp bands at 532 and 563 nm by adding Na_2S (Fig. 4d; Tables 1, S2). Addition of CO to this solution moved the Soret band from 429 to 425 nm in association with a shift and broadening of bands in the visible region, demonstrating formation of a heme Fe(II)–CO complex (Tables S2, S3). Interestingly, O_2, which was present in the solution, did not bind to the heme Fe(II) complex, unlike the case with the wild type and Met95His mutant. This is the first

demonstration of a stable, external-ligand–free heme Fe(II) complex formed by the addition of Na_2S to *Ec*DOS. It is possible that the O_2 molecule is converted to a reactive oxygen species such as H_2O_2 or O_2^- since Arg97, which is the key site for stabilizing the heme Fe(II)–O_2 complex, is replaced with a glutamate residue. Reactive oxygen species would not interact with the heme Fe(II) complex in the Arg97Glu mutant owing to ionic repulsion in the distal heme pocket.

For the full-length Arg97Ile mutant, the Soret band at 418 nm shifted toward 425 nm upon addition of H_2S, together with a decrease in its intensity and a concomitant appearance of a characteristic band at 657 nm (Fig. 4e; Tables 1, S2). The final spectrum is that of the verdoheme, based on the band positions (Table S5) (Ortiz de Montellano 1998; Matsui et al. 2010; Sakamoto et al. 2000). Verdoheme in the Arg97Ile mutant would be formed by reactive oxygen species generated by the mutant, reflecting the fact that the O_2 interaction that stabilizes the heme Fe(II)–O_2 complex is not possible in the absence of Arg97. It has been suggested that verdoheme in heme oxygenase forms via the heme Fe(III)-OOH complex (Ortiz de Montellano 1998) with the aid of a water molecule in the heme distal side (Matsui et al. 2010). Addition of CO to the final solution changed the visible bands, suggesting that the Fe(II) cation was present in the solution.

Mass spectral analysis of full-length wild type *Ec*DOS and the corresponding Arg97Glu and Arg97Ile mutants in the presence of Na_2S

An absorption spectral analysis suggested that protoporphyrin IX of the heme Fe(III) complex in the Arg97Ile mutant of full-length *Ec*DOS was modified by Na_2S and that verdoheme was formed, but indicated no heme modifications for the wild type or Arg97Glu mutant. To understand if protoporphyrin IX was modified by Na_2S, we performed mass spectral analyses of full-length wild-type *Ec*DOS and the corresponding Arg97Glu and Arg97Ile mutants (Fig. 5).

No mass spectral changes in the wild type or Arg97Glu mutants were observed even 300 min after adding Na_2S, clearly indicating that the addition of Na_2S caused no time-dependent heme modifications or formation of verdoheme in these *Ec*DOS variants (Fig. 5a–c). However, for the Arg97Ile mutant, the addition of Na_2S caused time-dependent formation of verdoheme and a simultaneous decrease in heme iron complex content (Fig. 5d). These mass spectral findings regarding verdoheme formation are consistent with the absorption spectral findings observed for the wild type and Arg97Glu and Arg97Ile mutants.

Proposed changes in coordination structure and redox state of full-length *Ec*DOS proteins

Table 1 and Fig. 6 summarize the proposed changes in coordination structure and redox state for full-length wild-type *Ec*DOS and the corresponding Met95 and Arg97 mutants caused by the addition of Na_2S based on absorption spectroscopic and mass spectrometric results. For the wild type and Met95His mutant, the heme Fe(III)–OH complex is converted into a heme Fe(III)–SH^- complex, which is then reduced, resulting in dissociation of SH^- from the heme Fe(II) complex and, instead, Met95 rebinds to the heme Fe(II) complex. O_2 then quickly binds to the heme Fe(II) complex. The heme Fe(II)–O_2 complex is gradually autoxidized back to the heme Fe(III)–OH complex for the wild type, but it is stable in the Met95His mutant, remaining reduced for more than 2 h. For the Met95Ala mutant, the heme Fe(III)–SH^- complex forms, but is not reduced to the heme Fe(II) complex.

For the Arg97Glu mutant, the stable heme Fe(II) complex is formed upon addition of H_2S. However, O_2, which should be present in the protein solution, does not bind to the heme Fe(II) complex. For the Arg97Ile mutant, it is clear that the addition of H_2S converts the initial heme Fe(III)–OH complex to verdoheme bound to the Fe(II) cation.

Verdoheme is the first product of the consecutive reactions from the heme Fe(III) complex of heme oxygenase that ultimately lead to bilirubin (Fig. S1) (Matsui et al. 2010; Ortiz de Montellano 1998). It has been suggested that the heme Fe(III)-OOH species and a water molecule in the heme distal side are critical for triggering the first oxygen-insertion reaction of heme oxygenase. Arg97 mutants of *Ec*DOS, which lack the side chain of Arg97, are unable to form the ionic bond with heme Fe(II) complex-bound O_2 that stabilizes the heme Fe(II)–O_2 complex, and instead would generate reactive oxygen species, such as H_2O_2 or O_2^-. Therefore, for the Arg97Ile mutant, H_2O_2 generated

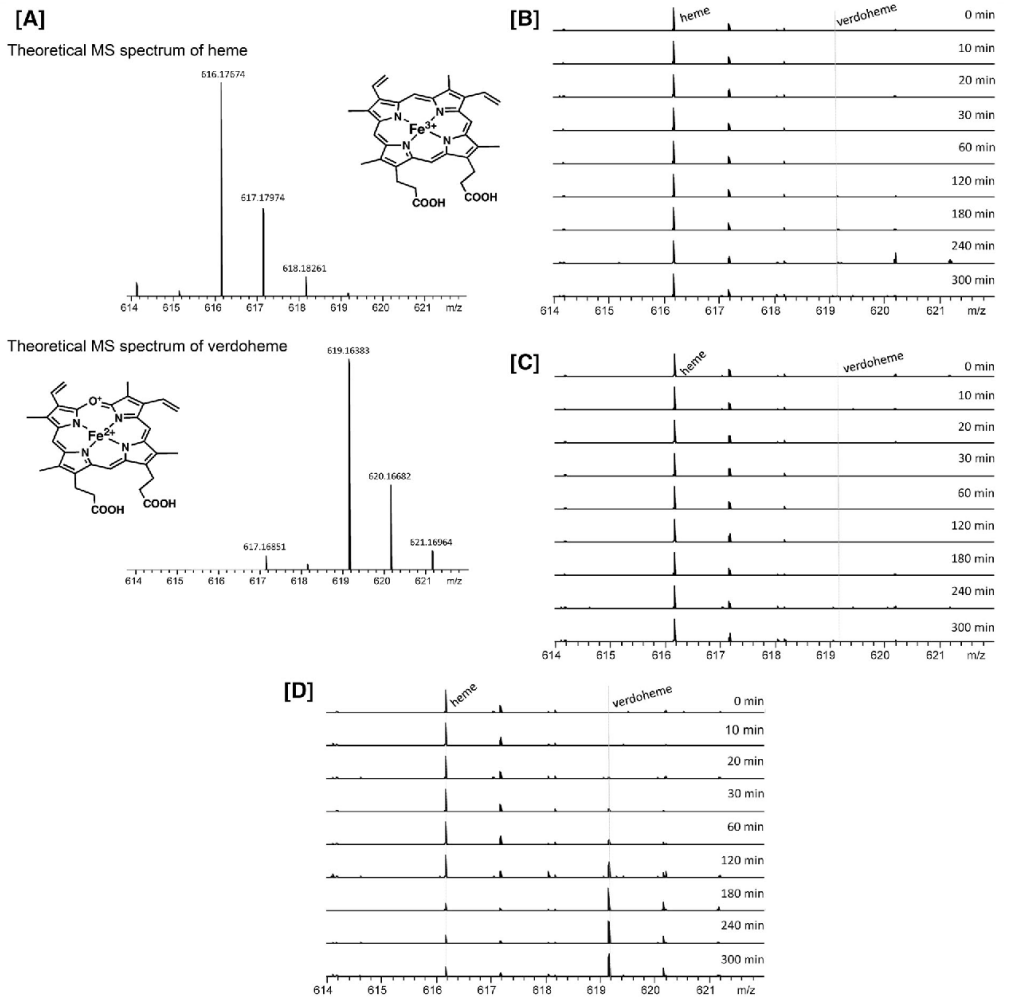


Fig. 5 Time resolved monitoring of heme to verdoheme conversion in selected *Ec*DOS variants by mass spectrometry. **a** Theoretical mass spectra of heme and verdoheme, and time-dependent mass spectral changes of **b** wild-type, **c** Arg97Glu, and **d** Arg97Ile of the heme Fe(III) complex of full-length *Ec*DOS caused by the addition of Na_2S. *Ec*DOS, 20 μM; Na_2S, 4 mM

during the reaction would interact with the heme Fe(III) complex and form the Fe(III)-OOH complex. The combination of these two factors—H_2O_2 and a water molecule—together with the characteristic structural and ionic properties of the heme distal side of the Arg97Ile mutant, would lead to optical conditions suitable for formation of verdoheme. For YddV, another heme-based O_2 sensor, introduction of a water molecule to the heme surroundings by mutations at the heme distal side converts the heme iron complex into verdoheme by mimicking heme oxygenase, even in the absence of Na_2S (Kitanishi et al. 2010; Nakajima et al. 2012; Stranava et al. 2014). Additionally, the high protein flexibility characteristic of the O_2-sensing

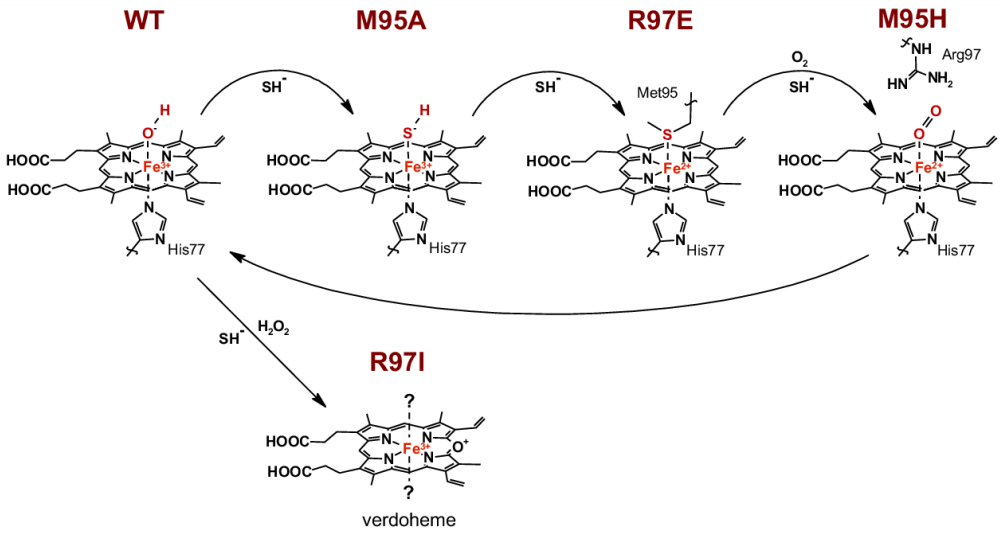


Fig. 6 Proposed changes in coordination structure and redox status of the heme Fe(III) complex of wild type and Met95 and Arg97 mutants of full-length *Ec*DOS caused by the addition of Na_2S

site of heme-based O_2 sensors would facilitate the facile formation of verdoheme; this is unlike the case for other prototypical hemoproteins, such as hemoglobin, myoglobin, and P450 (Anzenbacher et al. 2014). In contrast, for the Arg97Glu mutant, the ionic and/or stereochemical character of the heme surroundings would hamper the binding of reactive oxygen species to heme Fe(III) and Fe(II) complexes.

Catalytic activities of Met95 and Arg97 mutants of full-length *Ec*DOS in the presence of Na_2S

We successfully produced stable and pure heme Fe(III)–SH^-, external-ligand–free heme Fe(II), and heme Fe(II)–O_2 complexes by mutating the Met95 and Arg97 residues of full-length *Ec*DOS. To understand the role of the heme iron complex in the catalytic enhancement of full-length *Ec*DOS by Na_2S, we took advantage of the distinct characteristics of these separate forms, examining PDE catalytic activities of the corresponding Met95 and Arg97 mutants in the presence of Na_2S. Catalytic activities of the mutant enzymes were monitored by evaluating either the decrease in the substrate (c-di-GMP) or the increase in the product (l-di-GMP) using HPLC (Fig. 7). The results obtained were similar using both approaches, suggesting that this method is solid and reliable, and the catalytic activities of wild-type and mutant *Ec*DOS in the absence of Na_2S were consistent with those previously reported (Tanaka and Shimizu 2008).

For Met95 mutants, the addition of Na_2S enhanced catalytic activity, albeit to a slightly lesser degree than was the case for the wild type (Fig. 8). Since the Met95Ala mutant formed only the heme Fe(III)–SH^- complex but no the heme Fe(II)–O_2 complex, these results emphasize the critical involvement of the heme Fe(III)–SH^- complex in the catalytic enhancement. The addition of Na_2S also enhanced the catalytic activity of the Met95His mutant, which forms a stable heme Fe(II)–O_2 complex, demonstrating the involvement of the heme Fe(II)–O_2 complex in the observed catalytic enhancement of *Ec*DOS. Collectively, these results support the assumption that both the heme Fe(III)–SH^- complex and heme Fe(II)–O_2 complex are active species (Fig. 1c).

Unlike the case for Met95 mutants, the addition of Na_2S did not significantly enhance the catalytic of Arg97Glu or Arg97Ile mutants compared with the wild type. The addition of Na_2S to the Arg97Glu mutant caused formation of a heme Fe(II) complex

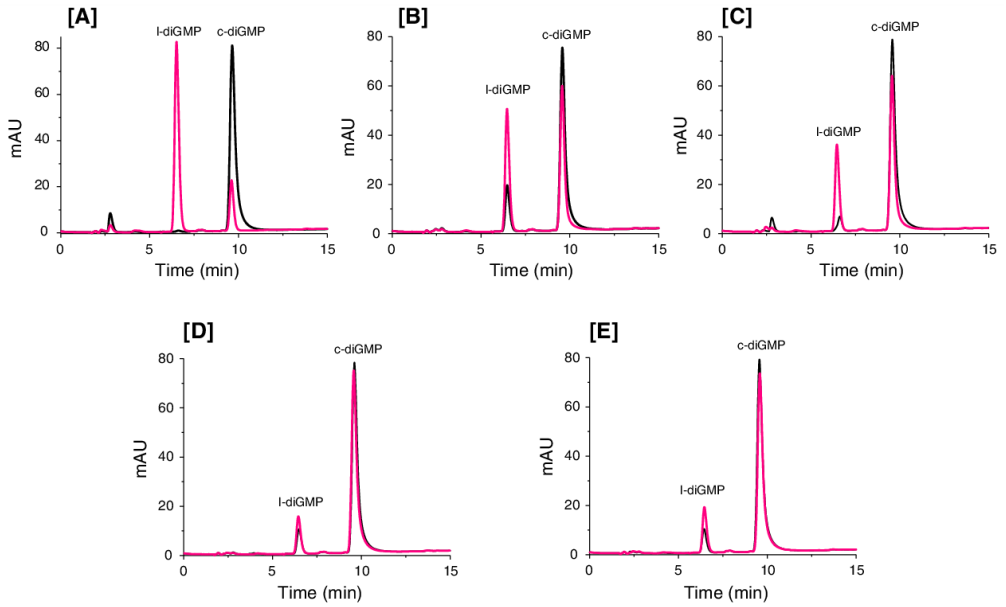


Fig. 7 Selected HPLC patterns of catalytic activities manifested as a time-dependent decrease in the substrate (c-di-GMP) and time-dependent increase in the product (linear di-GMP or pGpG) for **a** wild type and **b** Met95Ala, **c** Met95His, **d** Arg97Glu and **e** Arg97Ile mutants of full-length *Ec*DOS caused by the addition of Na_2S. *Black lines* without Na_2S; *red lines* 10 min after mixing with Na_2S. (Color figure online)

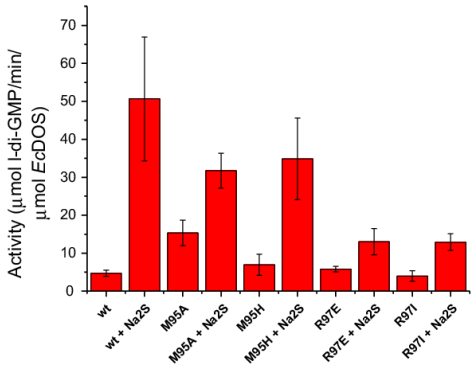


Fig. 8 Catalytic activities of wild type and Met95 and Arg97 mutants of full-length *Ec*DOS without and with Na_2S, evaluated by measuring the decrease in the substrate c-di-GMP by HPLC

that was free of an external axial ligand (Fig. 6; Tables 1, S1). These results thus reconfirm that external-axial-ligand–bound heme complexes, heme Fe(III)–SH^- and Fe(II)–O_2, rather than the axial-ligand–free heme Fe(II) complex, are significantly involved in mediating the catalytic enhancement of full-length *Ec*DOS by Na_2S. For the Arg97Ile mutant, the addition of Na_2S only slightly enhanced catalytic activity. In this study, we also found that verdoheme bound to the Fe(II) cation did not significantly contribute to the catalytic enhancement for *Ec*DOS compared with the heme iron complex, although it is not clear from our results whether external-ligand–bound or –free form(s) of verdoheme Fe(II) complex(es) are formed.

Roles of cysteine residues in the catalytic enhancement caused by Na_2S

The present study sought to determine the molecular mechanism by which the heme iron complex is involved in the Na_2S-induced catalytic activation of the heme-based O_2-sensor PDE, *Ec*DOS. The role of cysteine residues in the functional regulation by Na_2S

has been well documented in numerous physiological and pathological systems (Banerjee 2011; Kabil et al. 2014; Kimura 2014; Paul and Snyder 2012; Szabo 2010; Wang 2010).

The amino acid sequence of full-length *Ec*DOS reveals the presence of eight cysteines at residues 169, 180, 274, 287, 456, 624, 735, and 778. Our previously investigations of the catalytic involvement of cysteine residues (Takahashi et al. 2012) yielded a number of interesting findings. (1) Using 5, 5′-dithiobis-2-nitrobenzoic acid (DTNB) to determine the number of free thiolate residues on the full-length *Ec*DOS surface, we estimated that seven of the eight cysteine residues were present as free thiolates in the Fe(III)-bound form of *Ec*DOS, a number that increased to eight upon Na_2S treatment. This finding suggests that free thiolate residues formed by Na_2S may contribute to the catalytic enhancement of *Ec*DOS. (2) Treatment of full-length *Ec*DOS with the thiol blocking agent, *N*-ethylmaleimide, totally abolished the basal catalytic activity of *Ec*DOS. (3) Simultaneously mutating all eight cysteine residues in the full-length *Ec*DOS protein to alanines totally abolished both basal and ligand (O_2, NO, CO and H_2S)-induced catalytic activity. (4) The basal activity of a quadruple mutant in which Cys456, Cys624, Cys735 and Cys778 in the central and C-terminal PDE domains were simultaneously mutated to alanine residues was reduced to only ~15 % of that of the wild type in the presence of Na_2S. (5) Another quadruple mutant, in which Cys169, Cys180, Cys274 and Cys287 were simultaneously mutated to alanines, retained nearly 75 % of wild-type basal activity in the presence of Na_2S. (6) Basal activity of a Cys735Ala mutant in the presence of Na_2S was reduced to 35 % of that in the wild type. By comparison, activity was only slightly decreased compared with the wild type in all seven other single cysteine mutants.

Thus, cysteine residues are clearly involved in both basal as well as Na_2S-induced catalysis. Cysteine residues in the PDE domain, in particular, are unequivocally involved in catalysis. However, identification of specific cysteine residue(s) involved in the catalytic activity of full-length *Ec*DOS has not been feasible.

Summary

The following findings were obtained in the present study:

Coordination and redox changes

Changes in coordination structure and redox state of the heme Fe(III) complex in full-length *Ec*DOS Met95 and Arg97 mutants caused by Na_2S are distinct from those of the isolated heme-bound domain of *Ec*DOS, as demonstrated by absorption and mass spectral studies. Specifically:

(1) Changes in the heme redox state of the wild type and Met95 and at Arg97 mutants caused by Na_2S were not closely correlated with the proteins' reduction potential values. Namely, the heme Fe(III) complex of the Met95His mutant, with a minus reduction potential (−122 mV vs. SHE), was reduced and formed a heme Fe(II)–O_2 complex similar to the wild-type protein (+45 mV vs. SHE) upon addition of Na_2S. In contrast, the heme Fe(III) complex of the Met97Ala mutant, with a minus reduction potential (−26 mV vs. SHE) was not reduced by the same treatment, instead it was converted only to the heme Fe(III)–SH^- complex (Fig. 6; Tables 1, S2).

(2) The heme Fe(III) complex of the full-length *Ec*DOS Arg97Glu mutant was reduced and the addition of Na_2S resulted in formation of the heme Fe(II) complex (Fig. 6; Tables 1, S2). However, O_2, which should be present in the protein solution, did not bind to the heme Fe(II) complex of this mutant.

(3) The heme Fe(III) complex of the Arg97Ile mutant was converted to verdoheme bound to the Fe(II) cation upon addition of Na_2S, aided by reactive oxygen species generated by this mutant.

Catalytic activities

(1) The addition of Na_2S enhanced the catalytic activity of Met95Ala and Met95His mutants. The enhancement was slightly less than that for the wild type, probably because only one of the two active forms, the heme Fe(III)–SH^- or heme Fe(II)–O_2 complex, was formed for Met95Ala and Met95His mutants, respectively.

(2) Catalytic enhancement was diminished for the Arg97Glu mutant, since the addition of Na_2S

caused formation of an external-axial-ligand–free heme Fe(II) complex, which does not significantly contribute to catalytic enhancement.

(3) The addition of Na_2S only slightly enhanced the catalytic activity of the verdoheme-bound Arg97Ile mutant, suggesting that verdoheme bound to the Fe(II) cation, unlike the heme iron complex, is not capable of stimulating catalysis. However, it is not clear whether an external ligand is bound to the verdoheme Fe(II) cation.

Collectively, the results of the current study clearly indicate that the catalytic enhancement of heme Fe(III)-bound, full-length *Ec*DOS caused by Na_2S is mainly attributable to the heme Fe(III)–SH^- and heme Fe(II)–O_2 complexes in the sensor domain formed in response to Na_2S treatment. It is expected that interactions between HS^- and the heme iron complex are involved in various important physiological and pathological functions, but this question remains to be explored.

Acknowledgments This work was supported in part by Grants-in-Aid from Shantou University Medical College, and Grants from the National Natural Science Foundation of China (NSFC) (31170736, 31371333), Guangdong Natural Science Foundation (S2012030006289), Charles University in Prague (UNCE 204025/2012), the Grant Agency of Charles University in Prague (756214) and the Grant Agency of the Czech Republic (Grant 15-19883S). Mass spectrometry facility was supported by the Operational Program Prague—Competitiveness, project CZ.2.16/3.1.00/24023. We are grateful to Profs. Jikai Jiang and Wenhong Luo for technical assistance of HPLC at the initial stage of this work.

References

Anzenbacher P, Marchal S, Palacký J, Anzenbacherová E, Domaschke T, Lange R, Shimizu T, Kitanishi K, Stranava M, Stiborová M, Martínková M (2014) Pressure effects reveal that changes in the redox states of the heme iron complexes in the sensor domains of two heme-based oxygen sensor proteins, *Ec*DOS and YddV, have profound effects on their flexilibity. FEBS J 281:5208–5219

Aono A (2012) Novel bacterial gas sensor proteins with transition metal-containing prothethic groups as active sites. Antioxid Redox Signal 16:678–686

Banerjee R (2011) Hydrogen sulfide: redox metabolism and signaling. Antioxid Redox Signal 15:339–341

Delgado-Nixon VM, Gonzalez G, Gilles-Gonzalez MA (2000) Dos, a heme-binding PAS protein from *Escherichia coli*, is a direct oxygen sensor. Biochemistry 39:2685–2691

Du Y, Liu G, Yan Y, Huang D, Luo W, Martinkova M, Man P, Shimizu T (2013) Conversion of a heme-based oxygen sensor to a heme oxygenase by hydrogen sulfide: effects of mutatations in the heme distal side of a heme-based oxygen sensor phosphodiesterase (*Ec* DOS). Biometals 26:839–852

Germani F, Moens L, Dewilde S (2013) Haem-based sensors: a still growing old superfamily. Adv Microbiol Physiol 63:1–47

Gilles-Gonzalez MA, Gonzalez G (2005) Heme-bases sensors: defining characteristics, recent developents, and regulatory hypotheses. J Inorg Biochem 99:1–22

Girvan HM, Munro AW (2013) Heme sensor proteins. J Biol Chem 288:13194–13203

Green J, Crack JC, Thomson AJ, LeBrun NE (2009) Bacterial sensors of oxygen. Curr Opion Microbiol 12:145–151

Guengerich FP (2013) New trends in cytochrome P450 Research at the half-century mark. J Biol Chem 288:17063–17064

Hengge R (2009) Principles of c-di-GMP signalling in bacteria. Nat Rev Microbiol 7:263–273

Hirata S, Matsui T, Sasakura Y, Sugiyama S, Yoshimura T, Sagami I, Shimizu T (2003) Characterization of Met95 mutants of a heme-regulated phosphodiesterase from *Escherichia coli*: optical absorption, magnetic circular dichroism, circular dichroism, and redox potentials. Eur J Biochem 270:4771–4779

Honjo A, Takahashi H, Sekimoto M, Igarashi J, Shimizu T (2012) Novel effects of Mn^{2+} on the catalytic enhancement of the inactive form of the Fe(III) heme-bound *Ec* DOS, a heme-regulated phosphodiesterase from *Escherichia coli*. In: Qiu X (ed) Gas sensors: developments, efficacy and safety. Nova Science, Hauppauge, pp 251–261

Igarashi J, Kitanishi K, Shimizu T (2011) Emerging roles of heme as a signal and a gas-sensing site: Heme-sensing and gas-sensing proteins (chapter 73). In: Kadish KM, Smith KM, Guilard R (eds) Handbook of porphyrin science, vol 15., World Scientific Publishing Hackensack, NJ, pp 399–460

Ishitsuka Y, Araki Y, Tanaka A, Igarashi J, Ito O, Shimizu T (2008) Arg97 at the heme-distal side of the isolated heme-bound PAS domain of a heme-based oxygen sensor from *Escherichia coli* (*Ec* DOS) plays critical roles in autooxidation and binding of gases, particularly O_2. Biochemistry 47:8874–8884

Kabil O, Moti N, Banerjee R (2014) H_2S and its role in redox signaling. Biochim Biophys Acta 1844:1355–1366

Kimura H (2014) Hydrogen sulfide and polysulfides as biological mediators. Molecules 19:16146–16157

Kitanishi K, Kobayashi K, Kawamura Y, Ishigami I, Ogura T, Nakajima K, Igarashi J, Tanaka A, Shimizu T (2010) Important roles of Tyr43 at the putative heme distal side in the oxygen recognition and stability of the Fe(II)-O_2 complex of YddV, a globin-coupled heme-based oxygen sensor diguanylate cyclase. Biochemistry 49:10381–10393

Kitanishi K, Kobayashi K, Uchida T, Ishimori K, Igarashi J, Shimizu T (2011) Identification and functional and spectral characterization of a globin-coupled histidine kinase from *Anaeromyxobacter* sp. Fw109–5. J Biol Chem 286: 35522–35534

Kobayashi K, Tanaka A, Takahashi H, Igarashi J, Ishitsuka Y, Yokota N, Shimizu T (2010) Catalysis and oxygen binding of *Ec* DOS, a heme-based oxygen-sensor enzyme from *Escherichia coli*. J Biochem 148:693–703

Kurokawa H, Lee DS, Watanabe M, Sagami I, Mikami B, Raman CS, Shimizu T (2004) A redox-controlled molecular switch revealed by the crystal structure of a bacterial heme PAS sensor. J Biol Chem 279:20186–20193

Martínková M, Kitanishi K, Shimzu T (2013) Heme-based globin-coupled oxygen sensors: linking oxygen binding to functional regulation of diguanylate cyclase, histidine kinase, and methyl-accepting chemotaxis. J Biol Chem 288:27702–27711

Matsui T, Iwasaki M, Sugiyama R, Unno M, Ikeda-Saito M (2010) Dioxygen activation for self-degradation of heme: reaction mechanism and regulation of heme oxygenase. Inorg Chem 49:3602–3609

Nakajima N, Kitanishi K, Kobayashi K, Kobayashi N, Igarashi J, Shimizu T (2012) Leu65 in the heme distal side is critical for the stability of the Fe(II)-O_2 complex of YddV, a globin-coupled oxygen sensor diguanylate cyclase. J Inorg Biochem 108:163–170

Nicoletti FP, Comandini A, Bonamore A, Boechi L, Boubeta FM, Feis A, Smulvich G, Boffi A (2010) Sulfide binding properties of truncated hemoglobins. Biochemistry 49:1017–1026

Ortiz de Montellano PR (1998) Heme oxygenase mechanism: evidence for an electrophilic ferric peroxide species. Acc Chem Res 31:543–549

Ortiz de Montellano PR (2010) Hydrocarbon hydroxylation by cytochrome P450 enzymes. Chem Rev 110:932–948

Park H, Suquet C, Satterlee JD, Kang C (2004) Insights into signal transduction involving PAS domain oxygen-sensing heme proteins from the X-ray crystal structure of *Escherichia coli* DOS heme domain (*Ec* DOSH). Biochemistry 43:2738–2746

Paul BD, Snyder SH (2012) H_2S signaling through protein sulfhydration and beyond. Nat Rev Mol Cell Biol 13:499–507

Pietri R, Román-Morales E, López-Garriga J (2011) Hydrogen sulfide and hemeproteins: knowledge and mysteries. Antioxid Redox Sig 15:393–404

Poulos TL (2014) Heme enzyme structure and function. Chem Rev 114:3919–3962

Ramos-Alvarez C, Yoo BK, Pietri R, Lamarre I, Martin JL, Lopez-Garriga J, Nagrerie M (2013) Reactivity and dynamics of H_2S, NO, and O_2 interacting with hemoglobins from *Lucina pectinata*. Biochemistry 52:7007–7021

Ríos-González BB, Román-Morales EM, Pietri R, López-Garriga J (2014) Hydrogen sulfide activation in hemeproteins: the sulfheme scenario. J Inorg Biochem 133:78–86

Römling U, Gomelsky M, Galperin M (2005) C-di-GMP: the drawing of a novel bacterial signaling system. Mol Microbiol 57:629–639

Sakamoto H, Omata Y, Adachi Y, Palmer G, Noguchi M (2000) Separation and identification of regioisomers of verdoheme by reverse-phase ion-pair high-perfomance liquid chromatography, and characterization of their complexes with heme oxygenase. J Inorg Biochem 82:113–121

Sasakura Y, Hirata S, Sugiyama S, Suzuki S, Taguchi S, Watanabe M, Matsui T, Sagami I, Shimizu T (2002) Characterization of a direct oxygen sensor heme protein from *E. coli*: effects of the heme redox states and mutations at the heme binding site on catalysis and structure. J Biol Chem 277:23821–23827

Sasakura Y, Yoshimura-Suzuki T, Kurokawa H, Shimizu T (2006) Structure-function relationships of *Ec* DOS, a heme-regulated phosphodiesterase from *Escherichia coli*. Acc Chem Res 39:37–43

Sato A, Sasakura Y, Sugiyama S, Sagami I, Shimizu T, Mizutani Y, Kitagawa T (2002) Stationary and time-resolved resonance Raman spectra of His77 and Met95 mutants of the isolated heme domain of a direct oxygen sensor from *E. coli*. J Biol Chem 277:32650–32658

Schirmer T, Jenal U (2009) Structure and mechanistic determinants of c-di-GMP signaling. Nat Rev Microbiol 7:724–735

Shimizu T (2013a) The heme-based oxygen-sensor phosphodiesterase *Ec* DOS (DosP): structure–function relationships. Biosensor 3:211–237

Shimizu T (2013b) Revisit of the interactions between hydrogen sulfide and heme proteins. Curr Chem Biol 7:207–212

Stranava M, Martínková M, Stiborová M, Man P, Kitanishi K, Muchová L, Vítek L, Martínek V, Shimizu T (2014) Introduction of water into the heme distal side by Leu65 mutations of an oxygen sensor, YddV, generates verdoheme and carbon monoxide, exerting the heme oxygenase reaction. J Inorg Biochem 140:29–38

Szabo C (2010) Gaseotransmitters: new frontiers for translational science. Sci Transl Med 2:59ps54

Taguchi S, Matsui T, Igarashi J, Sasakura Y, Araki Y, Ito O, Sugiyama S, Sagami I, Shimizu T (2004) Binding of oxygen and carbon monoxide to a heme-regulated phosphodiesterase from *Escherichia coli*: kinetics and infrared spectra of the full-length wild-type enzyme, isolated PAS domain, and Met95 mutants. J Biol Chem 279:3340–3347

Takahashi H, Shimizu T (2006) Phosphodiesterase activity of *Ec*DOS, a heme-regulated enzyme from *Escherichia coli*, toward 3′, 5′-cyclic diguanylic acid is obviously enhanced by O_2 and CO binding. Chem Lett 35:970–971

Takahashi H, Sekimoto M, Tanaka M, Tanaka A, Igarashi J, Shimizu T (2012) Hydrogen sulfide stimulates the catalytic activity of a heme-regulated phosphodiesterase from *Escherichia coli* (*Ec* DOS). J Inorg Biochem 109:66–71

Tanaka A, Shimizu T (2008) Ligand binding to the Fe(III)-protoporphyrin IX complex of phosphodiesterase from *Escherichia coli* (*Ec* DOS) markedly enhances catalysis of cyclic di-GMP: roles of Met95, Arg97, and Phe113 of the putative heme distal side in catalytic regulation and ligand binding. Biochemistry 47:13438–13446

Tanaka A, Takahashi H, Shimizu T (2007) Critical role of the heme axial ligand, Met95, in locking catalysis of the phosphodiesterase from *Escherichia coli* (*Ec*DOS) toward cyclic diGMP. J Biol Chem 282:21301–21307

Tuckerman JR, Gonzalez G, Sousa EHS, Wan X, Saito JA, Alam M, Gilles-Gonzalez MA (2009) An oxygen-sensing diguanylate cyclase and phosphodiesterase couple for c-di-GMP control. Biochemistry 48:9764–9774

Uchida T, Kitagawa T (2005) Mechanism for transduction of the ligand-binding signal in heme-based gas sensory proteins revealed by resonance Raman spectroscopy. Acc Chem Res 38:662–670

Voet D, Voet JG (2011) Hemoglobin: protein function in microcosm. Biochemistry, 4th edn. Wiley, New York, pp 323–358

Wang R (2010) Hydrogen sulfide: the third gasotransmitter in biology and medicine. Antioxid Redox Signal 12: 1061–1064

Watanabe M, Matsui T, Sasakura Y, Sagami I, Shimizu T (2002) Unusual cyanide bindings to a heme-regulated phosphodiesterase from *Escherichia coli*: effect of Met95 mutations. Biochem Biophys Res Commun 299:169–172

Yamashita T, Bouzhir-Sima L, Lambry JC, Liebl U, Vos MH (2008) Ligand dynamics and early signaling events in the heme domain of the sensor protein Dos from *Escherichia coli*. J Biol Chem 283:2344–2352

4.2 Effects of hydrogen sulfide on the heme coordination structure and catalytic activity of the globin-coupled oxygen sensor *Af*GcHK

Fojtikova V., Bartosova M., Man P., Stranava M., Shimizu T., Martinkova M. *Biometals* (2016) 29, 715 (**IF_{2016} 2,2**)

Podíl předkladatelky na této práci: 65 % (exprese a purifikace proteinu *Af*GcHK v jeho přirozené a mutantních formách, spektroskopická měření, enzymové analýzy, zpracování a vyhodnocení výsledků)

Potvrzeno korespondujícím autorem, doc. RNDr. Markéta Martínková, Ph.D.

Biometals (2016) 29:715–729
DOI 10.1007/s10534-016-9947-z

Effects of hydrogen sulfide on the heme coordination structure and catalytic activity of the globin-coupled oxygen sensor *Af*GcHK

Veronika Fojtikova · Martina Bartosova · Petr Man · Martin Stranava · Toru Shimizu · Marketa Martinkova

Received: 29 April 2016 / Accepted: 1 July 2016 / Published online: 9 July 2016
© Springer Science+Business Media New York 2016

Abstract *Af*GcHK is a globin-coupled histidine kinase that is one component of a two-component signal transduction system. The catalytic activity of this heme-based oxygen sensor is due to its C-terminal kinase domain and is strongly stimulated by the binding of O_2 or CO to the heme Fe(II) complex in the N-terminal oxygen sensing domain. Hydrogen sulfide (H_2S) is an important gaseous signaling molecule and can serve as a heme axial ligand, but its interactions with heme-based oxygen sensors have not been studied as extensively as those of O_2, CO, and NO. To address this knowledge gap, we investigated the effects of H_2S binding on the heme coordination structure and catalytic activity of wild-type *Af*GcHK and mutants in which residues at the putative O_2-binding site (Tyr45) or the heme distal side (Leu68) were substituted. Adding Na_2S to the initial OH-bound 6-coordinate Fe(III) low-spin complexes transformed them into SH-bound 6-coordinate Fe(III) low-spin complexes. The Leu68 mutants also formed a small proportion of verdoheme under these conditions. Conversely, when the heme-based oxygen sensor *Ec*DOS was treated with Na_2S, the initially formed Fe(III)–SH heme complex was quickly converted into Fe(II) and Fe(II)–O_2 complexes. Interestingly, the autophosphorylation activity of the heme Fe(III)–SH complex was not significantly different from the maximal enzyme activity of *Af*GcHK (containing the heme Fe(III)–OH complex), whereas in the case of *Ec*DOS the changes in coordination caused by Na_2S treatment led to remarkable increases in catalytic activity.

Keywords Hydrogen sulfide · Heme-based oxygen sensor · Autophosphorylation · Histidine kinase · Intramolecular catalytic regulation · Two-component signal transduction

Abbreviations

*Af*GcHK	A globin-coupled oxygen sensor histidine kinase from *Anaeromyxobacter* sp. Fw109-5

Veronika Fojtikova and Martina Bartosova contributed equally to this work.

Electronic supplementary material The online version of this article (doi:10.1007/s10534-016-9947-z) contains supplementary material, which is available to authorized users.

V. Fojtikova · M. Bartosova · P. Man · M. Stranava · T. Shimizu · M. Martinkova (✉)
Department of Biochemistry, Faculty of Science, Charles University in Prague, Hlavova 2030, Prague 2 128 43, Czech Republic
e-mail: marketa.martinkova@natur.cuni.cz

P. Man
Biotechnology and Biomedicine Centre (BioCeV), Institute of Microbiology of the Czech Academy of Science, v.v.i., Prumyslova 595, Vestec 252 42, Czech Republic

*Ec*DOS	*Escherichia coli* direct oxygen sensor or heme-regulated phosphodiesterase from *E. coli* or *Ec*DosP
Fe(III)	Fe(III)–protoporphyrin IX complex, or hemin
Fe(II)	Fe(II)–protoporphyrin IX complex
GCS	Globin-coupled oxygen sensor
MALDI-MS	Matrix-assisted laser desorption/ionization mass spectrometry
MALDI-FT-ICR	Matrix-assisted laser desorption/ionization Fourier transform ion cyclotron resonance
PAS	An acronym derived from the words Per (*Drosophila* period clock protein)-Arnt (vertebrate aryl hydrocarbon receptor nuclear translocator)-Sim (*Drosophila* single-minded protein)
YddV	A globin-coupled diguanylate cyclase from *E. coli* or *Ec*DosC
YddV-heme	A sensor (globin) domain containing heme of YddV
WT	Wild type

Introduction

Oxygen (O_2) is a biologically important molecule and plays a vital role in aerobic metabolism as the final acceptor of electrons. Heme proteins such as hemoglobin and myoglobin transport and store O_2, respectively, whereas other hemoproteins such as cytochromes P450 and peroxidases activate or interact with O_2 or reactive oxygen species (Voet and Voet 2011; Poulos 2014). Cytochromes such as cytochrome *c* have functions in electron transfer. All of the hemoproteins discussed above are typical hemoproteins, in which the heme iron complex serves as the functional site. Conversely, in heme-based oxygen sensors, the heme iron complex is an O_2 sensing site that regulates the function of a separate catalytic domain. A great variety of catalytic domains have been identified, including histidine kinases, diguanylate cyclases, and phosphodiesterases, as well as domains that regulate methyl-accepting chemotaxis and transcription (Gilles-Gonzalez and Gonzalez 2005; Uchida and Kitagawa 2005; Green et al. 2009; Igarashi et al. 2011; Germani et al. 2013; Girvan and Munro 2013; Martínková et al. 2013; Shimizu et al. 2015).

*Af*GcHK is a heme-based O_2 sensor histidine kinase and a part of the two-component signaling system (Fig. 1) in the bacterium *Anaeromyxobacter* sp. strain Fw109-5 (Kitanishi et al. 2011; Nakajima et al. 2012; Fojtikova et al. 2015). Its N-terminal sensing domain is associated with an Fe(II) heme complex, and the binding of O_2 to the Fe(II) center triggers the autophosphorylation of His183 in the C-terminal kinase domain. The phosphate group is then transferred from His183 to an Asp residue in a cognate response regulator protein (Kitanishi et al. 2011). The enzyme retains its catalytic activity when the Fe(II) center is coordinated by CO instead of O_2. OH^--, CN^-- and imidazole-bound Fe(III) complexes exhibit similar activity to the Fe(II)–O_2 form (Fojtikova et al. 2015). However, the ligand-free 5-coordinate heme Fe(II) complex is catalytically inactive (Fojtikova et al. 2015). Both the Fe(II) and Fe(II)–O_2 complexes are stable; the latter was spectroscopically stable for more than 3 days at room temperature. The stability of the Fe(II) form is influenced by its redox environment because oxidative stress promotes its conversion into the Fe(III) form. It was suggested that *Af*GcHK is constitutively active under aerobic conditions because it exists as the Fe(II)–O_2 [or Fe(III)] complex, but is converted into the inactive Fe(II) complex under hypoxic or anaerobic conditions (Kitanishi et al. 2011).

While O_2, NO, and CO are the most well-known and extensively studied gaseous signaling molecules, H_2S is also an important biological signal in some

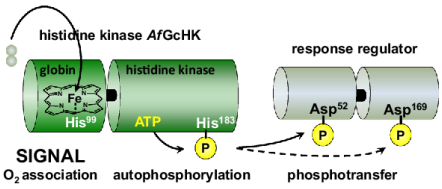


Fig. 1 The sensing and signaling mechanism of the two-component signal transduction system featuring the globin-coupled sensor (GCS) *Af*GcHK. O_2 binds to the Fe(II) heme complex of *Af*GcHK, which is bound to the N-terminal domain via the globin fold. Its binding strongly activates the histidine kinase in the C-terminal domain, resulting in its autophosphorylation at His183. This phosphate group is then transferred to the cognate response regulator. Although the enzyme is depicted as a monomer for the sake of simplicity, all histidine kinases reported to date, including *Af*GcHK, are dimers or tetramers. This figure was adapted from Martínková et al. (2013) and Shimizu et al. (2015)

systems (Banerjee 2011; Kimura 2015; Kimura et al. 2015; Mishanina et al. 2015; Paul and Snyder 2015). It has been proposed that persulfhydration of protein surfaces and/or the formation of polysulfides (H_2Sn) may be important in H_2S-mediated intermolecular signal transduction, making persulfhydrated proteins the active signaling species (Kimura 2015; Kimura et al. 2015; Mishanina et al. 2015; Paul and Snyder 2015).

Heme proteins with the globin fold such as hemoglobin and myoglobin reportedly interact with H_2S (Pietri et al. 2011; Shimizu 2013; Ríos-González et al. 2014). Because the pK_a of H_2S is around 6.9, HS^- can readily bind to the Fe(III) center of the heme protein in pH-neutral aqueous media (Shimizu 2013). The HS^--bound Fe(III) complex can be converted into the corresponding heme Fe(II) complex if the heme environment is suitable, which is followed by the dissociation of HS^- from the Fe(II) center (Pietri et al. 2011; Shimizu 2013; Ríos-González et al. 2014). In addition, a sulfheme iron complex (i.e. a protoporphyrin IX iron complex with a sulfur atom) is formed when hemoglobin or myoglobin are treated with both H_2S and H_2O_2 (Berzofsky et al. 1971; Andersson et al. 1984). The catalytic activity of the heme-based oxygen sensor phosphodiesterase *Ec*DOS (or *Ec*DosP) is reported to increase substantially following treatment with H_2S (Takahashi et al. 2012). This has been attributed to changes in the structure and coordination of the heme complex (Du et al. 2013; Yan et al. 2015). However, in contrast to hemoglobin and myoglobin, *Ec*DOS mutants with substitutions at the heme distal side form verdoheme iron complexes (i.e. protoporphyrin IX iron complexes in which one of the bridging methine groups of the porphyrin structure is replaced with an oxygen center) upon treatment with H_2S.

The heme-binding domain of *Ec*DOS adopts a PAS fold, which consists of several β-sheets, whereas the globin fold consists of several α-helices. In contrast, the heme-binding domain of the heme-based oxygen sensor *Af*GcHK adopts the globin fold, so the protein has been described as a globin-coupled oxygen sensor (GCS) (Fig. 2) (Martínková et al. 2013; Tarnawski et al. 2015; Zhang and Phillips 2003). The Fe(III) complexes of heme-based oxygen sensors such as *Ec*DOS and YddV are converted into the physiologically relevant Fe(II) or Fe(II)–O_2 forms by adding excess Na_2S, suggesting that their physiological functions could be activated under extreme conditions in the presence of H_2S (Takahashi et al. 2012). It seems likely that GCS and *Af*GcHK would also undergo similar redox state changes under comparable conditions. There is no published information on the interactions of H_2S with GCS proteins. To address this knowledge gap, we performed experiments to determine whether the heme coordination structure and kinase activity of *Af*GcHK are affected by treatment with H_2S. In addition, we performed experiments with *Af*GcHK mutants in which two key residues were substituted: Tyr45, which is assumed to be the O_2 binding site on the heme-distal side in the Fe(II)–O_2 complex (Kitanishi et al. 2011); and Leu68, which is assumed to be located on the heme distal side of the protein and to help prevent the coordination of water to the iron center (Nakajima et al. 2012; Stranava et al. 2014; Lambry et al. 2016). Using these mutants enabled us to study how structural changes at the corresponding positions affected the structure and coordination of the heme complex and the catalytic activity of *Af*GcHK. Supplemental spectroscopic experiments were performed with another GCS, YddV (Tuckerman et al. 2009; Kitanishi et al. 2010), to characterize its response to Na_2S treatment, and the structural behavior of these two GCS upon treatment with Na_2S was compared to that of *Ec*DOS.

Experimental procedures

Materials

Ampicillin and kanamycin were obtained from P-lab (Prague, Czech Republic). Isopropyl β-D-thiogalactopyranoside, hemin, and acrylamide were obtained from Sigma-Aldrich (St. Louis, MO, USA). Water, doubly distilled over quartz, was purified using a Milli-Q Plus system (EMD Millipore, Billerica, MA, USA). All glassware used for sample preparation was conditioned in advance by standing for 24 h in 10 % HCl suprapur (Merck, Darmstadt, Germany). Phos-tag was obtained from the Phos-tag consortium (Wako Pure Chemical Industries, Osaka, Japan). All other chemicals used were of the highest purity grade available from commercial sources and used without further purification.

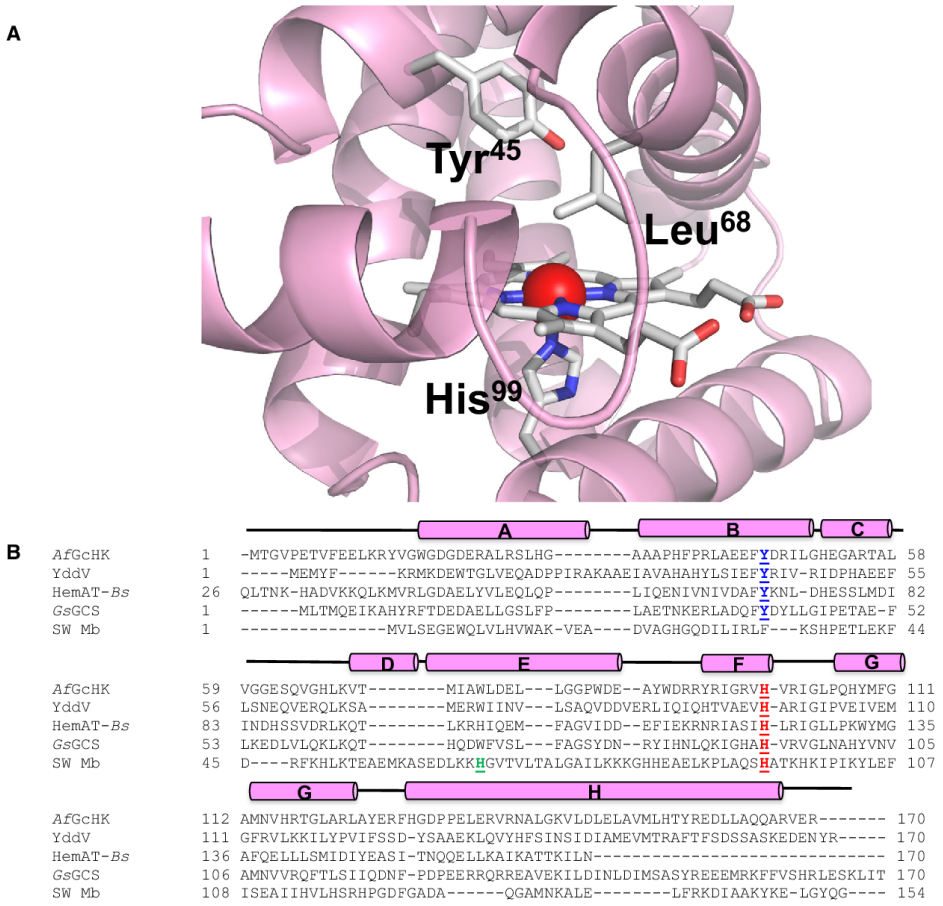


Fig. 2 Structure of the heme environment in the O_2 sensing domain of the GCS *Af*GcHK. **a** Putative structure of the Fe(III) complex of *Af*GcHK. The highlighted key residues were identified by considering the homology of *Af*GcHK with YddV (Tarnawski et al. 2015) and HemAT (Zhang and Phillips 2003). The structure was generated in SWISS-MODEL (http://swissmodel.expasy.org), which was used for homology modeling with PDB entry 1OR4 (the Fe(III)–CN^- moiety of HemAT) as the template. **b** Amino acid alignment of the heme distal side of *Af*GcHK, YddV, two other GCS proteins (HemAT-*Bs* and *Gs*GCS), and sperm whale myoglobin (Mb), with markers above the sequences indicating which residues belong to specific helices. The helix assignment was based on data for sperm whale Mb and HemAT (Martínková et al. 2013). The distal Tyr residue (B10), which binds to O_2 in the Fe(II)–O_2 complex, and the proximal heme-binding His residue (F8) are shown in *blue and red*, respectively. The distal His residue (E7) that interacts with O_2 in the Fe(II)–O_2 complex of sperm whale Mb is shown in *green*. (Color figure online)

Overexpression and purification of the wild-type and mutant proteins

Cloning and site-directed mutagenesis of *Af*GcHK were performed as previously described (Kitanishi et al. 2011). Overexpression in *Escherichia coli* and purification of His-tagged-*Af*GcHK were performed using a variant of a previously published protocol (Kitanishi et al. 2011; Fojtikova et al. 2015). Briefly, *E. coli* BL21(DE3) (Novagen) was transformed with

the appropriate pET 21c(+) plasmid containing a gene for WT *Af*GcHK or one of its mutants. Selection was then performed using 100 μg mL^{-1} ampicillin. After selection, the protein was expressed for 20 h at 15 °C in Terrific Broth containing the same antibiotic concentration after induction by the addition of 0.1 mM isopropyl β-D-thiogalactopyranoside. The *E. coli* cells were resuspended in buffer A [50 mM Tris–HCl (pH 8.0) and 100 mM NaCl] containing 1 mM phenylmethanesulfonyl fluoride and 1 mM ethylenediaminetetraacetic acid, and lysed with 0.2 mg mL^{-1} lysozyme. The crude extract was sonicated six times for 1 min each (with 1 min intervals between sonications) on ice and then centrifuged at 50,000×*g* for 60 min at 4 °C. The resulting supernatant was incubated for 20 min with hemin in dimethyl sulfoxide (300 μM) and then applied to a TALON Metal Affinity Resin column (Clontech Laboratories) that had been pre-equilibrated with buffer A. The column was then washed with buffer A, and *Af*GcHK fractions were eluted with 200 mM imidazole in buffer A. Protein fractions were pooled and applied to a Superdex 200 10/300 GL column (GE Healthcare) equilibrated with 20 mM Tris–HCl pH 8.0 buffer containing 150 mM NaCl. The desired eluates (identified by monitoring at 280 nm) were collected and concentrated with Amicon Ultra Centrifugal Filters (Millipore). Finally, the purified proteins were quickly frozen in liquid nitrogen and stored at −80 °C. Protein and heme concentrations were determined using the bicinchoninic acid assay with bovine serum albumin as a standard (Sunrise Absorbance Reader, TECAN) and the pyridine hemochromogen assay, respectively. Purified proteins were >90 % homogeneous, as confirmed by polyacrylamide gel electrophoresis in the presence of sodium dodecyl sulfate.

Cloning and site-directed mutagenesis of the isolated heme-bound domain of YddV (YddV-heme) were also performed according to a previously described protocol (Kitanishi et al. 2010; Nakajima et al. 2012). Overexpression in *E. coli* and purification of the His-tagged YddV-heme were performed using a variant of a previously published protocol (Kitanishi et al. 2010; Nakajima et al. 2012). Namely, wild-type and mutant proteins were expressed in *E. coli* BL21(DE3) harboring the pET28a(+) expression vector. Selection was performed with 50 μg mL^{-1} kanamycin. The protein was expressed after induction by the addition of 0.1 mM isopropyl β-D-thiogalactopyranoside for 20 h at 15 °C in Terrific Broth containing the same antibiotic concentration and 0.45 mM 5-aminolevulinic acid. *E. coli* cells were resuspended in 50 mM Tris–HCl, pH 8.0, 100 mM NaCl, 20 mM imidazole (buffer A), 1 mM phenylmethanesulfonyl fluoride, 1 mM ethylenediaminetetraacetic acid, and 0.2 mg mL^{-1} lysozyme. The solution was then sonicated and centrifuged at 100,000 × *g* for 30 min, and supernatant fractions were applied to a Ni–NTA agarose column. The YddV fractions were eluted with a linear gradient of 20–200 mM imidazole in buffer A. Protein fractions were pooled and loaded onto a Superdex 200 10/300 GL column (GE Healthcare) equilibrated with 20 mM Tris–HCl pH 8.0 buffer. The desired eluates (identified by monitoring at 280 nm) were collected and concentrated with Amicon Ultra Centrifugal Filters (Millipore). Finally, the purified proteins were quickly frozen in liquid nitrogen and stored at −80 °C. Protein and heme concentrations were determined using the bicinchoninic acid assay with bovine serum albumin as a standard (Sunrise Absorbance Reader, TECAN) and the pyridine hemochromogen assay, respectively. Purified proteins were >90 % homogeneous, as confirmed by polyacrylamide gel electrophoresis in the presence of sodium dodecyl sulfate.

Optical absorption spectroscopy

Optical absorption spectral data were obtained under aerobic conditions at 20 °C using a Cary 60 UV–Vis spectrophotometer (Agilent Technologies, CA, USA) and a Hewlett-Packard 8453 UV–Vis spectrophotometer (Agilent Technologies, CA, USA) for *Af*GcHK and YddV-heme spectra, respectively, as previously described (Du et al. 2013; Yan et al. 2015). To ensure that the solution was maintained at an appropriate temperature (20 °C), the reaction mixture was incubated for 5 min prior to spectroscopic measurement. Aliquots of a 200 mM Na_2S stock solution in 50 mM Tris–HCl buffer (pH 8.0) were added to a protein solution (2–5 μM) in the cuvette to yield final Na_2S concentrations ranging from 200 μM to 5 mM. To determine whether a heme-Fe(II) complex was formed as the final product, we added a CO solution to the mixture, since CO binds to heme–Fe(II) complexes but not to heme-Fe(III) complexes. A stock solution saturated with CO (~1 mM), prepared by bubbling

CO gas into the buffer, was used to achieve a final CO concentration of ~10 μM in the protein solution. Spectra of full-length *Af*GcHK and YddV-heme proteins were obtained in 20 mM Tris–HCl (pH 8.0). We confirmed that adding these reagents caused essentially no change in the pH of the protein solutions under the experimental conditions used.

Kinetic analysis of *Af*GcHK autophosphorylation

The autophosphorylation activities of WT *Af*GcHK and its mutants were assayed using a variant of a previously published protocol (Fojtikova et al. 2015). To estimate the effect of Na_2S on the kinetic parameters of the autophosphorylation of WT *Af*GcHK, experiments were performed using reaction mixtures containing 10 μM *Af*GcHK, 10 mM Na_2S, 5-1000 μM ATP, 50 mM Tris–HCl (pH 8.0), 50 mM KCl, and 5 mM $MgCl_2$ in a total volume of 100 μL. Initially, the protein was preincubated with Na_2S for various periods of time at 20 °C. All of the other components of the reaction mixture aside from ATP were then immediately added, after which the autophosphorylation reaction was initiated by adding ATP. The reaction mixtures for determination of kinetic parameters were incubated at 20 °C for 30 s; the reaction during this period was assumed to proceed under initial velocity conditions because of the reaction's linearity over the first minute. Apparent kinetic constants were determined from a Lineweaver–Burk plot (Supplementary Fig. S1). At least three replicate experiments were performed for each set of reaction conditions, and the results obtained for each replicate performed under a given set of conditions were usually within 10 % of those for the other replicates. The errors given in Table 2 relate to three independent calculations of K_m^{ATP} and V_{max}^{ATP} that were performed by constructing three Lineweaver–Burk plots corresponding to each set of reaction conditions.

The experiments comparing the kinetic activity of *Af*GcHK WT and its mutants (Y45F, Y45L, Y45W, L68F, L68G, L68N and L68V) were conducted in reaction mixtures containing 10 μM *Af*GcHK, 10 mM Na_2S, 50 mM Tris–HCl (pH 8.0), 50 mM KCl, 5 mM $MgCl_2$ and 1 mM ATP. Initially, the protein was preincubated with Na_2S for various time periods at 20 °C, then the other components of the reaction mixture were added, and finally the reaction was initiated by adding 1 mM ATP. The reaction time of the autophosphorylation reaction was 30 s.

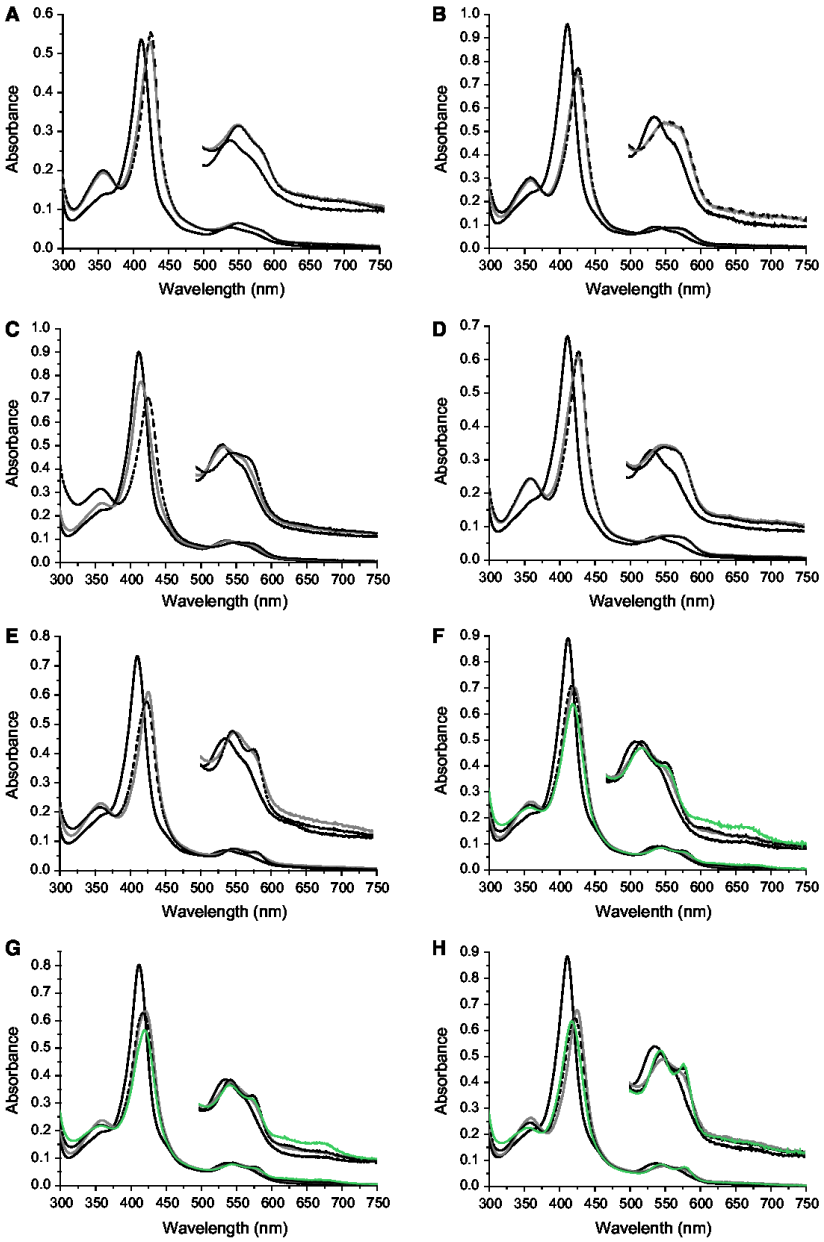
Fig. 3 Changes in the UV–visible spectra of the heme Fe(III) complexes of WT *Af*GcHK and its Y45 and L68 mutants (5 μM) upon treatment with Na_2S (5 mM). **a** Wild type; **b** Y45F; **c** Y45L; **d** Y45W; **e** L68F; **f** L68G; **g** L68N; **h** L68V. The spectra of the Fe(III) complexes before Na_2S treatment are shown in black, the spectra 75 s after Na_2S treatment are shown in grey, and the final spectra 75 min after Na_2S treatment are shown with dashed black lines. *Green lines* are used to show the spectra of the L68G, L68N, L68V mutants 120 min after Na_2S treatment; the new signals due to verdoheme formation are readily apparent. No peaks corresponding to verdoheme could be seen in the spectra of the WT protein or the other mutants. (Color figure online)

At the designated time, the *Af*GcHK autophosphorylation assay reaction was terminated by adding 100 μL aliquots of termination buffer [125 mM Tris–HCl (pH 6.8), 4 % SDS, 10 % 2-mercaptoethanol, 20 % glycerol, and 0.004 % bromophenol blue]. Samples of the quenched reaction mixtures were then loaded on a 10 % SDS–polyacrylamide gel containing 75 μM Phos-tag acrylamide and 0.2 mM $MnCl_2$. Each lane was loaded with a quantity of quenched reaction mixture containing 0.5 μg of *Af*GcHK. After electrophoresis, the phospo- and dephospho-proteins were visualized by staining with Coomassie Brilliant Blue R350 and the stained gels were imaged using a Scanjet G3010 (HP) scanner. The protein loadings were then quantified by analyzing the scanned images using the ImageJ software.

Mass spectrometry

Once the spectra of the *Af*GcHK solutions (5 μM) containing Na_2S (5 mM) had stopped changing, or, in the case of the incubations of the L68F, L68G, L68N, L68V mutants with Na_2S, after 0, 10, 60, 120 or 180 min, 0.5 μL of the solution was spotted onto a MALDI plate and overlaid with 0.5 μL of a saturated solution of α-cyano-4-hydroxycinnamic acid in methanol and water. Mass spectra were acquired with a MALDI-FT-ICR mass spectrometer equipped with a 15 T superconducting magnet (SolariX XR, Bruker Daltonics, Germany). Data were collected in positive ion mode over the mass range 350–1500 *m/z* at 4 M data points. The instrument was externally calibrated using singly-charged arginine clusters, resulting in sub-ppm accuracy. The spectra were processed and the theoretical isotopic envelopes of heme and verdoheme were modeled with DataAnalysis 4.2 (Bruker Daltonics).

Biometals (2016) 29:715–729



Results and discussion

UV–visible spectral changes of the full-length *Af*GcHK wild type (WT), Y45 and L68 mutants by adding Na_2S

The 412 nm Soret band of the WT 6-coordinate low-spin Fe(III)–OH complex was shifted to 424 nm upon treatment with Na_2S (Fig. 3a; Table 1). This band was stable over time, suggesting that the initially formed complex did not undergo further transformations. Based on previously published spectral data for hemoglobin, myoglobin, and *Ec*DOS, the peak at 424 nm was assigned to the Fe(III)–SH complex (Supplementary Table S1) (Nicoletti et al. 2010; Takahashi et al. 2012; Ramos-Alvarez et al. 2013). It is reasonable to expect that SH^- interacts with the heme iron in a similar way to CN^-, having a similar K_d in the range of hundreds of μM. Importantly, there was no evidence that the heme Fe(III)–SH complex is reduced to the Fe(II) complex followed by the formation of the Fe(II)–O_2 complex, in contrast to the reported behavior of *Ec*DOS under similar conditions (Takahashi et al. 2012; Du et al. 2013; Yan et al. 2015).

There are two key amino acids in the heme distal side of *Af*GcHK. The first, tyrosine 45, was assumed to be the O_2 binding site at the heme distal side. The O_2 dissociation rate constant of the WT protein, 0.10 s^{-1}, was increased substantially (to 8.0 s^{-1}) by the Y45L mutation. The second key residue, leucine 68, is located on the heme distal side of the protein and is assumed to help prevent the coordination of water to the iron center (Nakajima et al. 2012; Stranava et al. 2014; Lambry et al. 2016). The presence of water molecules in the heme distal side could lead to the decomposition of the heme molecule into verdoheme, as described for YddV (Stranava et al. 2014). Using these mutants enabled us to study how structural changes at the corresponding positions affected the structure and coordination of the heme complex and the catalytic activity of *Af*GcHK. Moreover, we tested the possibility that the key amino acids important for O_2 binding might influence the protein's interactions with SH^-.

The 6-coordinate low-spin Fe(III) complexes of the Y45F, Y45L and Y45W mutants in the resting state had Soret peaks at around 410–411 nm, similar to that of the WT protein (Fig. 3b–d). In keeping with the observations for the WT protein, the positions of these peaks shifted to 424–425 nm following treatment with Na_2S, indicating the formation of Fe(III)–SH complexes. No further spectral changes occurred, which is again consistent with the behavior of the WT.

Table 1 Positions of the Soret band and peaks in the visible region (nm) for 5 μM solutions of WT *Af*GcHK and its mutants at Y45 and L68 before and after treatment with Na_2S (5 mM)

Initial complex	Final complex	
6cLS Im-Fe(III)–OH	6cLS Im–Fe(III)–SH	Fe(II) Verdoheme
WT 412, 538	424, 551	
Y45F 410, 536	425, 552, 570	
Y45L 411, 536	425, 549, 570	
Y45W 411, 536	424, 551, 568	
L68F 410, 536	424, 546, 577	
L68G 411, 538	423, 545, 574	650
L68N 412, 538	420, 545, 576	650
L68V 411, 537	422, 545, 577	650

The proposed coordination structure of the heme complex in each case is indicated in the second row of the table: "6cLS Im-Fe(III)–OH" and "6cLS Im–Fe(III)–SH" stand for "six-coordinate low-spin Fe(III) complex coordinated by an imidazole ring of histidine and OH^-" and "six-coordinate low-spin Fe(III) complex coordinated by an imidazole ring of histidine and SH^-", respectively. The data presented here correspond to the spectra shown in Fig. 3

Although Y45 is assumed to be the residue that interacts directly with oxygen in the Fe(II)–O_2 complex, mutations at this position did not affect changes in the structure and coordination of the complex resulting from the replacement of the OH^- ligand in the 6-coordinate Fe(III)–OH complex with SH^-.

The L68F mutant exhibited similar spectral behavior to the WT protein and the Y45 mutants upon treatment with Na_2S (Fig. 3e). However, the spectra of the L68G, L68N and L68V mutants exhibited a characteristic broad peak at around 650 nm in addition to the Soret peak at around 420–423 nm (Fig. 3f–h, green lines). Broad peaks in the region between 610 and 680 nm are typical for modified hemes such as verdoheme or sulfheme, whose characteristic bands are located around 648–680 nm and 617 nm, respectively (Supplementary Table S1). The Soret peak of verdoheme is located around 352–400 nm, whereas those of sulfheme Fe(III) and Fe(II) complexes are located at 404 and 421 nm, respectively (Berzofsky et al. 1971; Andersson et al. 1984; Sakamoto et al. 2000). Because the solutions appeared to contain more than two species whose spectral bands overlapped, no useful information could be extracted from the position of the apparent Soret band in these cases. Therefore, the spectroscopic data were not sufficient to determine whether it was the verdoheme or the sulfheme that was formed as a result of Na_2S addition. To determine which species was formed, we performed mass spectrometry (MS) experiments on solutions of the L68 mutants after treatment with Na_2S.

Mass spectrometry analysis of WT *Af*GcHK and its mutants in the presence of Na_2S

We have shown previously that the heme modification (e.g. formation of verdoheme) can be also unambiguously monitored by mass spectrometry (Du et al. 2013; Yan et al. 2015). MALDI-MS spectra revealed time-dependent changes in the ratio between the heme (*m/z* 616.17674) and the verdoheme signal (*m/z* 619.16383) for solutions of the L68N (see Fig. 4), L68G, and L68V mutants after treatment with Na_2S. However, no verdoheme signal was observed for WT and Y45 mutants under the same conditions (Supplementary Fig. S3). These results confirm that the L68 mutants form verdoheme, as suggested by the UV–Vis

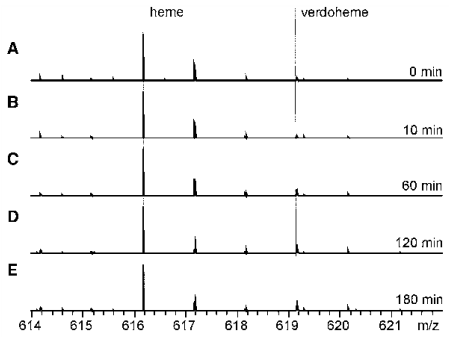


Fig. 4 MS spectra of the L68N mutant of *Af*GcHK at various time points after treatment with Na_2S, demonstrating the formation of the verdoheme complex. The figure shows the mass range covering heme (*m/z* 616.17674) and verdoheme (*m/z* 619.16383) species for the protein before Na_2S treatment (**a**) and after 10 min (**b**), 60 min (**c**), 120 min (**d**), and 180 min (**e**) of incubation with Na_2S. Position of the monoisotopic peaks for both heme species is marked with a *solid grey line*

spectroscopy data. The formation of verdoheme following Na_2S treatment has previously been observed for R97 *Ec*DOS mutants (Du et al. 2013). Moreover, L65 mutants of the globin-coupled oxygen sensor YddV form verdoheme even in the absence of Na_2S (Stranava et al. 2014), since the absence of the key leucine residue in the heme distal side allows the water molecules to enter the area. It has previously been shown that the presence of a water molecule in the heme distal side enables heme decomposition and verdoheme formation (Stranava et al. 2014).

Interestingly, there was no evidence of sulfheme formation in the case of WT *Af*GcHK or any of its mutants after treatment with Na_2S, in contrast to results reported for other hemoproteins with globin folds resembling the *Af*GcHK sensor domain. For example, myoglobin reportedly forms sulfmyoglobin after incubation with Na_2S (Berzofsky et al. 1971). It was recently shown that the formation of the sulfheme derivate requires a His residue in the heme distal side whose orientation permits the formation of an active ternary complex (Ríos-González et al. 2014). There is no such histidine residue on the heme distal side of *Af*GcHK (Fig. 2), which may explain its failure to form the sulfheme.

Effect of Na_2S on the autophosphorylation of WT *Af*GcHK and the Y45 and L68 mutants

The effect of Na_2S treatment on the autophosphorylation activity of the WT was investigated using the Phos-tag SDS PAGE method (Fojtikova et al. 2015). The initial velocities of the *Af*GcHK autophosphorylation reaction in the presence of Na_2S were very similar to those without Na_2S (Fig. 5). However, the K_m^{ATP} values of the enzyme with Na_2S were higher than those without, whereas its V_{max}^{ATP} values were not influenced by the presence of Na_2S (Table 2, Supplementary Fig. S1). Since the V_{max}^{ATP} values were not affected by Na_2S, the same was largely true for the k_{cat} values. However, the k_{cat}/K_m^{ATP} values in the presence of Na_2S were lower than those in its absence (Table 2, Supplementary Fig. S1). These kinetic parameters suggest that the changes in the coordination structure of *Af*GcHK following Na_2S treatment do not significantly affect its catalytic activity, but do appear to slightly reduce its affinity for ATP. It should be noted that the K_m^{ATP} value for the autophosphorylation of *Af*GcHK in the first few seconds after the addition of Na_2S is much higher than that without Na_2S or that observed in the long term after Na_2S addition (Table 2, Supplementary Fig. S1), when the initially formed Fe(III)–SH species may be partially converted back into the corresponding Fe(III) complex. It therefore seems that Na_2S treatment does not significantly affect the enzyme's catalytic activity but may slightly change its K_m^{ATP} value and catalytic effectiveness.

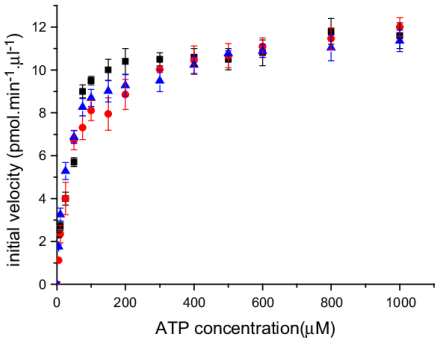


Fig. 5 Kinetic analysis of the autophosphorylation activity of WT *Af*GcHK before and after treatment with Na_2S (10 mM) based on Phos-tag experiments. The *black squares* show results obtained before Na_2S treatment, the *red circles* show the results after 75s' incubation with Na_2S, and the *blue triangles* show the results after 75 min' incubation with Na_2S. (Color figure online)

The catalytic effects observed for *Af*GcHK are very different to those seen for *Ec*DOS, whose catalytic activity was strongly increased by the addition of Na_2S and the subsequent changes in the coordination and structure of its heme complex (Yan et al. 2015). For *Ec*DOS, the binding of external axial ligands such as O_2 and CO to the Fe(II) complex, and SH^-, CN^-, or imidazole to the Fe(III) complex markedly enhanced catalytic activity. In contrast, the binding of SH^- to Fe(III) in the case of *Af*GcHK did not significantly affect its catalytic activity.

We also investigated the catalytic activity of Y45 and L68 mutants. The activities of the Y45F, Y45L, Y45W, L68F, L68G, L68N and L68V mutants after treatment with Na_2S were almost identical to that of the WT (Fig. 6), again suggesting that the changes in the structure and coordination of the heme complex following Na_2S treatment did not significantly affect the catalytic activity of *Af*GcHK.

Table 2 Effects of incubation with Na_2S on the kinetic parameters of the autophosphorylation reaction catalyzed by the functional domain of *Af*GcHK

Structure of the *Af*GcHK sensor domain's heme complex	K_m^{ATP} (µM)	V_{max}^{ATP} (pmol P-*Af*GcHK min^{-1} $µL^{-1}$)	k_{cat} (min^{-1})	k_{cat}/K_m^{ATP} (M^{-1} s^{-1})
Fe(III)–OH^- (WT, native form) (Fojtikova et al. 2015)	18.9 ± 2.3	10.8 ± 0.3	1.1	1000
Fe(III)–OH^- (no Na_2S) this work	19.0 ± 1.1	11.8 ± 0.6	1.2	1035
Fe(III)–SH^- (major) (75 s incubation with Na_2S) this work	47.1 ± 3.1	12.0 ± 1.2	1.2	425
Fe(III)–SH^- (minor) (75 min incubation with Na_2S) this work	25.7 ± 2.6	11.5 ± 0.7	1.2	746

Changes in the UV–visible spectra of the isolated heme-bound domain of another globin-coupled oxygen sensor (YddV-heme) upon treatment with Na_2S.

To compare the coordination chemistry of *Af*GcHK upon treatment with Na_2S to that of other GCSs, we examined the spectral behavior of the isolated heme-bound domain of another GCS–YddV, a heme-based oxygen sensor diguanylate cyclase (Tuckerman et al. 2009; Kitanishi et al. 2010). Both, the 5-coordinate high spin Fe(III) and the 6-coordinate low spin Fe(II)–O_2 complexes of YddV are associated with the highest activity of the diguanylate cyclase functional domain. On the other hand, the 5-coordinate high spin Fe(II) complex of YddV is inactive. It was suggested that YddV is constitutively active as the Fe(II)–O_2 [or Fe(III)] complex under aerobic conditions, but inactive as the Fe(II) complex under hypoxic or anaerobic conditions (Kitanishi et al. 2010). The heme complex of the over-expressed and purified WT YddV-heme has a 5-coordinate high-spin Fe(III) center, whose Soret band is located at 394 nm. Treatment with Na_2S rapidly shifted this band to 413 nm (Supplementary Fig. S2A), which was attributed to the formation of the heme Fe(II)–O_2 complex (Supplementary Table S2). No transient species such as Fe(III)–SH (425 nm) or Fe(II) (432 nm) complexes were observed before the formation of the Fe(II)–O_2 complex under the experimental conditions. The peak at 413 nm was gradually replaced by one at 432 nm, which was attributed to the Fe(II) complex. Surprisingly, it thus appears that the final Fe(II) complex does not feature O_2 as a ligand; it is possible that the O_2 ligand of the initially formed Fe(II)–O_2 complex is converted into the superoxide anion or H_2O_2. The behavior of the YddV-heme upon treatment with Na_2S is thus very different to that of both *Af*GcHK (for which only the Fe(III)–SH complex was observed; see Fig. 3 and Table 1) and *Ec*DOS (which underwent conversions from Fe(III)–OH → Fe(III)–SH → Fe(II) → Fe(II)–O_2) (Hirata et al. 2003; Takahashi et al. 2012; Du et al. 2013; Yan et al. 2015).

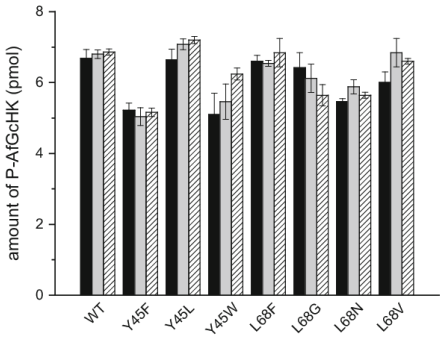


Fig. 6 Effects of mutations at Y45 and L68 on the autophosphorylation activity of *Af*GcHK (10 μM) after Na_2S treatment (10 mM). *Black bars* show the results obtained before Na_2S treatment; *grey bars* show results after 75 s' incubation with Na_2S; and the *dashed black bars* show results after 75 min' incubation with Na_2S

Fe(III) complexes of YddV-heme mutants at Y43 (which corresponds to Y45 in *Af*GcHK) have Soret peaks located around 391–393 nm, similar to the WT. The Soret peaks of the Fe(III) complexes of the Y43A and Y43F mutants shifted to 425–427 nm following the addition of Na_2S, suggesting that the heme Fe(III)–SH complex was formed (Supplementary Fig. S2B-D and Table S2). In addition, the intensities of the mutants' absorption bands decreased gradually, suggesting that the heme iron complex was slowly degraded. The Soret peak of the Fe(III) complex of the Y43W mutant shifted from 391 nm to 410–412 nm upon Na_2S treatment, suggesting that the heme Fe(II)–O_2 complex was formed, but again the intensities of the absorption bands gradually decreased, suggesting the degradation of the heme iron complex (Supplementary Fig. S2D).

Fe(III) complexes of L65 mutants of YddV-heme (which are analogous to L68 mutants of *Af*GcHK) had Soret peaks at around 403–405 nm, suggesting that they have low-spin Fe(III) heme complexes due to the incorporation of water into the heme's surroundings (Nakajima et al. 2012). The only change in the UV–Vis spectrum of L65G upon treatment with Na_2S was a decrease in the intensity of this peak, suggesting that the heme iron complex was simply degraded under these conditions (Supplementary Fig. S2E and Table S2). Conversely, the Soret bands of the L65M, L65Q and L65T mutants shifted to 421–425 nm after the addition of Na_2S, suggesting the formation of Fe(III)–SH complexes (Supplementary Fig. S2F–H and Table S2). However, the spectral intensities of these bands also decreased over time, indicating heme degradation. In the case of L65Q, this degradation

process was accompanied by the appearance of a transient peak at 413 nm, which was attributed to the formation of the Fe(II)–O_2 complex as an intermediate in heme degradation.

Overall, these results indicate that treating the WT YddV-heme with Na_2S caused the formation of Fe(II)–O_2 and Fe(II) complexes whereas most of the L65 and Y43 mutants were simply degraded under these conditions.

Physiological relevance

The concentrations of Na_2S used in this study were much higher than those of H_2S and HS^- that are used for signaling in biological systems. While this could potentially reduce the physiological relevance of our results, it enabled us to characterize the interactions of hydrogen sulfide with heme-based oxygen sensors. The observed differences between *Af*GcHK, YddV and *Ec*DOS in terms of their interactions with hydrogen sulfide improve our general understanding of the functions of these sensors. Moreover, our results suggest that all of these oxygen sensors could be more precisely regulated by a range of ligands, including hydrogen sulfide. While hydrogen sulfide enhances the activity of *Ec*DOS, it has no such effect on *Af*GcHK.

Bacteria in the mouth and gut generate H_2S and related sulfur compounds, as do intrinsic H_2S-generating enzymes such as cystathionine β-synthase and cystathionine γ-lyase (Washio et al. 2005; Rey et al. 2013). The activity of these enzymes could produce relatively high transient micro-localized concentrations of sulfur compounds, in the range of hundreds of μM. These sulfur derivatives could then interact with heme proteins in the mitochondria and impair important functions (Bostelaar et al. 2016). Additionally, sulfide is oxidized by chemolithotropic sulfur bacteria and dissimitory sulfate is reduced by sulfate-reducing bacteria (Muyzer and Stams 2008). These sulfur derivatives are found in hydrothermal vents, oil deposits, and hot springs, where concentrations of H_2S and related sulfur-derivatives could rise to the mM range. Although no heme-based H_2S sensors have yet been identified, it is possible that H_2S and its derivatives may interact with heme proteins when present at concentrations in the μM-mM range, inducing novel functions that could enable cells to survive under stress conditions.

Note that the Fe(III)-bound form of *Af*GcHK was obtained by incubating the overexpressed protein with hemin. The Fe(III)–SH complex was formed by adding Na_2S, but this complex was not converted into the Fe(II) complex even in the presence of excess Na_2S. However, it is speculated that the Fe(II)-bound form or the Fe(II)–O_2 complex may be physiologically relevant in that their activity may be regulated by the intracellular O_2 concentration. Our results suggest that *Af*GcHK might not be regulated by H_2S, whereas the Fe(III) complex of *Ec*DOS is reduced to the Fe(II) complex upon treatment with Na_2S. As such, Na_2S appears to modify the functional activity of this heme-based oxygen sensor. The structural differences between *Ec*DOS (which adopts a heme-bound PAS fold) and *Af*GcHK (which adopts a heme-bound truncated globin-fold) may account for the different ways their catalytic activity is regulated by H_2S.

Summary

1. Treatment with Na_2S caused the 6-coordinate Fe(III)–OH heme complex of the WT globin-coupled oxygen sensor *Af*GcHK and its mutants at Y45 to be converted into 6-coordinate Fe(III)–SH complexes (Fig. 7). In contrast to the results obtained for the heme-based oxygen sensor phosphodiesterase *Ec*DOS, these complexes did not undergo any further structural or redox changes.
2. L68 mutants of *Af*GcHK, in which water is incorporated into the heme environment, formed verdoheme iron complexes in addition to the corresponding Fe(III)–SH complexes upon treatment with Na_2S. It was thus suggested that a water molecule contributed to the heme modification reaction in these cases.
3. The autophosphorylation activity of *Af*GcHK was not significantly influenced by the addition of Na_2S. The formation of the Fe(III)–SH complex does not appreciably change the enzyme's apparent V_{max}^{ATP} value but does slightly increase its apparent K_m^{ATP}. This result contrasts strongly with the previously reported finding that the formation of the Fe(III)–SH complex of *Ec*DOS greatly enhances its catalytic activity.

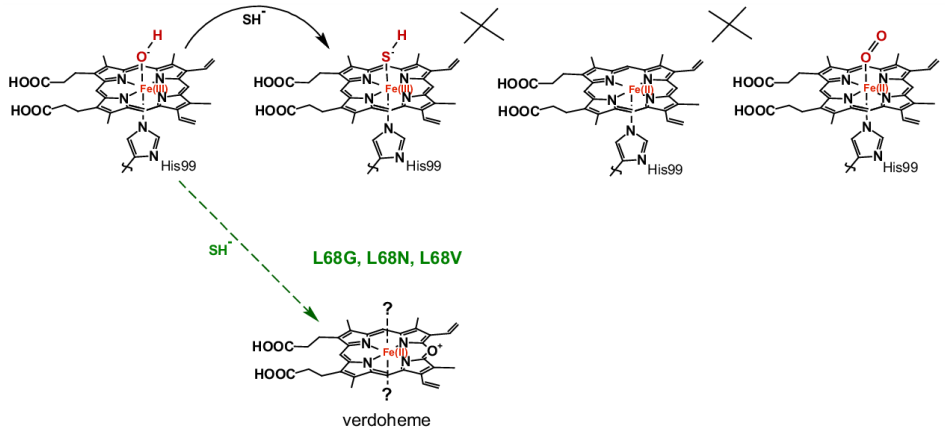


Fig. 7 Proposed changes in the coordination and structure of the heme complexes of WT *Af*GcHK and its Y45 and L68 mutants upon treatment with Na_2S. Note that the 6-coordinate low spin complexes with external axial ligands, such as the Fe(III)–SH complex, are the active forms. The L68 mutants (L68G, L68N and L68V) formed a small proportion of verdoheme upon prolonged incubation with Na_2S

4. The isolated WT heme domain of another GCS, YddV, formed distinct Fe(II)–O_2 and Fe(II) complexes upon treatment with Na_2S. However, Y43 and L65 mutants of this protein underwent heme degradation under these conditions. The changes in heme structure and coordination resulting from Na_2S treatment in this GCS were thus very different to those observed for *Af*GcHK.

Acknowledgments This work was supported in part by Charles University in Prague (UNCE 204025/2012), the Grant Agency of Charles University in Prague (362115) and the Grant Agency of the Czech Republic (Grant 15-19883S). The mass spectrometry facility used in this work was supported by the EU project CZ.1.05/1.1.00/02.0109. We are grateful to Dr. Kenichi Kitanishi for valuable discussion during the early stages of this project.

References

Andersson LA, Loehr TM, Lim AR, Mauk AG (1984) Sulfmyoglobin. Resonance Raman spectroscopic evidence for an iron-chlorin prosthetic group. J Biol Chem 259:15340–15349

Banerjee R (2011) Hydrogen sulfide: redox metabolism and signaling. Antioxid Redox Signal 15:339–341. doi:10.1089/ars.2011.3912

Berzofsky JA, Peisach J, Blumberg WE (1971) Sulfheme proteins. I. Optical and magnetic properties of sulfmyoglobin and its derivatives. J Biol Chem 246:3367–3377

Bostelaar T, Vitvitsky V, Kumutima J, Lewis BE, Yadav PK, Brunold TC, Filipovic M, Lehnert N, Stemmler TL, Banerjee R (2016) Hydrogen sulfide oxidation by myoglobin. J Am Chem Soc. doi:10.1021/jacs.6b03456

Du Y, Liu G, Yan Y, Huang D, Luo W, Martinkova M, Man P, Shimizu T (2013) Conversion of a heme-based oxygen sensor to a heme oxygenase by hydrogen sulfide: effects of mutations in the heme distal side of a heme-based oxygen sensor phosphodiesterase (Ec DOS). Biometals 26:839–852. doi:10.1007/s10534-013-9640-4

Fojtikova V, Stranava M, Vos MH, Liebl U, Hranicek J, Kitanishi K, Shimizu T, Martinkova M (2015) Kinetic analysis of a globin-coupled histidine kinase, AfGcHK: effects of the heme iron complex, response regulator, and metal cations on autophosphorylation activity. Biochemistry 54:5017–5029. doi:10.1021/acs.biochem.5b00517

Germani F, Moens L, Dewilde S (2013) Haem-based sensors: a still growing old superfamily. Adv Microb Physiol 63:1–47. doi:10.1016/B978-0-12-407693-8.00001-7

Gilles-Gonzalez M-A, Gonzalez G (2005) Heme-based sensors: defining characteristics, recent developments, and regulatory hypotheses. J Inorg Biochem 99:1–22. doi:10.1016/j.jinorgbio.2004.11.006

Girvan HM, Munro AW (2013) Heme sensor proteins. J Biol Chem 288:13194–13203. doi:10.1074/jbc.R112.422642

Green J, Crack JC, Thomson AJ, LeBrun NE (2009) Bacterial sensors of oxygen. Curr Opin Microbiol 12:145–151. doi:10.1016/j.mib.2009.01.008

Hirata S, Matsui T, Sasakura Y, Sugiyama S, Yoshimura T, Sagami I, Shimizu T (2003) Characterization of Met95

mutants of a heme-regulated phosphodiesterase from *Escherichia coli*. Optical absorption, magnetic circular dichroism, circular dichroism, and redox potentials. Eur J Biochem 270:4771–4779. doi:10.1046/j.1432-1033.2003.03879.x

Igarashi J, Kitanishi K, Shimizu T (2011) Emerging role of heme as a signal and the gas-sensing site: heme-sensing and gas-sensing. In: Kadish KM, Smith KM, Guilard R (eds) Handbook of porphyrin science, vol 15. World Scientific Publishing, Hackensack (**Chapter 73**)

Kimura H (2015) Signaling molecules: hydrogen sulfide and polysulfide. Antioxid Redox Signal 22:362–376. doi:10.1089/ars.2014.5869

Kimura Y, Toyofuku Y, Koike S, Shibuya N, Nagahara N, Lefer D, Ogasawara Y, Kimura H (2015) Identification of H2S3 and H2S produced by 3-mercaptopyruvate sulfurtransferase in the brain. Sci Rep 5:14774. doi:10.1038/srep14774

Kitanishi K, Kobayashi K, Kawamura Y, Ishigami I, Ogura T, Nakajima K, Igarashi J, Tanaka A, Shimizu T (2010) Important roles of Tyr43 at the putative heme distal side in the oxygen recognition and stability of the Fe(II)–O_2 complex of YddV, a globin-coupled heme-based oxygen sensor diguanylate cyclase. Biochemistry 49:10381–10393. doi:10.1021/bi100733q

Kitanishi K, Kobayashi K, Uchida T, Ishimori K, Igarashi J, Shimizu T (2011) Identification and functional and spectral characterization of a globin-coupled histidine kinase from *Anaeromyxobacter* sp. Fw109-5. J Biol Chem 286:35522–35534. doi:10.1074/jbc.M111.274811

Lambry J-C, Stranava M, Lobato L, Martinkova M, Shimizu T, Liebl U, Vos MH (2016) Ultrafast spectroscopy evidence for picosecond ligand exchange at the binding site of a heme protein: heme-based sensor YddV. J Phys Chem Lett 7:69–74. doi:10.1021/acs.jpclett.5b02517

Martínková M, Kitanishi K, Shimizu T (2013) Heme-based globin-coupled oxygen sensors: linking oxygen binding to functional regulation of diguanylate cyclase, histidine kinase, and methyl-accepting chemotaxis. J Biol Chem 288:27702–27711. doi:10.1074/jbc.R113.473249

Mishanina TV, Libiad M, Banerjee R (2015) Biogenesis of reactive sulfur species for signaling by hydrogen sulfide oxidation pathways. Nat Chem Biol 11:457–464. doi:10.1038/nchembio.1834

Muyzer G, Stams AJ (2008) The ecology and biotechnology of sulphate-reducing bacteria. Nat Rev Microbiol 6:441–454. doi:10.1038/nrmicro1892

Nakajima K, Kitanishi K, Kobayashi K, Kobayashi N, Igarashi J, Shimizu T (2012) Leu65 in the heme distal side is critical for the stability of the Fe(II)–O_2 complex of YddV, a globin-coupled oxygen sensor diguanylate cyclase. J Inorg Biochem 108:163–170. doi:10.1016/j.jinorgbio.2011.09.019

Nicoletti FP, Comandini A, Bonamore A, Boechi L, Boubeta FM, Feis A, Smulevich G, Boffi A (2010) Sulfide binding properties of truncated hemoglobins. Biochemistry 49:2269–2278. doi:10.1021/bi901671d

Paul BD, Snyder SH (2015) H2S: a novel gasotransmitter that signals by sulfhydration. Trends Biochem Sci 40:687–700. doi:10.1016/j.tibs.2015.08.007

Pietri R, Román-Morales E, López-Garriga J (2011) Hydrogen sulfide and hemeproteins: knowledge and mysteries. Antioxid Redox Signal 15:393–404. doi:10.1089/ars.2010.3698

Poulos TL (2014) Heme enzyme structure and function. Chem Rev 114:3919–3962. doi:10.1021/cr400415k

Ramos-Alvarez C, Yoo B-K, Pietri R, Lamarre I, Martin J-L, Lopez-Garriga J, Negrerie M (2013) Reactivity and dynamics of H_2S, NO, and O_2 interacting with hemoglobins from Lucina pectinata. Biochemistry 52:7007–7021. doi:10.1021/bi400745a

Rey FE, Gonzalez MD, Cheng J, Wu M, Ahern PP, Gordon JI (2013) Metabolic niche of a prominent sulfate-reducing human gut bacterium. Proc Natl Acad Sci USA 110:13582–13587. doi:10.1073/pnas.1312524110

Ríos-González BB, Román-Morales EM, Pietri R, López-Garriga J (2014) Hydrogen sulfide activation in hemeproteins: the sulfheme scenario. J Inorg Biochem 133:78–86. doi:10.1016/j.jinorgbio.2014.01.013

Sakamoto H, Omata Y, Adachi Y, Palmer G, Noguchi M (2000) Separation and identification of the regioisomers of verdoheme by reversed-phase ion-pair high-performance liquid chromatography, and characterization of their complexes with heme oxygenase. J Inorg Biochem 82:113–121

Shimizu T (2013) Revisit of the interactions between hydrogen sulfide and heme proteins. Curr Chem Biol 7:207–212

Shimizu T, Huang D, Yan F, Stranava M, Bartosova M, Fojtíková V, Martínková M (2015) Gaseous O_2, NO, and CO in signal transduction: structure and function relationships of heme-based gas sensors and heme-redox sensors. Chem Rev 115:6491–6533. doi:10.1021/acs.chemrev.5b00018

Stranava M, Martínková M, Stiborová M, Man P, Kitanishi K, Muchová L, Vítek L, Martínek V, Shimizu T (2014) Introduction of water into the heme distal side by Leu65 mutations of an oxygen sensor, YddV, generates verdoheme and carbon monoxide, exerting the heme oxygenase reaction. J Inorg Biochem 140:29–38. doi:10.1016/j.jinorgbio.2014.06.010

Takahashi H, Sekimoto M, Tanaka M, Tanaka A, Igarashi J, Shimizu T (2012) Hydrogen sulfide stimulates the catalytic activity of a heme-regulated phosphodiesterase from *Escherichia coli* (Ec DOS). J Inorg Biochem 109:66–71. doi:10.1016/j.jinorgbio.2012.01.001

Tarnawski M, Barends TRM, Schlichting I (2015) Structural analysis of an oxygen-regulated diguanylate cyclase. Acta Crystallogr D Biol Crystallogr 71:2158–2177. doi:10.1107/S139900471501545X

Tuckerman JR, Gonzalez G, Sousa EHS, Wan X, Saito JA, Alam M, Gilles-Gonzalez M-A (2009) An oxygen-sensing diguanylate cyclase and phosphodiesterase couple for c-di-GMP control. Biochemistry 48:9764–9774. doi:10.1021/bi901409g

Uchida T, Kitagawa T (2005) Mechanism for transduction of the ligand-binding signal in heme-based gas sensory proteins revealed by resonance Raman spectroscopy. Acc Chem Res 38:662–670. doi:10.1021/ar030267d

Voet D, Voet J (2011) Hemoglobin: Protein function in microcosm. Biochemistry, 4th edn. Wiley, New York, pp 323–358

Washio J, Sato T, Koseki T, Takahashi N (2005) Hydrogen sulfide-producing bacteria in tongue biofilm and their relationship with oral malodour. J Med Microbiol 54:889–895. doi:10.1099/jmm.0.46118-0

Yan F, Fojtikova V, Man P, Stranava M, Martínková M, Du Y, Huang D, Shimizu T (2015) Catalytic enhancement of the heme-based oxygen-sensing phosphodiesterase EcDOS by hydrogen sulfide is caused by changes in heme coordination structure. Biometals 28:637–652. doi:10.1007/s10534-015-9847-7

Zhang W, Phillips GN (2003) Structure of the oxygen sensor in Bacillus subtilis: signal transduction of chemotaxis by control of symmetry. Structure 11:1097–1110. doi:10.1016/S0969-2126(03)00169-2

5. Publikace BLOKU III

5.1 Structural characterization of the heme-based oxygen sensor, *Af*GcHK, its interactions with the cognate response regulator, and their combined mechanism of action in a bacterial two-component signaling system

Stranava M., Martínek V., Man P., **Fojtikova V**., Kavan D., Vaněk O., Shimizu T., Martinkova M. *Proteins* (2016) 84, 1375 (**IF_{2016} 2,3**)

Podíl předkladatelky na této práci: 15 % (exprese a purifikace proteinů, experimenty týkající se stanovení fosforylační aktivity RR proteinu)

Potvrzeno korespondujícím autorem, doc. RNDr. Markéta Martínková, Ph.D.

PROTEINS
STRUCTURE ■ FUNCTION ■ BIOINFORMATICS

Structural characterization of the heme-based oxygen sensor, *Af*GcHK, its interactions with the cognate response regulator, and their combined mechanism of action in a bacterial two-component signaling system

Martin Stranava,[1] Václav Martínek,[1,2] Petr Man,[1,3] Veronika Fojtikova,[1] Daniel Kavan,[1,3] Ondřej Vaněk,[1] Toru Shimizu,[1] and Marketa Martinkova[1]*

[1] Department of Biochemistry, Charles University in Prague, Hlavova (Albertov) 2030-8, Prague 2, Czech Republic

[2] Department of Chemical Education, Faculty of Science, Charles University in Prague, Hlavova (Albertov) 2030-8, Prague 2, Czech Republic

[3] Laboratory of Structure Biology and Cell Signalling, BioCeV - Institute of Microbiology, Czech Academy of Sciences, V.V.I, Prumyslova 595, Vestec, Czech Republic

ABSTRACT

The oxygen sensor histidine kinase *Af*GcHK from the bacterium *Anaeromyxobacter* sp. Fw 109-5 forms a two-component signal transduction system together with its cognate response regulator (RR). The binding of oxygen to the heme iron of its N-terminal sensor domain causes the C-terminal kinase domain of *Af*GcHK to autophosphorylate at His183 and then transfer this phosphate to Asp52 or Asp169 of the RR protein. Analytical ultracentrifugation revealed that *Af*GcHK and the RR protein form a complex with 2:1 stoichiometry. Hydrogen-deuterium exchange coupled to mass spectrometry (HDX-MS) suggested that the most flexible part of the whole *Af*GcHK protein is a loop that connects the two domains and that the heme distal side of *Af*GcHK, which is responsible for oxygen binding, is the only flexible part of the sensor domain. HDX-MS studies on the *Af*GcHK:RR complex also showed that the N-side of the H9 helix in the dimerization domain of the *Af*GcHK kinase domain interacts with the helix H1 and the β-strand B2 area of the RR protein's Rec1 domain, and that the C-side of the H8 helix region in the dimerization domain of the *Af*GcHK protein interacts mostly with the helix H5 and β-strand B6 area of the Rec1 domain. The Rec1 domain containing the phosphorylable Asp52 of the RR protein probably has a significantly higher affinity for *Af*GcHK than the Rec2 domain. We speculate that phosphorylation at Asp52 changes the overall structure of RR such that the Rec2 area containing the second phosphorylation site (Asp169) can also interact with *Af*GcHK.

Proteins 2016; 00:000–000.
© 2016 Wiley Periodicals, Inc.

Key words: heme-based oxygen sensor; histidine kinase; two-component signal transduction system; protein–protein interaction; hydrogen-deuterium exchange; analytical ultracentrifugation; homology modeling; protein–protein docking.

Additional Supporting Information may be found in the online version of this article.

Abbreviations: AA, amino acid; Aer-sal, a response regulator from *Aeromonas salmonicida*; *Af*GcHK, a globin-coupled histidine kinase from *Anaeromyxobacter* sp. Fw109-5; *Ec* DOS, *Escherichia coli* Direct Oxygen Sensor or a heme-regulated phosphodiesterase from *Escherichia coli* or *Ec* DosP; FixL, an oxygen-sensor histidine kinase with the heme-bound PAS domain that regulates nitrogen fixation in *Rhizobium meliloti* or *Bradyrhizobium japonicum*; GsGCS, a globin coupled sensor from *Geobacter sulfurreducens*; HDX, hydrogen-deuterium exchange; HK853, the sensor histidine kinase from *Thermotoga maritima*; MS, mass spectrometry; RR, response regulator; YddV, a heme-bound diguanylate cyclase from *Escherichia coli* or *Ec* DosC; WT, wild type

Grant sponsor: Charles University in Prague; Grant number: UNCE 204025/2012; Grant sponsor: Grant Agency of the Czech Republic; Grant number: 15-19883S; Grant sponsor: Grant Agency of Charles University in Prague; Grant numbers: 756214 and 362115; Grant sponsor: EU project; Grant number: CZ.1.05/1.1.00/02.0109; Grant sponsor: Czech Infrastructure for Integrative Structural Biology; Grant number: LM2015043.

*Correspondence to: Marketa Martinkova, Department of Biochemistry, Faculty of Science, Charles University in Prague, Hlavova (Albertov) 2030-8, Prague 2, Czech Republic. E-mail: marketa.martinkova@natur.cuni.cz

Received 11 March 2016; Revised 19 May 2016; Accepted 30 May 2016
Published online 7 June 2016 in Wiley Online Library (wileyonlinelibrary.com). DOI: 10.1002/prot.25083

© 2016 Wiley Periodicals, Inc.

INTRODUCTION

The globin-coupled histidine kinase *Af*GcHK originates from the bacterium *Anaeromyxobacter* sp. Fw 109–5 and belongs to a group of heme-based oxygen sensor proteins that are involved in bacterial two-component signal transduction systems, where they act in conjunction with cognate response regulators (RR proteins).[1] *Af*GcHK has two domains: an N-terminal sensor domain responsible for heme-based oxygen sensing and a C-terminal kinase domain.[1,2] The binding of an oxygen molecule to the heme iron complex in the sensor domain of *Af*GcHK represents the first signal and stimulates the functional domain, which then autophosphorylates at a conserved His residue (Supporting Information Fig. S1). This phosphate group is subsequently transferred to conserved Asp residues in the cognate RR, activating the output signal of the two-component system.[1] The RR protein has two tandem receiver domains (Rec1 and Rec2), each containing one conserved Asp residue (Supporting Information Fig. S1); other known RRs such as CheY have only a single receiver domain.[3–5] Once activated by phosphorylation, the RR proteins can affect the localization of other proteins, regulate transcription of important genes, function as phosphate sinks, and control chemotactic or chemokinetic responses.[3–5] Two-component systems with RR proteins similar to that found in *Anaeromyxobacter* sp. Fw 109–5 have been identified in *Anaeromyxobacter dehalogenans* and *Myxococcus xanthus*.[6,7] While *Anaeromyxobacter* can grow under both aerobic and anaerobic conditions, *Myxococcus* is an obligate aerobe and cannot survive without oxygen. Two-component systems may regulate physiological functions that require particular oxygen concentrations in these soil slime bacteria.

As two-component signal systems are involved in various important physiological functions in bacteria and lower eukaryotes,[8] their molecular mechanisms of action have been extensively analyzed in the last several years.[9–11] In particular, the interactions between the histidine kinases and the corresponding RR proteins are essential for our understanding of these systems. This work thus aims to shed new light on the *Af*GcHK and its cognate RR protein–protein and domain–domain interactions. In addition to its potential to provide fundamental scientific insights, this project has practical relevance because histidine kinases with heme-containing sensor domains (i.e., heme-based oxygen sensors) represent potential therapeutic targets for preventing and treating bacterial infections.[12–15] However, to control the functions of these proteins, we must first understand their functioning at the molecular level.

Many important functions of heme-responsive sensor proteins are regulated by the association/dissociation of the heme iron complex with or from the protein.[16–19] Conversely, in heme-based oxygen sensors such as FixL or *Ec*DOS, it is the association/dissociation of oxygen that regulates function.[20] It has been suggested that several heme-responsive sensor proteins have flexible structures, in contrast to well-known prototypical hemoproteins such as myoglobin, cytochrome *c*, and P450.[21–23] For example, heme-responsive sensor proteins have been observed to undergo global structural changes induced by the association or dissociation of the heme iron complex.[16–18] Heme-based oxygen sensor proteins differ from heme-responsive sensor proteins in that their catalytic functionality is localized in the C-terminal domain and is regulated by the binding of oxygen to the heme of the N-terminal sensing domain via intramolecular signal transduction.[1,2,20] However, they resemble heme-responsive sensor proteins in that the binding of oxygen to the heme is predicted to induce profound structural and conformational changes in the protein as a whole.[24] It thus seems that all heme sensor proteins, including both heme-responsive sensors and heme-based oxygen sensors, undergo large structural changes that are intimately linked to their functionality and mechanisms of action. The high flexibility of these systems means that they cannot be meaningfully studied using many conventional biochemical techniques.

One well-established method for studying the structural dynamics of flexible proteins under various conditions is hydrogen-deuterium exchange (HDX) coupled to mass spectrometry (MS). Among other things, the combination of HDX and MS has been used to distinguish between structured (α-helices and β-sheets) and unstructured parts of proteins, and to monitor the structural changes induced by protein–protein contacts.[25] A key advantage of HDX-MS is that it can be performed with samples dissolved in physiological buffers at physiological temperatures and pH values. Moreover, it yields results that can provide information on profound structural and conformational changes in the studied protein molecule under diverse conditions. It has been used for this purpose in a range of contexts. For example, HDX-MS was used to study conformational changes associated with osmosensing in the cytoplasmic domain of the histidine kinase EnvZ, which acts in conjunction with its cognate RR (OmpR) to regulate the expression of outer membrane proteins known as porins in response to osmotic stress.[26] HDX-MS has also been used in conjunction with a nuclear magnetic resonance approach to study the solution-phase conformational dynamics of the histidine-containing phosphotransfer signaling domain in the *Escherichia coli* sensor kinase ArcB, which transfers a phosphoryl group to a partner RR under anaerobic conditions.[27]

The experimental structural characterization of weak/transient protein–protein complexes is often challenging and requires the combined used of multiple analytical tools. One tool that is widely used to predict the structures of protein–protein complexes in such investigations is molecular docking.[28–30] Although docking methods

can be powerful, they frequently predict multiple binding positions when applied to weak complexes, making it necessary to use additional complementary methods to determine which of the predicted arrangements is most stable in reality.[31] Here, we describe the use of HDX-MS for this purpose.

The results presented herein help to address some unsettled questions regarding the molecular mechanism of action of *Af*GcHK and its interactions with its RR protein. HDX-MS was used in conjunction with analytical ultracentrifugation, protein homology modeling, and protein–protein docking methods to obtain important structural information on the *Af*GcHK:RR complex and to clarify its molecular mechanism of action.

MATERIALS AND METHODS

Materials

Ampicillin was obtained from P-lab (Prague, Czech Republic). Isopropyl β-D-thiogalactopyranoside and hemin were obtained from Sigma-Aldrich (St. Louis, MO). All other chemicals used were of the highest purity grade available from commercial sources and used without further purification. Deionized water was purified using a Milli-Q Plus system (EMD Millipore, Billerica, MA).

Overexpression and purification of the proteins

Cloning, overexpression in *E. coli* and purification of *Af*GcHK was performed as previously described.[1,32] Briefly, His-tagged *Af*GcHK was expressed in BL21(DE3) (Novagen, Madison, WI) harboring the pET 21c (+) plasmid. Cell lysates containing His-tagged *Af*GcHK were isolated by affinity chromatography on a TALON® Metal Affinity Resin column (Clontech Laboratories, Mountain View, CA) followed by size exclusion chromatography on a Superdex 200 GL 10/300 column (GE Healthcare, Amersham, UK). Protein and heme concentrations were determined using the BCA assay (Sunrise Absorbance Reader, TECAN, Männedorf, Switzerland) and the pyridine hemochromogen assay, respectively.[33] Purified proteins were >90% homogenous, as confirmed by SDS-PAGE.

Cloning, overexpression in *E. coli* and purification of RR was performed as described previously[1] with some modifications. His-tagged RR was expressed in BL21(DE3) (Novagen) harboring the pET 21c (+) plasmid and then purified as described previously with minor modifications. Cell lysates containing His-tagged RR were isolated by affinity chromatography on a TALON® Metal Affinity Resin column (Clontech Laboratories, Mountain View, CA) followed by size exclusion chromatography on a Superdex 200 GL 10/300 column (GE Healthcare). Purified RR was >97% homogeneous, as determined by SDS-PAGE, followed by staining with Coomassie Brilliant Blue. Protein concentrations were determined using the BCA assay (Sunrise Absorbance Reader, TECAN).

Analytical ultracentrifugation

Sedimentation velocity experiments were performed using a ProteomLab XL-I (Beckman Coulter, Brea, CA) analytical ultracentrifuge at loading concentrations of 6–15 μ*M* *Af*GcHK and 2–120 μ*M* RR protein, 20°C and a rotor speed of 36,000 rpm. Samples were dialyzed against a buffer containing 20 m*M* Tris-HCl (pH 8.0), 150 m*M* NaCl, and 5 m*M* $MgCl_2$ prior to analysis. All data were collected using Interference optics (used for weight-average sedimentation coefficient calculations) and absorbance optics at 411 nm (selective for hemoproteins). Examples of fitted sedimentation traces are shown in Supporting Information Figure S2. Data analysis was performed with the SEDFIT, SEDPHAT, and Gussi packages.[34–36] Sedimentation velocity data were analyzed using a continuous sedimentation coefficient distribution model, c(s). The resulting apparent sedimentation coefficients were utilized to compute sedimentation coefficients in water at 20°C ($s_{20,w}$). To determine apparent equilibrium dissociation constants (K_d values) for individual 2:1 and 2:2 *Af*GcHK:RR complexes, the weight-average sedimentation coefficients obtained by peak integration in the Gussi software package were analyzed by isotherm fitting in SEDPHAT using the A + B+B ↔ AB + B ↔ ABB model; the *Af*GcHK dimer (A) was presumed to have two symmetric and noncooperative binding sites for the RR protein (B).

HDX-MS analysis of AfGcHK, RR, and the AfGcHK:RR complex

HDX-MS experiments using samples of full length wild type *Af*GcHK (90 μ*M*), the RR protein (90 μ*M*), *Af*GcHK (90 μ*M*) + RR protein (90 μ*M*), *Af*GcHK (90 μ*M*) + RR protein (270 μ*M*), or *Af*GcHK (270 μ*M*) + RR protein (90 μ*M*) were initiated by 10-fold dilution in a deuterated buffer containing 20 m*M* Tris-HCl (pD 7.6), 150 m*M* NaCl at 20°C. The molar ratio of *Af*GcHK to RR was 1:1, 1:3, or 3:1. Aliquots (25 μL) were taken after 0.5 min, 5 min, 20 min, 60 min, and 180 min of exchange, the exchange reaction in the aliquots was immediately quenched by adding 25 μL of 1 *M* glycine (pH 2.3), and they were rapidly frozen in liquid nitrogen. HPLC-MS analysis of deuterated samples was performed using a HPLC (1200 Agilent Technologies, Waldbronn, Germany) connected to an ESI-FT-ICR MS (15T SolarixXR, Bruker Daltonics, Billerica, MA). The analysis was initiated by rapidly thawing the sample, followed by digestion on a pepsin or rhizopuspepsin column (66 μL bed volume, flow rate 100 μL min^{-1}). The

resulting peptides were desalted online using a Peptide MicroTrap (MichromBioresources, Auburn, CA) and separated on a C18 reversed phase column (0.5 × 50 mm, Jupiter, Phenomenex, Torrance, CA) using a linear gradient of 10–25% solvent B in 8 mins, where solvent A was 2% acetonitrile with 0.4% formic acid in water and solvent B was 95% acetonitrile/5% water with 0.4% formic acid. The injector and switching valve, pepsin column, peptide trap, and analytical column were placed in an ice box to minimize back-exchange. Peptide identification (mapping, HPLC-MS/MS) was done using the same system as described above, and MASCOT was used to compare the obtained MS/MS spectra to a database containing sequences for *Af*GcHK or RR. Deuterated data were processed using an in-house program called DeutEx (unpublished). The deuterium content of each peptide was reported as a percentage of the maximum achievable deuteration based on the number of exchangeable amide hydrogens in each peptide.[37] Fully deuterated controls were prepared by incubating the proteins at 37°C for 48 h in deuterated buffer containing 8 *M* urea. Correction for back-exchange was calculated as described previously.[38]

Homology modeling of the RR protein and AfGcHK's N-terminal (globin) and C-terminal (kinase) domains

We used SWISS-MODEL server[39] to construct homologous models of the globin and kinase domains of *Af*GcHK and RR from *Anaeromyxobacter* sp. Fw 109-5. The homology model of *Af*GcHK's globin domain was based on the structure of the *Gs*GCS protein from *Geobacter sulfurreducens* (PDB code 2W31).[40] This template exhibited the greatest amino acid sequence identity (35%) with the globin domain of *Af*GcHK of all proteins for which structural data are available (Supporting Information Fig. S6). The heme binding pocket was retained in this homology model; therefore the heme cofactor was inserted to the globin domain using its coordinates from the template. The kinase domain of *Af*GcHK was modeled as an asymmetric homodimer using subunits A and C of the sensor histidine kinase (HK853) from *Thermotoga maritima* (PDB code 3DGE).[41] Both subunits of HK853 that were used as templates show 34% amino acid sequence identity with the kinase domain of *Af*GcHK (Supporting Information Fig. S7). We used this template because it was cocrystalized with an RR protein homolog. The model of the RR from *Anaeromyxobacter* was constructed based on a homologous RR from *Aeromonas salmonicida* (Aer-sal) (PDB code 3MF4) that has 21.2% sequence identity with the target (Supporting Information Fig. S8) Although another possible template (RR-diguanylate cyclase with 23.6% sequence identity) was available, we preferred Aer-sal because it is more functionally relevant to our model.

Protein docking of the AfGcHK:RR complex

Protein–protein docking of the kinase domain of *Af*GcHK with RR was performed using a flexible docking protocol implemented in HADDOCK.[42] Exploring the entire surface during protein–protein docking is computationally very demanding, but HADDOCK utilizes experimental information to narrow the search to certain area of the protein surfaces. This process requires the user to define active residues (in this case, R185 in chain A of *Af*GcHK and P103 of RR) and passive residues (here, R186, N187, E193, T194 in chain A and N224 in chain B of *Af*GcHK; the residues E19, K102, V104 were used as passive residues in the RR protein). These constraints limited the conformational space searched during docking to the areas identified as being protected in the HDX-MS experiments.

RESULTS

Biophysical characterization of AfGcHK, its RR protein, and AfGcHK:RR complexes

Analytical ultracentrifugation was used for the initial biophysical characterization of *Af*GcHK, its RR protein, and their complexes. Figure 1(A) shows the sedimentation coefficient distributions obtained from the sedimentation velocity experiments. These data suggest that *Af*GcHK forms a dimer in solution [see the red line in Fig. 1(A)] because its sedimentation coefficient of $s_{20,w} = 4.74$ S corresponds to a molecular mass of 82 kDa but its molecular mass as computed from its amino acid sequence is 43 kDa. No evidence for the presence of monomeric *Af*GcHK was obtained even at the lowest detectable concentration of the protein (100 n*M*). However, a very minor trace corresponding to a tetramer was observed. The heme free form of *Af*GcHK (namely the H99A mutant lacking the ability to coordinate the heme iron) forms also a dimer structure (data not shown). The RR protein primarily exists as a monomer in solution [see the black line in Fig. 1(A)], with a sedimentation coefficient of $s_{20,w} = 2.34$ S and a calculated molecular weight of 27 kDa that is in good agreement with the theoretical molecular weight of the monomeric protein. However, approximately 5% of the RR protein forms a dimeric structure under the tested conditions (3.76 S; 52 kDa).

When *Af*GcHK was mixed with the RR protein, its sedimentation increased gradually in parallel with the RR protein's concentration [Fig. 1(B)], indicating that the *Af*GcHK:RR complex is very transient with a high dissociation rate constant ($k_{off} \geq 10^{-3} s^{-1}$). The sedimentation coefficients computed for the individual peaks in the distribution shown in Figure 1(B) thus correspond to the reaction boundary rather than true molecular species. The dimeric form of *Af*GcHK contains two equivalent

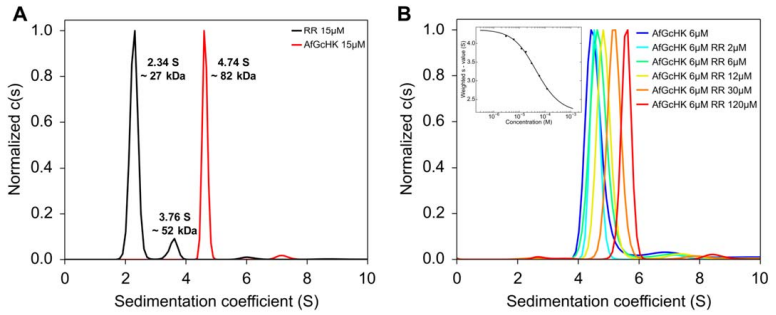


Figure 1

(A) Sedimentation coefficient distributions for the RR protein (15 μ*M*; black line) and *Af*GcHK (15 μ*M*; red line); (**B**) Changes in the sedimentation of *Af*GcHK (6 μ*M*) in the presence of different concentrations of the RR protein (2–120 μ*M*), monitored at 411 nm. The *inset* shows the isotherm curve obtained by fitting the weight-average sedimentation coefficients as a function of the loading protein concentration. The weight-average sedimentation coefficients were calculated from the interference data, providing signals for both the *Af*GcHK and RR proteins. For further details, see the 'Experimental Procedures' section. c(s) denotes the continuous sedimentation coefficient distribution.

binding sites for the RR protein, potentially allowing it to form *Af*GcHK:RR complexes with stoichiometries of 2:1 or 2:2. When solutions of *Af*GcHK were titrated with the RR protein [Fig. 1(B)], the 2:1 complex was initially formed; its sedimentation coefficient and apparent equilibrium dissociation constant (K_d) were determined to be $s_{20,w} = 5.42$ S and 18 μ*M*, respectively [Fig. 1(B), *inset*]. As the concentration of the RR protein was increased further, the sedimentation coefficient of the interaction boundary asymptotically approached that of the 2:2 complex, which was determined to have an $s_{20,w}$ value of 6.65 S based on its isotherm and calculations performed using the SEDPHAT software package.[43] In addition, it was determined to have a very high K_d of 158 μ*M*. This suggests that the 2:1 complex (one dimeric *Af*GcHK and one monomeric RR) is likely to predominate in the relatively dilute solutions studied in subsequent experiments.

Homology modeling of the AfGcHK globin and histidine kinase domains

Since no structural data for the full-length *Af*GcHK protein or its domains are available, we used homology modeling to construct an initial model of the protein. Due to the lack of suitable templates for predicting the structure of the whole protein, separate homology models of its globin and kinase domains were constructed. The structure of any homology model often depends on that of the template protein that is used. In the case of *Af*GcHK, the structures of the homology models of the globin domain and the globular part of the kinase domain did not prove to be strongly template-dependent but the spatial position of the N-terminal part of the kinase domain was very sensitive to the structure of the chosen template. The globin domain of *Af*GcHK was modeled on the *Gs*GCS protein (2W31) from *Geobacter sulfurreducens*[40] and the kinase domain was modeled as a homodimer whose structure was based on the sensor histidine kinase (HK853) from *Thermotoga maritima*.[41] Both templates exhibit low sequence similarity with *Af*GcHK (35% and 34% identity, respectively). Despite this, the homology models that were obtained can be considered reasonably accurate, although there is considerable uncertainty regarding the position of the N-terminal part of the kinase domain. Further optimization or new experimental data would be required to address this uncertainty. The homology models of the individual *Af*GcHK domains were used to visualize and interpret the results of the HDX-MS experiments (see Figs. 2–6, and 7).

The proposed structures of the AfGcHK globin and kinase domains are consistent with HDX-MS data

HDX-MS experiments were performed with the full-length *Af*GcHK protein having an Fe(III) ion bound to its heme moiety. This form has previously been shown to be the most enzymatically active in the way of autophosphorylation of its kinase domain.[32] The results obtained are summarized in the time-resolved protection plot shown in Figure 2. In addition, the deuteration levels of the globin and kinase domains at the initial time point (0.5 min) are visualized on the corresponding homology models in Figure 3, and the complete kinetic profile for the protein's deuteration is presented in Supporting Information Movie S1. The globin domain extends from the N-terminus to approximately His155,

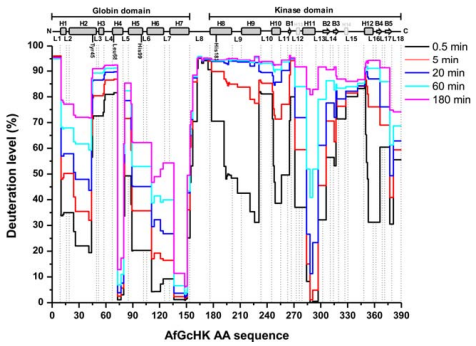


Figure 2

Protection plot showing the HDX-MS results for the full-length *Af*GcHK protein with an Fe(III)-bound heme. Levels of deuteration at 0.5, 5, 20, 60, and 180 min are plotted on the *y* axis, against the amino acid numbers of the *Af*GcHK primary sequence on the *x* axis. The putative secondary structural elements shown in the upper part of the protection plot are derived from the homology models developed within this work. The globin domain of *Af*GcHK consists of the putative secondary structural elements L1-H7; the kinase domain consists of H8-L18; and L8 is a loop connecting the two domains. Vertical dotted lines represent boundaries between individual secondary structural elements.

and includes seven helices (H1 – H7) and seven loops (L1 – L7) according to the homology model. It is connected to the kinase domain by loop L8. The kinase domain begins with helix H8 (Leu177) and contains five helices (H8 – H12), five β-strands (B1 – B5), and ten loops (L9 – L18).

The globin domain

The structural model of the *Af*GcHK globin domain developed from the *Gs*GCS structure (2W31) is in good agreement with most of the HDX-MS results [Figs. 2 and 3(A)]. It has a region formed by helices H6 and H7 along with the C-terminal part of helix H4 [the dark blue helices in Fig. 3(A) and Supporting Information Movie S1] with very low initial deuterium exchange levels. Interestingly, helix H7 and the second half of helix H4 were found to be negligibly deuterated even at the longest incubation time. This is partly due to their involvement in the formation of the hydrophobic core of the globin domain and in case of helix H7 the high level of protection can be also attributed to its participation in homodimer formation as suggested by homology modeling experiments. The hydrophobic core is partially excluded from contact with solvent, and its secondary structure elements may be stabilized by mutual contacts and contacts with helices H1 and H2. Those two helices together with helices H5 and H6 show higher deuteration levels at longer incubation times but they do not reach highest levels of deuteration typical for unstructured regions. Therefore, we may conclude that these regions indeed contain structured elements but with slightly higher solvent accessibility which agrees well with the proposed model. The higher solvent accessibility and flexibility of the end of helix H2 and of the beginning of H4 maybe also essential for oxygen sensing since the possible O_2 binding site at the heme distal side formed by Tyr45 and Leu68,[1] are located within this regions.

Figure 2 shows that together with the N-terminus, loops L3 and L4 and the short helix H3 are the most flexible parts of the globin domain. These segments form the heme distal side that is responsible for oxygen binding. Schematic and surface representations of the globin domain [Fig. 3(A) and Supporting Information Movie S1] indicate that the heme distal side [red arrow in Fig. 3(A)] of the globin domain model is partially unstructured and highly solvent-accessible. The HDX-MS data agree quite well with most of the globin domain helices predicted by the homology model. In addition, the model's predictions concerning the C-terminal part of helix H4 [Fig. 3(A)] also agree with the corresponding HDX-MS data (Fig. 2). However, there is some disagreement between the model and the HDX-MS data relating to the N-terminal part of this helix, which seems to be quite flexible according to the HDX-MS experiment. The discrepancy is tentatively attributed to the comparatively poor resolution of the HDX-MS data for this region covered only by one large peptide including, besides the N-terminal part of helix H4, also the highly flexible loop L4.

The HDX-MS pattern shown in Figure 2 indicates that the globin domain, which is terminated by helix H7, is connected to the kinase domain via the long and very flexible loop L8. The level of deuteration in this loop, which lies between helices H7 and H8, is clearly much higher than that in other parts of the protein; the HDX-MS pattern for L8 is a typical deuteration profile for an unstructured and fully solvent-accessible region.

The kinase domain

The model of the *Af*GcHK kinase domain was constructed using the HK853 histidine kinase structure (3DGE) as a template because its structure has been solved in complex with its RR.[44–46] The kinase consists of two relatively flexible and loosely interconnected subdomains: (i) the ATP binding subdomain, which (unlike the globin domain) contains a relatively high proportion of β-strand structures; and (ii) the dimerization subdomain, which consists of two long solvent-exposed helices [Fig. 3(B)]. The structural motifs of both subdomains suggest that the kinase domain should be more flexible and solvent-accessible than the globin domain. This is consistent with the HDX-MS data. Figure 2 shows that

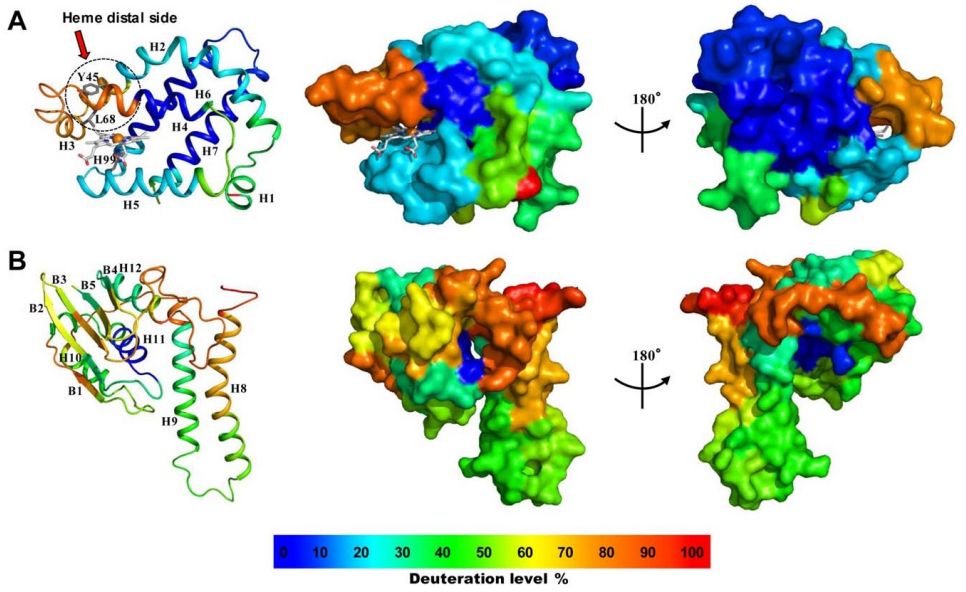


Figure 3

The structure of the full length *Af*GcHK protein with an Fe(III)-bound heme, colored according to the deuteration levels (recorded as percentages) of individual peptide fragments after 0.5 min of deuterium exchange. Because different templates[40,41] were used for homology modeling of (**A**) the globin domain and (**B**) the kinase domain, the domains' structures are shown separately even though the HDX-MS experiments were performed with the full length protein. Representations of the domains' structures (left) and surfaces (right) are shown. Note that the templates utilized for homology modeling of the globin and kinase domains are both dimers, and the full length *Af*GcHK protein also predominantly exists in solution as a dimer. However, the globin and histidine kinase domains are shown as monomers for the sake of simplicity.

the globin domain exchanges significantly less than the kinase domain.

The region of the kinase domain that has the lowest deuterium exchange level over short time scales is helix H11. The homology model predicts that this helix is located in the center of the ATP binding subdomain, where it is well shielded from the solvent. H11 is also stabilized by its interactions with helices H10 and H12 and the domain's large β-sheet, particularly β-strands B3 and B5 [Fig. 3(B)]. The HDX-MS data also indicate that helix H11 has a more pronounced time-dependent increase in its deuterium exchange level than any other structural element of the kinase domain, suggesting that it participates in slow but extensive conformational dynamics [Fig. 3(B)]. The bimodal isotope pattern shown in Supporting Information Figure S3 indicates that helix H11, unlike the rest of the *Af*GcHK protein, exhibits mixed EX1/EX2 deuteration kinetics. EX1 kinetics is associated with exchange occurring via larger cooperative unfolding processes, highlighting the dynamic nature of this helix. However, pure EX1 kinetics is very rare; it is more common for proteins to exhibit a mixture of EX1 and EX2 exchange kinetics. Indeed, EX2 kinetics was observed for all the other structural elements of *Af*GcHK. In contrast to EX1 kinetics, EX2 kinetics is indicative of exchange that occurs during uncorrelated brief unfolding events.

The two long helices H8 and H9 are the major components of the dimerization subdomain. They both exchange deuterons more readily than the domain's other secondary structural elements, which reflects their solvent accessibility and their loose contacts with neighboring structures [Figs. 2 and 3(B)]. The solvent accessibility of the dimerization domain is probably preserved after dimer formation because dimerization protects only approximately 25% of its solvent-accessible surface (Fig. 7 and Supporting Information Fig. S4). Helix H9 exhibits a higher initial level of protection than helix H8. This is consistent with the homology model, which predicts that the latter helix is distorted by the presence of a proline residue in its center.

Interestingly, the *Af*GcHK histidine kinase structural model based on the HK853 template suggests that the

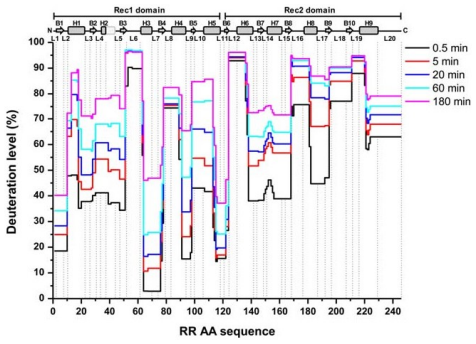


Figure 4

Protection plot showing the HDX-MS results for the RR protein. Levels of deuteration at 0.5, 5, 20, 60, and 180 min are plotted on the *y* axis, against the protein's amino acid sequence on the *x* axis. The protein's putative secondary structure elements shown in the upper part of the protection plot were derived from the homology model created in this work. Vertical dotted lines represent boundaries between individual elements of the RR secondary structure.

*Af*GcHK dimer consists of subunits with slightly different structures (Supporting Information Fig. S4). The first subunit (on the left in Supporting Information Fig. S4) has a short helix (H13) in the region covered by the loop L12. The second subunit (on the right in Supporting Information Fig. S4) has no helix covered by loop L12; instead, its H14 helix is predicted to lie within the loop L15. Both of these helices are very short and contain proline residues, and no conclusions regarding their presence or absence can be drawn based on the HDX-MS data. The speculative helices H13 and H14 are shown in grey in the structure alignment at the top of Figure 2.

Homology modeling of the RR protein

The RR protein consists of two receiver domains, Rec1 and Rec2, which contain the phosphorylable aspartic acid residues Asp52 and Asp169 (Fig. 4). The sequence identity between the Rec1 and Rec2 domains is 22.8%. Homology modeling of this protein was performed using the solved structure of the RR from *Aeromonas salmonicida* (Aer-sal) as the template (PDB code 3MF4). The template exhibits 21.2% amino acid sequence identity with the RR protein and consists of two CheY-like receiver domains. The final homology model of the RR protein was compared to the corresponding HDX-MS data (see below). The secondary structures of the RR protein suggested by the homology model are indicated in Figure 4, which also presents the corresponding HDX-MS data.

Correlation of the RR model's structure with the HDX-MS data

The deuteration profiles for the RR protein show that it has a high overall level of deuterium uptake, indicating a relatively high degree of structural flexibility (Fig. 4). The level of deuteration of the RR protein is comparable to the average deuteration of the *Af*GcHK protein as a whole but significantly higher than that of the *Af*GcHK globin sensor domain. The deuteration kinetics data for RR were matched to its homology model in order to validate the predicted structure and visualize its flexibility and dynamics (Fig. 5 and Supporting Information Movie S2). According to the model, the RR protein contains 9 α-helices, 10 β-strands, and 20 unstructured loops, with loop L11 forming a short linker between the Rec1 and Rec2 domains. These domains are organized into a structure with a central β-sheet formed from five parallel β-strands that is surrounded by α-helices. The model also suggests that Rec1 has a lower proportion of unstructured

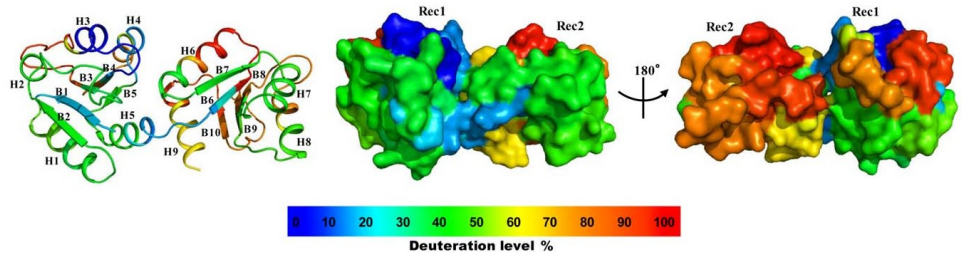


Figure 5

The structure of the RR protein showing the Rec1 and Rec2 domains, colored according to the deuteration levels (recorded as percentages) of individual fragments after 0.5 min of deuterium exchange. The structure shown is based on the homology model created in this work. Representations of the protein's structure (left) and surface (right) are shown.

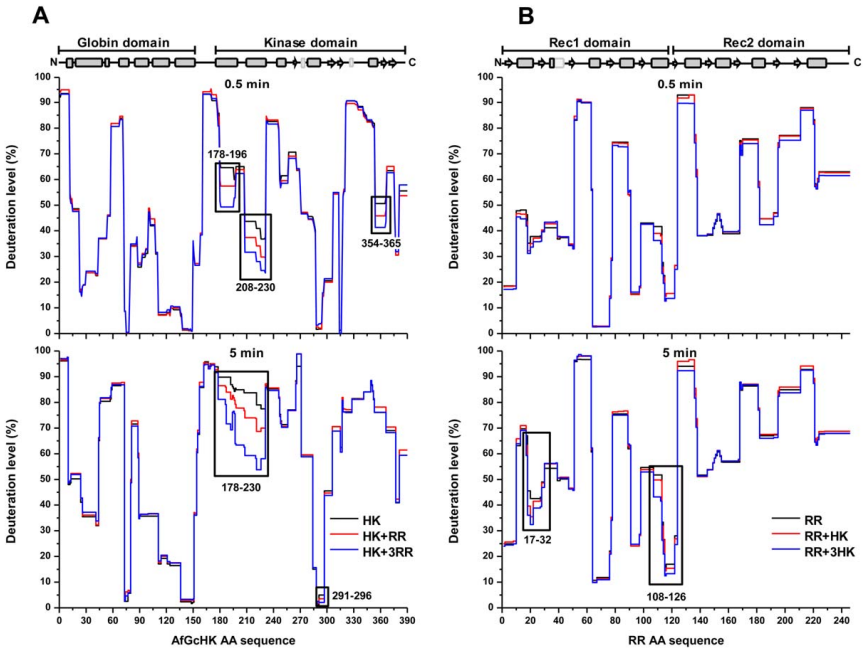


Figure 6

Protection plot showing the HDX-MS results for the complex of *Af*GcHK with its RR protein. (**A**) Results obtained for *Af*GcHK in the absence (HK) and the presence of two different molar ratios of RR (HK + RR; HK + 3RR). The deuteration level (*y* axis) at 0.5 min (upper) and 5 min (lower) is plotted against the *Af*GcHK amino acid sequence (*x* axis). To increase the resolution of the analysis, HDX-MS data obtained using two digestion protocols employing two different proteases (pepsin and rhizopuspepsin) were merged. The protein segments influenced by the presence of RR are enclosed in black boxes. (**B**) Results obtained for RR in the absence (RR) and the presence of two different molar ratios of *Af*GcHK (RR + HK; RR + 3HK). The deuteration level (*y* axis) at 0.5 min (upper) and 5 min (lower) is plotted against the RR amino acid sequence (*x* axis), and protein segments influenced by the presence of *Af*GcHK are enclosed in black boxes.

regions than Rec2 (Fig. 5). In addition, the HDX-MS data indicate that the Rec2 domain is on average slightly more accessible for deuteration than the Rec1 domain (Fig. 4).

The Rec1 domain contains 5 β-strands and 5 α-helices (Figs. (4 and 5) and Supporting Information Movie S2). A segment corresponding to the β-strand B3, which forms the core of the protein, exhibited low deuteration relative to the protein's other secondary structure elements. However, this β-strand was dynamic over longer time scales (hours): its level of deuteration had almost doubled after the longest tested incubation period. The α-helices in the Rec1 domain are mostly positioned on the periphery and are therefore solvent-accessible, which is reflected by their relatively fast deuteration (Figs. (4 and 5) and Supporting Information Movie S2). The α-helices H1, H3, and H5 exhibit similar deuteration levels and kinetics. The homology model predicts that helix H2 consists of only four amino acids. However, the HDX-MS data show that the deuteration rates for the residues covering this part of the structure and the residues immediately downstream are comparatively low, suggesting that the H2 α-helix may be longer at its C-end than predicted by the homology model. If so, its structure would be similar to that of the corresponding helix (H7) of the Rec2 domain. Another inconsistency between the HDX-MS results and the homology model of the Rec1 domain is that helix H4 is predicted to be 10 residues long but the corresponding sequence shows high deuteration levels even at the shortest incubation time, suggesting that this structural element is actually quite unstructured. Similar deuteration properties were observed for the corresponding segment of the Rec2 domain but that segment is predicted to be a loop (L18), which is more consistent with the HDX-MS data.

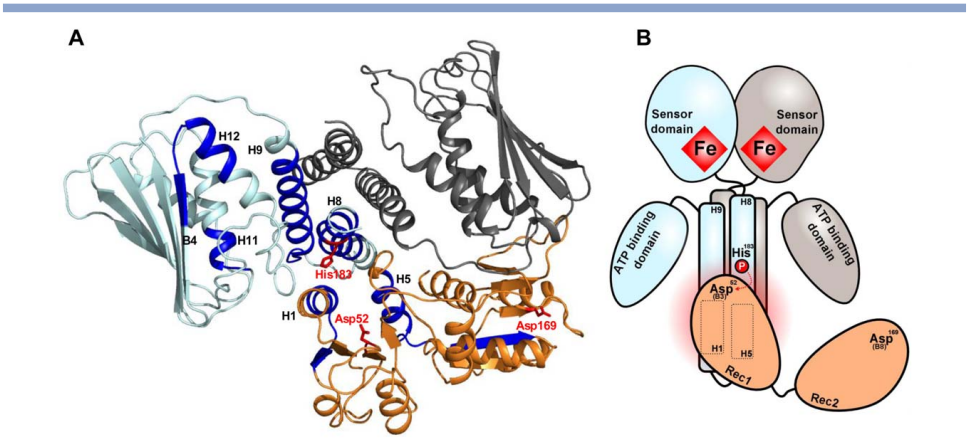


Figure 7

A structural model of the *Af*GcHK:RR protein complex based on the homology modeling and protein–protein docking of the *Af*GcHK kinase domain and the RR protein validated by the HDX-MS data. (**A**) The individual *Af*GcHK monomers are shown in light blue and light grey, while the RR protein is shown in orange; regions influenced by *Af*GcHK:RR complex formation are shown in dark blue. (**B**) A simplified cartoon model highlighting the most important contact area between the Fe(III)-bound full length *Af*GcHK and RR proteins.

The Rec2 domain has the same length as Rec1 and contains 5 β-strands but, in keeping with the discussion above, only 4 α-helices (Figs. (4 and 5) and Supporting Information Movie S2). The homology model for this domain is in better agreement with the HDX-MS data than that for Rec1, which exhibited at least two discrepancies (see above). The second helix (H7) of the Rec2 domain is predicted to be longer than helix H2 of the Rec1 domain. Moreover, the model does not predict there to be a helix between the last two β-strands (B9 and B10) of this domain; again, this is consistent with the HDX-MS data (Figs. 4 and 5). The segment corresponding to this loop includes three proline residues that would strongly destabilize helical structures; we therefore consider the model's prediction of an unstructured loop 18 to be correct. The β-strand B8, which contains the phosphorylable Asp169 residue, was the least deuterated region of the Rec2 domain and was consistently predicted to be in the center of the Rec2 domain (Figs. (4 and 5) and Supporting Information Movie S2). The deuteration profile of the C-terminal sequence confirms the presence of a structured part (helix H9). However, the poor spatial resolution of the HDX-MS data for this region (which is due to the nature of the corresponding proteolysis steps) made it impossible to establish an exact fit between the HDX-MS data and the model.

Overall, the Rec2 domain contains a higher proportion of easily deuterated regions than Rec1, suggesting that it is probably slightly more flexible and solvent-accessible and/or less structured (Figs. 4 and 5). The deuteration levels of these two domains differ significantly in some cases, especially at shorter incubation times, the Rec2 domain seems to be more accessible (exchange more) than the Rec1 domain.

Mapping of the Interaction Interface between the AfGcHK and RR proteins using HDX-MS

The analytical ultracentrifugation experiments revealed that the predominant complex of *Af*GcHK and RR proteins in solution consists of an *Af*GcHK dimer and one RR monomer. HDX-MS experiments and computer modeling for protein–protein docking were used to further characterize this protein–protein complex. The contact interface on the *Af*GcHK protein was mapped using HDX-MS data. To increase the spatial resolution of this experiment, HDX-MS data obtained from two digestion protocols employing two different proteases (pepsin and rhizopuspepsin[47]) were merged. In addition, we monitored the effects of equimolar and excess concentrations of RR on the deuteration of *Af*GcHK [Fig. 6(A)], revealing that RR protected *Af*GcHK against deuteration in a concentration-dependent fashion. Changes in deuteration were considered as significant if the difference in deuteration exceeded the standard deviation calculated from the replicate measurements.[48] Additional criterion applicable in this study was the concentration dependency of the protection levels observable at the sites with altered deuteration kinetics (Supporting Information Fig. S5).

The protective effect was primarily observed in the segments comprising amino acid residues 178–196 and 208–230, which correspond to the central parts of helices H8 and H9, respectively. The deuteration kinetics of peptides corresponding to both segments shows that the protective effect of RR is only observed for short incubation times; no protection was observed for 1 or 3 h long incubations, even when an excess of the RR was used [Supporting Information Fig. S5(A)]. All these findings are consistent with the central parts of H8 and H9, which are localized in the middle part of the *Af*GcHK dimerization domain, participating in weak but direct interactions with the RR protein. We also observed smaller but reproducible decreases in the deuteration of segments 291–296 and 354–365, indicating a weak or indirect stabilizing influence of the RR protein on these *Af*GcHK regions. These slightly protected segments correspond to the C-terminal part of helix H11, the beginning of loop L13 (residues 291–296), parts of helix H12, loop L16, and parts of β-strand B4 (residues 354–365), respectively. The helix H11 is located within the ATP binding site (ATP was not added into the mixture during the HDX-MS experiments) and as described above this region exhibits mixed EX1/EX2 exchange kinetics. However, this behavior was unaffected by the interaction with RR protein (Supporting Information Fig. S3). Interestingly, the other slightly protected segment, which included helix H12, loop L16, and part of β-strand B4, was located on the opposite side of the ATP binding subdomain and should thus be unable to interact directly with the RR protein based on the homology model [Fig. 7(A)]. It should also be noted that the stabilizing effect in this relatively long region is weak and was only significant for the shortest incubation period [Supporting Information Fig. S5(A)]. The presence of the RR protein had no detectable effect on the deuteration of the *Af*GcHK globin domain.

The segments of the RR protein influenced by interaction with the *Af*GcHK protein were similarly investigated by studying its protection plots based on experimental data gathered using equimolar and excess concentrations of *Af*GcHK [Fig. 6(B)]. The RR segments that were stabilized by contact with *Af*GcHK include residues 17–32 and 108–126. Residues 17–32 correspond to the second part of helix H1 and β-strand B2 as well as the adjacent loops, while residues 108–126 represent the C-terminal end of helix H5 together with loop L11 and β-strand B6 [Figs. 6(B) and Supporting Information S5(B)]. It is obvious that the presence of *Af*GcHK has no effect on the deuteration propensity of the RR Rec2 domain because all of the *Af*GcHK interaction sites are located in the Rec1 domain.

A plausible model of the 2:1 *Af*GcHK:RR complex was obtained by soft–soft protein–protein docking of the corresponding homology models [Fig. 7(A)], and the contacts observed in the model were compared to the HDX-MS data for the complex. Overall, the results obtained indicate that the N-terminal side of the H9 helix of the *Af*GcHK kinase domain interacts with the H1 helix of the RR protein, while the C-side of the H8 helix region of the kinase domain interacts mostly with the H5 helix of the RR protein. No interactions between the RR protein and the globin domain of *Af*GcHK were detected.

DISCUSSION

Most histidine kinases involved in two-component signal transduction systems form homodimers under physiological conditions.[49,50] *Af*GcHK has also been proposed to form a homodimer on the basis of gel filtration experiments.[1] We confirmed that suggestion by analytical ultracentrifugation and proved that heme coordinated in the globin domain is not responsible for the *Af*GcHK dimerization. Moreover, it was found that the RR protein predominantly exists as a monomer. When *Af*GcHK and the RR protein are present in solution together, they predominantly form a complex with 2:1 stoichiometry. If the RR protein is present in large excess, a second RR molecule interacts with the 2:1 *Af*GcHK:RR complex to form a weak, physiologically less relevant, 2:2 complex whose K_d value is an order of magnitude greater than that of the 2:1 complex. It should also be noted that both *Af*GcHK:RR complexes are transient, with a high dissociation rate constant.

The overall structure of the *Af*GcHK globin domain is rigid and well-organized based on its low level of deuteration in the HDX-MS experiments, especially when compared to the histidine kinase domain (Figs. 2 and 3). Importantly, the deuterium exchange kinetics of the C-terminal end of helix H4 and the entirety of helices H6 and H7 are very slow in comparison to the other helices, suggesting that these helices form the hydrophobic core of the globin domain. In contrast, the structural elements of the heme distal side (mainly loops L3 and L4 and the short helix H3) responsible for oxygen binding to the heme form the most flexible part of the *Af*GcHK globin domain. This protein area is responsible for the binding and dissociation of O_2 and thus for the detection of the first signal involved in the recognition of aerobic/anaerobic conditions in the sensor protein's surroundings. The high flexibility of this region is consistent with our findings concerning two other oxygen sensor proteins, YddV and *Ec*DOS, in which the sensor domains containing the ferric heme complex exhibit high flexibility in the vicinity of the heme.[24]

The *Af*GcHK kinase domain contains many unstructured loops, which naturally provide weaker stabilizing effects than α-helices (Figs. 2 and 3). Moreover, the two long central α-helices of this domain (H8 and H9) are solvent-accessible. These helices are probably responsible for kinase domain dimer formation, as in other histidine

kinases.[9,49] Participation in dimer formation could thus influence the behavior of H8 and H9 in solution. On the other hand, the ATP binding site formed partially by helix H11 was found to be the most rigid region in the kinase domain. Moreover, the bimodal distribution of changes in the isotope profile for the peptides covering H11 indicates that this helix exhibits partial EX1 deuteration kinetics (Supporting Information Fig. S3), which is associated with exchange involving larger cooperative unfolding processes. It thus appears that this region of the kinase domain experiences higher levels of destabilization and is more flexible than its other parts.[51] In contrast, the remaining regions of *Af*GcHK exhibit classical EX2 deuteration kinetics. Since H11 is involved in ATP binding, this difference in behavior might also play some role in the processes associated with the autophosphorylation activity of *Af*GcHK.

The ultracentrifugation results revealed that *Af*GcHK forms a dimer in solution. It seems to contain at least two dimerization sites; the first may be located within the globin domain, which would explain the unusually high resistance of helix H7 to deuterium exchange (and maybe also that of helix H6). Other globin domains from globin-coupled sensor proteins have been observed to form dimeric structures when isolated without their functional domains.[40,52] It should be noted, that the heme absence in the globin domain has no effect of the *Af*GcHK oligomerization state. The second dimerization site of *Af*GcHK is located within the kinase domain and consists of its two long central α-helices, H8 and H9.[49] The homology modeling suggested that the individual chains forming the *Af*GcHK dimer could have slightly different structures (Supporting Information Fig. S4). According to the AA sequence (Supporting Information Fig. S7) of the first subunit, the loop L12 contains two proline residues that would strongly destabilize an α-helix, so the entirety of the L12 loop region is probably unstructured. In the second subunit, helix H14 (which consists of only four amino acids) appears to be only transient (Supporting Information Fig. S4). We were unable to obtain more information on the structures of these regions using HDX-MS.

In comparison to *Af*GcHK, the HDX-MS data for the RR protein indicate that as a whole it is flexible and solvent-accessible. Moreover, the homology model of the Rec2 domain was in better agreement with the experimental data than that for the Rec1 domain. The RR protein contains two phosphorylable aspartates, namely Asp52 and Asp169.[1] While Asp52 is located on the edge of β-strand B3 and loop L6 in Rec1, Asp169 is situated between β-strand B8 and loop L16 of Rec2. The region containing Asp52 is more flexible and solvent-accessible than that containing Asp162, which may be important in the protein's mechanism of action and function. On the basis of these HDX-MS results, it was suggested that the RR protein interacts only with the *Af*GcHK kinase domain and that its two main contact areas are formed by the central α-helices of the histidine kinase domain, H8 and H9 [Fig. 7(B)]. Moreover, we can assume that the binding of the RR protein induces conformational changes in the ATP binding region (helix H11) of *Af*GcHK. Such induced conformational changes could increase the enzyme's K_m^{ATP} value, in keeping with recent findings.[32] Moreover, the deuteration profiles of the peptides derived from the aforementioned areas [Fig. 6(A) and Supporting Information Fig. S5(A)] indicate that these interaction sites are flexible. This is consistent with the known behavior of other histidine kinases.[53] Interestingly, contact with the RR protein also appears to stabilize an additional segment of the *Af*GcHK kinase domain, which includes helix H12, loop L16 and part of β-strand B4. This segment is located on the opposite side of the ATP binding region, so the homology model predicts that it is unable to interact with the RR protein directly [Fig. 7(A)]. The protection of this region may thus reflect an allosteric effect of RR binding on the structure of the *Af*GcHK kinase domain. In contrast, RR binding has no detectable effect on the deuteration propensity of the *Af*GcHK globin domain. It appears that only the Rec1 domain of the RR protein, which contains the phosphorylable Asp52 residue, interacts with the *Af*GcHK kinase domain. However, it should be noted that both aspartates of the RR protein (Asp52 in Rec1 and Asp169 in Rec2) are phosphorylated when RR is incubated with *Af*GcHK in the presence of ATP.[1] In contrast, our current HDX-MS studies were performed in the absence of ATP. It is possible that the Rec1 domain of RR, which contains Asp52, has a significantly higher affinity for *Af*GcHK than the Rec2 domain, which would explain why contact was only observed between Rec1 and *Af*GcHK. This would be consistent with previous observations indicating that over short incubation periods, Asp52 is the preferred phosphorylation site of RR.[1] It is also possible that the phosphorylation of Asp52 changes the overall structure of RR, facilitating the interaction of the Rec2 domain containing the second phosphorylation site (Asp169) with *Af*GcHK. In this way, Asp52 phosphorylation could play an important role in the allosteric regulation of RR phosphorylation. Further experiments will be required to test this hypothesis. Namely, examination of conformational changes during sensing and signaling is underway in our laboratory.

The homology models of the proteins considered in this work were all based on structural alignments with low homology templates, so some segments of the models may be less accurate than others. Indeed, comparisons with the experimental HDX-MS data revealed several potentially inaccurate segments of the models. The predicted structures of these segments could be improved in the future by using combinations of several templates, with each individual segment of the target protein being modeled with the template that most closely matches the

relevant experimental data. The structure of the resulting hybrid homology model could be refined by molecular dynamics. The model of *Af*GcHK:RR complex presented here that is based on the current generation of homology models should be seen as a low resolution model. We can conclude that the N-side of helix H9 in the *Af*GcHK protein interacts with the region of the RR protein comprising residues 17–32, and that the C-side of the helix H8 region of the *Af*GcHK protein interacts mostly with the region comprising residues 108–126 in the RR protein (Fig. 7). The residues Asp52 and His183 are in the model positioned 11.5 Å apart. This distance does not exclude the phosphate-transfer between these residues; however, it is by 3–4 Å longer than that observed in crystal structure of a HK853–RR complex from *Thermotoga maritima*.[41] It should be noted, that the docking and HDX-MS studies were performed in the absence of ATP and therefore with the un-phosphorylated form of His183. For that reason, the structure of the nascent phosphate-transfer complex could be slightly different from our model. Although the model of the complex is consistent with most of the data from the HDX-MS experiments, it cannot explain the RR-induced protection of the distant segment featuring H12 and B4. It seems that the asymmetric structural transitions and asymmetric receiver binding is a general feature of two component signaling systems.[9–11] We believe that the complex model presented herein could be significantly improved by combining next generation models of the RR and *Af*GcHK proteins with more rigorous computational approaches such as flexible docking in combination with classical and steered molecular dynamics. These techniques have been used to characterize and predict the structures of other transient protein–protein complexes,[31,54] and could make it possible to investigate the potential allosteric behavior of the ATP-binding domain of *Af*GcHK.

SUMMARY

The heme-regulated oxygen sensor histidine kinase *Af*GcHK is the first component of a two-component signal transduction system. On the binding to oxygen to the heme iron complex of its N-terminal sensing domain, it autophosphorylates His183 in its C-terminal kinase domain. This phosphate group is then transferred to either Asp52 or Asp169 of its cognate response receptor (RR) protein. Ultracentrifugation experiments indicated that the predominant complex of *Af*GcHK and RR in solution consists of an *Af*GcHK dimer and an RR monomer that has an apparent equilibrium dissociation constant (K_d) of 18 μ*M*. HDX-MS data obtained for the *Af*GcHK protein indicated that its N-terminal globin domain is less flexible than its C-terminal kinase domain and that the most flexible part of the whole protein is the loop connecting the N-terminal globin and C-terminal kinase domains. Our data also showed that the heme distal side, responsible for oxygen binding formed by loops L3, L4 and the short helix H3, is the only flexible part of the globin domain. Studies on the *Af*GcHK:RR complex showed that the N-side of the H9 helix of *Af*GcHK interacts with the helix H1 and the β-strand B2 area of the RR protein's Rec1 domain, and that the C-side of the H8 helix region of the *Af*GcHK protein interacts mostly with the helix H5 and β-strand B6 area of the Rec1 domain. Only the Rec1 domain containing the phosphorylable Asp52 interacts with the *Af*GcHK kinase domain because the Rec1 domain probably has a significantly higher affinity for *Af*GcHK than the Rec2 domain. We speculate that phosphorylation at Asp52 changes the overall structure of RR such that the Rec2 area containing the second phosphorylation site (Asp169) can also interact with *Af*GcHK.

ACKNOWLEDGMENT

We are grateful to Dr. Kenichi Kitanishi for technical assistance during the early stages of this work.

AUTHOR CONTRIBUTIONS

M.S. planned experiments, performed experiments and analyzed data; V.M. performed and interpreted protein models, discussed and interpreted data; P.M. planned, performed and interpreted MS experiments; V.F. performed experiments; D.K. helped with MS data processing and wrote the program DeutEx for HDX-MS data analysis; O.V. participated in ultracentrifugation experiments; T.S. discussed and interpreted data; M.M. discussed and interpreted data, and wrote the article.

REFERENCES

1. Kitanishi K, Kobayashi K, Uchida T, Ishimori K, Igarashi J, Shimizu T. Identification and functional and spectral characterization of a globin-coupled histidine kinase from *Anaeromyxobacter* sp. Fw109-5. J Biol Chem 2011;286:35522–35534.
2. Shimizu T, Huang D, Yan F, Stranava M, Bartosova M, Fojtíková V, Martínková M. Gaseous O2, NO, and CO in signal transduction: structure and function relationships of heme-based gas sensors and heme-redox sensors. Chem Rev 2015;115:6491–6533.
3. Gao R, Mack TR, Stock AM. Bacterial response regulators: versatile regulatory strategies from common domains. Trends Biochem Sci 2007;32:225–234.
4. Galperin MY. Diversity of structure and function of response regulator output domains. Curr Opin Microbiol 2010;13:150–159.
5. Jenal U, Galperin MY. Single domain response regulators: molecular switches with emerging roles in cell organization and dynamics. Curr Opin Microbiol 2009;12:152–160.
6. Shi X, Wegener-Feldbrügge S, Huntley S, Hamann N, Hedderich R, Søgaard-Andersen L. Bioinformatics and experimental analysis of proteins of two-component systems in *Myxococcus xanthus*. J Bacteriol 2008;190:613–624.

7. Zusman DR, Scott AE, Yang Z, Kirby JR. Chemosensory pathways, motility and development in *Myxococcus xanthus*. Nat Rev Microbiol 2007;5:862–872.
8. Stock AM, Robinson VL, Goudreau PN. Two-component signal transduction. Annu Rev Biochem 2000;69:183–215.
9. Bhate MP, Molnar KS, Goulian M, DeGrado WF. Signal transduction in histidine kinases: insights from new structures. Structure 2015;23:981–994.
10. Podgornaia AI, Casino P, Marina A, Laub MT. Structural basis of a rationally rewired protein-protein interface critical to bacterial signaling. Structure 2013;21:1636–1647.
11. Willett JW, Herrou J, Briegel A, Rotskoff G, Crosson S. Structural asymmetry in a conserved signaling system that regulates division, replication, and virulence of an intracellular pathogen. Proc Natl Acad Sci USA 2015;112:E3709–E3718.
12. Müller S, Chaikuad A, Gray NS, Knapp S. The ins and outs of selective kinase inhibitor development. Nat Chem Biol 2015;11:818–821.
13. Wu P, Nielsen TE, Clausen MH. FDA-approved small-molecule kinase inhibitors. Trends Pharmacol Sci 2015;36:422–439.
14. Dean SN, van Hoek ML. Screen of FDA-approved drug library identifies maprotiline, an antibiofilm and antivirulence compound with QseC sensor-kinase dependent activity in Francisella novicida. Virulence 2015;6:487–503.
15. Kim W, Conery AL, Rajamuthiah R, Fuchs BB, Ausubel FM, Mylonakis E. Identification of an antimicrobial agent effective against methicillin-resistant *Staphylococcus aureus* persisters using a fluorescence-based screening strategy. PLoS One 2015;10:e0127640
16. Igarashi J, Kitanishi K, Martinkova M, Murase M, Iizuka A, Shimizu T. The roles of thiolate-heme proteins, other than the P450 cytochromes, in the regulation of hemesensor proteins. Acta Chim Slov 2008;55:67–74.
17. Igarashi J, Murase M, Iizuka A, Pichierri F, Martinkova M, Shimizu T. Elucidation of the heme binding site of heme-regulated eukaryotic initiation factor 2alpha kinase and the role of the regulatory motif in heme sensing by spectroscopic and catalytic studies of mutant proteins. J Biol Chem 2008;283:18782–18791.
18. Shimizu T. Binding of cysteine thiolate to the Fe(III) heme complex is critical for the function of heme sensor proteins. J Inorg Biochem 2012;108:171–177.
19. Girvan HM, Munro AW. Heme sensor proteins. J Biol Chem 2013; 288:13194–13203.
20. Martínková M, Kitanishi K, Shimizu T. Heme-based globin-coupled oxygen sensors: linking oxygen binding to functional regulation of diguanylate cyclase, histidine kinase, and methyl-accepting chemotaxis. J Biol Chem 2013;288:27702–27711.
21. Frank DJ, Waddling CA, La M, Ortiz de Montellano PR. Cytochrome P450 125A4, the third cholesterol C-26 hydroxylase from *Mycobacterium smegmatis*. Biochemistry 2015;54:6909–6916.
22. Casadei CM, Gumiero A, Metcalfe CL, Murphy EJ, Basran J, Concilio MG, Teixeira SCM, Schrader TE, Fielding AJ, Ostermann A, Blakeley MP, Raven EL, Moody PCE. Neutron cryocrystallography captures the protonation state of ferryl heme in a peroxidase. Science 2014;345:193–197.
23. Poulos TL. Heme enzyme structure and function. Chem Rev 2014; 114:3919–3962.
24. Anzenbacher P, Marchal S, Palacký J, Anzenbacherová E, Domaschke T, Lange R, Shimizu T, Kitanishi K, Stranava M, Stiborová M, Martinkova M. Pressure effects reveal that changes in the redox states of the heme iron complexes in the sensor domains of two heme-based oxygen sensor proteins, EcDOS and YddV, have profound effects on their flexibility. FEBS J 2014;281:5208–5219.
25. Engen JR. Analysis of protein conformation and dynamics by hydrogen/deuterium exchange MS. Anal Chem 2009;81:7870–7875.
26. Foo YH, Gao Y, Zhang H, Kenney LJ. Cytoplasmic sensing by the inner membrane histidine kinase EnvZ. Prog Biophys Mol Biol 2015;118:119–129.
27. Ikegami T, Okada T, Ohki I, Hirayama J, Mizuno T, Shirakawa M. Solution structure and dynamic character of the histidine-containing phosphotransfer domain of anaerobic sensor kinase ArcB from Escherichia coli. Biochemistry 2001;40:375–386.
28. Guo Q, Jureller JE, Warren JT, Solomaha E, Florián J, Tang W-J. Protein-protein docking and analysis reveal that two homologous bacterial adenylyl cyclase toxins interact with calmodulin differently. J Biol Chem 2008;283:23836–23845.
29. Sulc M, Jecmen T, Snajdrova R, Novak P, Martinek V, Hodek P, Stiborova M, Hudecek J. Mapping of interaction between cytochrome P450 2B4 and cytochrome b5: the first evidence of two mutual orientations. Neuroendocrinol Lett 2012;33:41–47.
30. Perkins JR, Diboun I, Dessailly BH, Lees JG, Orengo C. Transient protein-protein interactions: structural, functional, and network properties. Structure 2010;18:1233–1243.
31. Jeřábek P, Florián J, Stiborová M, Martínek V. Flexible docking-based molecular dynamics/steered molecular dynamics calculations of protein–protein contacts in a complex of cytochrome P450 1A2 with cytochrome b5. Biochemistry 2014;53:6695–6705.
32. Fojtikova V, Stranava M, Vos MH, Liebl U, Hranicek J, Kitanishi K, Shimizu T, Martinkova M. Kinetic analysis of a globin-coupled histidine kinase, AfGcHK: effects of the heme iron complex, response regulator, and metal cations on autophosphorylation activity. Biochemistry 2015;54:5017–5029.
33. Antonini EB., Brunori M. Hemoglobin and myoglobin in their reactions with ligands. Amsterdam: North-Holland; 1971.
34. Houtman JCD, Brown PH, Bowden B, Yamaguchi H, Appella E, Samelson LE, Schuck P. Studying multisite binary and ternary protein interactions by global analysis of isothermal titration calorimetry data in SEDPHAT: application to adaptor protein complexes in cell signaling. Protein Sci 2007;16:30–42.
35. Schuck P. Size-distribution analysis of macromolecules by sedimentation velocity ultracentrifugation and lamm equation modeling. Biophys J 2000;78:1606–1619.
36. Brautigam CA. Calculations and publication-quality illustrations for analytical ultracentrifugation data. Methods Enzymol 2015;562:109–133.
37. Trcka F, Durech M, Man P, Hernychova L, Muller P, Vojtesek B. The assembly and intermolecular properties of the Hsp70-Tomm34-Hsp90 molecular chaperone complex. J Biol Chem 2014;289:9887–9901.
38. Zhang Z, Smith DL. Determination of amide hydrogen exchange by mass spectrometry: a new tool for protein structure elucidation. Protein Sci 1993;2:522–531.
39. Biasini M, Bienert S, Waterhouse A, Arnold K, Studer G, Schmidt T, Kiefer F, Cassarino TG, Bertoni M, Bordoli L, Schwede T. SWISS-MODEL: modelling protein tertiary and quaternary structure using evolutionary information. Nucleic Acids Res 2014;42: W252–W258. Web Server issue):–.
40. Pesce A, Thijs L, Nardini M, Desmet F, Sisinni L, Gourlay L, Bolli A, Coletta M, Van Doorslaer S, Wan X, Alam M, Ascenzi P, Moens L, Bolognesi M, Dewilde S. HisE11 and HisF8 provide bis-histidyl heme hexa-coordination in the globin domain of Geobacter sulfurreducens globin-coupled sensor. J Mol Biol 2009;386:246–260.
41. Casino P, Rubio V, Marina A. Structural insight into partner specificity and phosphoryl transfer in two-component signal transduction. Cell 2009;139:325–336.
42. Vries SJ, de Dijk M, Bonvin AM. The HADDOCK web server for data-driven biomolecular docking. Nat Protoc 2010;5:883–897.
43. Cole JL, Lary JW, P Moody T., Laue TM, Analytical ultracentrifugation: sedimentation velocity and sedimentation equilibrium. Methods Cell Biol 2008;84:143–179.
44. Casino P, Miguel-Romero L, Marina A. Visualizing autophosphorylation in histidine kinases. Nat Commun 2014;5:3258
45. Ashenberg O, Keating AE, Laub MT. Helix bundle loops determine whether histidine kinases autophosphorylate in cis or in trans. J Mol Biol 2013;425:1198–1209.

46. Cai S-J, Inouye M. Spontaneous subunit exchange and biochemical evidence for trans-autophosphorylation in a dimer of Escherichia coli histidine kinase (EnvZ). J Mol Biol 2003;329:495–503.
47. Rey M, Man P, Brandolin G, Forest E, Pelosi L. Recombinant immobilized rhizopuspepsin as a new tool for protein digestion in hydrogen/deuterium exchange mass spectrometry. Rapid Commun Mass Spectrom 2009;23:3431–3438.
48. Leurs U, Lohse B, Ming S, Cole PA, Clausen RP, Kristensen JL, Rand KD. Dissecting the binding mode of low affinity phage display peptide ligands to protein targets by hydrogen/deuterium exchange coupled to mass spectrometry. Anal Chem 2014;86:11734–11741.
49. Wolanin PM, Thomason PA, Stock JB. Histidine protein kinases: key signal transducers outside the animal kingdom. Genome Biol 2002;3:REVIEWS3013
50. Surette MG, Levit M, Liu Y, Lukat G, Ninfa EG, Ninfa A, Stock JB. Dimerization is required for the activity of the protein histidine kinase CheA that mediates signal transduction in bacterial chemotaxis. J Biol Chem 1996;271:939–945.
51. Weis DD, Wales TE, Engen JR, Hotchko M, Ten Eyck LF. Identification and characterization of EX1 kinetics in H/D exchange mass spectrometry by peak width analysis. J Am Soc Mass Spectrom 2006;17:1498–1509.
52. Tarnawski M, Barends TRM, Schlichting I. Structural analysis of an oxygen-regulated diguanylate cyclase. Acta Crystallogr D Biol Crystallogr 2015;71:2158–2177.
53. Childers WS, Xu Q, Mann TH, Mathews II, Blair JA, Deacon AM, Shapiro L. Cell fate regulation governed by a repurposed bacterial histidine kinase. PLoS Biol 2014;12:e1001979
54. Jeřábek P, Florián J, Martínek V. Membrane-anchored cytochrome P450 1A2-cytochrome b5 complex features an X-shaped contact between antiparallel transmembrane helices. Chem Res Toxicol 2016;29:626–636.

5.2 Coordination and redox state-dependent structural changes of the heme-based oxygen sensor *Af*GcHK associated with intraprotein signal transduction

Stranava M., Man P., Skálová T., Kolenko P., Blaha J., **Fojtikova V.**, Martínek V., Dohnálek J., Lengalova A., Rosůlek M., Shimizu T., Martínková M. *J Biol Chem*. (2017) 292, 20921 (**IF_{2016} 4,1**).

Podíl předkladatelky na této práci: 10 % (exprese a purifikace proteinů, experimenty týkající se stanovení autofosforylační aktivity *Af*GcHK)

Potvrzeno korespondujícím autorem, doc. RNDr. Markéta Martínková Ph.D.

JBC ARTICLE

Coordination and redox state–dependent structural changes of the heme-based oxygen sensor *Af*GcHK associated with intraprotein signal transduction

Received for publication, September 12, 2017, and in revised form, October 18, 2017 Published, Papers in Press, November 1, 2017, DOI 10.1074/jbc.M117.817023

Martin Stranava[‡], Petr Man[‡§1], Tereza Skálová[¶], Petr Kolenko[¶‖], Jan Blaha[‡], Veronika Fojtikova[‡], Václav Martínek[‡], Jan Dohnálek[¶], Alzbeta Lengalova[‡], Michal Rosůlek[‡§1], Toru Shimizu[‡], and Markéta Martínková[‡2]

From the [‡]Department of Biochemistry, Faculty of Science, Charles University, Hlavova (Albertov) 2030/8, Prague 2, 128 43 Czech Republic, the [§]Institute of Microbiology of the Czech Academy of Sciences, v.v.i., Biocev, 252 50 Vestec, Czech Republic, the [¶]Institute of Biotechnology of the Czech Academy of Sciences, v.v.i., Biocev, 252 50 Vestec, Czech Republic, and the [‖]Department of Solid State Engineering, Faculty of Nuclear Sciences and Physical Engineering, Czech Technical University in Prague, Brehova 7, 115 19 Praha 1, Czech Republic

Edited by F. Peter Guengerich

The heme-based oxygen sensor histidine kinase *Af*GcHK is part of a two-component signal transduction system in bacteria. O_2 binding to the Fe(II) heme complex of its N-terminal globin domain strongly stimulates autophosphorylation at His^{183} in its C-terminal kinase domain. The 6-coordinate heme Fe(III)-OH^- and -CN^- complexes of *Af*GcHK are also active, but the 5-coordinate heme Fe(II) complex and the heme-free apo-form are inactive. Here, we determined the crystal structures of the isolated dimeric globin domains of the active Fe(III)-CN^- and inactive 5-coordinate Fe(II) forms, revealing striking structural differences on the heme-proximal side of the globin domain. Using hydrogen/deuterium exchange coupled with mass spectrometry to characterize the conformations of the active and inactive forms of full-length *Af*GcHK in solution, we investigated the intramolecular signal transduction mechanisms. Major differences between the active and inactive forms were observed on the heme-proximal side (helix H5), at the dimerization interface (helices H6 and H7 and loop L7) of the globin domain and in the ATP-binding site (helices H9 and H11) of the kinase domain. Moreover, separation of the sensor and kinase domains, which deactivates catalysis, increased the solvent exposure of the globin domain-dimerization interface (helix H6) as well as the flexibility and solvent exposure of helix H11. Together, these results suggest that structural changes at the heme-proximal side, the globin domain-dimerization interface, and the ATP-binding site are important in the signal transduction mechanism of *Af*GcHK. We conclude that *Af*GcHK functions as an ensemble of molecules sampling at least two conformational states.

The heme-based oxygen sensor kinase from the soil bacterium *Anaeromyxobacter* sp. Fw109-5, *Af*GcHK is a globin-coupled oxygen sensor (GCS)[3] consisting of an N-terminal heme-binding globin domain and a C-terminal histidine kinase domain (1, 2). *Af*GcHK is an element of a two-component signal transduction system (3–6) in which the binding of O_2 to the heme Fe(II) complex of its oxygen-sensing globin domain significantly enhances the autophosphorylation activity of its kinase domain via intramolecular signal transduction (Fig. 1). The phosphate group is subsequently transferred from His^{183} of the *Af*GcHK to the Asp^{52} and Asp^{169} residues of its cognate response regulator protein (1, 2, 7) (supplemental Fig. S1). Like the 6-coordinate heme Fe(II)-O_2 complex, the 6-coordinate heme Fe(III)-OH^- and CN^- complexes are also active, despite having a different redox state at the iron center (8). However, *Af*GcHK containing a globin domain with a 5-coordinate Fe(II) heme complex or a heme-free apo-globin domain exhibits low kinase activity (8). This strongly suggests

This work was supported in part by Charles University Grant UNCE 204025/2012; Grant Agency of the Czech Republic Grant 15-19883S; Grant Agency of Charles University Grants 362115 and 704217; Ministry of Education, Youth, and Sports of the Czech Republic Grant LM2015043 CIISB, Biocev - Crystallization, Diffraction and LTC17065 in frame of COST Action CA15126 MOBIEU; ERDF fund Grants CZ.02.1.01/0.0/0.0/16_013/0001776 and CZ.1.05/1.1.00/02.0109; and Grant Agency of the Czech Technical University in Prague Grant SGS16/246/OHK4/3T/14. This work was also partly funded by Instruct, part of the European Strategy Forum on Research Infrastructures (ESFRI) and supported by national member subscriptions. The authors declare that they have no conflicts of interest with the contents of this article.

This article contains supplemental information on the crystal structure of *Af*GcHK globin domain, a structural comparison of the isolated globin domains of *Af*GcHK and other GCSs, supplemental Table S1, and supplemental Figs. S1–S8.

The atomic coordinates and structure factors (codes 5OHE and 5OHF) have been deposited in the Protein Data Bank (http://wwpdb.org/).

[1] Recipient of financial support from NPU II (LQ1604).

[2] To whom correspondence should be addressed. Tel.: 420-22-195-1242; Fax: 420-22-195-1283; E-mail: marketa.martinkova@natur.cuni.cz.

[3] The abbreviations used are: GCS, globin-coupled oxygen sensor; *Af*GcHK, a globin-coupled histidine kinase from *Anaeromyxobacter* sp. Fw109-5; *Ec*DOS, *E. coli* direct oxygen sensor or heme-regulated phosphodiesterase from *E. coli* or *Ec*DosP; Fe(III), Fe(III)-protoporphyrin IX complex, or hemin; Fe(II), Fe(II)-protoporphyrin IX complex; FixL, an oxygen-sensor histidine kinase with the heme-bound PAS domain that regulates nitrogen fixation in *Rhizobium meliloti* or *Bradyrhizobium japonicum*; GAF, domain conserved in cyclic GMP-specific and stimulated phosphodiesterases, adenylate cyclases, and *E. coli* formate hydrogenlyase transcriptional activator; *Gs*GCS, globin-coupled sensor from *G. sulfurreducens*; HDX–MS, hydrogen/deuterium exchange coupled with mass spectrometry; HK853, the sensor histidine kinase from *T. maritima*; PAS, Per (*Drosophila* period clock protein)-Arnt (vertebrate aryl hydrocarbon receptor nuclear translocator)-Sim (*Drosophila* single-minded protein); YddV, heme-bound diguanylate cyclase from *E. coli* or *Ec*DosC; PDB, Protein Data Bank; RMSD, root mean square deviation.

© 2017 by The American Society for Biochemistry and Molecular Biology, Inc. Published in the U.S.A.

Protein structures of a heme-based oxygen sensor kinase AfGcHK

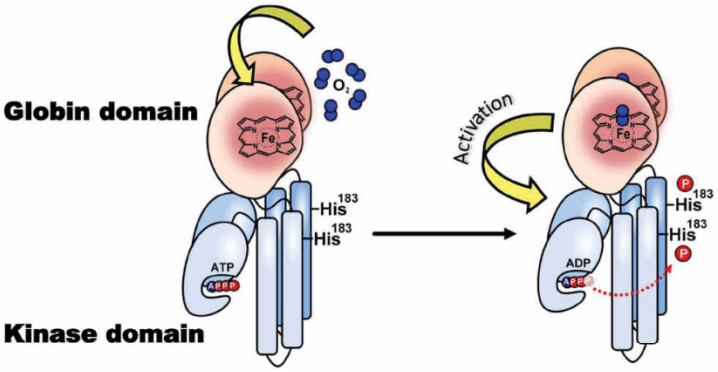


Figure 1. Intramolecular signal transduction of homodimeric *Af*GcHK. O_2 binds to the heme Fe(II) complex in the globin domain at the N terminus, changing the structure of the protein surrounding the heme. These structural changes function as a signal that is transduced to the kinase domain (at the C terminus), activating the kinase reaction and inducing autophosphorylation at His^{183}.

that structural changes near the heme-binding site in the globin domain are tightly linked to the catalytic regulation of the kinase domain via intraprotein signal transduction.

To understand the molecular mechanism of this intramolecular signal transduction, it is important to know 1) how the structure of the globin domain differs between the Fe(III) (active) and Fe(II) (inactive) heme complex–bound forms and between forms with and without axial ligands; 2) how structural changes in the globin domain propagate to the kinase domain; and 3) how the transition from the inactive to the active state in response to the transduction of the globin domain signal affects the kinase domain.

The structure–function relationships of oxygen sensors containing a heme-bound globin, PAS, and GAF folds have been investigated in various proteins (2). Both heme iron reduction and the binding of external axial ligands such as O_2 can induce global structural changes (affecting both the heme surroundings and more distant regions) in the isolated heme-bound PAS domains of oxygen sensors, such as FixL (9, 10) and *Ec*DOS (11, 12). However, these effects were found to be less pronounced in the isolated heme-bound GAF domains of oxygen sensors, such as DosS/DosT, than those observed for the PAS domain (13–15). Additionally, changes in heme redox state or external ligand binding had no significant impact on the structure of the isolated heme-bound globin domain of GCS (16–18). In this work, we present the first X-ray crystal structures of heme Fe(III) and Fe(II) complexes of the isolated dimeric globin domain of *Af*GcHK, revealing large structural differences between the active and inactive forms in the vicinity of the heme and at the globin dimerization interface.

Importantly, no X-ray crystal structure of any full-length heme-based oxygen sensor has yet been reported. We previously studied the full-length *Af*GcHK protein in solution by combining hydrogen/deuterium exchange coupled with mass spectrometry (HDX–MS) with homology modeling (7). However, the structural changes in this protein caused by heme redox state changes and the binding of different axial ligands (both of which are closely linked to catalytic regulation) have not been characterized.

This work uses HDX–MS to describe the structural differences between the active and inactive forms of full-length *Af*GcHK and its isolated globin and kinase domains in solution and analyzes structural differences between the active and inactive forms of the *Af*GcHK globin domain revealed by X-ray crystallography. It was found that changes in the heme redox state and axial ligand binding to the heme iron complex lead to structural alterations in the heme-proximal side of the globin domain and affect domain-domain interactions within the dimeric globin domains. Differences were also observed around the two helices forming the ATP-binding site necessary for autophosphorylation in the kinase domain. These structural changes associated with catalytic regulation revealed by HDX–MS corroborated the conclusions drawn by analyzing the X-ray crystal structures of the isolated globin domain in two redox states.

Results

We first determined the X-ray crystal structures of isolated *Af*GcHK globin domains bearing heme in the Fe(III)-CN^- form (active state) and containing heme Fe(II) (inactive state) complexes and then compared them with HDX–MS data for the full-length *Af*GcHK protein.

Crystal structure of the isolated heme Fe(III)-CN^- globin domain (PDB code 5OHE)

The crystal structure of the isolated globin domain in the presence of KCN was solved at a resolution of 1.85 Å. Relevant data processing parameters and structure characteristics are presented in Table 1.

Overall structure—The asymmetric unit of the crystal consists of four dimers (Fig. 2*A*) formed by eight protein chains (AB, CD, EF, and GH) positioned in a disphenoidal arrangement. The crystal structure confirms that the domain adopts the characteristic globin fold of GCSs (Fig. 2*B*). Each monomer consists of seven helices, H1–H7 (also known as helices A–G (2)), and seven loops, L1–L7. RMSD values of coordinates of C^α atoms of the aligned protein chains (monomers) are in the range of 0.2–0.5 Å with no significant difference between the

Table 1
Data processing statistics and structure refinement parameters
Values in parentheses refer to the highest-resolution shell.

	Globin domain of *Af*GcHK with heme Fe(III)-CN^-	Globin domain of *Af*GcHK with cyanide, partially reduced (the dithionite-soaked crystal)
PDB code	5OHE	5OHF
Data processing statistics		
Space group	$P4_12_12$	$P4_12_12$
Unit-cell parameters		
a, *b*, *c* (Å)	78.1, 78.1, 441.8	77.7, 77.7, 441.2
α, β, γ (degrees)	90.0, 90.0, 90.0	90.0, 90.0, 90.0
Resolution range (Å)	46.82–1.85 (1.88–1.85)	49.17–1.8 (1.83–1.80)
No. of observations	1,413,447 (62,729)	931,937 (47,063)
No. of unique reflections	118,539 (5739)	127,077 (6192)
Data completeness (%)	100 (100)	100 (100)
Average redundancy	11.9 (10.9)	7.3 (7.6)
Mosaicity (degrees)	0.118	0.07
Average $I/\sigma(I)$	11.1 (1.9)	16.7 (2.7)
Solvent content (%)	46	46
Matthews coefficient ($Å^3$/Da)	2.27	2.27
R_{merge}[a]	0.139 (1.157)	0.059 (0.761)
$R_{p.i.m.}$[a]	0.059 (0.517)	0.034 (0.442)
CC1/2	0.998 (0.804)	0.993 (0.844)
Structure refinement parameters		
R_{work}[a]	0.192	0.190
R_{free}	0.241	0.239
R_{all}	0.194	0.192
Average *B*-factor ($Å^2$)	24	28
RMSD bond lengths from ideal (Å)	0.015	0.009
RMSD bond angles from ideal (degrees)	1.653	1.267
Number of non-hydrogen atoms	11,456	12,325
Dimers per asymmetric unit (chains)	AB, CD, EF, GH	AB, CD, EF, GH
No. of water molecules	1117	1017
Ramachandran statistics		
Residues in favored regions (%)	100	99.9
No. of outliers	0	0

[a] $R_{merge} = \Sigma_h\Sigma_i|I_{hi} - \langle I_h\rangle|/\Sigma_h\Sigma_i I_{hi}$, $R_{p.i.m.} = \Sigma_h\Sigma_i(n_h - 1)^{-1/2}|I_{hi} - \langle I_h\rangle|/\Sigma_h\Sigma_i I_{hi}$, and $R = \Sigma_h||F_{h,obs}| - |F_{h,calc}||/\Sigma_h|F_{h,obs}|$, where I_{hi} is the observed intensity, $\langle I_h\rangle$ is the mean intensity of multiple observations of symmetry-related reflections, and $F_{h,obs}$ and $F_{h,calc}$ are the observed and calculated structure factor amplitudes. R_{work} is the *R* factor calculated on 95% of reflections excluding a random subset of 5% of reflections marked as "free." The final structure refinement was performed on all observed structure factors.

structures of the monomers. The fold of the dimer is most similar to that of the globin domain of *Geobacter sulfurreducens* GCS (PDB code 2W31 (17), 34% sequence identity); the RMSD between the C^α atom coordinates of the aligned dimers is 1.4 Å (PDBeFold (19)).

Crystal contacts, electron density, and B-factors; differences among the chains—All four dimers in the asymmetric unit have approximately the same contact surface area at the dimer interface (as determined by a PISA assembly analysis (20)) except in the region of residues Arg^{55}–Val^{65}. This region is very well localized in the electron density map in chains A and D due to stabilizing interchain contacts within the asymmetric unit. The remaining chains form weaker water-mediated contacts with symmetry-related chains. In chains C and G, this region exhibits higher disorder and weaker electron density. This is also reflected in *B*-factors of the protein chains; the C and G chains of the dimer had higher chain-averaged *B*-factors than the other chains (28 and 31 $Å^2$, respectively, compared with 21–23 $Å^2$ for the others). The higher average *B*-factors of both chains are primarily due to *B*-factor "hot spots" around residues 55–65, which are close to the heme-binding pocket. These observations are in agreement with the greater susceptibility of chains C and G to structural changes and in part explain why the effects of the dithionite soaking were observed only in chain G (see below).

Dimer interface—Interestingly, the dimer interface largely consists of water-mediated hydrogen bonds. The interface between protein chains A and B features 28 water molecules involved in water-mediated hydrogen bonds, of which 12 participate in residue-water-residue and four participate in residue-water-water-residue bonds (Fig. 2*C*). Another eight water molecules together with a chloride ion fill a large cavity in the upper part of the dimerization interface (the area labeled *part I* of the dimerization interface in Fig. 2*C*), which is located opposite the kinase domain in the full-length protein. The total interface area varies between 1722 and 1800 $Å^2$, depending on the pair of chains analyzed, and accounts for around 21% of the total monomer surface area of 8500 $Å^2$. The interface can be divided into two regions (Fig. 2*C*): part I and part II. Part I features mainly van der Waals interactions and water-mediated hydrogen bonds and has no direct protein–protein hydrogen bonds. Part II is close to the C-terminus (and thus close to the kinase domain in the full-length protein) and features 19 interchain protein–protein hydrogen bonds, hydrophobic interactions, and several water-mediated hydrogen bonds. Part I of the interface therefore allows for more variability in the relative arrangement of the two monomers, whereas part II functions as a more tightly tethered hinge. Together, the two parts allow the monomers' relative positions and orientations to be quite well defined and controlled near the heme sites while also permitting a highly dynamic arrangement, especially in the part I region (Fig. 2*C*).

Heme surroundings—The heme is bound in a hydrophobic pocket formed by residues from helices H2–H7. The 6-coordi-

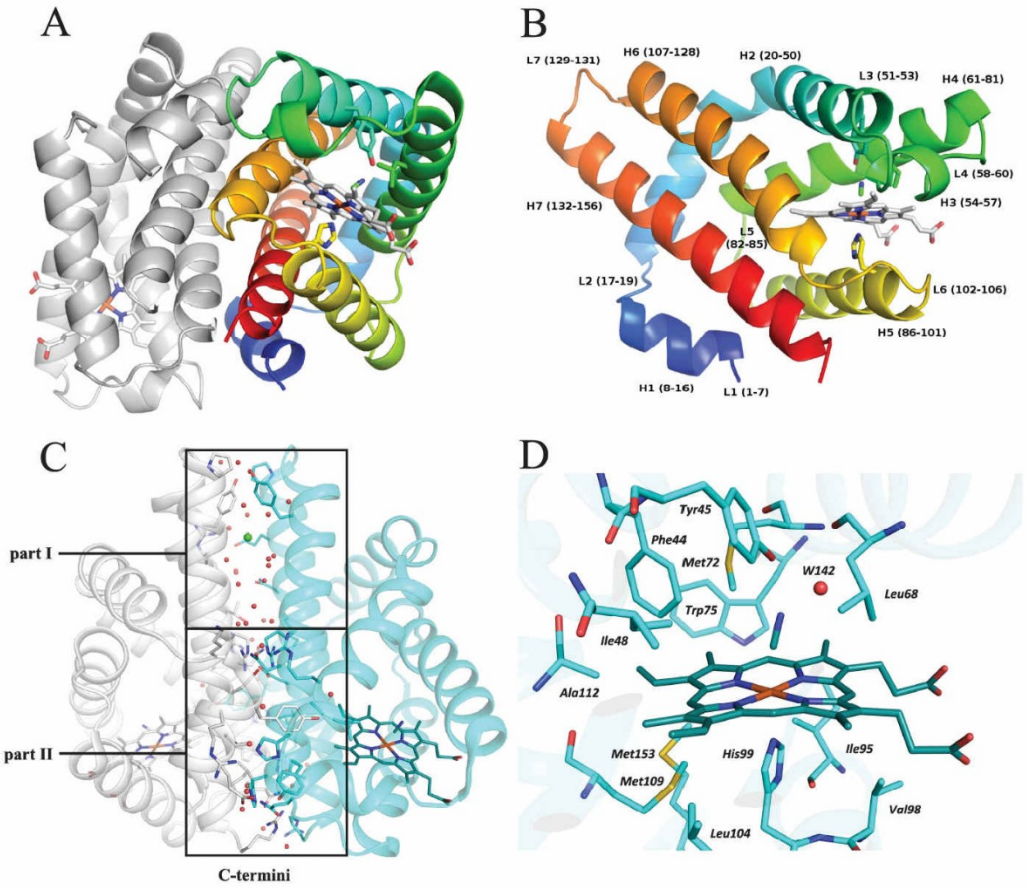


Figure 2. Crystal structure of a dimer of the globin domain of *Af*GcHK with an Fe(III)-CN^- heme complex (active state, PDB code 5OHE) and a *close-up view* of the heme surroundings. *A*, secondary structure representation of the dimer with the N terminus of chain A in *blue*, the C terminus of chain A in *red*, and chain B in *gray*. The heme, selected neighboring residues, and bound cyanide molecule are shown using a *stick representation*. *B*, *close-up view* of the molecular architecture of protein chain A, using the same *color coding* and representations as in *A*; individual α-helices, loops, and the corresponding residue numbers are marked. *C*, dimerization interface of the isolated globin domain dimer, showing its division into parts I and II; part I is situated opposite the kinase domain in the full-length protein and relies only on van der Waals interactions and water-mediated hydrogen bonds, with no direct protein–protein hydrogen bonds, whereas part II is near the C terminus (close to the kinase domain in the full-length protein) and features 19 interchain protein–protein hydrogen bonds, hydrophobic interactions, and several water-mediated hydrogen bonds. *Red dots*, water molecules; *green sphere*, a chloride ion. *D*, the heme pocket residues (whose carbon atoms are shown in *cyan*), the heme group (carbon atoms shown in *dark cyan*), and the cyanide ligand (carbon atom shown in *dark cyan*) are shown in a *stick representation* with *color coding* according to atom type. The graphics were generated using PyMOL (Schrödinger, LLC, New York).

nate Fe(III) ion is stabilized by direct interactions with His^{99} (belonging to H5) at the proximal side and Tyr^{45} (belonging to H2) at the distal side, with the latter interaction being mediated by a small ligand (Fig. 2*D*). In most chains, the small ligand can be interpreted as a CN^- ion, but the electron density maps for chains D and F lack the diatomic character and were interpreted as water molecules.

The distal side of the heme-binding pocket is formed from eight residues located within 4 Å of the heme: Phe^{44}, Tyr^{45}, Ile^{48}, Leu^{68}, Met^{72}, Trp^{75}, Ala^{112}, and Met^{113}. Additionally, Tyr^{15} from the neighboring chain completes the binding pocket. The Leu^{68} residue is located at the entrance to the heme-binding pocket and represents a "gate" for incoming ligand molecules. The proximal side is formed from residues Ile^{95}, Val^{98}, His^{99} (which binds directly to the Fe(III) center), Ile^{102}, Leu^{104}, Tyr^{108}, Met^{109}, and Met^{153}. As observed in our crystal structure, the distance between the Fe(III) center and the $N^{\epsilon 2}$ center of His^{99} is 2.1 Å.

The observed position of Tyr^{45} is consistent with resonance Raman data on its interaction with O_2 bound to Fe(II) (1). In addition, mutation of Tyr^{45} destabilizes the Fe(II)-O_2 complex, increasing its autoxidation rate several hundred-

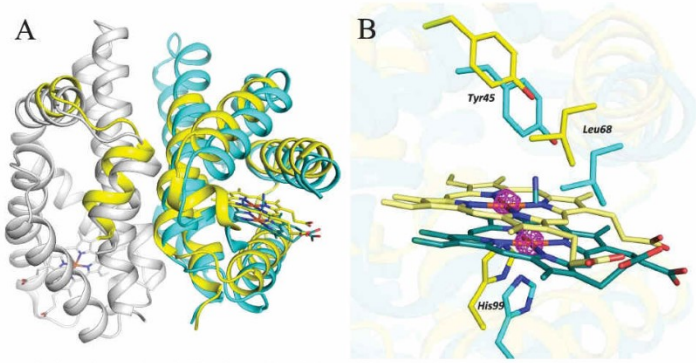


Figure 3. Structural changes induced by sodium dithionite soaking (PDB code 5OHF). *A*, chains G and H are shown using a secondary structure representation (in *cyan* and *gray*, respectively) except for their heme and CN^- moieties, which are shown using a *stick representation* (*colored* in *dark cyan* for chain G and *dark gray* for chain H). Alternative B is shown in *yellow*, and the position of its heme group is shown in *light yellow* using a *stick representation*. Most of the residues adopting different positions in alternative B are in chain G. *B*, detailed view of the shift of the heme group and the surrounding heme pocket upon dithionite soaking. The active Fe(III)-CN^- form is shown in *cyan*, and the inactive Fe(II) form is shown in *yellow*. The anomalous difference map (*magenta*, contoured at 5σ) confirms the presence of iron in two positions (observed in chain G only). The graphics were generated using PyMOL (Schrödinger, LLC).

fold (supplemental Table S1 and Figs. S2 and S3). The corresponding Tyr residue (Tyr^{43}) of the homologous GCS sensor protein, YddV, is also assumed to interact with O_2 bound to the heme Fe(II) center. Accordingly, mutation of this residue significantly changes the O_2-binding behavior of YddV: the Y43A and Y43L mutants do not bind O_2, and the autoxidation rates of the Y43F and Y43W mutants are more than 10 times higher than that of the wild type (supplemental Table S1) (1, 21–24). Leu^{68}, which is located between the small heme ligand and the bulk solvent, also has important effects on the activity of *Af*GcHK. Its role in stabilizing the Fe(II)-O_2 complex has been confirmed using site-directed mutagenesis; the L68G, L68N, and L68V mutations all significantly increased the heme iron autoxidation rate (supplemental Table S1 and Figs. S2 and S3).

Crystal structure of the AfGcHK globin domain after reduction with sodium dithionite (PDB code 5OHF)

To obtain a crystal structure of the *Af*GcHK globin domain with an Fe(II) heme complex, the crystal of the Fe(III)-CN^--containing globin domain was soaked in a solution of the strong reductant sodium dithionite. The resulting diffraction data were processed at a resolution of 1.8 Å. The data processing parameters and structure characteristics for the reduced crystal are presented in Table 1.

The reduced crystal retains the unit cell and asymmetric unit ordering of the parent (non-soaked) crystal. However, the structure of protein chain G (which had the highest *B*-factors in the parent crystal) differs sharply from that in the parent crystal (Fig. 3*A*). The iron center of the heme group from chain G was found in two distinct positions, each having an occupancy of 0.5 (confirmed by anomalous scattering; see Fig. 3*B*). Similarly, the heme group and protein chain were also observed in two alternative positions designated A and B (supplemental Fig. S4). In alternative A, the structure of the G chain resembles that of the other chains, and the sixth ligand is visible above the heme; if the sixth ligand is not modeled, there is a positive difference peak in the position it would occupy. Alternative A thus represents an Fe(III)-CN^--bound form. Omit electron density does not contain any significant positive difference peak that would justify building of a small ligand in the expected position above heme in alternative B. Therefore, alternative B contains a heme with no sixth ligand and thus represents a reduced heme iron complex formed by the action of dithionite. Based on the experimental conditions and the lack of a small axial ligand, we assume that the iron center in this alternative is 5-coordinate and exists in the Fe(II) oxidation state (Fig. 3*B*). In alternative A, the atomic coordinates for all amino acid residues in chain G and all of the other protein chains are consistent with those for the corresponding amino acids in the original 6-coordinate Fe(III)-CN^- structure. In alternative B, the positions of most residues in chain G and some in chain H (its dimerization partner protein chain) differed significantly from those in alternative A. In total, 93 residues in chain G were modeled in alternative positions: Pro^{38}–Leu^{58}, Gln^{64}–Leu^{120}, and Gly^{143}–Arg^{158} at the end of the chain (residues Val^{59}–Ser^{63} could not be localized and therefore were not modeled). Residues in chain H that required interpretation by two alternative positions were Thr^{7}–Ala^{25}, located at the beginning of the chain (Fig. 3*A*). All residues built in two alternatives belong to helices H2–H7 of chain G and helices H1 and H2 of its partner chain H. The positional changes in chain H are clearly due to those in chain G rather than any redox process affecting the chain H heme complex. The heme and heme pocket in alternative B are shifted away from the globin dimer interface by 2.5 Å relative to their position in alternative A, and much of the positional difference between the protein chains in two alternatives is due to the displacement of residues to follow and accommodate this shift. The residue exhibiting the greatest displacement from its position in alternative A (3.6 Å) is Ile^{102}, which forms van der Waals interactions with the heme.

The crystal structure presented in Fig. 3 is the best from a series of eight diffraction data sets obtained by soaking of the original crystals of the *Af*GcHK globin domain in sodium

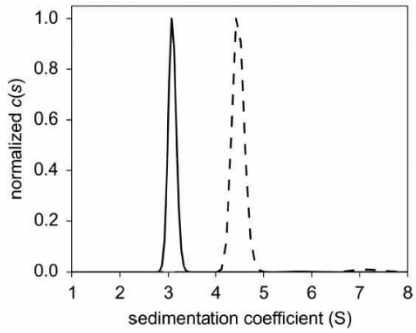


Figure 4. Sedimentation coefficient distributions for the isolated globin domain of *Af*GcHK (15 μM; *black solid line*) and the full-length *Af*GcHK (15 μM; *black dashed line*). The weight average sedimentation coefficients were calculated from the absorbance data. For further details, see "Experimental procedures." *c*(*s*) denotes the continuous sedimentation coefficient distribution.

dithionite for various periods. All eight data sets were checked, and similar trends of structural changes were observed. The data set allowing the most accurate interpretation of the data in terms of structural changes was selected. For details, see the supplemental materials.

Determination of the oligomeric state of the isolated globin domain and the full-length protein in solution by analytical ultracentrifugation

The full-length *Af*GcHK protein forms a dimer in solution (Fig. 4) because its sedimentation coefficient of $s_{20,w} = 4.74$ S corresponds to a molecular mass of 82 kDa, but its molecular mass as computed from its amino acid sequence is 43 kDa. The isolated globin domain of *Af*GcHK also forms a dimer in solution (Fig. 4) because its sedimentation coefficient of $s_{20,w} = 3.20$ S corresponds to a molecular mass of 39 kDa, but its molecular mass as computed from its amino acid sequence is 19 kDa.

Similarities and differences between the active Fe(III)-OH⁻ and inactive Fe(II) forms of the full-length AfGcHK protein revealed by HDX–MS data

The structure of the isolated globin domain of *Af*GcHK containing Fe(III)-CN^- determined by X-ray crystallography in this work and our previously reported model structure of the isolated kinase domain (7) were used to visualize the changes in the functional states of *Af*GcHK that were observed by HDX–MS, which are summarized in Fig. 5.

Reduction of the Fe(III)-OH^- complex in *Af*GcHK changes the iron coordination number from 6 to 5 and is accompanied by changes in deuteration across the entire protein. This is shown in Fig. 6, which presents the relative differences in deuteration between the active full-length *Af*GcHK protein containing the Fe(III)-OH^- complex and the inactive 5-coordinate Fe(II) complex with no sixth ligand. The greatest decrease in deuteration was observed in the globin domain, and the magnitude and extent of the decrease observed 5 min after reduction were similar to those seen after 60 min (Fig. 6). Regions of the protein that were stabilized or more shielded from deuteration included helices H2 and H3 (residues 44–72), and H5 and H6 (residues 89–120); these helices are shown in *blue* in the *top left* structure in Fig. 5*B*. On the other hand, heme iron reduction increased deuteration in part I of the globin dimerization interface, which is distant from the connection to the kinase domain. Regions exhibiting pronounced increases in deuteration included the end of H6, loop L7, and the beginning of H7 (residues 121–150); see the *red areas* in the *top left* structure in Fig. 5*B*. The HDX–MS results are consistent with the globin domain structure determined by X-ray crystallography (Fig. 2*C*); part I shows greater dynamics, whereas part II functions as a more tightly tethered hinge. This behavior was observed for the isolated globin domain with an Fe(III)-CN^- heme complex and is readily apparent in the HDX–MS results for the active and inactive forms of the full-length *Af*GcHK protein (compare the *top left* structures shown in Fig. 5, *A* and *B*). The structural data suggest that the globin dimerization interface undergoes a sort of scissor motion as the protein transitions from the active to the inactive state.

Interestingly, reduction of the heme iron center has little effect on the deuteration profile of the kinase domain outside two distinct regions: residues 221–231 of H9 and residues 284–296 of H11 (Figs. 5*B* (*bottom left*) and 6). The largest changes occur in the part of the kinase domain (helix H11) that forms the ATP binding site, which is more flexible and solvent-exposed in the inactive Fe(II)-bound form. It may be that heme iron reduction increases the separation of H9 and H11 (the ATP binding site), indirectly hindering His^{183} (at H8) phosphorylation.

The differences in deuteration between the active Fe(III)-OH^- and inactive Fe(II) forms of the full-length *Af*GcHK protein were analogous in all tested incubation times. Data for the 5- and 60-min time points were selected as representative results (Fig. 6); the measurements for the other time points (0.5, 20, and 180 min) showed similar trends (supplemental Fig. S5).

Similarities and differences between the other active and inactive forms of the full-length AfGcHK protein revealed by HDX–MS data

To determine whether the changes in the deuteration profile of *Af*GcHK upon reduction of the active Fe(III)-OH^- globin domain heme complex to the inactive Fe(II) form are consistent with those observed for other active and inactive forms (supplemental Fig. S6), we performed HDX–MS experiments with three other full-length variants: the inactive heme-free apoprotein (the H99A mutant), the active Fe(III)-CN^- complex, and the active Fe(II)-O_2 complex (Fig. 7).

The differences in deuteration between the Fe(III)-OH^- form and the other active forms containing CN^- and O_2 were rather small and confined to the heme-distal side of the globin domain, specifically residues 30–60 and 120–130 in helices H2, H3, and H6 (represented as *blue ribbons* in the *top left* and *central structures* in Fig. 5*A*). It thus seems that the nature of the sixth heme ligand affects the protein's dynamics and the solvent accessibility in the vicinity of the heme prosthetic group on the heme-distal side but has little effect on the transduction of dynamic effects between the globin and kinase domains (repre-

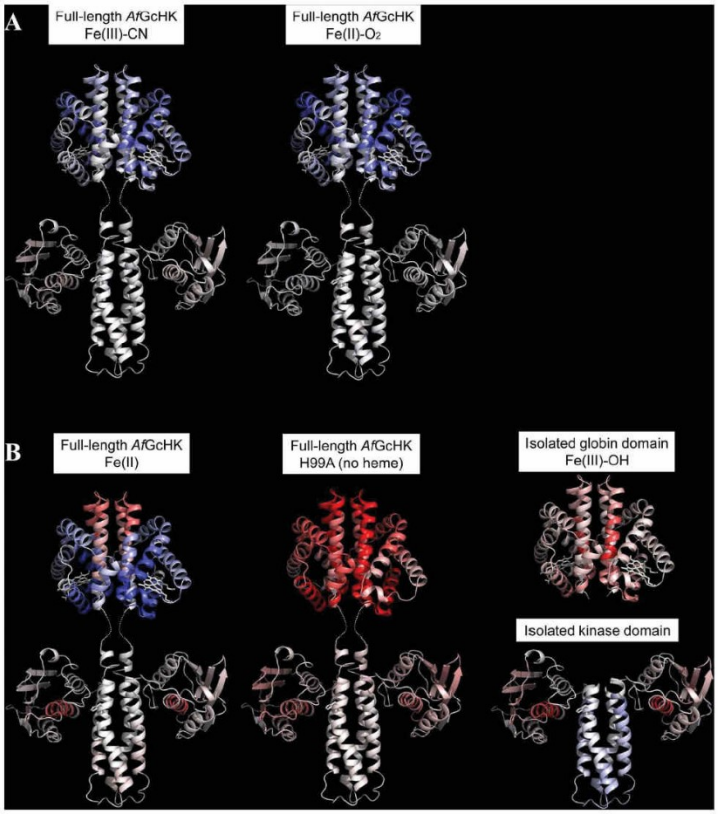


Figure 5. Conformational changes revealed by HDX–MS after 60 min of deuteration of the full-length *Af*GcHK proteins and the separated domains, visualized on the protein's structure. Differences between the Fe(III)-OH^- form and other active or inactive forms are *color-coded*; *gray* indicates no difference, whereas higher and lower levels of deuteration in the specified protein form are indicated by increasingly intense *red* and *blue* coloration, respectively. *A*, active full-length *Af*GcHK proteins with Fe(III)-CN^- (*left*) and Fe(II)-O_2 (*center*) heme complexes. *B*, inactive structures, including the full-length *Af*GcHK protein with an Fe(II) heme complex (*left*), the full-length heme-free (apo) H99A mutant (*center*), the isolated globin domain (*top right*), and the isolated kinase domain (*bottom right*). The globin domain structure is based on the X-ray crystal data (PDB code 5OHE) presented in this work, and the kinase domain was modeled as an asymmetric homodimer using subunits A and C of the sensor histidine kinase (HK853) from *Thermotoga maritima* (PDB code 3DGE). This approach was validated by experiments presented elsewhere (7).

sented as *gray ribbons* in the *bottom left* and *central structures* of Fig. 5*A*).

The HDX–MS patterns for the two inactive forms, the 5-coordinate Fe(II) complex and the H99A apo-mutant, differ significantly from those for the active forms. In particular, their globin domains have deuteration patterns very different from those of the active Fe(III)-OH^- form; the 5-coordinate Fe(II) complex is much less extensively deuterated on the heme-proximal side (helices H2, H3, and H5) but more strongly deuterated around the dimerization interface (helices H6 and H7) (see the *top part* of the *left structure* in Fig. 5*B*). On the other hand, the entire globin domain of the apo-form is completely deprotected (Fig. 5*B*, *top part* of the *central structure*). Interestingly, despite these differences in the globin domains, the kinase domains of the two inactive forms exhibit rather similar deuteration patterns, with sharply increased deuteration in helix H11(284–296) (see the *bottom parts* of the *left* and *central structures* in Fig. 5*B*). Increases in the solvent accessibility and dynamic behavior of helix H11 were also identified as the major changes associated with domain separation and kinase inactivation (Fig. 5*B*, *bottom right*). This may indicate that this area is involved in intramolecular signal transduction. The deuteration patterns of the active and inactive forms of *Af*GcHK did not vary appreciably over the incubation times considered in this work.

Comparison of the full-length AfGcHK protein with its isolated globin and kinase domains based on HDX–MS data

We also compared the HDX–MS exchange profile of the Fe(III)-OH^- complex of the full-length *Af*GcHK protein with those of the isolated Fe(III)-OH^- globin domain and the isolated kinase domain (Fig. 8).

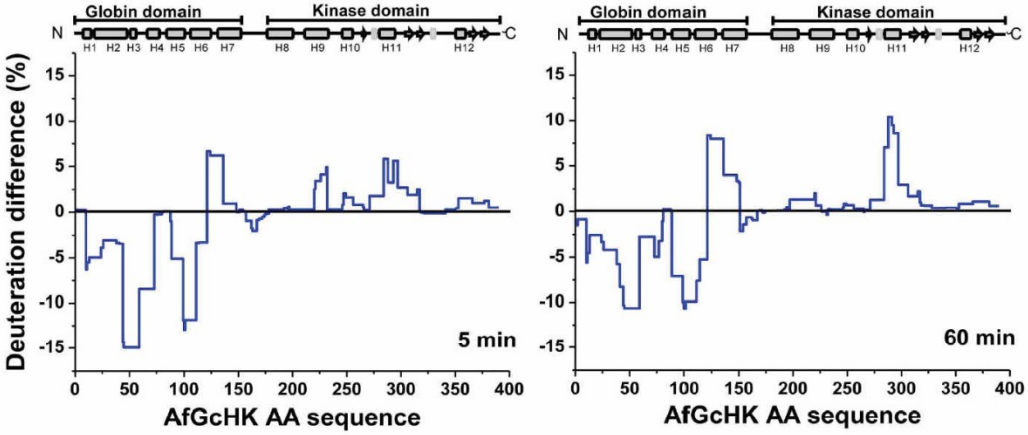


Figure 6. HDX–MS protection plots showing the differences in deuteration after 5 min (*left*) and 60 min (*right*) of exchange for the full-length Fe(III)-OH$^-$ bound (active) and Fe(II)-bound (inactive) forms of *Af*GcHK. The deuteration levels of the active form were subtracted from those of the inactive form and plotted against the protein's sequence (*x* axis). The *blue line* thus represents the structural changes caused by reducing the heme iron center in the globin domain of the full-length protein.

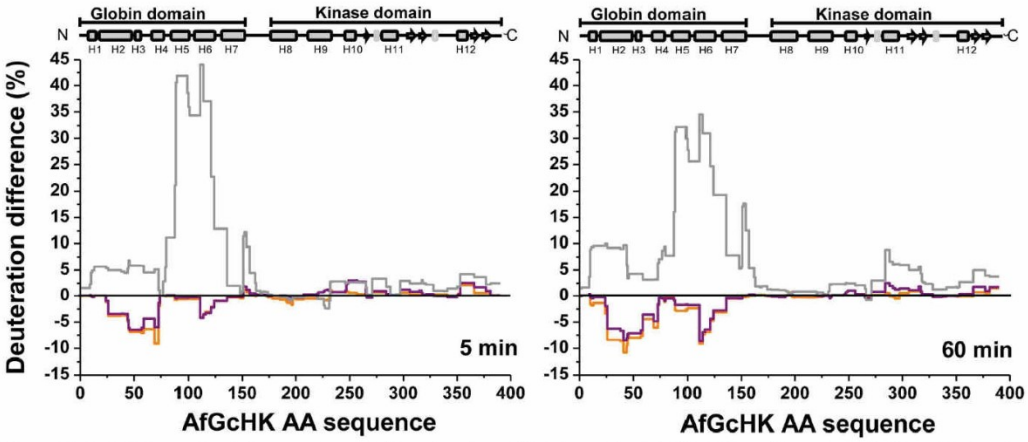


Figure 7. HDX–MS deuteration differences for the full-length active Fe(II)-O_2 (*orange*) and Fe(III)-CN (*purple*) forms of *Af*GcHK and the inactive full-length heme-free H99A mutant (*gray*) after 5 and 60 min of exchange. The deuteration differences for each form are computed relative to the deuteration of the full-length *Af*GcHK protein with the Fe(III)-OH$^-$ heme complex.

The globin domain of the full-length protein is dimeric, and ultracentrifugation experiments showed that the isolated globin domain is too (Fig. 4). However, the absence of the covalently attached kinase domain increases the solvent accessibility of the globin domain contact interface (H6 and L7) in the isolated domain (Fig. 5*B*, *top right structure*). Interestingly, another region showing increased deuteration upon isolation of the globin domain was helix H5 on the heme-proximal side (shown in *pink* in the *bottom parts* of the *top right structure* in Fig. 5*B*; see also Fig. 8). This helix is in direct contact with both the heme and the C terminus of the globin domain, the latter of which is attached to the kinase domain via a short linker. Therefore, H5 might be important in intraprotein signal transduction.

The separation of the kinase domain from the globin domain eliminates its autokinase activity, suggesting that the attachment of the globin domain in the full-length *Af*GcHK protein is required for the functioning of the kinase domain (supplemental Fig. S7). HDX–MS experiments indicated that the isolated kinase domain is more solvent-accessible than that in the full-length protein. The *dark red ribbon* in the *bottom part* of the *right structure* in Fig. 5*B* shows the significant structural destabilization of helix H11 (residues 284–292) associated with the isolation of the kinase domain in the full-length protein. The

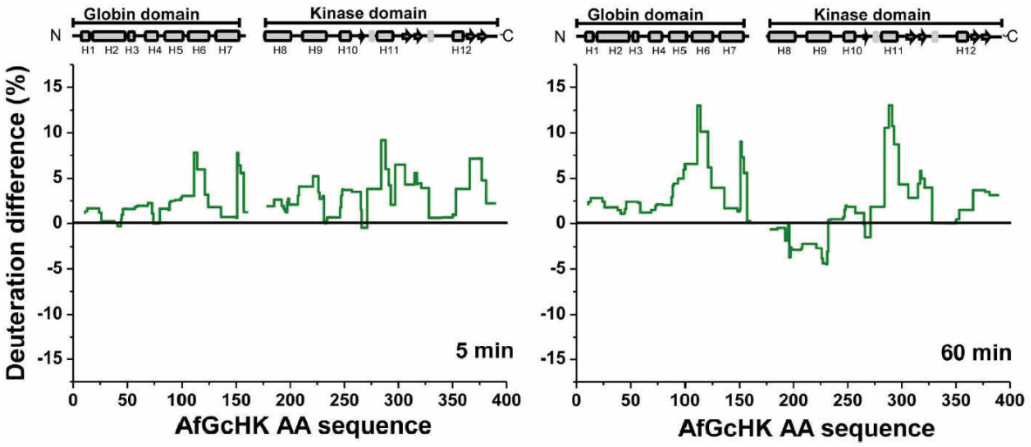


Figure 8. HDX–MS deuteration differences between the active full-length Fe(III)-OH$^-$ form of *Af*GcHK and a mixture of its isolated Fe(III)-OH$^-$-bound globin domain with its isolated inactive kinase domain. Deuteration differences are shown for incubation times of 5 and 60 min *lined* in *dark green*, and the plotted values were obtained by subtracting the deuteration levels of the active full-length Fe(III)-OH$^-$ form from those for the isolated domains.

isolation of the kinase domain, which inactivates it, also affects helix H9, which is slightly deprotected over short deuteration times (Fig. 8) but moderately protected over longer deuteration times (see the *light blue ribbons* in the *bottom right structure* in Fig. 5*B*). Conversely, both incubation times make helix H11 more solvent-accessible. A slight increase in deuteration was also observed for the large β-sheet–forming solvent-exposed part of the ATP-binding subdomain (*pink arrows* in the *bottom right* structure in Fig. 5*B*).

The deuteration profiles of the isolated globin (Fig. 5*B*, *top right*) and kinase (Fig. 5*B*, *bottom right*) domains show several similarities to the inactive forms of the full-length protein (*i.e.* the 5-coordinate heme Fe(II) form and the H99A apo-form) (Figs. 5–8). Specifically, helices H6 and H11 behave similarly when the heme iron is reduced and when the domains are separated.

Characterization of the contact interface between the globin and kinase domains based on HDX–MS data for isolated domains and mixtures of isolated domains

HDX–MS can be used to map interaction interfaces between proteins or domains if they interact in a way that affects solvent accessibility and/or hydrogen bonding. However, as shown in supplemental Fig. S8, the deuteration profiles of the isolated globin and kinase domains when measured in isolation (*dark green lines*) did not differ from those seen with an equimolar mixture of the two (*light green lines*). This implies that the domains are not in direct close contact with a clearly defined interaction interface. The absence of protection in a HDX–MS experiment does not necessarily mean the absence of a direct interaction; weak and/or transient interactions are not captured by this method (25–27). However, such weak interactions would probably not explain the efficient signal transduction between the sensor and kinase domains.

Discussion

Full-length heme-based gas sensor proteins are very difficult to crystallize. X-ray structures have been reported for a small full-length heme-based CO-sensing transcription activator, CooA (28, 29), but not for any full-length heme-based oxygen sensors. HDX–MS is a powerful complementary tool to crystallography for mapping the folding, interactions, and conformational changes of proteins in solution, including those that are not readily crystallized. For example, it was used to characterize significant conformational changes in the heme-based NO sensor soluble guanylate kinase induced by NO binding (30). In addition, we have previously studied the folding, interactions, and conformational changes of heme Fe(III) complexes of *Af*GcHK in the presence and absence of its response regulator partner protein (7). In this work, we determined the X-ray crystal structures of the isolated globin domain of *Af*GcHK with 6-coordinate Fe(III)-CN$^-$ and 5-coordinate Fe(II) complexes and compared these structures with conformational changes observed by HDX–MS.

X-ray structures of the AfGcHK globin domain in various forms

The X-ray structure of *Af*GcHK globin domain containing the Fe(III)-CN$^-$ complex (Fig. 2) revealed slight differences between the individual chains, mainly in the long loop (L3) connecting helices H3 and H4. This segment, which consists of residues Ala^{57}–Met^{71}, has the highest absolute hydrogen/deuterium exchange level in both the isolated globin domain and the full-length *Af*GcHK protein, suggesting that it is very flexible and solvent-accessible. The large contact area observed between the two chains of the *Af*GcHK dimer supports the proposed physiological relevance of the dimerization of its globin domain, in keeping with the results of ultracentrifugation experiments (Fig. 4) and predictions based on earlier HDX–MS experiments (7). Moreover, all globin domains from homo-

Protein structures of a heme-based oxygen sensor kinase AfGcHK

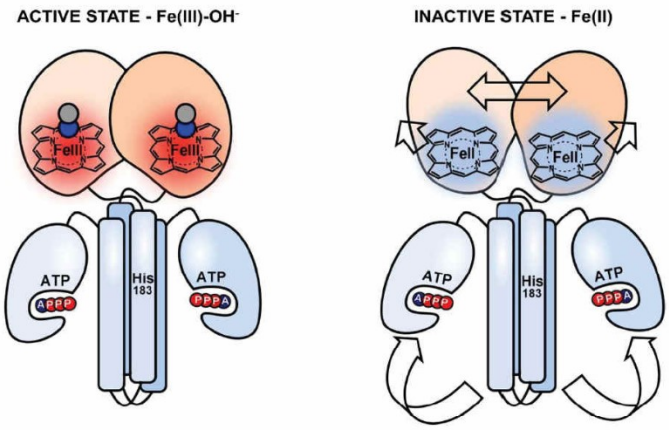


Figure 9. Proposed intramolecular signal transduction mechanism in the full-length *Af*GcHK protein that explains its catalytic inactivation upon heme reduction. Heme reduction induces conformational changes in the globin domain, simultaneously widening and splitting its internal dimeric interface, and making the initial residues of H7 accessible to the solvent. This signal is propagated down to the kinase domain via the linker, causing the ATP binding site to be separated from His^{183}, hindering the autophosphorylation of the latter residue. Data previously obtained by our group indicated that heme reduction increases the enzyme's K_m^{ATP} value and thus reduces the ATP affinity of the kinase domain (8).

logous GCS proteins with known structures form analogous dimers (16–18). The unique organization of the globin domain dimerization interface, with its flexible part I and tightly bound part II (see Fig. 2*C*), implies a high capacity for dynamic rearrangement (31). This is consistent with the HDX–MS data for active and inactive forms of the full-length *Af*GcHK protein (Figs. 5 (*A* and *B*), *top parts* in *left structures*), which suggest that the globin domain dimerization interface undergoes a "scissor" motion as the protein transitions between active and inactive forms (Fig. 9). A scissor-like dynamic motion was inferred for another oxygen sensor, *Ec*DOS, based on the crystal structure of its dimeric isolated heme-bound PAS domain (11). A structural comparison of the isolated globin domains of *Af*GcHK with other GCSs is presented in the supplemental material.

Interestingly, reducing the heme iron in the crystallized Fe(III)-CN^- form of the isolated globin domain induced a structural change (Fig. 3). The most significant changes were observed in chain G, in the chain with elevated temperature factors and weaker protein–protein contacts of the H3–L3 segment in the crystal. Surprisingly, only some heme iron molecules populating chain G were reduced upon soaking the original crystal in the dithionite solution, resulting in the observation of two different alternatives, A and B. Observations of alternative localization of protein atoms in crystal structures are common and can provide vital insights into how conformational changes enable proteins to function (32). Alternative A is consistent with the original atomic coordinates of the chains in the 6-coordinate Fe(III)-CN^- structure, whereas alternative B represents the reduced state of the heme complex. Because this change occurred under strongly reducing conditions and the heme of the B alternative lacks a distal ligand, we conclude that the heme in chain G was partially reduced to form a 5-coordinate Fe(II) complex. Therefore, the two alternatives represent globin domain structures associated with one active form (Fe(III)-CN^- complex) and one inactive form (Fe(II) complex).

The most important result is the observation that the heme and a significant part of the protein chain G and minor part of the protein chain H are shifted in the case of the heme iron reduction. There is thus a clear structural difference between the globin domains associated with the active and inactive forms. Conversely, Tarnawski *et al.* (16) found that heme iron reduction had no significant structural effect on the isolated globin domain of YddV from *Escherichia coli* (PDB entries 4ZVA and 4ZVB). They reached this conclusion by preparing two different crystals and superimposing their structures, whereas we prepared a single protein crystal containing *Af*GcHK in a mixture of two states. In our case, the four dimers in the asymmetric unit formed luckily a scaffold in which it is possible to see larger changes in one of the dimers without destroying the crystal. If all of the protein chains of this asymmetric crystal underwent similar reduction-induced changes, it would probably cause major structural changes in the crystal lattice; indeed, prolonged soaking in the dithionite solution led to macroscopic crystal reshaping. Based on the consistent experimental results for crystals soaked in the strong reducing agent and the adverse effects of long soaking times, we suggest that the concurrent observation of both states in the crystal was only possible because the heme of chain G in the asymmetric crystal reacts more rapidly than the hemes of the other chains.

Signal transduction in the full-length AfGcHK protein observed by HDX–MS

For the first time, we have observed conformational changes associated with signal transduction in a full-length heme-containing sensor protein. All known active forms of the full-length *Af*GcHK protein, namely the Fe(III)-CN^--, Fe(III)-OH^-- and Fe(II)-O_2-containing forms, exhibit very similar dynamic behavior and solvent accessibility, unlike the inactive Fe(II)- and heme-free forms (Fig. 5). The most important differences between the active and inactive forms were found 1) near the

heme in the globin domain; 2) in the dimerization interface (helices H6 and H7) of the globin domain, where the end of helix H6, loop L7, and the beginning of helix H7 are more solvent-accessible in the inactive forms; and 3) in helices H11 and (to a lesser extent) H9 in the kinase domain, which undergo faster hydrogen/deuterium exchange after heme iron reduction or in the absence of heme. The faster hydrogen/deuterium exchange in H11 and H9 could be caused by their opening or an increase in the mobility of this region, which is consistent with the hypothesis that the distance between the helices increases in the inactive states. These changes are probably significant because the HDX–MS results for the three active forms were similar, as were those for the two inactive forms, especially with respect to the kinase domain. The HDX–MS data thus highlighted the key regions involved in the molecular signal transduction mechanism and important structural differences between the active and inactive forms.

We have previously shown that the heme Fe(III)-OH^--, Fe(III)-CN^--, and Fe(II)-O_2-bound forms of full-length *Af*GcHK are active, whereas heme-free and heme Fe(II)-bound forms are inactive (1, 8). Here we reported for the first time that the isolated kinase domain is inactive, and its His^{183} residue is not autophosphorylated (supplemental Fig. S7). Importantly, the HDX–MS profile of the isolated kinase domain (and especially that of H11) is similar to that of the kinase domain joined to the "inactive" Fe(II)-bound and heme-free globin domains in full-length *Af*GcHK (Fig. 5*B*).

Mechanism of signal transduction in AfGcHK

Two mechanisms have been proposed to explain how the kinase domain's autophosphorylation activity could be altered in response to signaling from the globin domain. The first is based on steric hindrance, with autophosphorylation being suppressed by physically blocking the autophosphorylation site (33). A similar mechanism was proposed to explain signal transduction in gas sensors; the protein surface of the heme-bound globin domain was suggested to directly contact the protein surface of the kinase domain such that signals from the globin domain could directly modulate the kinase domain's activity (34). The second mechanism involves indirect regulation of the autophosphorylation activity, with no direct blocking ("touching") of the phosphorylation site in the kinase domain (35). The data presented here for *Af*GcHK strongly support this mechanism; there does not seem to be any direct interaction between the globin and kinase domains, which are only connected by a 15-residue-long covalent linker peptide in the full-length protein (supplemental Fig. S8).

The indirect mechanism of *Af*GcHK signal transduction loosely resembles that proposed for transmembrane signal propagation in membrane-bound two-component systems (3–6), although *Af*GcHK is not a membrane-bound protein.

In terms of dynamics, *Af*GcHK can be regarded as an ensemble of molecules sampling at least two conformational states. The kinase domains in these states feature different mutual arrangements of segments, including helices H11 (the ATP-binding site) and H9. In one state, the orientation of the H11 and H9 segments supports autophosphorylation; in the other, these segments occupy catalytically unfavorable positions. We suggest that the oxygen-binding signal is propagated from the heme to the kinase domain via the globin dimerization interface and the long helices (H8 and H9) that form the dimerization interface of the kinase domain. The short and structurally undetermined linker sequence connecting the globin and kinase domains may also play some role. On the contrary, there was no difference in its behavior under the studied conditions; therefore, its functional significance is currently unknown. Finally, the signal is propagated throughout the kinase domain, reorienting helices H11 and H9 in a way that impairs autophosphorylation and possibly ATP binding, as suggested by an increase in the domain's K_m^{ATP} value (8). This signal transduction process may involve a scissor-like motion as was discussed above or a larger-scale dynamic rearrangement of the globin domain that transfers the signal to the kinase domain (Fig. 9). The X-ray crystallography and HDX–MS experiments performed in this study provided complementary information on the functional and structural behavior of *Af*GcHK. For the first time, the conformational changes associated with signal transduction were studied in a full-length globin-coupled oxygen sensor protein and linked to directly observed structural changes in the globin domain. As such, this work represents an important step toward a deeper understanding of the mechanism of heme-containing sensor regulation.

Experimental procedures

Materials

Ampicillin was obtained from P-lab (Prague, Czech Republic). Isopropyl β-D-thiogalactopyranoside, hemin, and acrylamide were obtained from Sigma-Aldrich. Water, doubly distilled over quartz, was purified using a Milli-Q Plus system (EMD Millipore, Billerica, MA). All glassware used for sample preparation was conditioned in advance by standing for 24 h in 10% (v/v) HCl Suprapur (Merck, Darmstadt, Germany). Phos-tag was from the Phos-tag consortium, Wako Pure Chemical Industries (Osaka, Japan). All chemicals used were of the highest purity grade available from commercial sources and used without further purification.

Protein production and purification

Cloning, overexpression in *E. coli*, and purification of the full-length wild-type, Y45F, Y45L, Y45W, L68N, L68F, L68G, L68W, and H99A *Af*GcHK proteins were performed as described previously (1, 7, 8). Briefly, His-tagged *Af*GcHK was expressed in BL21(DE3) (Novagen, Madison, WI) harboring the pET21c(+) plasmid. Cell lysates containing the His-tagged *Af*GcHK were isolated by affinity chromatography on a TALON® metal affinity resin column (Clontech), followed by size-exclusion chromatography on a Superdex Increase 200 GL 10/300 column (GE Healthcare). Protein and heme concentrations were determined using the BCA assay (Sunrise Absorbance Reader, TECAN, Männedorf, Switzerland) and the pyridine hemochromogen assay, respectively (36). Purified proteins were >90% homogeneous, as confirmed by SDS-PAGE.

The isolated globin domain of *Af*GcHK was prepared as follows. 500 ml of TB medium containing 100 μg/ml ampicillin was inoculated with 500 μl of O/N BL21(DE3) cells containing the appropriate pET21c(+) plasmid. Cells were grown at 37 °C

for 5 h (220 rpm), and then the temperature was lowered to 18 °C (160 rpm), and protein expression was initiated by adding 0.1 mM isopropyl 1-thio-β-D-galactopyranoside followed by further shaking for 18 h. Cells were then harvested by centrifugation at 4 °C and 5000 × *g*, and stored at −80 °C. The pellets were resuspended in 50 mM Tris, 150 mM NaCl, pH 8, containing 1 mM PMSF, 1 mM EDTA, and 0.2 mg/ml lysozyme. After sonication (10 × 1 min), reconstitution with 300 μM hemin for 20 min, and 70 min of centrifugation at 50,000 × *g*, the supernatant was applied to a TALON® metal affinity resin column (Clontech), and the protein was eluted using 200 mM imidazole. The eluted protein was concentrated to a volume of 2 ml and desalted on Sephadex G10 column equilibrated with 20 mM Tris, 150 mM NaCl, pH 8. The protein was then diluted to 0.5 mg/ml, and the His tag was cleaved with the tobacco etch virus protease (final concentration 0.05 mg/ml, 48 h at 10 °C). The tobacco etch virus protease and uncleaved protein were removed using a TALON® metal affinity resin column, leaving the isolated protein in the flow-through fraction. Finally, size-exclusion chromatography was performed using a Superdex Increase 200 GL 10/300 column (GE Healthcare), and the final protein preparation was frozen in liquid nitrogen for further use. SDS-PAGE experiments showed that the purified isolated globin domain of *Af*GcHK was >99% homogeneous.

The isolated kinase domain (Δ161) of *Af*GcHK was prepared as follows. 500 ml of TB medium containing 100 μg/ml ampicillin was inoculated with 500 μl of O/N BL21(DE3) cells containing the appropriate pET21c(+) plasmid. Cells were grown at 37 °C for 5 h (220 rpm), and then the temperature was lowered to 18 °C (160 rpm), and protein expression was initiated by adding 0.1 mM isopropyl 1-thio-β-D-galactopyranoside followed by further shaking for 18 h. Cells were harvested by centrifugation at 4 °C and 5000 × *g* and stored at −80 °C. Pellets were resuspended in 50 mM Tris, 150 mM NaCl, pH 8, containing 1 mM PMSF, 1 mM EDTA, and 0.2 mg/ml lysozyme. After sonication (5 × 1 min) and 70 min of centrifugation at 50,000 × *g*, the supernatant was applied to a TALON® metal affinity resin column (Clontech), and the protein was eluted using 200 mM imidazole. The protein was concentrated to a volume of 0.5 ml, size-exclusion chromatography was performed on a Superdex 200 GL 10/300 column (GE Healthcare), and the final protein preparation was frozen in liquid nitrogen for further use. SDS-PAGE experiments showed that the purified isolated kinase domain of *Af*GcHK was >70% homogeneous.

Crystallization of the isolated AfGcHK globin domain

A 5.4 mg/ml solution of the *Af*GcHK globin domain with the Fe(III)-OH^- complex in 150 mM NaCl, 20 mM Tris, pH 8.0, was crystallized using the hanging-drop vapor diffusion method at 25 °C. The drops contained 2 μl of protein and 1 μl of reservoir. The reservoir contained 20.7% (w/v) PEG 3350, 0.1 M MMT buffer (DL-malic acid, MES, and Tris base in a molar ratio of 1:2:2), pH 6.7, 0.2 M $MgCl_2$, 10 mM KCN, and 7.5% (v/v) glycerol. This yielded red wedge block–shaped crystals with dimensions of up to 80 × 80 × 300 μm. The crystals were vitrified in liquid nitrogen without any cryoprotection. Before vitrification, the dithionite-soaked crystal was soaked for 15 min in a maternal drop containing 0.2 μl of added 100 mM sodium dithionite (giving a final dithionite concentration of ~10 mM). Soaking did not cause any visible changes in the crystal.

Diffraction data collection, structure determination, and refinement

Data for the crystal with the Fe(III)-CN^- complex were collected at the Helmholtz-Zentrum Berlin (Bessy II) on beamline 14.1 equipped with a Dectris Pilatus 6M detector at 100 K, using wavelength 0.918409 Å, detector distance 0.375 m, Δφ 0.1° per image, and exposure time 0.5 s. Data for the sodium dithionite–soaked crystal were collected at the synchrotron light source Petra III in Hamburg on beamline PX13 equipped with a Dectris Pilatus 6M detector at 100 K using wavelength 0.92010 Å, detector distance 0.369 m, Δφ 0.05° per image, and exposure time 0.1 s.

The diffraction images were processed using XDS (37) and scaled using AIMLESS from the CCP4 program package (38). Data processing statistics are presented in Table 1. The phase problem was solved by molecular replacement using the MORDA program (39) and the structure of the globin domain of the globin-coupled sensor from *G. sulfurreducens* (PDB code 2W31 (17)). Structures were refined using REFMAC5 with manual editing using COOT (40), with 5% of reflections used as the testing set (the R_{free} set). The last cycle of the refinement was performed using all reflections. Structure quality was checked using the validation tools implemented in MOLPROBITY (41) and COOT.

The atomic coordinates and structure factors have been deposited in the Protein Data Bank under the codes 5OHE (globin domain of *Af*GcHK with cyanide) and 5OHF (globin domain of *Af*GcHK with cyanide, partially reduced).

HDX–MS

HDX–MS experiments using samples of full-length wild type *Af*GcHK (80 μM), the globin domain of *Af*GcHK (80 μM), the kinase domain of *Af*GcHK (80 μM), and a 1:1 mixture of the globin and kinase domains with a total protein concentration of 160 μM were initiated by 10-fold dilution in a deuterated buffer containing 20 mM Tris-HCl (pD 7.6), 150 mM NaCl, 50 mM KCl, and 5 mM $MgCl_2$ at 20 °C. Solutions of *Af*GcHK with different heme iron ligands in the globin domain were prepared as follows: Fe(III)-CN^-, 1-h incubation of the protein in 10 mM KCN solution and use of a deuterated buffer containing 10 mM KCN; Fe(II)-O_2, 2-min incubation of the protein in 10 mM sodium dithionite followed by desalting on a Sephadex G10 column equilibrated with 20 mM Tris and 150 mM NaCl, pH 8; Fe(II), prepared in an anaerobic glove box (Jacomex GP-Concept; oxygen concentration <1 ppm) by 2-min incubation of the protein in 10 mM sodium dithionite followed by desalting on a Sephadex G10 column equilibrated with degassed 20 mM Tris, 150 mM NaCl, pH 8, buffer. All solutions used in this experiment were thoroughly degassed and equilibrated in the anaerobic box, and UV-visible spectra were recorded throughout the procedure to ensure the exclusive presence of the Fe(II) form.

Aliquots (25 μl) were taken after 0.5, 5, 20, 60, and 180 min of exchange. The exchange reaction in the aliquots was immediately quenched by adding 25 μl of 1 M glycine (pH 2.3), and the

samples were then rapidly frozen in liquid nitrogen. HPLC-MS analysis of deuterated samples was performed using a high-performance liquid chromatograph (1200 Agilent Technologies, Waldbronn, Germany) connected to an ESI-FT-ICR mass spectrometer (15T solariX XR, Bruker Daltonics, Billerica, MA). The analysis was initiated by rapidly thawing the sample, followed by digestion on a pepsin column (66-μl bed volume, flow rate 100 μl min^{-1}). The resulting peptides were desalted online using a Peptide MicroTrap (MichromBioresources, Auburn, CA) and separated on a C18 reversed phase column (0.5 × 50 mm; Jupiter, Phenomenex, Torrance, CA) using a linear gradient of 10–45% (v/v) solvent B over 7 min, where solvent A was 2% (v/v) acetonitrile with 0.4% (v/v) formic acid in water and solvent B was 95% (v/v) acetonitrile, 5% (v/v) water with 0.4% (v/v) formic acid. The injector and switching valve, pepsin column, peptide trap, and analytical column were placed in an ice box to minimize back-exchange. Peptide identification (mapping, HPLC-MS/MS) was done using the system described above, and MASCOT was used to compare the obtained MS/MS spectra with a database containing a sequence for *Af*GcHK. Deuterated data were processed using an in-house program called DeutEx,[4] which records the average mass for each peptide at each time point and each condition studied and calculates the percentage of deuteration relative to the maximum achievable deuteration based on the number of exchangeable amide hydrogens in each peptide. The deuterium content of each peptide was reported as a percentage of the maximum achievable deuteration based on the number of exchangeable amide hydrogens in each peptide (42).

Mass spectrometric analysis of AfGcHK phosphorylation at His^{183}

The above-mentioned LC-MS setup designed for HDX–MS samples was also used to analyze the phosphorylation status of His^{183} in the full-length *Af*GcHK and the isolated kinase domain. Extracted ion chromatograms for non-phosphorylated and phosphorylated peptides including His^{183} were plotted in Data Analysis (Bruker Daltonics).

UV-visible spectroscopy and autoxidation rate estimation

Optical absorption spectral data were obtained using an HP 8453 UV-visible spectrophotometer (Agilent Technologies) at 20 °C under aerobic conditions as described previously (1). Proteins were diluted to 300 μl in 20 mM Tris/Cl, 150 mM NaCl, pH 8. A dithiothreitol solution (2 M) was then added to a final concentration of 0.5 M, and the protein sample was reduced for 60 min; the reduction was monitored by UV-visible spectrophotometry. Excess dithiothreitol was removed using a Sephadex G-25 desalting chromatography column, and the eluate was placed in a cuvette and diluted such that its absorbance at 413 nm was around 0.8. Spectra were collected every 15 or 30 min (depending on the protein) for 48 h at 25 °C (supplemental Fig. S2). The k_{ox} value was calculated under the assumption of first order kinetics based on the time-dependent decrease of the α band (577–580 nm) absorbance.

[4] D. Kavan, P. Man, and G. Kruppa, unpublished data.

Enzyme activity of the isolated kinase domain of AfGcHK

A reaction mixture containing 10 μM full-length wild-type *Af*GcHK or its isolated kinase domain, 50 mM Tris-HCl, pH 8.0, 50 mM KCl, and 5 mM $MgCl_2$ was preincubated for 5 min at 20 °C, and then the reaction was initiated by adding 1 mM ATP at 20 °C. At designated times, the autophosphorylation reaction was terminated by adding 100-μl aliquots of termination buffer (125 mM Tris-HCl, pH 6.8, 4% (w/v) SDS, 10% (v/v) 2-mercaptoethanol, 20% (v/v) glycerol, 0.004% (w/v) bromphenol blue). Samples of the quenched reaction mixtures were then loaded on a 10% (w/v) SDS-polyacrylamide gel containing 75 μM Phos-tag acrylamide and 0.2 mM $MnCl_2$. Each lane was loaded with a quantity of quenched reaction mixture containing 0.5 μg of *Af*GcHK. Phosphorylated proteins in the sample interacted with the Phos-tag manganese complex in the gel, reducing their mobility relative to phosphate-free proteins (1, 43, 44). After electrophoresis, the proteins were visualized by staining with Coomassie Brilliant Blue R350, and the stained gels were imaged using a Scanjet G3010 (HP) scanner. The protein loadings were then quantified by analyzing the scanned images using ImageJ.

Analytical ultracentrifugation

Sedimentation velocity experiments were performed using a ProteomeLab XL-I (Beckman Coulter, Brea, CA) analytical ultracentrifuge at loading concentrations of 6–15 μM for the isolated globin domain of *Af*GcHK and the full-length protein, at 20 °C and a rotor speed of 36,000 rpm. All data were collected using absorbance optics at 411 nm (selective for hemoproteins). Data analysis was performed with the SEDFIT, SEDPHAT, and Gussi packages (45–47). Sedimentation velocity data were analyzed using a continuous sedimentation coefficient distribution model, $c(s)$. The resulting apparent sedimentation coefficients were used to compute sedimentation coefficients in water at 20 °C ($s_{20,w}$).

Author contributions—M. S. planned experiments, performed experiments and analyzed data; P. M. planned, performed and interpreted MS experiments; T. S., P. K., and J. B. designed, performed, and analyzed the crystallization, diffraction data collection, structure determination, and refinement experiments; V. F. performed experiments; V. M. performed and interpreted protein models and discussed and interpreted data; J. D. performed interpretation and validation of structures and contributed to the manuscript; A. L. provided technical assistance and contributed to the preparation of the figures; M. R. provided technical assistance; T. S. discussed and interpreted data; M. M. discussed and interpreted data and wrote the paper. All authors reviewed the results and approved the final version of the manuscript.

Acknowledgments—We are grateful to Dr. Kenichi Kitanishi and Dr. Ondrej Vanek for technical assistance during the early stages of this work.

References

1. Kitanishi, K., Kobayashi, K., Uchida, T., Ishimori, K., Igarashi, J., and Shimizu, T. (2011) Identification and functional and spectral characterization of a globin-coupled histidine kinase from *Anaeromyxobacter* sp. Fw109-5. *J. Biol. Chem.* **286,** 35522–35534

2. Martínková, M., Kitanishi, K., and Shimizu, T. (2013) Heme-based globin-coupled oxygen sensors: linking oxygen binding to functional regulation of diguanylate cyclase, histidine kinase, and methyl-accepting chemotaxis. *J. Biol. Chem.* **288,** 27702–27711
3. Gushchin, I., Melnikov, I., Polovinkin, V., Ishchenko, A., Yuzhakova, A., Buslaev, P., Bourenkov, G., Grudinin, S., Round, E., Balandin, T., Borshchevskiy, V., Willbold, D., Leonard, G., Büldt, G., Popov, A., and Gordeliy, V. (2017) Mechanism of transmembrane signaling by sensor histidine kinases. *Science* 10.1126/science.aah6345
4. Abriata, L. A., Albanesi, D., Dal Peraro, M., and de Mendoza, D. (2017) Signal sensing and transduction by histidine kinases as unveiled through studies on a temperature sensor. *Acc. Chem. Res.* **50,** 1359–1366
5. Willett, J. W., and Crosson, S. (2017) Atypical modes of bacterial histidine kinase signaling. *Mol. Microbiol.* **103,** 197–202
6. Zschiedrich, C. P., Keidel, V., and Szurmant, H. (2016) Molecular mechanisms of two-component signal transduction. *J. Mol. Biol.* **428,** 3752–3775
7. Stranava, M., Martínek, V., Man, P., Fojtikova, V., Kavan, D., Vaněk, O., Shimizu, T., and Martinkova, M. (2016) Structural characterization of the heme-based oxygen sensor, AfGcHK, its interactions with the cognate response regulator, and their combined mechanism of action in a bacterial two-component signaling system. *Proteins* **84,** 1375–1389
8. Fojtikova, V., Stranava, M., Vos, M. H., Liebl, U., Hranicek, J., Kitanishi, K., Shimizu, T., and Martinkova, M. (2015) Kinetic analysis of a globin-coupled histidine kinase, AfGcHK: effects of the heme iron complex, response regulator, and metal cations on autophosphorylation activity. *Biochemistry* **54,** 5017–5029
9. Gong, W., Hao, B., and Chan, M. K. (2000) New mechanistic insights from structural studies of the oxygen-sensing domain of *Bradyrhizobium japonicum* FixL. *Biochemistry* **39,** 3955–3962
10. Hao, B., Isaza, C., Arndt, J., Soltis, M., and Chan, M. K. (2002) Structure-based mechanism of O2 sensing and ligand discrimination by the FixL heme domain of *Bradyrhizobium japonicum*. *Biochemistry* **41,** 12952–12958
11. Kurokawa, H., Lee, D.-S., Watanabe, M., Sagami, I., Mikami, B., Raman, C. S., and Shimizu, T. (2004) A redox-controlled molecular switch revealed by the crystal structure of a bacterial heme PAS sensor. *J. Biol. Chem.* **279,** 20186–20193
12. Park, H., Suquet, C., Satterlee, J. D., and Kang, C. (2004) Insights into signal transduction involving PAS domain oxygen-sensing heme proteins from the X-ray crystal structure of *Escherichia coli* Dos heme domain (Ec DosH). *Biochemistry* **43,** 2738–2746
13. Cho, H. Y., Cho, H. J., Kim, Y. M., Oh, J. I., and Kang, B. S. (2009) Structural insight into the heme-based redox sensing by DosS from *Mycobacterium tuberculosis*. *J. Biol. Chem.* **284,** 13057–13067
14. Podust, L. M., Ioanoviciu, A., and Ortiz de Montellano, P. R. (2008) 2.3 Å X-ray structure of the heme-bound GAF domain of sensory histidine kinase DosT of *Mycobacterium tuberculosis*. *Biochemistry* **47,** 12523–12531
15. Yukl, E. T., Ioanoviciu, A., Nakano, M. M., de Montellano, P. R., and Moënne-Loccoz, P. (2008) A distal tyrosine residue is required for ligand discrimination in DevS from *Mycobacterium tuberculosis*. *Biochemistry* **47,** 12532–12539
16. Tarnawski, M., Barends, T. R. M., and Schlichting, I. (2015) Structural analysis of an oxygen-regulated diguanylate cyclase. *Acta Crystallogr. D* **71,** 2158–2177
17. Pesce, A., Thijs, L., Nardini, M., Desmet, F., Sisinni, L., Gourlay, L., Bolli, A., Coletta, M., Van Doorslaer, S., Wan, X., Alam, M., Ascenzi, P., Moens, L., Bolognesi, M., and Dewilde, S. (2009) HisE11 and HisF8 provide bis-histidyl heme hexa-coordination in the globin domain of *Geobacter sulfurreducens* globin-coupled sensor. *J. Mol. Biol.* **386,** 246–260
18. Zhang, W., and Phillips, G. N. (2003) Structure of the oxygen sensor in *Bacillus subtilis*: signal transduction of chemotaxis by control of symmetry. *Structure* **11,** 1097–1110
19. Krissinel, E., and Henrick, K. (2004) Secondary-structure matching (SSM), a new tool for fast protein structure alignment in three dimensions. *Acta Crystallogr. D* **60,** 2256–2268
20. Krissinel, E., and Henrick, K. (2007) Inference of macromolecular assemblies from crystalline state. *J. Mol. Biol.* **372,** 774–797
21. Nakajima, K., Kitanishi, K., Kobayashi, K., Kobayashi, N., Igarashi, J., and Shimizu, T. (2012) Leu65 in the heme distal side is critical for the stability of the Fe(II)-O2 complex of YddV, a globin-coupled oxygen sensor diguanylate cyclase. *J. Inorg. Biochem.* **108,** 163–170
22. Zhang, W., Olson, J. S., and Phillips, G. N. (2005) Biophysical and kinetic characterization of HemAT, an aerotaxis receptor from *Bacillus subtilis*. *Biophys. J.* **88,** 2801–2814
23. Aono, S., Kato, T., Matsuki, M., Nakajima, H., Ohta, T., Uchida, T., and Kitagawa, T. (2002) Resonance Raman and ligand binding studies of the oxygen-sensing signal transducer protein HemAT from *Bacillus subtilis*. *J. Biol. Chem.* **277,** 13528–13538
24. Springer, B. A., Sligar, S. G., Olson, J. S., and Phillips, G. N. J. (1994) Mechanisms of ligand recognition in myoglobin. *Chem. Rev.* **94,** 699–714
25. Engen, J. R. (2003) Analysis of protein complexes with hydrogen exchange and mass spectrometry. *Analyst* **128,** 623–628
26. Kadek, A., Kavan, D., Marcoux, J., Stojko, J., Felice, A. K. G., Cianférani, S., Ludwig, R., Halada, P., and Man, P. (2017) Interdomain electron transfer in cellobiose dehydrogenase is governed by surface electrostatics. *Biochim. Biophys. Acta* **1861,** 157–167
27. Rezabkova, L., Man, P., Novak, P., Herman, P., Vecer, J., Obsilova, V., and Obsil, T. (2011) Structural basis for the 14-3-3 protein-dependent inhibition of the regulator of G protein signaling 3 (RGS3) function. *J. Biol. Chem.* **286,** 43527–43536
28. Lanzilotta, W. N., Schuller, D. J., Thorsteinsson, M. V., Kerby, R. L., Roberts, G. P., and Poulos, T. L. (2000) Structure of the CO sensing transcription activator CooA. *Nat. Struct. Biol.* **7,** 876–880
29. Komori, H., Inagaki, S., Yoshioka, S., Aono, S., and Higuchi, Y. (2007) Crystal structure of CO-sensing transcription activator CooA bound to exogenous ligand imidazole. *J. Mol. Biol.* **367,** 864–871
30. Underbakke, E. S., Iavarone, A. T., Chalmers, M. J., Pascal, B. D., Novick, S., Griffin, P. R., and Marletta, M. A. (2014) Nitric oxide-induced conformational changes in soluble guanylate cyclase. *Structure* **22,** 602–611
31. Skálová, T., Dohnálek, J., Spiwok, V., Lipovová, P., Vondrácková, E., Petroková, H., Dusková, J., Strnad, H., Králová, B., and Hasek, J. (2005) Cold-active β-galactosidase from *Arthrobacter* sp. C2-2 forms compact 660 kDa hexamers: crystal structure at 1.9 Å resolution. *J. Mol. Biol.* **353,** 282–294
32. Keedy, D. A., Fraser, J. S., and van den Bedem, H. (2015) Exposing hidden alternative backbone conformations in X-ray crystallography using qFit. *PLoS Comput. Biol.* **11,** e1004507
33. Cunningham, K. A., and Burkholder, W. F. (2009) The histidine kinase inhibitor Sda binds near the site of autophosphorylation and may sterically hinder autophosphorylation and phosphotransfer to Spo0F. *Mol. Microbiol.* **71,** 659–677
34. Shimizu, T., Huang, D., Yan, F., Stranava, M., Bartosova, M., Fojtíková, V., and Martínková, M. (2015) Gaseous O_2, NO, and CO in signal transduction: structure and function relationships of heme-based gas sensors and heme-redox sensors. *Chem. Rev.* **115,** 6491–6533
35. Rao, M., Herzik, M. A., Jr., Iavarone, A. T., and Marletta, M. A. (2017) Nitric oxide-induced conformational changes govern H-NOX and histidine kinase interaction and regulation in *Shewanella oneidensis*. *Biochemistry* **56,** 1274–1284
36. Antonini, E., and Brunori, M. (1971) *Hemoglobin and myoglobin in their reactions with ligands*, North-Holland Publishing Co., Amsterdam, The Netherlands
37. Kabsch, W. (2010) XDS. *Acta Crystallogr. D* **66,** 125–132
38. Winn, M. D., Ballard, C. C., Cowtan, K. D., Dodson, E. J., Emsley, P., Evans, P. R., Keegan, R. M., Krissinel, E. B., Leslie, A. G. W., McCoy, A., McNicholas, S. J., Murshudov, G. N., Pannu, N. S., Potterton, E. A., Powell, H. R., *et al.* (2011) Overview of the CCP4 suite and current developments. *Acta Crystallogr. D* **67,** 235–242
39. Vagin, A., and Lebedev, A. (2015) MoRDa, an automatic molecular replacement pipeline. *Acta Crystallogr. A* **71,** s19
40. Emsley, P., Lohkamp, B., Scott, W. G., and Cowtan, K. (2010) Features and development of Coot. *Acta Crystallogr. D* **66,** 486–501
41. Chen, V. B., Arendall, W. B., 3rd, Headd, J. J., Keedy, D. A., Immormino, R. M., Kapral, G. J., Murray, L. W., Richardson, J. S., and Richardson, D. C.

(2010) MolProbity: all-atom structure validation for macromolecular crystallography. *Acta Crystallogr. D* **66,** 12–21
42. Trcka, F., Durech, M., Man, P., Hernychova, L., Muller, P., and Vojtesek, B. (2014) The assembly and intermolecular properties of the Hsp70-Tomm34-Hsp90 molecular chaperone complex. *J. Biol. Chem.* **289,** 9887–9901
43. Yamada, S., Nakamura, H., Kinoshita, E., Kinoshita-Kikuta, E., Koike, T., and Shiro, Y. (2007) Separation of a phosphorylated histidine protein using phosphate affinity polyacrylamide gel electrophoresis. *Anal. Biochem.* **360,** 160–162
44. Igarashi, J., Murase, M., Iizuka, A., Pichierri, F., Martinkova, M., and Shimizu, T. (2008) Elucidation of the heme binding site of heme-regulated eukaryotic initiation factor 2α kinase and the role of the regulatory motif in heme sensing by spectroscopic and catalytic studies of mutant proteins. *J. Biol. Chem.* **283,** 18782–18791
45. Houtman, J. C. D., Brown, P. H., Bowden, B., Yamaguchi, H., Appella, E., Samelson, L. E., and Schuck, P. (2007) Studying multisite binary and ternary protein interactions by global analysis of isothermal titration calorimetry data in SEDPHAT: application to adaptor protein complexes in cell signaling. *Protein Sci.* **16,** 30–42
46. Schuck, P. (2000) Size-distribution analysis of macromolecules by sedimentation velocity ultracentrifugation and Lamm equation modeling. *Biophys. J.* **78,** 1606–1619
47. Brautigam, C. A. (2015) Calculations and publication-quality illustrations for analytical ultracentrifugation data. *Methods Enzymol.* **562,** 109–133

6. Závěr

Předkládaná disertační práce se zabývá studiem hemových senzorových proteinů detekujících kyslík. Byly studovány tři modelové senzorové proteiny, z nichž dva sdílely podobnou (homologní) strukturu senzorové domény. Hlavním cílem této práce bylo popsat intraproteinový/interdoménový přenos signálu u proteinu *Af*GcHK a YddV a také interproteinový přenos signálu mezi proteinem *Af*GcHK a jeho partnerem ve dvousložkovém signálním systému – RR proteinem. Neméně důležitým cílem bylo prostudovat vliv sulfidu sodného na spektrální a enzymové vlastnosti hemových senzorových proteinů *Af*GcHK, YddV a *Ec*DOS. Nejdůležitější výsledky předkládané disertační práce jsou shrnuty v těchto bodech:

1. Studium intraproteinového/interdoménového přenosu signálu přineslo tyto výsledky:
   - Kinetická studie enzymové aktivity proteinů *Af*GcHK a YddV odhalila, že redoxní stav hemového železa a vazba ligandů k tomuto iontu v senzorové doméně má výrazný vliv na aktivitu hemových senzorových proteinů (více viz kapitola 3.2).
   - Na základě hodnot naměřených kinetických parametrů bylo zjištěno, že absence molekuly hemu a redukce hemového železa výrazným způsobem snižuje katalytickou aktivitu hemových senzorových proteinů s globinovou strukturou senzorové domény (více viz kapitola 3.2).
   - Pomocí strukturně biologických metod byly odhaleny rozdíly ve struktuře senzorové domény po redukci hemového železa, a to zejména v řetězci G a H, dále v oblasti dimerizace globinové domény (helixy H6 a H7) a v helixech H11 a H9 kinasové domény (více viz kapitola 5.2).
   - Na základě těchto výsledků byl odvozen a objasněn intraproteinový přenos signálu u modelového hemového senzorového proteinu *Af*GcHK (více viz kapitola 3.2, 5.2).

2. Studium interproteinového přenosu signálu přineslo následující výsledky:
   - Interakce proteinu *Af*GcHK s jeho reakčním partnerem (RR protein) vyvolá snížení afinity *Af*GcHK k ATP, což má za následek snížení autofosforylační aktivity proteinu *Af*GcHK (více viz kapitola 3.2).

- V roztoku dochází k tvorbě komplexu – dimerní *Af*GcHK a monomerní RR protein (více viz kapitola 5.1).
- Na základě těchto výsledků byl odvozen a objasněn interproteinový přenos signálu mezi proteinem *Af*GcHK a RR proteinem (více viz kapitola 5.1).

3. Studium vlivu sulfidu sodného na spektrální vlastnosti a enzymovou aktivitu hemových senzorových proteinů přineslo následující výsledky:

- Po inkubaci hemových senzorových proteinů (konkrétně *Af*GcHK, *Ec*DOS a senzorové domény YddV) se sulfidem sodným došlo ke změně jejich spektrálních vlastností, což se projevilo posunem Soretova pásu (více viz kapitola 4.1, 4.2).
- U mutantní formy Arg97Ile proteinu *Ec*DOS a určitých mutantních forem Leu68 proteinu *Af*GcHK došlo vlivem působení sulfidu sodného ke vzniku verdohemu (více viz kapitola 4.1).
- U proteinu *Ec*DOS došlo vlivem koordinace SH^- k iontu železa hemu v PAS senzorové doméně ke zvýšení enzymové aktivity v porovnání s formou Fe(III). Katalytická účinnost *Af*GcHK, kdy hemové železo v jeho globinové senzorové doméně bylo ve formě Fe(III)-SH^- nebyla odlišná od stavu, kdy hemové železo bylo ve formě Fe(III) (více viz kapitola 4.1, 4.2).

7. Curicullum vitae Veroniky Fojtíkové včetně seznamu publikací

Vzdělání:

2014 - dosud **Přírodovědecká fakulta, Univerzita Karlova, Praha**
doktorské studium Biochemie
Téma disertační práce: Kinetická analýza enzymové aktivity modelových hemových senzorových proteinů

2014 **Přírodovědecká fakulta, Univerzita Karlova, Praha**
magisterské studium Klinická a toxikologická analýza
Téma diplomové práce: Určení kinetických parametrů pro enzymovou reakci katalyzovanou histidinkinasou s globinovou strukturou senzorové domény
Státní zkouška: Aplikovaná analytická chemie, biochemie regulací a působení vnějších vlivů, toxikokinetika a farmakologie; prospěla s vyznamenáním

2012 **Přírodovědecká fakulta, Univerzita Karlova, Praha**
bakalářské studium Klinická a toxikologická analýza
Téma bakalářské práce: Důležité role hemu: signál pro hem-detekující proteiny a detekční místo v plyn-detekujících proteinech
Státní zkouška: Analytická chemie, obecná a anorganická chemie, biochemie, organická chemie, toxikologie

Pracovní zkušenosti:

2017 - dosud Medicínské centrum Praha, odborný pracovník v laboratorních metodách

2014 - 2018 pedagogická účast v praktických laboratorních cvičeních (Praktikum z klinické biochemie), Přírodovědecká fakulta, Univerzita Karlova

2016 - 2018 vědecký pracovník, Přírodovědecká fakulta, Univerzita Karlova

Jazykové znalosti:

anglický jazyk - aktivně slovem i písmem, úroveň B2 (FCE, prosinec 2015)

německý jazyk - mírně pokročilý

Vědecká činnost:

Příspěvky na konferencích:

1. 77th Harden Conference: Two Component Signalling in Bacteria: Integrating Approaches and Science (Anglie, 2015) - poster
2. 9th International Conference on Heme Oxygenase (Česká republika, 2016) - poster
3. XIX Conference on Oxygen-Binding and Sensing Proteins (Německo, 2016) - poster
4. XXV. Biochemický sjezd (Česká republika, 2016) - poster, cena za nejlepší poster
5. XVI. mezioborové setkání mladých biologů, biochemiků a chemiků (Česká republika, 2016) – přednáška
6. The 42nd FEBS congress (Israel, 2017) - poster

Účast v soutěži:

- Finálové kolo soutěže pořádané francouzskou ambasádou Sanofi Prize in Pharmacy (Česká republika, 2015)

Řešené grantové projekty:

- Hlavní řešitel projektu Grantové agentury Univerzity Karlovy (Studium modelových senzorových proteinů obsahujících hem (konkrétně histidinkinasy, *Af*GcHK a fosfodiesterasy, *Ec*DOS) se zaměřením na vysvětlení mechanismu přenosu signálu prostřednictvím modulace enzymové aktivity těchto proteinů, 2015 - 2017)
- Účast na řešení projektu Grantové agentury České republiky (Molecular mechanisms of intraprotein/interdomain signal transduction in model heme sensor proteins, 2015 - 2017)

Publikace:

1. **Fojtikova V**, Stranava M, Vos MH, Liebl U, Hranicek J, Kitanishi K, Shimizu T, Martinkova M (2015) Kinetic Analysis of a Globin-Coupled Histidine Kinase,

AfGcHK: Effects of the Heme Iron Complex, Response Regulator, and Metal Cations on Autophosphorylation Activity. *Biochemistry* 54, 5017-29.

2. Shimizu T, Huang D, Yan F, Stranava M, Bartosova M, **Fojtíková V**, Martínková M (2015) Gaseous O2, NO, and CO in signal transduction: structure and function relationships of heme-based gas sensors and heme-redox sensors. *Chem Rev* 115, 6491-533
3. Yan F, **Fojtikova V**, Man P, Stranava M, Martínková M, Du Y, Huang D, Shimizu T. (2015) Catalytic enhancement of the heme-based oxygen-sensing phosphodiesterase EcDOS by hydrogen sulfide is caused by changes in heme coordination structure. *Biometals* 28, 637-52
4. **Fojtikova V**, Bartosova M, Man P, Stranava M, Shimizu T, Martinkova M. (2016) Effects of hydrogen sulfide on the heme coordination structure and catalytic activity of the globin-coupled oxygen sensor AfGcHK. *Biometals* 29, 715-29
5. Stranava M, Martínek V, Man P, **Fojtikova V**, Kavan D, Vaněk O, Shimizu T, Martinkova M (2016) Structural characterization of the heme-based oxygen sensor, AfGcHK, its interactions with the cognate response regulator, and their combined mechanism of action in a bacterial two-component signaling system. *Proteins* 84, 1375-89
6. Mináriková M, **Fojtikova V**, Vyskočilová E, Sedláček J, Šikut M, Borek-Dohalska L, Stiborová M, Martinkova M (2017) The capacity and effectiveness of diosmectite and charcoal in trapping the compounds causing the most frequent intoxications in acute medicine: A comparative study. *Environ Toxicol Pharmacol*. 52, 214-220
7. Stranava M, Man P, Skálová T, Kolenko P, Blaha J, **Fojtikova V**, Martínek V, Dohnálek J, Lengalova A, Rosůlek M, Shimizu T, Martínková M. (2017) Coordination and redox state-dependent structural changes of the heme-based oxygen sensor AfGcHK associated with intraprotein signal transduction. *J Biol Chem,* 292, 20921-20935
8. **Fojtikova V**., Lengalova A., Vávra J., Kraus D., Stranava M., Shimizu T, Martinkova M. (2018) Kinetic Analysis of a Globin-coupled Diguanylate Cyclase, YddV: Effects of the Various Heme Iron Redox and Ligand States on Diguanylate Cyclase Activity *in preparation*